
Universidad Autónoma de Madrid

Programa de Doctorado en Biociencias Moleculares

TESIS DOCTORAL

# Nuevos modelos preclínicos en insuficiencia cardiaca: caracterización con técnicas de imagen avanzada y aplicación de nuevas terapias

**Autor:** Jaume Agüero Ramón-Llin

**Director:** Borja Ibáñez Cabeza

Madrid, 2017

Departamento de Bioquímica.

Programa de Doctorado en Biociencias Moleculares

Universidad Autónoma de Madrid.

Título de la Tesis: “Nuevos modelos preclínicos en insuficiencia cardiaca: caracterización con técnicas de imagen avanzada y aplicación de nuevas terapias”.

Doctorando: Jaume Agüero Ramón-Llin. Licenciado en Medicina por la Universidad de Valencia.

Director: Borja Ibáñez Cabeza.

Lugar de realización. Centro Nacional de Investigaciones Cardiovasculares Carlos III (CNIC), Madrid.

BORJA IBÁÑEZ CABEZA, DOCTOR EN MEDICINA Y DIRECTOR DEL DEPARTAMENTO DE INVESTIGACIÓN CLÍNICA DEL CENTRO NACIONAL DE INVESTIGACIONES CARDIOVASCULARES CARLOS III (CNIC), Y LEANDRO SASTRE GASCÓN, PROFESOR TITULAR DEL DEPARTAMENTO DE BIOQUÍMICA DE LA UNIVERSIDAD AUTÓNOMA DE MADRID,

INFORMAN: Que D. Jaume Agüero Ramón-Llin ha realizado durante los últimos tres años bajo nuestra dirección la Tesis Doctoral “Nuevos modelos preclínicos en insuficiencia cardiaca: caracterización con técnicas de imagen avanzada y aplicación de nuevas terapias”. Estimamos que este trabajo contribuye de forma original y significativamente al campo de la investigación traslacional en enfermedades cardiovasculares.

BORJA IBAÑEZ CABEZA

LEANDRO SASTRE GASCÓN

**Dedicatoria.**

Para Iratxe, Josu y Manel.

*You can't connect the dots looking forward;*

*you can only connect them looking backward.*

*So you have to trust that the dots will somehow connect in your future.*

***Steve Jobs***

**Agradecimientos.**

A Borja Ibañez, Roger J Hajjar y Valentin Fuster, por haberme dado la oportunidad de dedicarme a la investigación durante estos años, y haberme dado la motivación necesaria en los momentos difíciles.

A mis compañeros y amigos de Mount Sinai en Nueva York, en especial Kiyotake Ishikawa y Carlos Santos-Gallego por su inestimable ayuda en éste otros trabajos, y su gran amistad.

A toda la gente de mi grupo en CNIC, muy en especial a Carlos Galán, Rodrigo Fernández, Javier Sánchez, Gonzalo López, Austin Bruce, David Sanz-Rosa, Andrés Pun y Jaime García-Prieto con quienes he tenido la suerte de compartir tantas horas de trabajo, por su inagotable entusiasmo y dedicación, y el apoyo que me han dado dentro y fuera del trabajo en estos años.

A mis colegas y amigos de los hospitales La Fe de Valencia, Francesc de Borja de Gandía, y General de Castellón, por haberme dado la visión clínica con la que he intentado dirigir mi trabajo como investigador.

Muy especialmente, a mis padres Celia y Antonio, y a mis hermanos Cristina, Elena, Antonio, Celia y Alberto, por darme siempre su cariño y apoyo, y enseñarme a no rendirme nunca.

# Índice.

## 1. Resumen.

La insuficiencia cardíaca crónica (IC) se caracteriza por una alta prevalencia en los países occidentales, un impacto dramático en la calidad de vida del paciente y su capacidad funcional, y una enorme carga económica para los sistemas de salud. En la IC crónica, la transformación de los nuevos descubrimientos en investigación básica en mejoras en el cuidado de los pacientes es una prioridad, y se basa en una validación preclínica de nuevos conceptos diagnósticos y terapéuticos. Se han desarrollado modelos animales que recapitulan la IC en el laboratorio. Sin embargo, al igual que en otras enfermedades crónicas, el modelado de IC es un desafío debido a la heterogeneidad fisiopatológica. Los modelos de IC en animales grandes son costosos y técnicamente complejos, pero proporcionan una oportunidad única para evaluar nuevos conceptos y terapias de imagen utilizando herramientas clínicamente relevantes. Aunque los intentos de reproducir el cuadro clínico completo junto con anomalías hemodinámicas y estructurales graves de la IC crónica no han tenido éxito, la recapitulación de fenotipos específicos puede ser factible y clínicamente relevante. Este documento incluye un trabajo de Tesis doctoral centrado en la creación y caracterización de modelos animales grandes sobre características clave de la IC: 1) hipertensión pulmonar crónica y remodelado ventricular derecha; 2) remodelado ventricular izquierdo de causa isquémica y por sobrecarga de presión. Finalmente, se evalúan nuevas estrategias de terapia génica en la IC ventricular derecha asociada a hipertensión pulmonar crónica en el contexto preclínico. En general, este trabajo contribuye con nuevos hallazgos en investigación preclínica sobre terapias innovadoras para una mejor atención al paciente.

### Summary

Chronic heart failure (HF) is characterized by a high prevalence in the aging western countries, dramatic impact in the patient quality of life and functional performance, and overwhelming economic burden for health systems. In chronic HF, translation of basic research knowledge into innovative patient care is a priority, and relies on the preclinical testing and validation of new diagnostic and therapeutic concepts. Animal models have been developed that recapitulate HF in the laboratory setting. However, as in other chronic diseases, modeling of HF is challenging due to the heterogeneous and complex pathophysiology. Models of HF in large animals are costly and technically complex, but provide a unique opportunity to evaluate novel imaging concepts and therapies using clinically relevant tools, and therefore accelerate the potential translation. While attempts to reproduce the full clinical picture along with severe hemodynamic and structural

abnormalities of chronic HF have been unsuccessful, recapitulation of specific phenotypes may be feasible and clinically relevant. This document summarizes a PhD Thesis compendium focused on the creation and characterization of large animal models of key HF features: 1) chronic pulmonary hypertension and right ventricular remodeling, 2) ischemic and pressure overload left ventricular remodeling. Finally, novel strategies of gene therapy in chronic PH-associated right ventricular heart failure are evaluated in the preclinical setting. Overall, this work contributes with novel findings in a challenging field of preclinical research in the search of innovative therapies for better patient care.

## 2. Abreviaturas.

HTP: hipertensión pulmonar.

IC: insuficiencia cardíaca.

VD: ventrículo derecho.

VI: ventrículo izquierdo.

HF: heart failure.

# 3. Introducción general

## 3.1. La insuficiencia cardiaca crónica como problema cardiovascular de primera magnitud y necesidad de investigación preclínica.

La insuficiencia cardíaca (IC) es un síndrome clínico caracterizado por disnea, intolerancia al esfuerzo, y congestión a nivel sistémico y pulmonar. Estas manifestaciones se deben a la incapacidad del corazón para proporcionar un gasto cardíaco suficiente que permita el normal funcionamiento de los tejidos. La IC es una de las primeras de causas de morbimortalidad en los países desarrollados, con una prevalencia y gasto sanitario en progresivo aumento debido, entre otros factores, al envejecimiento de la población[1].

Pese a los avances que se han producido en el manejo integral de la IC en la última década, se considera un área prioritaria de investigación para mejorar el pronóstico vital y la calidad de vida de estos pacientes. Un aspecto clave de esta investigación es la identificación de nuevos tratamientos que sean más eficaces para prevenir, enlentecer o revertir la progresión de la enfermedad. En este sentido, un limitación importante ha sido la falta de modelos animales clínicamente relevantes en los que poder evaluar la eficacia y seguridad de nuevos tratamientos.

## 3.2. Modelos preclínicos en insuficiencia cardíaca como herramienta en investigación traslacional.

Los modelos animales son un eslabón clave para trasladar los nuevos descubrimientos en investigación básica al ámbito clínico. La validación de tratamientos en distintos modelos animales se considera un requerimiento para la aprobación de los mismos para su ensayo en humanos (Figura 1). Esto pone de manifiesto la importancia de desarrollar modelos clínicamente relevantes[2]. El modelo animal preclínico suele hacer referencia a modelos de animal grande (cerdo, oveja, etc), por su mayor semejanza fisiológica al ser humano, en particular en el sistema cardiovascular[2]. Esto hace que, aunque muchos estudios en investigación cardiovascular se desarrollan inicialmente en modelos de roedor, posteriormente sea necesario una validación en un modelo de mayor complejidad biológica[3-4].

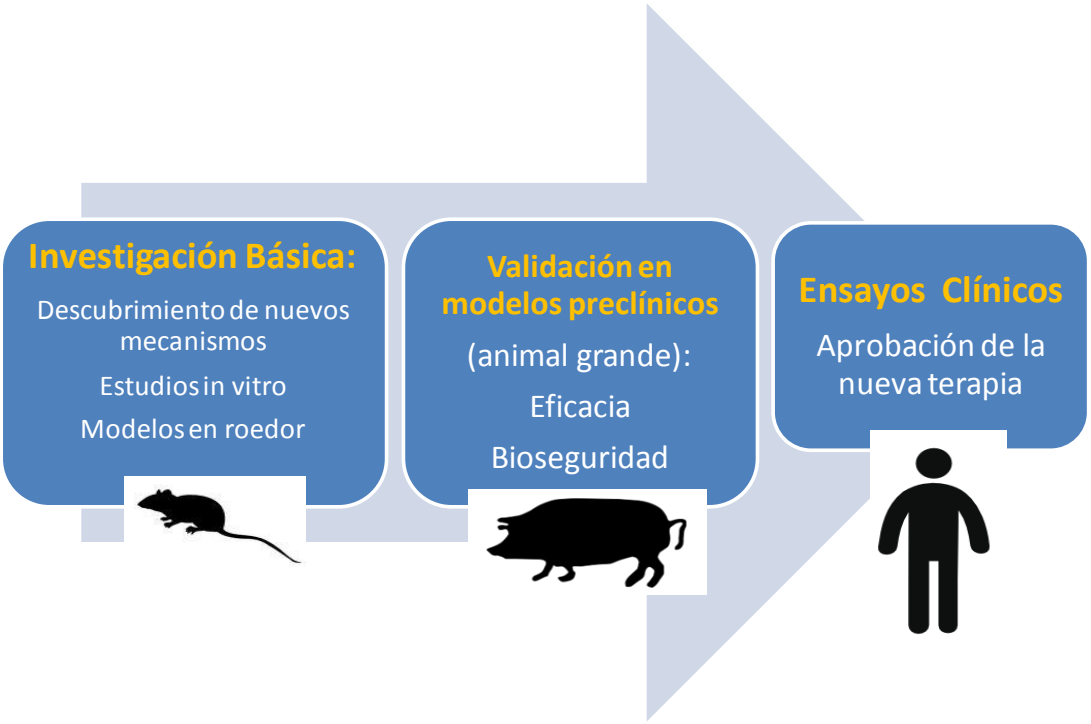


*Figura 1. Descubrimiento, validación y fase clínica en el desarrollo de nuevas terapias, empleando modelos in vitro e in vivo de diferente complejidad.*

Además de la relevancia respecto a las características clínicas que se busca recapitular en el modelo, otro aspecto clave a tener en cuenta en estudios preclínicos de intervención es el potencial traslacional de la misma. Este término hace referencia a la similitud de la metodología de la intervención (modo de administración de un fármaco, regeneración celular o terapia génica, por ejemplo), así como los métodos para evaluar el éxito de la misma. En este aspecto, la caracterización de los modelos preclínicos cardiovasculares en animal grande, que permite el uso de técnicas de imagen y estrategias terapéuticas (administración intracoronaria de tratamientos, implante de dispositivos percutáneos, nuevas técnicas quirúrgicas) similares a las que se utilizan en pacientes con la patología de interés es de vital importancia para garantizar la validez de los resultados.

3.3. Heterogeneidad clínica y fenotipos específicos en IC como principal problema en la creación de modelos.

La IC es un síndrome muy heterogéneo en cuanto a las causas subyacentes (cardiopatía isquémica, hipertensión arterial, enfermedad valvular cardíaca, miocardiopatías, miocarditis, etc), así como en cuanto a la forma de manifestación clínica. En los últimos años la percepción de que esta heterogeneidad clínica es de gran importancia ha dado lugar a la definición de distintos “fenotipos clínicos” en pacientes con IC, haciendo referencia

a las alteraciones estructurales y funcionales predominantes. Desde esta nueva perspectiva, las técnicas diagnósticas deben ser orientadas a describir adecuadamente los distintos perfiles clínicos, y estos a su vez deben guiar el tratamiento[5].

Tradicionalmente, las alteraciones en la estructura y función del ventrículo izquierdo (VI) se han considerado el aspecto clave en el tratamiento de la IC. Esto se debe a que a menudo es la alteración primaria de la cardiopatía, como ocurre tras un infarto agudo de miocardio, o en respuesta a la sobrecarga de presión crónica en la hipertensión arterial. Sin embargo, y gracias a los avances en técnicas de imagen, se ha comprobado que a menudo son alteraciones a otros niveles las que determinan el pronóstico y las respuesta al tratamiento. Los fenotipos clínicos en IC tienen en cuenta no sólo alteraciones estructurales o funcionales específicas (como la presencia o ausencia de disfunción sistólica, fibrilación auricular crónica, insuficiencia mitral funcional, hipertensión pulmonar (HTP) y fallo ventricular derecho [VD]), sino también características clínicas relacionadas con comorbilidades, como la edad avanzada, diabetes mellitus, obesidad, enfermedad renal crónica, anemia y fragilidad[5].

### 3.4. Modelos preclínicos actuales en IC: características y principales limitaciones.

A continuación se resumen brevemente las características y limitaciones de los principales modelos preclínicos que se han desarrollado en investigación sobre IC[2, 6]:

a. *Modelos de cardiopatía isquémica crónica.* Se han empleado modelos basados en infarto agudo de miocardio mediante isquemia coronaria transitoria seguida de reperfusión, oclusión coronaria sin reperfusión, isquemia crónica mediante estenosis progresiva (dispositivos de constricción coronaria progresiva, conocidos como ameroides), y menos frecuentemente microembolizaciones coronarias repetidas. Estos modelos simulan diferentes escenarios clínicos en cardiopatía isquémica aguda como daño inicial, cuya consecuencia a largo plazo es el remodelado ventricular progresivo. Se considera un modelo altamente traslacional porque recapitula aspectos esenciales de la IC de etiología isquémica. Se han empleado ampliamente en estudios de regeneración miocárdica mediante terapia celular. Como modelo de IC, las principales limitaciones son: 1) falta de caracterización de las diferencias entre infartos en diferentes territorios coronarios, 2) incertidumbre respecto a los cambios estructurales y funcionales en el miocardio no infartado (“remoto” al infarto, y en gran parte responsable del remodelado global), 3) fenotipo de HTP y disfunción del VD no reproducible.

b. *Modelos de sobrecarga de presión crónica emulando cardiopatía hipertensiva.* El modelo más empleado ha sido la estenosis o constricción aórtica supravalvular. Este modelo simula determinadas características de la respuesta ventricular ante una estenosis aórtica, y en menor medida una situación de hipertensión arterial crónica. Este modelo induce un aumento de la masa ventricular relacionada con la gravedad de la sobrecarga de presión (es decir, el grado de estenosis inducida) y la duración del seguimiento. Las principales limitaciones son: 1) no recapitular un escenario clínico concreto (las estenosis aórticas son patologías lentamente progresivas de años de evolución, mientras que el tipo de sobrecarga de presión no es equiparable a la cardiopatía hipertensiva), 2) no está caracterizada en modelos preclínicos una transición desde hipertrofia compensadora a una situación de IC por criterios clínicos o hemodinámicos.

c. *Modelos de sobrecarga de volumen para recapitular lesiones valvulares.* El modelo de insuficiencia mitral orgánica mediante rotura quirúrgica de las cuerdas tendinosas ha sido descrito como un modelo relevante de IC aguda o subaguda, asociado a HTP y grados variables de disfunción del ventrículo izquierdo. Este modelo se asocia a una elevada mortalidad lo que ha limitado mucho su utilización en el ámbito preclínico, y es complejo llevar a cabo un seguimiento a largo plazo por la gravedad del mismo.

d. *Modelos de estimulación ventricular rápida emulando "taquimiocardiopatias".* Consisten en una estimulación ventricular rápida durante varias semanas mediante el implante de un marcapasos. Se recapitulan características esenciales de la IC, como la activación neurohormonal, la dilatación de cavidades y los signos congestivos. La principal limitación es la reversibilidad en gran parte, y en ocasiones impredecible, de las alteraciones fenotípicas una vez interrumpida la estimulación, lo cual suele ser necesario para caracterizar los cambios estructurales y funcionales mediante técnicas de imagen.

e. *Otros modelos.* La inducción de toxicidad cardiaca por antraciclinas se ha descrito en algunos modelos, si bien la consistencia del fenotipo en relación a las dosis administradas no está bien caracterizada en la literatura, así como las dosis mínimas y duración del seguimiento necesarios, y el daño inducido por el tóxico en tejidos extracardíacos ha limitado su aplicación en el ámbito preclínico.

**3.5.** Nuevos enfoques en modelos preclínicos de IC: caracterización de fenotipos específicos y su aplicación para desarrollo de nuevas terapias.

El trabajo de la presente Tesis Doctoral se ha centrado en aspectos concretos de los modelos animales de IC que consideramos muy relevantes desde el punto de vista clínico. Según se ha indicado, los siguientes aspectos no se habían caracterizado en descripciones previas y que son fundamentales para llevar a cabo un estudio traslacional en IC. En relación a cada uno de estos aspectos, se indican los trabajos publicados como parte de la presente Tesis Doctoral.

3.5.1. *Modelos preclínicos de hipertensión pulmonar crónica.*

Los pacientes con IC desarrollan con frecuencia HTP en su evolución, lo cual determina un elemento adicional de sobrecarga hemodinámica, en este caso en el VD. Multitud de estudios han demostrado que la aparición de HTP y sobretodo disfunción del VD determina una mayor morbimortalidad en estos pacientes. En los últimos años ha surgido un gran interés por las implicaciones de la HTP en la IC. Así pues, la presencia de HTP junto al remodelado y la disfunción del VD constituyen un fenotipo específico por sus principales características: 1) se asocian a un mal pronóstico independientemente de las lesiones estructurales asociadas (disfunción del VI sistólica o diastólica, valvulopatías mitral o aórtica, miocardiopatías de cualquier etiología), 2) el diagnóstico y caracterización son más compleja, por las dificultades de las técnicas no invasivas para estimar el estado de la hemodinámica pulmonar y la complejidad anatómica del VD, y 3) la falta de tratamientos efectivos dirigidos a tratar este aspecto de la enfermedad en pacientes con IC. A esto se añade una heterogeneidad fisiopatológica en las causas de HTP en la IC: 1) congestión venosa pulmonar (HTP pasiva), 2) vasoconstricción (HTP precapilar reactiva), 3) remodelado vascular distal y reducción del lecho vascular (HTP precapilar fija), 4) HTP de mecanismo mixto. En todos los casos, el aumento de la poscarga del VD da lugar a un fenómeno de remodelado que deteriora la función cardíaca más allá de la cardiopatía subyacente a todo el proceso.

Como parte de esta Tesis Doctoral, hemos contribuido en este campo con dos artículos originales de los que como doctorando soy el primer autor:

*Artículo 1: "Characterization of right ventricular remodeling and failure in a chronic pulmonary hypertension model"* [7]*.* En este trabajo hemos demostrado que un modelo de HTP pasiva (constricción venosa pulmonar) es capaz de inducir un fenotipo de HTP mixto (es decir, pre y postcapilar) que progresa tanto en la gravedad de los parámetros hemodinámicos como en el remodelado del VD. Este trabajo contribuyó de forma original con los siguientes hallazgos: 1) demostramos que el remodelado adaptativo evoluciona a una fase de fallo del VD y aparición de síntomas cuando se produce un desacoplamiento de

la unidad ventrículo-arterial. Este fenómeno sólo fue posible demostrarlo mediante el patrón oro para definir el desacoplamiento basado en análisis de curvas de presión-volumen en el VD. A nivel de histología y molecular, observamos un aumento progresivo de fibrosis intersticial y alteración de la homeostasis del calcio en el tejido miocárdico; 2) demostramos a través de histología de la vasculatura pulmonar el efecto del incremento crónico de las presiones venosas pulmonares, siendo este remodelado vascular en vasos pulmonares distales un factor responsable de aumento de resistencias vasculares, y relacionado con el fallo ventricular derecho; 3) en este modelo de HTP crónica se demostró una activación de la vía de la aldosterona, apoyando estudios clínicos que sugieren un potencial beneficio del bloqueo de este mecanismo en pacientes con HTP.

*Artículo 2: "Combination Proximal Pulmonary Artery Coiling and Distal Embolization Induces Chronic Pulmonary Hypertension in Swine"* [8]*.* En este estudio evaluamos el efecto de la oclusion progresiva del lecho vascular pulmonar, para determinar el efecto aislado del componente precapilar de la HTP en la hemodinámica pulmonar y su impacto en el VD. Si bien este modelo ha sido evaluado previamente, la persistencia del efecto a largo plazo de embolizaciones repetidas y la repercusión en el VD no han sido abordados en estudios previos. Las principales contribuciones de este estudio son: 1) se requiere un elevado número de embolizaciones para inducir HTP a largo plazo, lo que sugiere que, en respuesta a daño precapilar o reducción del lecho vascular pulmonar, el incremento de presiones pulmonares es un marcador de una fase avanzada de la enfermedad; 2) el remodelado ventricular derecho en este contexto es tardío y por tanto poco sensible en fases iniciales del proceso; 3) en presencia de una obstrucción proximal en el árbol pulmonar (como suele ocurrir en pacientes con tromboembolismo pulmonar), se produce una mayor sobrecarga del VD y un mayor remodelado; 4) con todo ello, se trata de un modelo adecuado para estudiar fases iniciales de HTP precapilar, pero el fenotipo observado no permite llevar a cabo estudios sobre fallo del VD.

3.5.2. *Modelos de remodelado ventricular izquierdo post-infarto agudo de miocardio, y secundarios a sobrecarga de presión crónica.* Este apartado se compone de tres trabajos (dos artículos ya publicados, y un manuscrito pendiente de publicación).

*Artículo 3."Characterizing Preclinical Model of Ischemic Heart Failure: Difference Between LAD and LCx Infarctions"* [9]*.* En este estudio comparamos los dos modelos más utilizados en cardiopatía isquémica. Los principales hallazgos y contribuciones al campo son: 1) la idoneidad del modelo de oclusión de la arteria descendente anterior proximal como modelo de IC, debido a su mayor remodelado ventricular, y su mayor repercusión en

la función longitudinal, y 2) la moderada disfunción del miocardio remoto detectada mediante ecocardiografía avanzada (técnica de *strain* miocárdico) como potencial diana terapéutica en estudios preclínicos.

*Manuscrito 1. Left atrial remodeling after acute myocardial infarction: insight into the role of atrial infarction.* El remodelado ventricular extenso, en particular en determinadas localizaciones, se ha asociado a la aparición de insuficiencia mitral funcional. Se trata de una alteración morfológica de la válvula mitral secundaria al remodelado ventricular, y que es a su vez un marcador de mal pronóstico, y que aumenta el riesgo de HTP por sobrecarga de volumen en la aurícula izquierda. En este estudio, que profundiza en la caracterización de los principales modelos de IC de etiología isquémica del artículo 3, hemos demostrado que tras un infarto agudo de miocardio, la insuficiencia mitral funcional y la isquemia auricular contribuyen de forma decisiva a la progresión de la IC post-infarto. En comparación con otros modelos de cardiopatía isquémica crónica (como los evaluados en el artículo 3), se trata de un modelo con características únicas y potencialmente muy relevantes para estudios relacionados con: 1) estudios diagnósticos y terapéuticos asociados a remodelado auricular izquierdo y fibrosis, 2) diagnóstico y tratamiento quirúrgico o percutáneo de la insuficiencia mitral isquémica.

*Artículo 4. "Increased Stiffness is the Major Early Abnormality in a Pig Model of Severe Aortic Stenosis and Predisposes to Congestive Heart Failure in the Absence of Systolic Dysfunction"* [10]*.* En este trabajo evaluamos un modelo de sobrecarga de presión del VI a largo plazo mediante constricción aórtica supravalvular. Como principales hallazgos, observamos que en este modelo la principal alteración fisiopatológica se encuentra en el aumento de elastancia ventricular diastólica, mientras que la relajación rápida al inicio de la diástole, y la función sistólica permanecen normales. La principal contribución de este trabajo es demostrar las limitaciones como modelo de IC avanzada, y el potencial como herramienta para estudio de alteraciones funcionales precoces en la hipertrofia cardiaca en el ámbito preclínico.

3.5.3. Aplicación de modelos preclínicos en hipertensión pulmonar crónica: Desarrollo de nuevas terapias experimentales. Este apartado se compone de dos publicaciones (un artículo original, y un artículo metodológico basado en el anterior):

*Artículo 5. "Intratracheal Gene Delivery of SERCA2a Ameliorates Chronic Post-Capillary Pulmonary Hypertension in a Large Animal Preclinical Model"* [11]*.* En este estudio desarrollamos una metodología para administración de terapia génica en modelo de animal grande por vía aérea mediante un dispositivo específico. Los vectores virales basados en

virus adeno-asociados tenían como objetivo la sobreexpresión vascular de la ATPasa 2a del retículo sarcoplásmico (SERCA2a) en células musculares lisas. Esta terapia se había validado previamente en un modelo de roedor (HTP por monocrotalina en ratas)[12], y en humanos en el ensayo clínico CUPID (*Calcium Up-regulation by Percutaneous administration of Gene Therapy in Cardiac Disease Phase 2b*[13]) desarrollado en la última década. Para probar el beneficio de esta terapia empleamos el modelo animal caracterizado en el artículo 1 por reunir los aspectos idóneos de la enfermedad potencialmente tratable mediante sobreexpresión vascular de SERCA2a (remodelado de la capa media muscular, deterioro progresivo de la hemodinámica pulmonar y disfunción ventricular derecha). Los resultados han demostrado el potencial de esta estrategia terapéutica y ha sido el primer trabajo sobre esta metodología en un modelo preclínico. Por otra parte, se trata de una contribución relevante al demostrar las limitaciones y necesidad de mejoras en la tecnología de vectores y administración de los mismos para aumentar las posibilidades de éxito en pacientes.

*Artículo 6. "Inhaled Gene Transfer for Pulmonary Circulation"* [14]*.* Se trata deuna revisión detallada sobre la metodología empleada en la creación de modelos, caracterización de los mismo, y administración de terapia génica, basada en los artículos 1 y 5.

## 4. Objetivos.

**Objetivo 1.** Desarrollo de nuevos modelos experimentales que permitan una caracterización integral de fenotipos específicos de enfermedades cardiovascular crónica: 1) hipertensión pulmonar crónica y disfunción ventricular derecha, 2) disfunción y remodelado ventricular izquierdo (cardiopatía isquémica y por sobrecarga de presión) e insuficiencia mitral funcional.

**Objetivo 2.** Caracterización de modelos preclínicos mediante técnicas de imagen y a nivel de las principales alteraciones histológicas y moleculares, que permita evaluar su valor traslacional.

**Objetivo 3.** Desarrollo de nuevas opciones de intervención sobre dichos modelos con especial atención a nuevas dianas y vectores en terapia génica.

## 5. Materiales, Métodos y Resultados.

Los aspectos metodológicos de esta Tesis Doctoral pueden resumirse según los tres grandes Objetivos:

1. Capacitación para diseño y ejecución de procedimientos experimentales en modelos de animal grande. Se han desarrollado modelos animales que han requerido entrenamiento en técnicas quirúrgicas, de cateterización percutánea y procedimientos de intervencionismo intracoronarios, así como instrumentación invasiva para estudio de la circulación pulmonar, y de las relaciones de presión-volumen en ambos ventrículos. El doctorando ha adquirido amplia experiencia en experimentación preclínica tras pasar 5 años con dedicación exclusiva a esta metodología en distintos laboratorios (Cardiovascular Research Center, Icahn School of Medicine, Nueva York, y CNIC, Madrid). Esta capacitación ha permitido la creación y caracterización de los modelos animales descritos en el siguiente apartado.

2. Caracterización de los modelos experimentales mediante técnicas de imagen, histología y biología molecular. Se han desarrollado protocolos de adquisición y análisis en el ámbito preclínico basados en ecocardiografía avanzada y resonancia magnética nuclear. Además se ha llevado a cabo una caracterización histológica y molecular del remodelado miocárdico y vascular pulmonar en los modelos descritos, contribuyendo a incrementar el conocimiento sobre dichos escenarios preclínicos, así como para establecer una correlación clínico-patológica entre los cambios estructurales y la información estructural y funcional procedente de las técnicas de imagen.

3. Descripción de tipos de vectores y métodos de transferencia génica en modelos de insuficiencia cardiaca. Desarrollo de métodos traslacionales de transferencia génica sobre el modelo preclínico. Tras una estancia de 2 años en un grupo de investigación centrado en la terapia génica cardiovascular, el doctorando ha llevado a cabo protocolos para administrar terapia génica en modelos de animal grande. Esta metodología incluye el manejo in vivo de vectores virales basados en virus adeno-asociados recombinantes así como la puesta a punto de métodos para evaluar los mecanismos inmunes ante estos vectores, tanto existentes previamente al tratamiento, como inducidos por el mismo. Además se han desarrollado protocolos para detección de expresión génica en muestras de tejido miocárdico. Finalmente, los experimentos basados en una intervención basada en terapia génica han sido evaluados en modelos animales descritos en trabajos anteriores del

mismo doctorando y grupo de investigación, empleando técnicas de diagnóstico descritas en los puntos anteriores.

En base a la temática de las publicaciones, estas se han agrupado en tres partes:

Parte 1. Modelos de hipertensión pulmonar crónica (artículos 1 y 2).

Parte 2. Modelos de disfunción ventricular izquierda.

Parte 3. Desarrollo de nuevas terapias experimentales en hipertensión pulmonar.

**Parte 1. Modelos de hipertensión pulmonar crónica.**

**<u>Introducción a los artículos 1 y 2.</u>**

Como parte de esta Tesis Doctoral, hemos contribuido en este campo con dos artículos originales de los que como doctorando soy el primer autor. En ambos trabajos fui responsable de llevar a cabo gran parte de los procedimientos experimentales, incluida la creación de los modelos animales mediante técnica quirúrgica o percutánea, de la adquisición de parámetros estructurales y funcionales mediante técnicas invasivas y de imagen (cateterismos cardiacos, ecocardiografía), análisis de los datos brutos (curvas de presión volumen, hemodinámica pulmonar, postprocesado de imagen avanzada tridimensional y análisis de la mecánica cardiaca mediante *strain* miocárdico), análisis estadístico de los datos, y redacción de los manuscritos. En ambos trabajos se planteó una metodología de trabajo similar, con la diferencia de los tiempos de seguimiento que se adaptaron a las características de la cada modelo. La Figura 2 resume los principales hallazgos y compara ambos modelos en las dos vertientes más importantes: el remodelado vascular pulmonar, y el remodelado del VD.

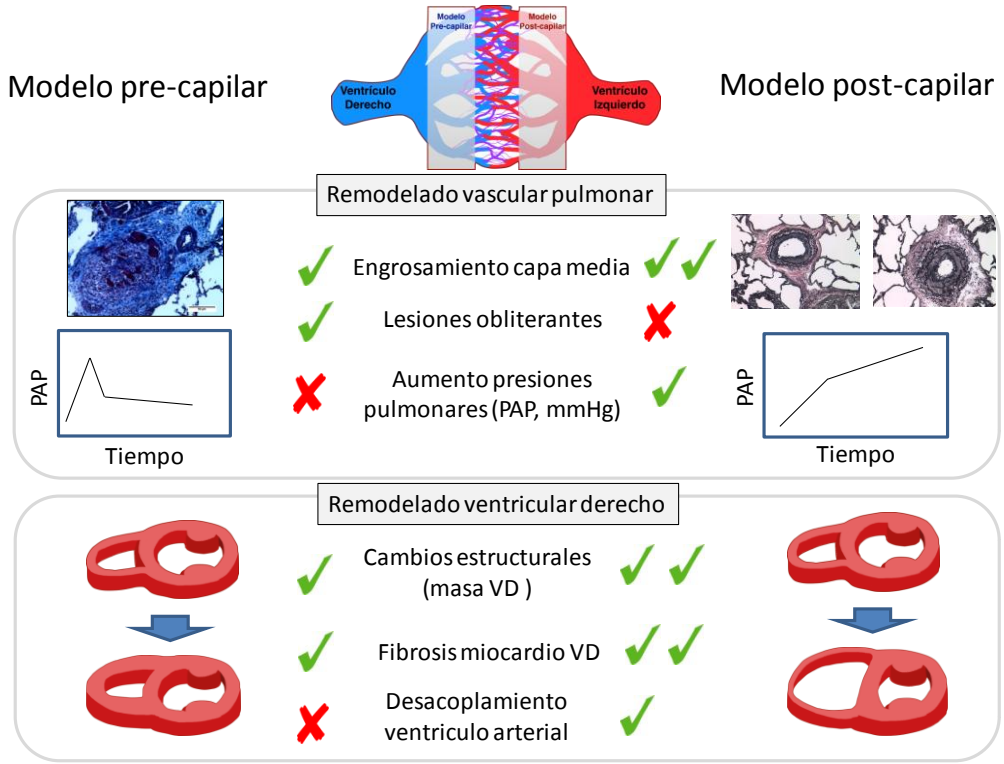


*Figura 2 (Resumen Parte 1, Modelos de hipertensión pulmonar). Según el modelo, los efectos a nivel de remodelado vascular pulmonar y del VD difieren. Esto permite seleccionar la opción más adecuada en función del los objetivos del estudio preclínico.*

Referencias de los artículos.

Artículo 1 [7].

*Aguero J, Ishikawa K, Hadri L, Santos-Gallego CG, Fish K, Hammoudi N, Chaanine AH, Torquato S, Naim C, Ibanez B, Pereda D, Garcia-Alvarez A, Fuster V, Sengupta PP, Leopold JA, Hajjar RJ. Characterization of right ventricular remodeling and failure in a chronic pulmonary hypertension model. Am J Physiol Heart Circ Physiol. 2014 Oct 15;307(8):H1204-15.*

Artículo 2 [8].

*Aguero J, Ishikawa K, Fish KM, Hammoudi N, Hadri L, Garcia-Alvarez A, Ibanez B, Fuster V, Hajjar RJ, Leopold JA. Combination Proximal Pulmonary Artery Coiling and Distal Embolization Induces Chronic Pulmonary Hypertension in Swine. PLoS One. 2015 Apr 29;10(4):e0124526. doi: 10.1371/journal.pone.0124526.*

Artículo 1 [7].

*Aguero J, Ishikawa K, Hadri L, Santos-Gallego CG, Fish K, Hammoudi N, Chaanine AH, Torquato S, Naim C, Ibanez B, Pereda D, Garcia-Alvarez A, Fuster V, Sengupta PP, Leopold JA, Hajjar RJ. Characterization of right ventricular remodeling and failure in a chronic pulmonary hypertension model. Am J Physiol Heart Circ Physiol. 2014 Oct 15;307(8):H1204-15.*

*Am J Physiol Heart Circ Physiol* 307: H1204–H1215, 2014.
First published August 22, 2014; doi:10.1152/ajpheart.00246.2014.

# Characterization of right ventricular remodeling and failure in a chronic pulmonary hypertension model

**Jaume Aguero,[1,2] Kiyotake Ishikawa,[1] Lahouaria Hadri,[1] Carlos Santos-Gallego,[3] Kenneth Fish,[1] Nadjib Hammoudi,[1] Antoine Chaanine,[1] Samantha Torquato,[4] Charbel Naim,[1] Borja Ibanez,[2] Daniel Pereda,[2] Ana García-Alvarez,[2] Valentin Fuster,[2,3] Partho P. Sengupta,[3] Jane A. Leopold,[4]* and Roger J. Hajjar[1]***

[1]*Cardiovascular Research Center, Icahn School of Medicine at Mount Sinai, New York, New York;* [2]*Centro Nacional de Investigaciones Cardiovasculares Carlos III-Epidemiology, Atherothrombosis and Imaging Department, Madrid, Spain;* [3]*Zena and Michael A. Wiener Cardiovascular Institute, Icahn School of Medicine at Mount Sinai, New York, New York; and* [4]*Cardiovascular Medicine, Brigham and Women's Hospital, Harvard Medical School, Boston, Massachusetts*

Submitted 11 April 2014; accepted in final form 13 August 2014

**Aguero J, Ishikawa K, Hadri L, Santos-Gallego C, Fish K, Hammoudi N, Chaanine A, Torquato S, Naim C, Ibanez B, Pereda D, García-Alvarez A, Fuster V, Sengupta PP, Leopold JA, Hajjar RJ.** Characterization of right ventricular remodeling and failure in a chronic pulmonary hypertension model. *Am J Physiol Heart Circ Physiol* 307: H1204–H1215, 2014. First published August 22, 2014; doi:10.1152/ajpheart.00246.2014.—In pulmonary hypertension (PH), right ventricular (RV) dysfunction and failure is the main determinant of a poor prognosis. We aimed to characterize RV structural and functional differences during adaptive RV remodeling and progression to RV failure in a large animal model of chronic PH. Postcapillary PH was created surgically in swine ($n = 21$). After an 8- to 14-wk follow-up, two groups were identified based on the development of overt heart failure (HF): PH-NF (nonfailing, $n = 12$) and PH-HF ($n = 8$). In both groups, invasive hemodynamics, pressure-volume relationships, and echocardiography confirmed a significant increase in pulmonary pressures and vascular resistance consistent with PH. Histological analysis also demonstrated distal pulmonary arterial (PA) remodeling in both groups. Diastolic dysfunction, defined by a steeper RV end-diastolic pressure-volume relationship and longitudinal strain, was found in the absence of HF as an early marker of RV remodeling. RV contractility was increased in both groups, and RV-PA coupling was preserved in PH-NF animals but impaired in the PH-HF group. RV hypertrophy was present in PH-HF, although there was evidence of increased RV fibrosis in both PH groups. In the PH-HF group, RV sarcoplasmic reticulum $Ca^{2+}$-ATPase2a expression was decreased, and endoplasmic reticulum stress was increased. Aldosterone levels were also elevated in PH-HF. Thus, in the swine pulmonary vein banding model of chronic postcapillary PH, RV remodeling occurs at the structural, histological, and molecular level. Diastolic dysfunction and fibrosis are present in adaptive RV remodeling, whereas the onset of RV failure is associated with RV-PA uncoupling, defective calcium handling, and hyperaldosteronism.

right ventricular remodeling; pulmonary hypertension model; pressure-volume relationships; echocardiography; SERCA2a; aldosterone

PULMONARY HYPERTENSION (PH) is a complex clinical condition that may be associated with cardiac, pulmonary, or other systemic diseases. At present, PH is categorized into five distinct groups on the basis of pathological, pathophysiological, and therapeutic commonalities shared by patients with different forms of the disease (14). Right ventricular (RV) failure is a common consequence of chronic PH of any etiology and is currently considered the strongest indicator of prognosis in these patients (44). RV failure occurs when contractility of the hypertrophied RV is insufficient to compensate for the increase in pulmonary vascular resistance, or RV afterload, and RV-pulmonary artery (PA) uncoupling occurs. Although distal pulmonary vascular disease severity is a major determinant of RV hypertrophy and subsequent failure in Group 1 PH (pulmonary arterial hypertension), less is known about the mechanisms leading to maladaptive RV remodeling in Group 2 patients (left heart disease). In heart failure (HF) patients, concomitant PH is a frequent diagnosis, but the relevance of distal pulmonary vascular remodeling and the passive increase in venous pulmonary pressure for RV function and RV-PA coupling has not been well characterized (43).

In PH, understanding the RV remodeling process and RV-PA uncoupling remains challenging as the anatomical and pathophysiological responses to chronically increased afterload differ significantly from that of the left ventricle (LV) (44). RV-PA uncoupling in chronic PH has been quantified directly in experimental models (19, 20, 34) and estimated in clinical studies (26, 38). Although RV-PA uncoupling is now recognized as a critical event leading to RV failure, the temporal relationship between RV-PA uncoupling and the onset of RV failure remains less clear (45). Some studies have suggested that uncoupling is a late complication of severe long-standing PH (34), which is preceded by RV adaptive remodeling (35), whereas others have suggested that RV-PA uncoupling is an early phenomenon in chronic PH (19, 20). Exposure of the RV to chronic pressure overload also promotes cellular and molecular remodeling, which may underlie the early changes in RV cardiomyocyte function that occur prior to RV failure (3, 45). Pathologic cardiomyocyte growth, abnormal calcium handling (21, 31), and increased apoptosis (3, 10) as well as RV ischemia and neurohormonal activation (5) have all been identified as mechanisms that promote RV remodeling and transition to failure.

Given the importance of RV function for prognosis in PH, few studies have provided a comprehensive RV hemodynamic, cellular, and molecular profile that differentiates compensatory RV hypertrophy from RV failure associated with RV-PA uncoupling (9). This knowledge deficit has resulted, in part, from both the aforementioned complexity in RV functional characterization as well as the lack of availability of relevant

* J. A. Leopold and R. J. Hajjar contributed equally to this study.
Address for reprint requests and other correspondence: J. Aguero, Cardiovascular Research Center, Icahn School of Medicine at Mount Sinai, One Gustave L. Levy Place, Box 1030, New York, NY 10029-6574 (e-mail: jaimeaguero30@hotmail.com).

large animal models that recapitulate different stages of RV remodeling. Experimental models of PH in large animals offer a unique opportunity to analyze RV structure and function with clinical relevance for human disease; however, large animal models of PH have been difficult to create and have not mimicked completely the pulmonary vascular and RV pathophysiology observed in human PH. We hypothesized that there are physiological, cellular, and phenotypic differences in the RV that differentiate between adaptive and maladaptive remodeling in a large animal model of pulmonary hypertension. To examine this hypothesis, we chose to study the porcine pulmonary vein banding model of postcapillary PH as a representative large animal model of PH that would allow us to identify unique hemodynamic parameters using invasive pressure-volume loops and noninvasive echocardiographic imaging, in association with key molecular abnormalities in the myocardium, that differentiate adaptive from maladaptive RV remodeling.

## METHODS

The study was performed in accordance with the *Guidelines for the Care and Use of Laboratory Animals* and was approved by the Icahn School of Medicine at Mount Sinai Institutional Animal Care and Use Committee.

## EXPERIMENTAL PROCEDURES

*Experimental design.* Twenty-five Yorkshire pigs were included in this study. The postcapillary PH model was created by surgical banding of the inferior pulmonary venous drainage (PH Group, $n = 21$). The pigs were housed in the animal facility for up to 16 wk and developed PH gradually during this period. A sham-operated group ($n = 4$) undergoing a left lateral thoracotomy without pulmonary vein banding was included as a control. The pigs were considered to have signs of RV HF when they showed progressively increased respiratory rate at rest, loss of appetite and water intake, and weight loss or slower weight gain as compared with controls. Accordingly, at the onset of RV HF, the PH group was divided into two groups based on the RV response to pulmonary venous banding: adaptive (PH-NF, pulmonary hypertension with nonfailing RV) and maladaptive (PH-HF, pulmonary hypertension with RV HF). At the end of the study, animals were euthanized with pentobarbital sodium and the heart and lungs were removed for analysis.

*Surgical and periprocedural anesthesia.* Animals were premedicated using 6.0 mg/kg Telazol (tiletamine/zolazepam), intubated, and ventilated using the following parameters: 40% oxygen, 10 ml/kg tidal volume at 15 respirations per minute to maintain an end-tidal $CO_2$ between 35 and 45 mmHg. General anesthesia was maintained with 5–8 $mg \cdot kg^{-1} \cdot h^{-1}$ propofol except during the surgical procedures that required a thoracotomy that were performed under isoflurane (1.5–3%) anesthesia. Before a thoracotomy procedure, animals were given 25 mg/kg im cefazolin and 2 mg/kg iv gentamicin; 25 mg/kg im cefazolin twice daily was given for 10 days after the thoracotomy. Animals postoperatively received a 25–50 mcg/h fentanyl patch.

*Postcapillary PH model.* The procedure was adapted from the a previous description by Silove et al. (39) and Pereda et al. (33) and performed in 9–13 kg pigs with minor modifications. Briefly, through a left lateral thoracotomy at the fifth intercostal space, the superior left pulmonary vein and the common inferior pulmonary vein (drains both right and left diaphragmatic veins) were dissected in the extrapericardial space close to the left atrium. To provide consistency in the degree of venous stenosis created between animals, each vein was constricted initially with a 3.5-mm diameter plastic cylinder; after the fabric tape is placed around the vein and secured with a 2-0 silk suture, the cylinder is removed. The optimal degree of constriction was determined from the experience of three pilot experiments that varied the degree of the constriction. In this case, a band with restriction $<3.5$ mm created no hemodynamic effects at follow-up, whereas a more severe restriction ($>3.5$ mm) led to refractory pulmonary edema in the first 24 h. All animals received a single dose of furosemide (4 mg/kg) immediately after the surgery.

*Pulmonary hemodynamic evaluation.* At the final follow-up, a 7.5-Fr Swan-Ganz (Edwards Lifesciences) catheter was advanced through a femoral vein to the right heart. Right atrial (RA) pressure and systolic, diastolic, and mean pressures were recorded in the pulmonary artery (PA) and PA wedge position (PAWP) positions. PAWP is reported as the average of measurements obtained from both right and left lung. Cardiac output (CO) was measured using the thermodilution method. Pulmonary vascular resistance (PVR) was calculated as (mean PA − PAWP)/CO and PA capacitance as SV/PP, where SV is stroke volume and PP is pulse pressure. CO, SV, PVR, and PA capacitance were indexed to the body surface area as reported previously (24). All parameters were recorded during brief periods of end-expiratory breath-hold in anesthetized ventilated animals.

*Pressure-volume relationships.* RV pressure-volume loops were obtained with a 7-Fr conductance micromanometer catheter (Millar Instruments, Houston, TX) connected to a MPVS Ultra Control Interface (Millar Instruments, Houston, TX). The position of the conductance catheter inside the RV chamber was coordinated using a customized 7-Fr XB3.5 guide catheter (Cordis, Johnson & Johnson) that was advanced into the center of the RV cavity via femoral vein access. A small dose of iodinated contrast agent was injected through the catheter to delineate the RV shape. Under fluoroscopic guidance, the tip of the catheter was placed in the RV apex and, typically, 5–7 electrodes, depending on the chamber size, were included to compute the total RV volume. Simultaneous pressure-volume data were acquired under steady-state conditions and during transient inferior vena cava occlusion using a Fogarty Occlusion catheter (Edwards Lifesciences). All measurements were performed during brief periods of breath-hold in anesthetized and ventilated animals.

Pressure-volume data were analyzed using Iox2 Software (EMKA Technologies). For calibration, the $\alpha$ gain factor was calculated using the simultaneously determined SV (obtained from thermodilution cardiac output) as a reference method and volumes were corrected using the values obtained by three-dimensional (3D) echocardiography. The following parameters were subsequently obtained from steady-state or occlusion series loops: peak RV pressure rate of rise ($+dP/dt$) maximum and decline ($-dP/dt$) minimum, $\tau$ value (time constant of isovolumic relaxation), RV stroke work (SW) index, preload recruitable stroke work [as the slope of SW and end-diastolic volume (6)], RV end-systolic elastance slope [end-systolic pressure-volume relationship (ESPVR)] and volume intercept (Vo), pulmonary artery elastance (Ea), and the ratio ESPVR/Ea as an estimate of RV-PA coupling, as described previously (6). The RV diastolic properties were quantified further by the end-diastolic pressure-volume relationship (EDPVR) defined as its linear slope. The assumption of linearity for both ESPVR and EDPVR was confirmed by a Pearson correlation coefficient $>0.9$ within the physiological range of pressures and volumes within the occlusion series for all studies.

### *Echocardiography*

Echocardiographic data were collected at baseline and final follow-up in all animals by using a Philips iE33 ultrasound system (Philips Medical Systems, Andover, MA). According to current recommendations of the American Society of Echocardiography for RV assessment (35), cardiac performance was analyzed by measuring the following parameters: *1*) anatomical M-mode tricuspid annulus plane systolic excursion (TAPSE), *2*) tissue Doppler-derived tricuspid annular systolic velocity, *3*) myocardial performance index (MPI), *4*) RV volumes and ejection fraction (RVEF) obtained from 3D datasets that were analyzed offline with QLAB software (Philips Medical

Systems, Andover, MA) and a disk summation method validated previously using magnetic resonance imaging (MRI) as a reference method (32), and *5*) RV free wall mechanics. Modified four-chamber views were used to measure the RV free wall peak longitudinal strain and strain rate. Two-dimensional (2D) speckle tracking-derived strain and strain rate were measured offline in three consecutive beats using Cardiac Performance Analysis (TomTec, Munich, Germany). The 2D clip acquisition protocol focused on the endocardial border definition while ensuring frame rates between 50 and 70 frames/s for an appropriate performance of the tracking algorithm (15).

LV volumes and ejection fraction were also assessed using 3D datasets, and LV diastolic function was quantified by the E/A ratio of the mitral inflow. All measurements were averaged from three consecutive beats obtained during brief periods of breath-hold.

The severity of pulmonary vein banding was estimated by the mean gradient of the common inferior pulmonary vein flow using the velocity-time integral from the pulsed wave echo-Doppler signal.

### *Heart and Lung Morphology*

After the animals were euthanized, the RV and LV were sectioned and weighed, and RV hypertrophy was assessed by the ratio RV/(LV + septum). Heart and lung tissue samples were placed in 10% formaldehyde solution and subsequently fixed, processed, embedded in paraffin, and sectioned into 5-μm-thick sections for analysis. From randomly selected segments of upper and lower lobes from both lungs, the relative medial thickness (MT) was measured as: MT = (WT × 2) × 100/ED, where WT is wall thickness and ED is external diameter). MT for each PH group was compared with the sham at different sizes of ED (in μm): <50, 50–100, 100–150, and >150. In the upper and lower lobes of both lungs, we measured MT in 30–40 randomly identified arteries/pig with an external diameter <300 μm. PA vessel characterization and morphometric quantification were performed after staining with Elastica Van Gieson. Cardiomyocyte cross-sectional area was measured in cardiac sections stained with wheat germ agglutinin (conjugated to Oregon Green 488, 10 μg/ml; Invitrogen) and costained with phalloidin (conjugated to Alexa fluor 546, 165 nM; Invitrogen). Images of RV cardiomyocyte cell membranes were captured digitally and analyzed by image analysis using ImageJ software (National Institutes of Health). RV myocardial fibrosis was assessed with Masson's Trichrome staining, quantified, and reported as percent area.

### *Myocardial Tissue and Serum Sample Analysis*

Protein lysates were obtained from RV tissue that was homogenized in radioimmunoprecipitation assay buffer containing protease and phosphatase inhibitors (Pierce, Rockford, IL). Twenty micrograms of total protein extracts were mixed with Laemmli sample buffer containing 5% β-mercaptoethanol (Bio-Rad, Hercules, CA). Samples were heated at 95°C for 5 min, with the exception of those used for phospholamban (PLN) analysis, which were incubated at 37°C for 30 min. Samples then were loaded onto 4–20% SDS-PAGE gels. After electrophoresis proteins were transferred onto polyvinylidene difluoride membrane (Millipore, Billerica, MA). Membranes were blocked with 5% fat-free milk in Tris-buffered saline (TBS) for 1 h at room temperature and incubated with the primary antibodies diluted in blocking buffer overnight at 4°C. The following primary antibodies were used: GAPDH (Sigma, St. Louis, MO; 1:10,000 dilution), sarco(endo)plasmic reticulum $Ca^{2+}$-ATPase 2a (SERCA2a; 21st Century Biochemicals, Marlboro, MA; 1:3,000 dilution), PLN (Badrilla Leeds innovation center, Leeds, United Kingdom; 1:5,000 dilution), and CCAAT/enhancer binding protein homology protein (CHOP; Cell Signaling, Danvers, MA; 1:1,000 dilution). The second day, after three washing steps with TBS-0.05% Tween-20, the membrane was incubated with secondary horseradish peroxidase conjugated antibody (Thermo Scientific, Barrington, IL; 1:10,000 dilution) for 45 min. The blot was washed three times with TBS-0.05% Tween-20, and then a SuperSignal West Pico chemiluminescent substrate (Thermo Scientific, Barrington, IL) was used for the detection of protein bands. Band density was quantified using Photoshop. Values were normalized to GAPDH to correct for variation in protein loading.

Aldosterone levels were measured using the Aldosterone EIA kit-Monoclonal (Cayman Chemical) as reported previously (30) Briefly, serum samples were subjected to methylene chloride extraction to remove corticosteroids that may interfere with the assay. After extraction, samples were dissolved in 0.5 ml of assay buffer and aldosterone levels were determined according to the manufacturer's instructions and read on a Spectramax 190 plate reader (Molecular Devices).

### *Statistical Analysis*

Continuous variables are expressed as median [percentiles 25th-75th] unless indicated otherwise. The distribution of each continuous variable was graphically assessed using histograms, and normality was analyzed using Q-Q plots. Continuous variables were compared at the final follow-up time point using the independent samples *t*-test, Mann-Whitney test, one-way ANOVA, or the nonparametric Kruskal-Wallis test as appropriate. Post hoc analysis (Hochberg method) was used to correct for multiple pairwise comparisons. The association between two continuous variables was analyzed using the Pearson correlation coefficient. The differences in pulmonary arteriole MT between groups were analyzed using a mixed model regression for arterial media thickness to account for repeated measurements on the same animals at different vessel diameters. All statistical analyses were performed using R software version 2.15.3 (http://cran.r-project.org/) and OriginPro 9.1 package (Northampton, MA).

## RESULTS

### *Survival and Heart Failure Occurrence in the Chronic Postcapillary PH Model*

Of the 21 animals that underwent pulmonary venous banding to create postcapillary PH, only one animal died postoperatively due to acute pulmonary edema. Of the remaining group of 20 postcapillary PH pigs, 8 animals developed overt signs of HF characterized by increased respiratory rate, decreased food intake, and impaired weight gain as determined by daily examination by the veterinary team. Based on this assessment, the final follow-up examination for these animals was expedited (median follow-up: 8[7–9] wk). The final follow-up of the remaining 12 pigs was performed at wk 14[13–16]. Because 40% of the animals in the PH group exhibited early signs of RV failure, we sought to compare RV functional, cellular, and molecular parameters to differentiate a compensatory from a failing RV phenotype in our model of chronic postcapillary PH. Accordingly, we divided animals into two groups: PH-NF ($n = 8$) and PH-HF ($n = 12$).

### *Cardiopulmonary Hemodynamics and PA Remodeling*

The hemodynamic measurements obtained from the sham-operated controls, PH-NF, and PH-HF groups are summarized in Table 1. Although both PH groups developed elevated pulmonary pressures and hemodynamic profiles consistent with PH, the mean pulmonary arterial pressure (42[39–47] vs. 28[25–33] mmHg; $P = 0.03$) and PVR index (8.8[6.8–12.3] vs. 3.0[2.1–3.9] WU*$m^2$; $P = 0.02$) were higher in PH-HF compared with PH-NF animals, indicating the presence of

Table 1. *Invasive hemodynamics in PH with adaptive or maladaptive RV remodeling*

| | Sham | PH-NF | PH-HF | *P*, ANOVA | Pairwise Comparisons* | | |
|---|---|---|---|---|---|---|---|
| | | | | | Sham vs. PH-NF | Sham vs. PH-HF | PH-NF vs. PH-HF |
| *n* | 4 | 12 | 8 | | | | |
| Body weight, kg | 30.5 (29.5–31.3) | 29.0 (26.8–32.2) | 20.0 (17.5–22.5) | 0.0000007 | 0.67 | 0.00013 | 0.000013 |
| Hemodynamics | | | | | | | |
| Heart rate, beats/min | 65 (53–76) | 73 (61–79) | 75 (72–86) | 0.17 | | | |
| Mean aorta, mmHg | 96 (84–108) | 106 (83–126) | 75 (68–80) | 0.03 | 0.43 | 0.36 | 0.027 |
| Pressure, mmHg | | | | | | | |
| Pulmonary artery wedge | 5 (4–6) | 12 (11–15) | 12 (11–14) | 0.005 | 0.007 | 0.007 | 0.94 |
| Mean pulmonary artery | 15 (13–15) | 28 (25–33) | 42 (29–47) | 0.0009 | 0.019 | 0.0007 | 0.03 |
| Right atrial | 2 (1–2) | 3 (3–4) | 3 (1–4) | 0.2 | | | |
| Transpulmonary gradient, mmHg | 9 (8–10) | 14 (11–22) | 29 (27–33) | 0.014 | 0.12 | 0.015 | 0.09 |
| Cardiac index, l/min*m$^2$ | 4.4 (4.1–4.7) | 4.7 (3.8–5.0) | 3.0 (2.8–4.2) | 0.056 | 0.056 | | |
| Stroke volume index, ml/m$^2$ | 69 (62–77) | 64 (58–76) | 41 (39–46) | 0.007 | 0.58 | 0.019 | 0.016 |
| PVR index, wood units*m$^2$ | 2.0 (1.7–2.3) | 3.0 (2.1–3.9) | 8.8 (6.8–12.3) | 0.004 | 0.21 | 0.008 | 0.02 |
| PVR-to-systematic vascular resistance ratio | 0.12 (0.11–0.13) | 0.18 (0.13–0.33) | 0.58 (0.43–0.59) | 0.001 | 0.18 | 0.003 | 0.006 |
| Pulmonary artery capacitance index, ml/mmHg*m$^2$ | 5.7 (5.2–5.9) | 3.3 (2.6–3.8) | 1.7 (1.5–1.9) | 0.00001 | 0.0017 | 0.000012 | 0.0017 |

PH-NF, pulmonary hypertension, adaptive right ventricular (RV) remodeling, and no failure; PH-HF, pulmonary hypertension, maladaptive RV remodeling, and heart failure; PVR, pulmonary vascular resistance. *Presented if ANOVA $P < 0.05$.

more severe disease in PH-HF animals (Fig. 1, *A* and *B*). Furthermore, the finding that the transpulmonary gradient and the PVR index were increased in both PH groups identifies a precapillary factor as a contributor to elevated pulmonary pressures in this model of chronic postcapillary PH. The inverse curvilinear relationship between the PA capacitance (pulsatile) and PVR index (resistive) components that determine RV afterload identified a transition from adaptive to maladaptive RV remodeling that was determined by the rise in PVR index: an early decrease in PA capacitance without a rise in PVR was associated with adaptive RV remodeling, whereas maladaptive RV remodeling occurred in the setting of a marked increase in PVR index (Fig. 1*C*). As expected, a decrease in the cardiac index (3.0[2.8–4.2] vs. 4.4[4.1–4.7] vs.

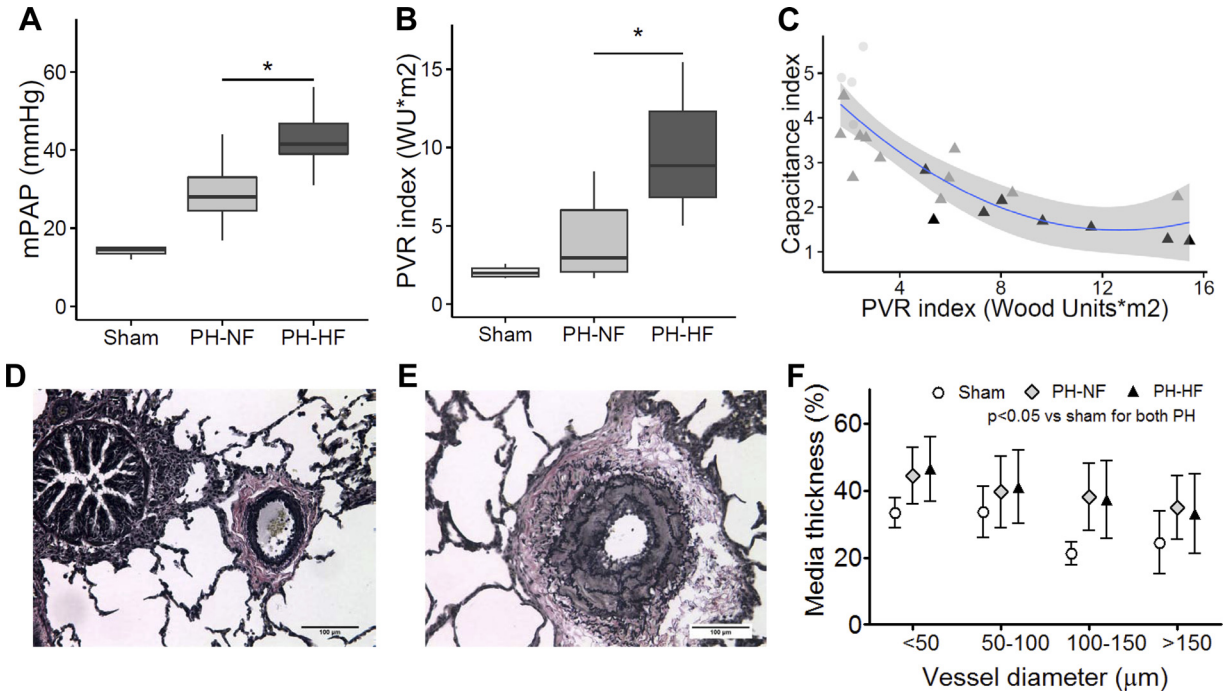


Fig. 1. Pulmonary pressures and vascular remodeling in pigs with pulmonary hypertension (PH) and adaptive versus maladaptive right ventricular (RV) remodeling. In comparison with pigs that had PH, adaptive RV remodeling, and no failure (PH-NF), pigs with PH, maladaptive RV remodeling, and failure (PH-HF) had a higher mean pulmonary arterial (PA) pressure (mPAP; *A*) and pulmonary vascular resistance (PVR) index (*B*). *C*: inverse curvilinear relationship between PA capacitance (pulsatile component) and PVR index (steady component) of RV afterload shows the transition from RV adaptive to maladaptive remodeling in PH-NF (light gray triangles) and PH-HF (dark gray triangles) as compared with shams (light gray circles). Representative lung vascular morphometry (×20) showing pulmonary arteriole remodeling stained with Elastica Van Gieson staining for a sham-operated (*D*) and PH (*E*) pig. *F*: quantification of pulmonary arteriole medial thickness comparing sham (white), PH-NF (gray), and PH-HF (black) stratified by vessel diameter, $P < 0.05$ for sham vs. PH (*$P < 0.05$ vs. PH-NF). WU, wood units.

4.7[3.8–5.0] l/min*m$^2$; $P = 0.056$ by ANOVA) and stroke volume index were found only in PH-HF animals as compared with sham-operated controls or PH-NF pigs.

To examine the precapillary contribution to elevated pulmonary pressures and resistance, histopathological analysis of lung sections was performed, which revealed that significant pulmonary arteriole remodeling occurred in this model of chronic postcapillary PH. In distal pulmonary arterioles <300 μm from both PH-NF and PH-HF animals, there was evidence of medial hypertrophy, severe narrowing and regression of the vessel lumen, and disruption of the internal elastic lamina (Fig. 1, *D–F*). Although there were no quantitative differences found in the number of remodeled vessels between the PH-NF and PH-HF groups, the presence of pulmonary arteriole hypertrophic remodeling identifies structural precapillary vascular changes as a consequence of chronically increased pulmonary venous pressures in this model.

### *Functional and Structural Parameters in the Chronically Overloaded RV Assessed by Invasive Pressure-Volume Loops and Echocardiography*

As differences in pulmonary vascular remodeling alone could not explain the adaptive versus maladaptive RV responses observed in the chronic postcapillary PH model, detailed RV functional and structural analyses were performed. Summary data for pressure-volume relationships are shown in Table 2, and representative examples are displayed in Fig. 2*A*. With the use of steady state high-fidelity micromanometry, the adjusted (dP/d*t*) maximum revealed that there was a decrease in RV function in the PH-NF and PH-HF groups compared with shams (19.7 [17.4–22.4] vs. 14.5 [13.3–20.3] vs. 14.6 [12.3–15.7] (s − 1); $P = 0.052$). SW index was also increased in both PH group despite the lower stroke volume. From the inferior vena cava occlusion study, we observed that RV elastance (as the ESPVR linear slope) was increased in both groups, as was the arterial elastance. This resulted in compensated RV-PA coupling (ESPVR/Ea) in the PH-NF adaptive group, which markedly impaired in the maladaptive PH-HF animals, consistent with RV-PA uncoupling (Fig. 2*B*). Among invasive parameters of RV diastolic function, a significantly longer τ constant was observed in both PH groups compared with shams indicative of diastolic dysfunction; however, there were no differences found between the PH groups. Regardless, other indexes of RV relaxation, including a less negative absolute value of (dP/d*t*) minimum and EDPVR slope, revealed RV relaxation was impaired to

Table 2. *Pressure-volume loop and echocardiographic assessment of RV function*

| | | | | | Pairwise Comparisons* | | |
|---|---|---|---|---|---|---|---|
| | Sham | PH-NF | PH-HF | *P*, ANOVA | Sham vs. PH-NF | Sham vs. PH-HF | PH-NF vs. PH-HF |
| *n* | 4 | 12 | 8 | | | | |
| | | Pressure-volume analysis | | | | | |
| Systolic function | | | | | | | |
| dP/d$t_{max}$, mmHg/s | 551 (511–618) | 690 (592–746) | 783 (702–896) | 0.1 | | | |
| Adjusted dP/d$t_{max}$, s$^{-1}$ | 19.7 (17.4–22.4) | 14.5 (13.3–20.3) | 14.6 (12.3–15.7) | 0.052 | 0.22 | 0.05 | 0.23 |
| RV stroke work index, (mmHg*ml)/m$^2$ | 1,060 (1,041–1,079) | 1,817 (1,619–2,070) | 1,931 (1,495–2,157) | 0.19 | | | |
| Arterial elastance index, (mmHg/ml)*m$^2$ | 0.81 (0.73–0.91) | 1.27 (1.18–1.33) | 5.10 (2.50–5.70) | 0.0004 | 0.57 | 0.002 | 0.0009 |
| ESPVR slope, mmHg/ml | 0.48 (0.48–0.53) | 0.7 (0.59–0.81) | 1.7 (1.25–1.58) | 0.0002 | 0.45 | 0.0009 | 0.0006 |
| ESPVR volume intercept, ml | −10 ([−21]–2) | −5 ([−23]–4) | 24 ([−7.5]–30) | 0.22 | | | |
| ESPVR/Ea | 0.59 (0.54–0.66) | 0.58 (0.46–0.69) | 0.30 (0.26–0.50) | 0.041 | 0.75 | 0.08 | 0.07 |
| Preload recruitable stroke work slope | 12 (11–13) | 18 (17–19) | 25 (22–28) | 0.002 | 0.037 | 0.002 | 0.037 |
| Diastolic function | | | | | | | |
| dP/d$t_{min}$, mmHg/s | −301 ([−331]–[−293]) | −532 ([−646]–[−443]) | −844 ([−1019]–[−605]) | 0.0006 | 0.08 | 0.0009 | 0.0005 |
| τ, ms | 22 (16–25) | 31 (30–40) | 29 (24–37) | 0.041 | 0.04 | 0.19 | 0.28 |
| End-diastolic pressure-volume relationship slope, mmHg/ml | 0.13 (0.10–0.16) | 0.19 (0.18–0.23) | 0.43 (0.36–0.47) | 0.005 | 0.12 | 0.006 | 0.03 |
| | | Echocardiography | | | | | |
| RV | | | | | | | |
| RV EDV, ml/m$^2$ | 103 (101–104) | 125 (115–134) | 130 (118–138) | 0.087 | | | |
| RV ESV, ml/m$^2$ | 30 (28–32) | 41 (36–47) | 58 (54–65) | 0.002 | 0.09 | 0.002 | 0.0016 |
| RV ejection fraction, % | 70 (69–72) | 67 (63–70) | 54 (41–61) | 0.001 | 0.32 | 0.0037 | 0.0037 |
| Myocardial performance index | 0.377 (0.369–0.411) | 0.406 (0.390–0.480) | 0.590 (0.460–0.650) | 0.06 | 0.52 | 0.014 | 0.014 |
| S′, Doppler tissue imaging, cm/s | 9.7 (9.5–10.3) | 8.8 (7.9–8.2) | 8.4 (8.1–8.7) | 0.024 | 0.024 | 0.024 | 0.85 |
| Tricuspid annular plane systolic excursion, mm | 25 (23–26) | 20 (19–22) | 15 (14–18) | 0.0003 | 0.028 | 0.0003 | 0.012 |
| Longitudinal strain, % | −31 ([−32]–[−29]) | −25 ([−25]–[−22]) | −20 ([−21]–[−18]) | 0.00006 | 0.006 | 0.00005 | 0.006 |
| Longitudinal strain rate, s$^{-1}$ | −3.0 ([−3.2]–[−2.8]) | −2.0 ([−2.2]–[−1.9]) | −1.5 ([−1.6]–[−1.4]) | 0.00002 | 0.0024 | 0.00019 | 0.0024 |
| LV | | | | | | | |
| LV EDV, ml/m$^2$ | 88 (76–95) | 96 (84–100) | 75 (60–83) | 0.12 | | | |
| LV ESV, ml/m$^2$ | 17 (15–19) | 19 (16–19) | 14 (11–19) | 0.36 | | | |
| LV ejection fraction, % | 80 (79–81) | 80 (76–82) | 80 (78–83) | 0.97 | | | |
| Mitral E/A | 1.0 (0.9–1.1) | 1.2 (1.1–1.3) | 1.4 (1.1–1.5) | 0.24 | | | |

dP/d*t*, rate of pressure change in the ventricle; Ea, arterial elastance; ESPVR, end-systolic pressure volume relationship; LV, left ventricle; EDV, end-diastolic volume; ESV, end-systolic volume. *Presented if ANOVA $P < 0.05$.

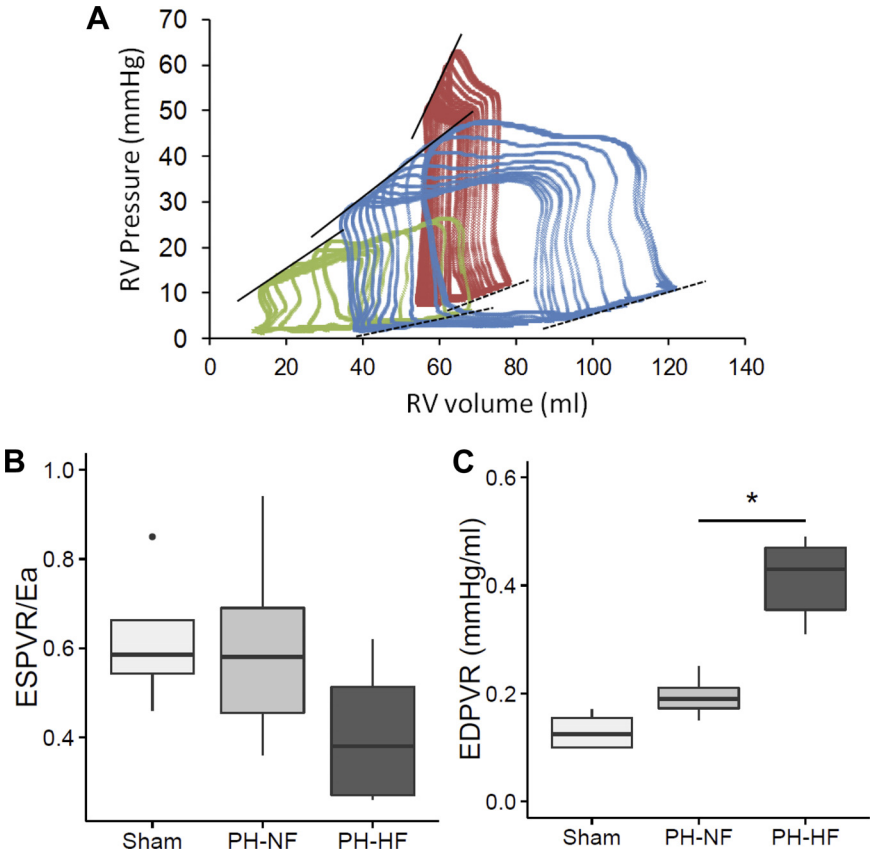


Fig. 2. Pressure-volume relationships in adaptive versus maladaptive RV remodeling. *A*: representative RV pressure-volume loops during inferior vena cava occlusion showing end-systolic pressure-volume relationships (ESPVR) and end-diastolic pressure-volume relationships (EDPVR) in a sham-operate pig (green), a pig with adaptive RV remodeling with increased EDPVR (0.24) and preserved RV-PA coupling/pulmonary arterial elastance (ESPVR/Ea) (0.84; blue), and a pig with maladaptive RV remodeling, high EDPVR slope (0.31), and impaired ESPVR/Ea (0.26; red). Solid lines: end-systolic pressure-volume (Ees) slope; dashed lines: EDPVR. *B*: ESPVR/Ea was determined as a measure of RV-PA coupling. *C*: EDPVR was assessed as measure of diastolic function. *$P < 0.05$ vs. PH-NF.

a significantly greater degree in PH-HF as compared with PH-NF animals (Fig. 2*C*).

An echocardiographic assessment of cardiac function was also performed and data are summarized in Table 2. RV remodeling quantified using 3D-echocardiography revealed increases in indexed RV end-diastolic and end-systolic volumes in both PH groups compared with sham-operated controls. RV remodeling was associated with RV dysfunction with decreased RVEF, TAPSE, and an increase in the MPI in the PH groups compared with shams. Moreover, the RVEF was significantly lower in the PH-HF compared with the PH-NF animals (54 [41–61] vs. 67 [63–70] %; $P = 0.004$), as was TAPSE (15 [14–18] vs. 20 [19–22] mm; $P = 0.012$), and MPI was significantly higher (0.059 [0.46–65] vs. 0.41 [0.39–0.48]; $P = 0.014$). Longitudinal strain was also reduced in PH-HF compared with PH-NF animals (−20 [−21 −18] vs. −25 [−25-22] %; $P = 0.006$; Fig. 3, *A* and *B*).

At the final follow-up, the inferior pulmonary vein was also interrogated using pulsed-wave Doppler echocardiography to determine if there was increased severity of the pulmonary vein luminal restriction over time as a cause of RV maladaptive remodeling. This demonstrated that the mean gradient at the common inferior vein was <1 mmHg in the sham-operated group and increased significantly in both PH groups. Interestingly, the mean gradient was significantly higher in the PH-HF group compared with the PH-NF (17[16–18] vs. 12 [11–13] mmHg, respectively; adjusted $P = 0.047$) despite a similar degree of venous banding at the index procedure to create the model.

### *Chronic Postcapillary PH is Associated With RV Cardiomyocyte Hypertrophy and Fibrosis*

Additional evidence of RV remodeling in the chronic postcapillary PH model was obtained from the explanted heart by measurement of the weight of the RV free wall relative to that of the LV + septum indexed to the animal body weight. When compared with sham-operated controls, the PH groups had a marked increase in RV weight consistent with RV hypertrophy (Fulton index: 0.40 [0.38–0.43] vs. 0.62 [0.54–0.77]; $P <$ 0.05; RV weight/body weight: 1.13 [1.11–1.16] vs 1.56 [1.38–1.98] g/kg; $P < 0.05$; Fig. 3, *C* and *D*).

On histopathological analysis of the RV myocardium, there was evidence of RV cardiomyocyte hypertrophy with increased cardiomyocyte cross-sectional area in both PH-NF and PH-HF animals compared with sham-operated controls and no difference identified between the PH groups (Fig. 4, *A–C*). There was also an increase in fibrosis detected in the RV of animals with PH compared with sham-operated controls with a predilection for the perivascular space and no observed differences between the PH groups (Fig. 4, *D–F*).

### *Myocardial SERCA2a and Endoplasmic Reticulum Stress-Related Protein Expression*

To determine whether there were appreciable differences in the RV of PH-NF versus PH-HF animals at the molecular level, we analyzed the expression of calcium handling proteins since studies performed in a canine model of severe RV pressure overload found a decrease in SERCA and PLN phos-

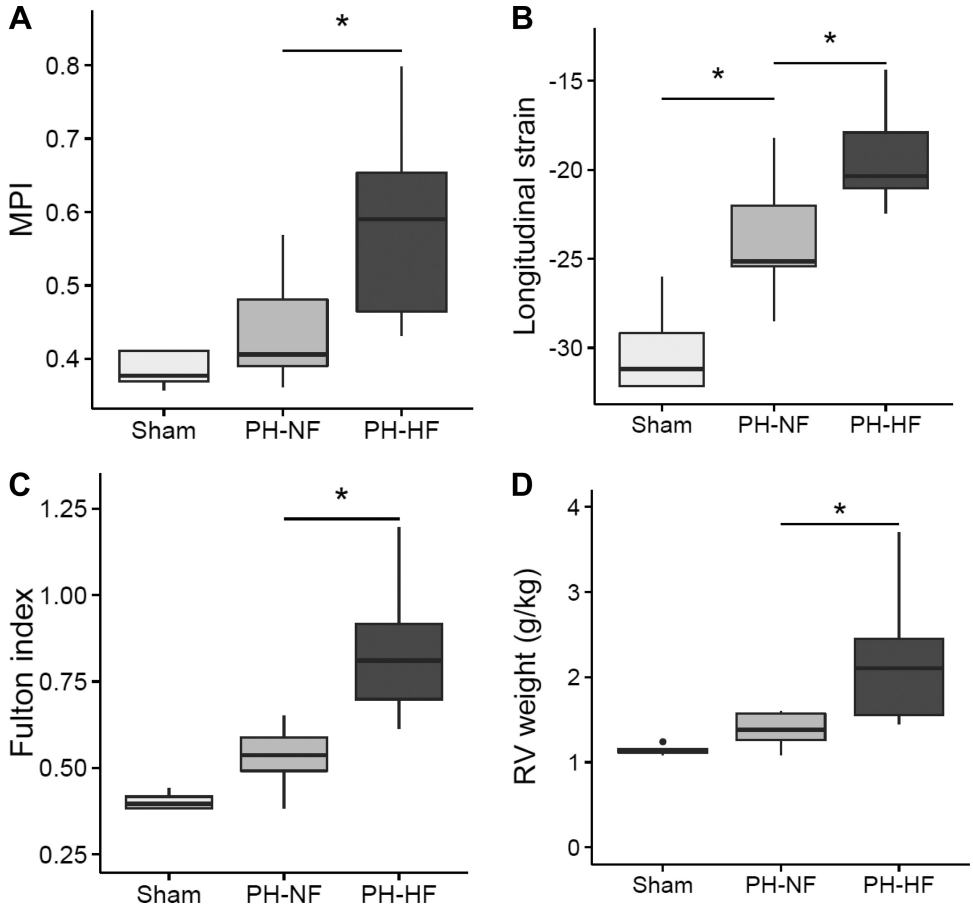


Fig. 3. RV function and hypertrophy. In sham-operated and PH pigs, myocardial performance index (MPI) was measured as an index of RV contractile reserve (*A*) and RV longitudinal strain was assessed (*B*). *C*: RV hypertrophy was evaluated by RV weight relative to left ventricle (LV) + septum (Fulton index) and indexed for body weight. *D*: RV weight. *$P < 0.05$ vs. PH-NF or vs. sham.

phorylation (31). In the RV myocardium, SERCA2a protein expression was decreased significantly in the PH-HF animals compared with PH-NF animals and sham-operated controls (Fig. 5*A*). Interestingly, RV SERCA2a levels correlated linearly with indexes of RV remodeling, including RV hypertrophy determined by the RV/LV + septum weight ratio (Pearson $r = -0.71$, $P = 0.040$), RV-PA coupling determined by ESPVR/Ea ($R = 0.68$, $P = 0.061$), and EDPVR slope ($r = -0.70$, $P = 0.052$) reflecting an association of SERCA2a downregulation with more severe RV functional impairment. We also examined the expression and phosphorylation status of PLN, which is the main regulator of SERCA2a activity. In the RV myocardium from PH-HF animals, phosphorylation of PLN at Ser16 was decreased (inhibition of SERCA2a activity) compared with PH-NF and sham-operated control animals (Fig. 5*B*). As SERCA2a activity has been inversely related to endoplasmic reticulum (ER) stress, we also examined the expression of the pro-apoptotic ER stress-related protein CCAAT/enhancer binding protein homology protein (CHOP). Increased expression of CHOP was detected in the PH-HF group as compared with the PH-NF and sham-operated controls (Fig. 5*C*). Taken together, these findings indicate that at a molecular level, the RV in PH-HF animals is characterized by a decrease in SERCA2a expression and activation with a concomitant increase in ER stress.

*Hyperaldosteronism Occurs in Chronic Postcapillary PH*

Aldosterone levels were also examined in PH animals since aldosterone has been shown to mediate pulmonary arteriole remodeling and fibrosis in PA hypertension (28–30) and aldosterone is a recognized indicator of HF status. Aldosterone levels were elevated in chronic postcapillary PH pigs compared with sham-operated controls with the highest levels detected in PH-HF animals (28.12 ± 4.56 vs. 60.69 ± 6.47 vs. 190.90 ± 61.44 mg/dL; $P < 0.02$ by ANOVA; Fig. 6).

## DISCUSSION

RV dysfunction and progression to RV failure is a major determinant of adverse prognosis that underlies the unacceptably high mortality rate associated with PH (2). It is increasingly recognized that the spectrum of RV remodeling that occurs in PH ranges from adaptive remodeling, characterized by RV hypertrophy with overall preserved ventricular function and RV-PA coupling, to maladaptive remodeling associated with RV hypertrophy, diastolic, and systolic dysfunction, and RV-PA uncoupling (45). To date, much of the mechanistic insight to understand RV remodeling and dysfunction has been provided by studies performed in rodent models of experimental PH; however, detailed RV mechanical studies using invasive hemodynamic monitoring are difficult to perform in these models and highlight the need for clinically relevant large animal models (18). In the present study, we analyzed the RV remodeling response in a swine pulmonary vein banding model to define hemodynamic, structural, and functional characteristics that differ between compensated or adaptive RV remodeling and decompensated or maladaptive RV remodeling. We found that elevated pulmonary artery pressures, pulmonary vascular resistance index, and distal pulmonary arterial remod-

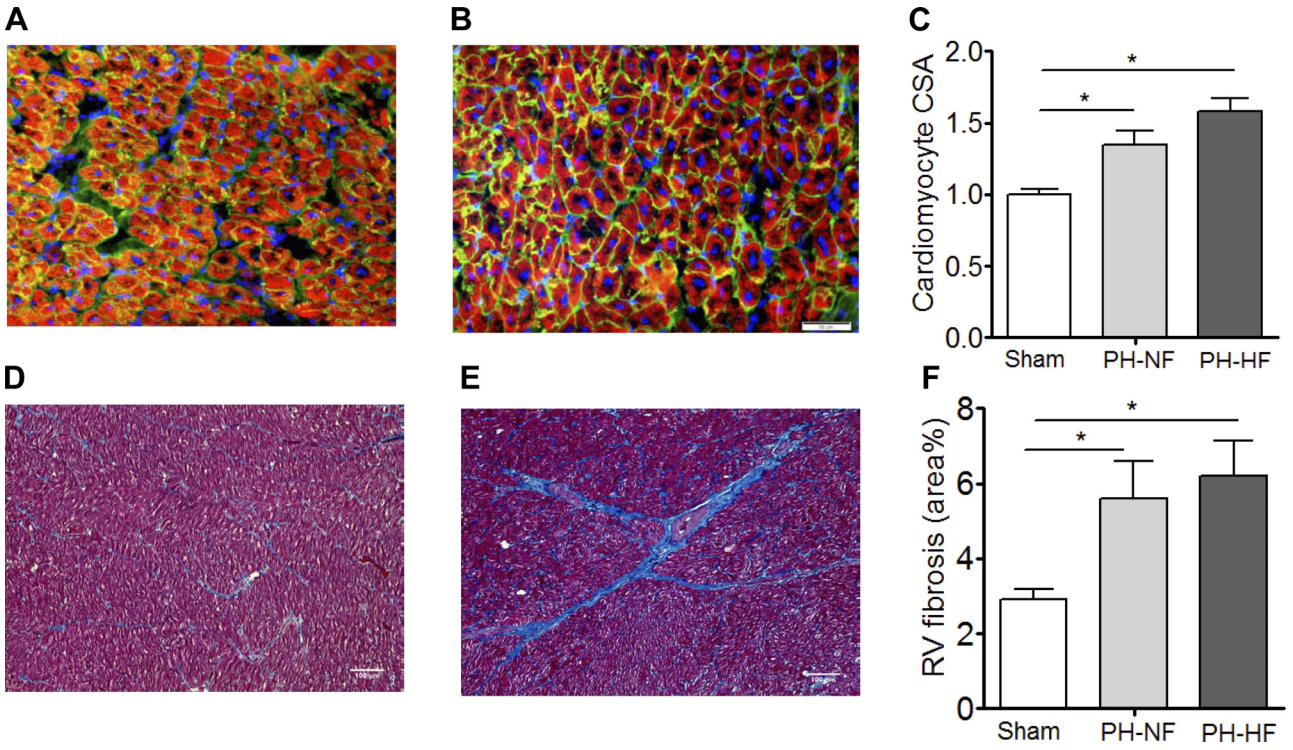


Fig. 4. Cardiomyocyte hypertrophy and RV fibrosis. RV cardiomyocyte cross-sectional area (CSA) was examined by staining with wheat germ agglutinin to evaluate RV sections for cardiomyocyte hypertrophy. Representative sections are shown for sham-operated (*A*) and PH (*B*) pigs, with quantification of pooled data (*C*). RV sections were stained with Masson's trichrome to examine fibrosis. Representative sections are shown for sham-operated (*D*) and PH (*E*) pigs with quantification of pooled quantification (*F*). *$P < 0.05$.

eling, all measures of increased afterload, all occur consistently with pulmonary vein banding model. Using invasive pressure-volume relationships and multi-parameter noninvasive imaging, we confirmed that RV diastolic dysfunction and chamber dilatation are present in early adaptive RV remodeling, whereas RV-PA uncoupling is related to the onset of RV failure. At a cellular level, we found that RV cardiomyocyte hypertrophy and RV fibrosis are present in both adaptive and maladaptive RV remodeling; however, only RV failure is associated with abnormalities in calcium handling protein expression and the ER stress-related protein CHOP. We also observed that RV adaptive and maladaptive remodeling is associated with hyperaldosteronism with higher levels present in the setting of RV failure. Based on these observations, we are now able to define RV maladaptive remodeling on the basis of indexes of RV systolic and diastolic dysfunction, increased RV contractility and decreased arterial elastance, RV-PA uncoupling, and abnormal SERCA2a-related calcium handling.

Despite the growing interest in understanding adaptive and maladaptive RV remodeling in PH, a major hurdle to defining these pathophenotypes has been the lack of clinically relevant large animal models that allow for a comprehensive analysis of RV structure and function (41). One other porcine model of chronic pressure overload that is created by left pulmonary artery banding and weekly right pulmonary artery infusion of cyanoacrylate beads is amenable to subsequent unloading of the RV through the creation of a PA-PA conduit. This model develops PH with RV dysfunction over time, similar to pulmonary vein banding model, but requires several surgical interventions and alters pulmonary artery flow patterns (19, 20). The advantage of the pulmonary vein swine banding model is that, ultimately, the degree of inferior pulmonary vein constriction is determined by animal somatic growth leading to gradual onset but sustained elevations in RV afterload, consistent with the clinical course in humans. Moreover, owing to differences in the imposed RV afterload, the remodeling pattern in the RV may differ between animals, leading some to develop PH with maladaptive RV remodeling and failure while others undergo adaptive RV remodeling as we observed. Although a swine pulmonary vein banding model has been described previously (33, 39), this is the first study that focuses specifically on characterizing RV structure and function in PH during the remodeling process in this model.

RV pressure-volume relationships, which have been used widely to evaluate LV performance under different loading conditions (6), were performed and shown to provide detailed information pertaining to RV systolic and diastolic function in adaptive and maladaptive RV remodeling the porcine pulmonary vein banding model of PH. Interestingly, we found that RV remodeling considered to be adaptive was associated with systolic dysfunction as well as early diastolic dysfunction assessed by a longer $\tau$ constant, less negative ($dP/dt$) minimum, and EDPVR slope, but RV-arterial coupling was preserved. Although these abnormalities were also observed in RV maladaptive remodeling, the difference between adaptive and maladaptive remodeling and failure was the association with RV-arterial uncoupling. This occurred when the increase in ventricular elastance was insufficient to match pulmonary arterial elastance concomitant with a further increase in the EDPVR. Although this finding is in contradistinction with

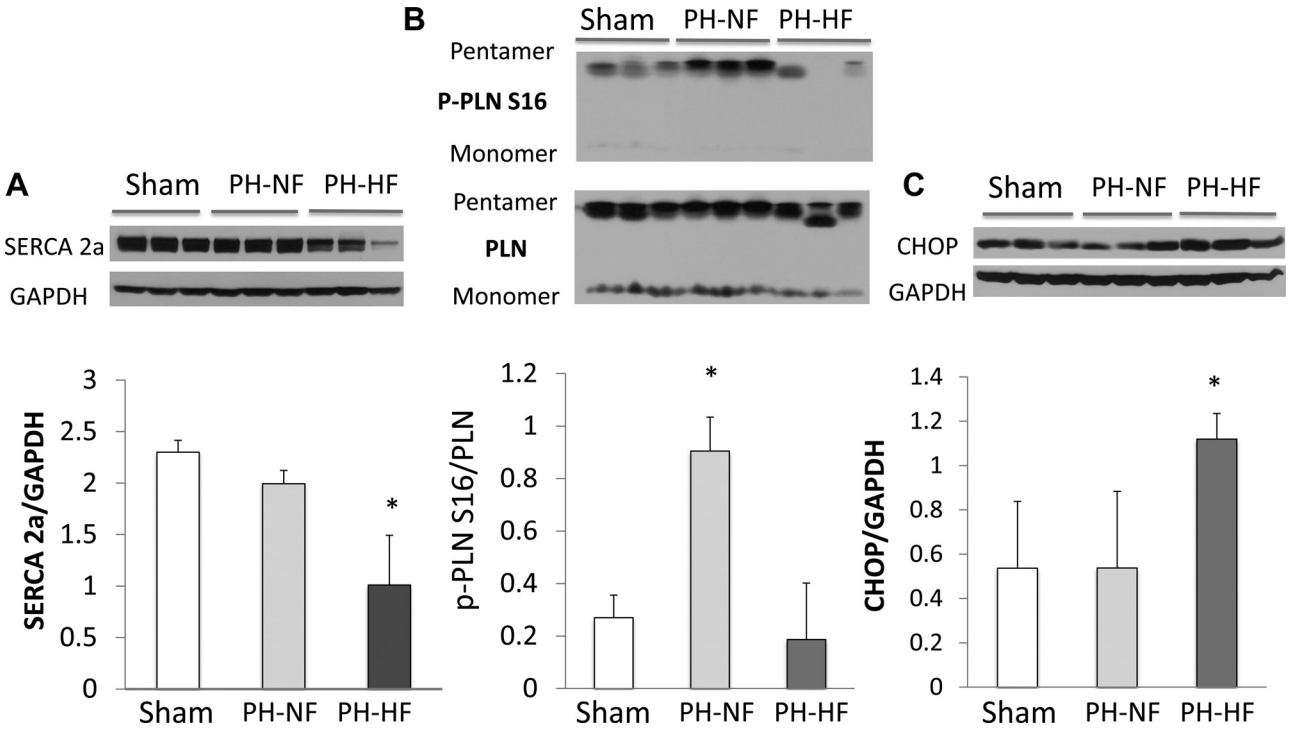


Fig. 5. Molecular remodeling occurs in RV maladaptive remodeling. Myocardial protein quantification and representative blots for SERCA2a (*A*), relative phosphorylation of phospholamban (PLN) at serine 16 (p-PLNS16/PLN; *B*), and CCAAT/enhancer binding protein homology protein (CHOP; *C*) as markers of molecular remodeling in PH-HF. *$P < 0.05$ vs. sham (for SERCA2a, CHOP); *$P < 0.05$ vs. sham and PH-NF for p-PLNS16/PLN.

prior studies that reported early abnormalities in RV-PA coupling (19, 20), our observations are supported by other works in large animal models showing that RV-PA uncoupling occurred with RV failure; however, in this model, RV-PA uncoupling was related to RV hypertrophy and systolic dysfunction (19, 20). The difference between our observations and the aforementioned study is likely related to how the large animal models were created. In our study, we also observed an increase in RVSWI in the setting of maladaptive remodeling in failure. Although an increase in this measure of RV workload and contractility is counterintuitive, this finding has been reported previously in other large animal models of pulmonary hypertension and in patients with Group 2 pulmonary hypertension (20, 25).

The concept of using pressure-volume relationships to define RV-PA coupling as a measure of RV remodeling in PH has merit (4, 8, 9, 26, 36). Studies analyzing RV pressure-volume relationships in experimental or clinical PH have reported increased RV contractility as determined by the ESPVR slope as well as some degree of RV-PA uncoupling (19, 20, 26, 34, 38). Although invasive measures of RV-PA coupling are not always feasible clinically, there is preclinical evidence demonstrating a direct relationship between RV-PA coupling and noninvasive indexes of RV function (19, 20). In patients with PH, noninvasive estimations of RV-PA coupling have been reported using the single beat method and maximal time varying elastance ($E_{max}$) has been estimated as the ratio mean pulmonary arterial pressure/ESV, thus neglecting the volume axis intercept of ESPVR (26, 38). In this study, noninvasive imaging using 3D volumetry and 2D speckle-tracking strain was used to evaluate RV remodeling. With the use of these tools, adaptive RV remodeling was characterized noninvasively by increased RV volumes and mildly abnormal parameters of longitudinal function, such as TAPSE or strain, whereas RVEF or MPI was preserved. Further impairment of longitudinal function along with decreased RVEF and high MPI defined the maladaptive RV remodeling and failure condition. The present study uses 2D strain techniques within the context of the pressure-volume framework and shows that 2D-derived longitudinal strain is afterload dependent, consistent with other studies evaluating RV strain using speckle-tracking algorithms, and correlates with RV-PA coupling (13, 22). These observations also confirm other reports that support

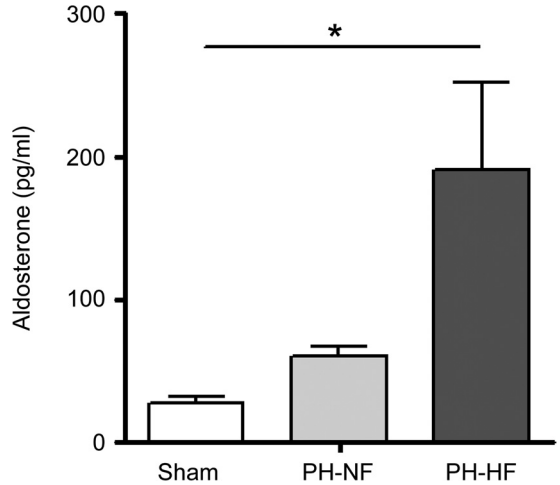


Fig. 6. Hyperaldosteronism is present in PH with RV maladaptive remodeling. Serum aldosterone levels were measured at the end of the study in sham-operated and PH pigs. *$P < 0.02$ by ANOVA.

the clinical feasibility and validity of longitudinal strain as a prognostic marker in chronic PH (10, 12, 22, 37).

In this study, RV dysfunction and failure in the PH-HF subset of animals is likely related to differences in the severity of PH (indicated by the hemodynamic profile) that occurred as a result of the surgical banding resulting in greater constriction of the pulmonary vein. Although the degree of constriction was similar between all animals at baseline, differences in somatic growth may have influenced the ultimate degree of afterload imposed on the RV. Hemodynamically, RV failure was associated with reactive PH (higher PVR) and severe impairment of PA capacitance as indicators of the steady and pulsatile components of afterload. Stiffness parameters, including capacitance, are independent markers of prognosis and RV failure in chronic PH (27, 40).

RV cardiomyocyte hypertrophy and fibrosis were identified as histolopathological markers of both adaptive and maladaptive RV remodeling in PH. These abnormalities may underlie the early diastolic dysfunction observed in the functional studies in animals without heart failure. We also found that SERCA2a expression was downregulated in the failing RV but maintained in the adaptive stage of RV remodeling. This is similar to what has been described in chronic pressure overload by PA banding (31) and in the rat monocrotaline-PH model (21). In addition to defects in calcium handling, other molecular mechanisms have been associated to RV failure in response to chronic pressure overload, such as abnormal cardiomyocyte growth ($\alpha/\beta$ MHC switch) (3) and increased oxidative stress and apoptosis (34). We explored ER stress, which has been reported to mediate pulmonary vascular remodeling (42), in the RV in our model and found evidence of ER stress in animals developing RV failure. Interestingly, increased ER stress in the myocardium has been recently described in response to ischemia (16) possibly as a result of capillary rarefaction and decreased blood supply to the hypertrophied RV, which has been suggested to contribute to RV failure in PH (1, 10, 17). Neurohormonal activation has also been identified as potential contributor to RV failure (3). In support of this, we measured elevated levels of aldosterone in animals with maladaptive RV remodeling and failure. Hyperaldosteronism has been described in patients with PH (28) and is a clinically relevant biomarker of disease severity (28, 29).

### *Limitations of the Study*

There are several limitations to the findings from the present study. An established definition of maladaptive RV remodeling that incorporates functional and structural parameters down to the cellular level is not currently available. We, therefore, chose an arbitrary definition of maladaptive RV remodeling based on the onset of RV failure, as assessed by clinical signs, that was corroborated by structural, functional, and molecular changes consistent with maladaptive remodeling. Although it is possible that the differences between adaptive to maladaptive remodeling to RV failure may have been identified more precisely for each animal by repeated hemodynamic assessments over time, we did not perform these studies owing to the morbidity associated with repeat instrumentation as well as the fact that the time course of disease has been established (33). In our model, the mean RA pressure in PH-HF subjects was not increased compared with PH-NF or controls. Although it is expected that the mean RA pressure would be increased under these circumstances, similar findings have been reported in other studies (33). Our study used 2D and 3D echocardiography as opposed to magnetic resonance imaging to assess the RV. This technique is subject to interoperator variability and can underestimate RV volumes when RV dilation is present (7, 12). MRI might also have provided additional insight into the role of RV myocardial ischemia in RV dysfunction by allowing for an assessment of coronary flow reserve (23).

In conclusion, we provide evidence that the porcine pulmonary vein banding model of PH is an excellent clinically relevant model to characterize adaptive and maladaptive remodeling in PH using invasive and noninvasive structural and functional quantification tools, as well as histological and molecular analysis. Cardiomyocyte hypertrophy and fibrosis underlie early RV adaptive remodeling and diastolic dysfunction, whereas abnormal calcium cycling protein expression, increased ER stress, and hyperaldosteronism are associated with RV-PA uncoupling and the onset of RV failure.


## ACKNOWLEDGMENTS

We thank Lauren Leonardson for expertise and valuable technical support.

## GRANTS

This work is supported by National Heart, Lung, and Blood Institute Grants NIH RO1-HL083156, HL-093183, HL-119046, and P20HL-100396 and Program of Excellence in Nanotechnology Award Contract No. HHSN268201000045C (to R. J. Hajjar) and NIH RO1-105301 (to J. A. Leopold). Part of the work was funded by a Leducq Foundation grant (to R. J. Hajjar). J. Aguero was supported by the Fundacion Alfonso Martin-Escudero.


## DISCLOSURES

No conflicts of interest, financial or otherwise, are declared by the author(s).

## AUTHOR CONTRIBUTIONS

Author contributions: J.A., K.I., L.H., K.F., B.I., D.P., A.G.-A., V.F., P.P.S., J.A.L., and R.J.H. conception and design of research; J.A., K.I., L.H., C.G.S.-G., N.H., A.H.C., S.T., C.N., and A.G.-A. performed experiments; J.A., K.I., C.G.S.-G., K.F., N.H., A.H.C., S.T., J.A.L., and R.J.H. analyzed data; J.A., K.I., L.H., K.F., A.H.C., S.T., C.N., B.I., D.P., V.F., P.P.S., J.A.L., and R.J.H. interpreted results of experiments; J.A., L.H., A.H.C., and S.T. prepared figures; J.A., K.I., and J.A.L. drafted manuscript; J.A., K.I., A.H.C., S.T., J.A.L., and R.J.H. edited and revised manuscript; J.A., K.I., L.H., C.G.S.-G., K.F., N.H., A.H.C., C.N., B.I., D.P., A.G.-A., V.F., P.P.S., J.A.L., and R.J.H. approved final version of manuscript.

## REFERENCES


1. **Archer SL, Fang YH, Ryan JJ, Piao L.** Metabolism and bioenergetics in the right ventricle and pulmonary vasculature in pulmonary hypertension. *Pulm Circ* 3: 144–152, 2013.
2. **Benza RL, Miller DP, Gomberg-Maitland M, Frantz RP, Foreman AJ, Coffey CS, Frost A, Barst RJ, Badesch DB, Elliott CG, Liou TG, McGoon MD.** Predicting survival in pulmonary arterial hypertension: insights from the Registry to Evaluate Early and Long-Term Pulmonary Arterial Hypertension Disease Management (REVEAL). *Circulation* 122: 164–172, 2010.
3. **Bogaard HJ, Abe K, Vonk Noordegraaf A, Voelkel NF.** The right ventricle under pressure: cellular and molecular mechanisms of right-heart failure in pulmonary hypertension. *CHEST J* 135: 794–804, 2009.
4. **Brimioulle S, Wauthy P, Ewalenko P, Rondelet B, Vermeulen F, Kerbaul F, Naeije R.** Single-beat estimation of right ventricular end-systolic pressure-volume relationship. *Am J Physiol Heart Circ Physiol* 284: H1625–H1630, 2003.
5. **Burke MA, Katz DH, Beussink L, Selvaraj S, Gupta DK, Fox J, Chakrabarti S, Sauer AJ, Rich JD, Freed BH, Shah SJ.** Prognostic

importance of pathophysiologic markers in patients with heart failure and preserved ejection fraction. *Circ Heart Fail* 7: 288–299, 2014.

6. **Burkhoff D, Mirsky I, Suga H.** Assessment of systolic and diastolic ventricular properties via pressure-volume analysis: a guide for clinical, translational, and basic researchers. *Am J Physiol Heart Circ Physiol* 289: H501–H512, 2005.
7. **Crean AM, Maredia N, Ballard G, Menezes R, Wharton G, Forster J, Greenwood JP, Thomson JD.** 3D echo systematically underestimates right ventricular volumes compared to cardiovascular magnetic resonance in adult congenital heart disease patients with moderate or severe RV dilatation. *J Cardiovasc Magn Reson* 13: 78, 2011.
8. **Dell′Italia LJ, Walsh RA.** Application of a time varying elastance model to right ventricular performance in man. *Cardiovasc Res* 22: 864–874, 1988.
9. **Dickstein ML, Yano O, Spotnitz HM, Burkhoff D.** Assessment of right ventricular contractile state with the conductance catheter technique in the pig. *Cardiovasc Res* 29: 820–826, 1995.
10. **Drake JI, Bogaard HJ, Mizuno S, Clifton B, Xie B, Gao Y, Dumur CI, Fawcett P, Voelkel NF, Natarajan R.** Molecular signature of a right heart failure program in chronic severe pulmonary hypertension. *Am J Resp Cell Mol Biol* 45: 1239–1247, 2011.
11. **Fine NM, Chen L, Bastiansen PM, Frantz RP, Pellikka PA, Oh JK, Kane GC.** Outcome prediction by quantitative right ventricular function assessment in 575 subjects evaluated for pulmonary hypertension. *Circ Cardiovasc Imaging* 6: 711–721, 2013.
12. **Forfia PR, Vachiéry JL.** Echocardiography in pulmonary arterial hypertension. *Am J Card* 110: S16–S24, 2012.
13. **Fukuda Y, Tanaka H, Sugiyama D, Ryo K, Onishi T, Fukuya H, Nogami M, Ohno Y, Emoto N, Kawai H, Hirata KI.** Utility of right ventricular free wall speckle-tracking strain for evaluation of right ventricular performance in patients with pulmonary hypertension. *J Am Soc Echocardiogr* 24: 1101–1108, 2011.
14. **Galie N, Hoeper MM, Humbert M, Torbicki A, Vachiery JL, Barbera JA, Beghetti M, Corris P, Gaine S, Gibbs JS, Gomez-Sanchez MA, Jondeau G, Klepetko W, Opitz C, Peacock A, Rubin L, Zellweger M, Simonneau G.** Guidelines for the diagnosis and treatment of pulmonary hypertension: the Task Force for the Diagnosis and Treatment of Pulmonary Hypertension of the European Society of Cardiology (ESC) and the European Respiratory Society (ERS), endorsed by the International Society of Heart and Lung Transplantation (ISHLT). *Eur Heart J* 30: 2493–2537, 2009.
15. **Geyer H, Caracciolo G, Abe H, Wilansky S, Carerj S, Gentile F, Nesser HJ, Khandheria B, Narula J, Sengupta PP.** Assessment of myocardial mechanics using speckle tracking echocardiography: fundamentals and clinical applications. *J Am Soc Echocardiogr* 23: 351–369, 2010.
16. **Glembotski CC.** Endoplasmic reticulum stress in the heart. *Circ Res* 101: 975–984, 2007.
17. **Gómez A, Bialostozky D, Zajarias A, Santos E, Palomar A, Martínez MaL, Sandoval J.** Right ventricular ischemia in patients with primary pulmonary hypertension. *J Am Coll Card* 38: 1137–1142, 2001.
18. **Gomez-Arroyo J1, Saleem SJ, Mizuno S, Syed AA, Bogaard HJ, Abbate A, Taraseviciene-Stewart L, Sung Y, Kraskauskas D, Farkas D, Conrad DH, Nicolls MR, Voelkel NF.** A brief overview of mouse models of pulmonary arterial hypertension: problems and prospects. *Am J Physiol Lung Cell Mol Physiol* 302: L977–L991, 2012.
19. **Guihaire J, Haddad F, Boulate D, Decante B, Denault AY, Wu J, Hervé P, Humbert M, Dartevelle P, Verhoye JP, Mercier O, Fadel E.** Non-invasive indices of right ventricular function are markers of ventricular-arterial coupling rather than ventricular contractility: insights from a porcine model of chronic pressure overload. *Eur Heart J Cardiovasc Imaging* 14: 1140–1149, 2013.
20. **Guihaire J, Haddad F, Boulate D, Capderou A, Decante B, Flécher E, Eddahibi S5, Dorfmüller P, Hervé P, Humbert M, Verhoye JP, Dartevelle P, Mercier O, Fadel E.** Right ventricular plasticity in a porcine model of chronic pressure overload. *J Heart Lung Transplant* 33: 194–202, 2014.
21. **Hadri L, Kratlian RG, Benard L, Maron BA, Dorfmuller P, Ladage D, Guignabert C, Ishikawa K, Aguero J, Ibanez B, Turnbull IC, Kohlbrenner E, Liang L, Zsebo K, Humbert M, Hulot JS, Kawase Y, Hajjar RJ, Leopold JA.** Therapeutic efficacy of AAV1. SERCA2a in monocrotaline-induced pulmonary arterial hypertension. *Circulation* 128: 512–523, 2013.
22. **Haeck MLA, Scherptong RWC, Marsan NA, Holman ER, Schalij MJ, Bax JJ, Vliegen HW, Delgado V.** Prognostic value of right ventricular longitudinal peak systolic strain in patients with pulmonary hypertension. *Circ Cardiovasc Imaging* 5: 628–636, 2012.
23. **Ibrahim T, Nekolla SG, Schreiber K, Odaka K, Volz S, Mehilli J, Güthlin M, Delius W, Schwaiger M.** Assessment of coronary flow reserve: comparison between contrast-enhanced magnetic resonance imaging and positron emission tomography. *J Am Coll Cardiol* 39: 864–870, 2002.
24. **Kelley KW, Curtis SE, Marzan GT, Karara HM, Anderson CR.** Body surface area of female swine. *J Anim Sci* 36: 927–930, 1973.
25. **Khush KK, Tasissa G, Butler J, McGlothlin D, De Marco T; Investigators ESCAPE.** Effect of pulmonary hypertension on clinical outcomes in advanced heart failure: analysis of the Evaluation Study of Congestive Heart Failure and Pulmonary Artery Catheterization Effectiveness (ESCAPE) database. *Am Heart J* 157: 1026–1034, 2009.
26. **Kuehne T, Yilmaz S, Steendijk P, Moore P, Groenink M, Saaed M, Weber O, Higgins CB, Ewert P, Fleck E, Nagel E, Schulze-Neick I, Lange P.** Magnetic resonance imaging analysis of right ventricular pressure-volume loops: in vivo validation and clinical application in patients with pulmonary hypertension. *Circulation* 110: 2010–2016, 2004.
27. **Mahapatra S, Nishimura RA, Sorajja P, Cha S, McGoon MD.** Relationship of pulmonary arterial capacitance and mortality in idiopathic pulmonary arterial hypertension. *J Am Coll Cardiol* 47: 799–803, 2006.
28. **Maron BA, Opotowsky AR, Landzberg MJ, Loscalzo J, Waxman AB, Leopold JA.** Plasma aldosterone levels are elevated in patients with pulmonary arterial hypertension in the absence of left ventricular heart failure: a pilot study. *Eur J Heart Fail* 15: 277–283, 2013.
29. **Maron BA, Waxman AB, Opotowsky AR, Gillies H, Blair C, Aghamohammadzadeh R, Loscalzo J, Leopold JA.** Effectiveness of spironolactone plus ambrisentan for treatment of pulmonary arterial hypertension (from the [ARIES] Study 1 and 2 Trials). *Am J Card* 112: 720–725, 2013.
30. **Maron BA, Zhang YY, White K, Chan SY, Handy DE, Mahoney CE, Loscalzo J, Leopold JA.** Aldosterone inactivates the endothelin-b receptor via a cysteinyl thiol redox switch to decrease pulmonary endothelial nitric oxide levels and modulate pulmonary arterial hypertension. *Circulation* 126: 963–974, 2012.
31. **Moon MR, Aziz A, Lee AM, Moon CJ, Okada S, Kanter EM, Yamada KA.** Differential calcium handling in two canine models of right ventricular pressure overload. *J Surg Res* 178: 554–562, 2012.
32. **Morikawa T, Murata M, Okuda S, Tsuruta H, Iwanaga S, Satoh T, Ogawa S, Fukuda K.** Quantitative analysis of right ventricular function in patients with pulmonary hypertension using three-dimensional echocardiography and a two-dimensional summation method compared to magnetic resonance imaging. *Am J Cardiol* 107: 484–489, 2011.
33. **Pereda D, García-Alvarez A, Sánchez-Quintana D, Nuño M, Fernández-Friera L, Fernández-Jiménez R, García-Ruíz J, Sandoval E, Aguero J, Castellá M, Hajjar R, Fuster V, Ibáñez B.** Swine model of chronic postcapillary pulmonary hypertension with right ventricular remodeling: long-term characterization by cardiac catheterization, magnetic resonance, and pathology. *J Cardiovasc Transl Res* 7: 494–506, 2014.
34. **Rondelet B, Dewachter C, Kerbaul F, Kang X, Fesler P, Brimioulle S, Naeije R, Dewachter L.** Prolonged overcirculation-induced pulmonary arterial hypertension as a cause of right ventricular failure. *Eur Heart J* 33: 1017–1026, 2012.
35. **Rondelet B, Kerbaul F, Motte S, van Beneden R, Remmelink M, Brimioulle S, McEntee K, Wauthy P, Salmon I, Ketelslegers JM, Naeije R.** Bosentan for the prevention of overcirculation-induced experimental pulmonary arterial hypertension. *Circulation* 107: 1329–1335, 2003.
36. **Rudski LG, Lai WW, Afilalo J, Hua L, Handschumacher MD, Chandrasekaran K, Solomon SD, Louie EK, Schiller NB.** Guidelines for the echocardiographic assessment of the right heart in adults: a report from the American Society of Echocardiography endorsed by the European Association of Echocardiography, a registered branch of the European Society of Cardiology, and the Canadian Society of Echocardiography. *J Am Soc Echocardiogr* 23: 685–713, 2010.
37. **Sachdev A, Villarraga HR, Frantz RP, McGoon MD, Hsiao JF, Maalouf JF, Ammash NM, McCully RB, Miller FA, Pellikka PA, Oh JK, Kane GC.** Right ventricular strain for prediction of survival in patients with pulmonary arterial hypertension. *Chest J* 139: 1299–1309, 2011.
38. **Sanz J, García-Alvarez A, Fernández-Friera L, Nair A, Mirelis JG, Sawit ST, Pinney S, Fuster V.** Right ventriculo-arterial coupling in pulmonary hypertension: a magnetic resonance study. *Heart* 98: 238–243, 2012.

39. **Silove ED, Tavernor WD, Berry CL.** Reactive pulmonary arterial hypertension after pulmonary venous constriction in the calf. *Cardiovasc Res* 6: 36–44, 1972.
40. **Stevens GR, Garcia-Alvarez A, Sahni S, Garcia MJ, Fuster V, Sanz J.** RV dysfunction in pulmonary hypertension is independently related to pulmonary artery stiffness. *J Am Coll Cardiol Cardiovasc Imaging* 5: 378–387, 2012.
41. **Sutendra G, Michelakis ED.** Pulmonary arterial hypertension: challenges in translational research and a vision for change. *Sci Transl Med* 5: 208sr5, 2013.
42. **Sutendra G1, Dromparis P, Wright P, Bonnet S, Haromy A, Hao Z, McMurtry MS, Michalak M, Vance JE, Sessa WC, Michelakis ED.** The role of Nogo and the mitochondria-endoplasmic reticulum unit in pulmonary hypertension. *Sci Transl Med* 3: 88, 2012.
43. **Vachiéry JL, Adir Y, Barberà JA, Champion H, Coghlan JG, Cottin V, De Marco T, Galiè N, Ghio S, Gibbs JSR, Martinez F, Semigran M, Simonneau G, Wells A, Seeger W.** Pulmonary hypertension due to left heart diseases. *J Am Coll Cardiol* 62: D100–D108, 2013.
44. **Voelkel NF, Quaife RA, Leinwand LA, Barst RJ, McGoon MD, Meldrum DR, Dupuis J, Long CS, Rubin LJ, Smart FW, Suzuki YJ, Gladwin M, Denholm EM, Gail DB.** Right ventricular function and failure: report of a national heart, lung, and blood institute working group on cellular and molecular mechanisms of right heart failure. *Circulation* 114: 1883–1891, 2006.
45. **Vonk-Noordegraaf A, Haddad F, Chin KM, Forfia PR, Kawut SM, Lumens J, Naeije R, Newman J, Oudiz RJ, Provencher S, Torbicki A, Voelkel NF, Hassoun PM.** Right heart adaptation to pulmonary arterial hypertension: physiology and pathobiology. *J Am Coll Cardiol* 62: D22–D33, 2013.

Artículo 2 [8].

*Aguero J, Ishikawa K, Fish KM, Hammoudi N, Hadri L, Garcia-Alvarez A, Ibanez B, Fuster V, Hajjar RJ, Leopold JA. Combination Proximal Pulmonary Artery Coiling and Distal Embolization Induces Chronic Pulmonary Hypertension in Swine. PLoS One. 2015 Apr 29;10(4):e0124526. doi: 10.1371/journal.pone.0124526.*

PLOS | ONE

RESEARCH ARTICLE

# Combination Proximal Pulmonary Artery Coiling and Distal Embolization Induces Chronic Elevations in Pulmonary Artery Pressure in Swine

**Jaume Aguero[1,2]*, Kiyotake Ishikawa[1], Kenneth M. Fish[1], Nadjib Hammoudi[1], Lahouaria Hadri[1], Ana Garcia-Alvarez[2], Borja Ibanez[2], Valentin Fuster[2,3], Roger J. Hajjar[1‡], Jane A. Leopold[4‡]**

**1** Cardiovascular Research Center, Icahn School of Medicine at Mount Sinai, New York, New York, United States of America, **2** Centro Nacional de Investigaciones Cardiovasculares Carlos III (CNIC)- Epidemiology, Atherothrombosis and Imaging Department, Madrid, Spain, **3** Zena and Michael A. Wiener Cardiovascular Institute, Icahn School of Medicine at Mount Sinai, New York, New York, United States of America, **4** Cardiovascular Medicine Division, Brigham and Women's Hospital, Harvard Medical School, Boston, Massachusetts, United States of America

‡ These authors are co-senior authors on this work.
* jaimeaguero30@hotmail.com





**Citation:** Aguero J, Ishikawa K, Fish KM, Hammoudi N, Hadri L, Garcia-Alvarez A, et al. (2015) Combination Proximal Pulmonary Artery Coiling and Distal Embolization Induces Chronic Elevations in Pulmonary Artery Pressure in Swine. PLoS ONE 10(4): e0124526. doi:10.1371/journal.pone.0124526

**Academic Editor:** Harm Bogaard, VU University Medical Center, NETHERLANDS

**Received:** August 29, 2014

**Accepted:** March 15, 2015

**Published:** April 29, 2015



**Data Availability Statement:** All relevant data are within the paper and its Supporting Information files.

**Funding:** This work is supported by National Institutes of Health RO1 HL083156, HL093183, HL119046, P20HL100396 and a NHLBI Program of Excellence in Nanotechnology Award, Contract # HHSN268201000045C (RJH) and NIH R01 105301 (JAL). Part of the work was funded by a Leducq Foundation grant (RJH). JA was supported by the Fundacion Alfonso Martin-Escudero.

## Abstract

Pulmonary hypertension (PH) is associated with aberrant vascular remodeling and right ventricular (RV) dysfunction that contribute to early mortality. Large animal models that recapitulate human PH are essential for mechanistic studies and evaluating novel therapies; however, these models are not readily accessible to the field owing to the need for advanced surgical techniques or hypoxia. In this study, we present a novel swine model that develops cardiopulmonary hemodynamics and structural changes characteristic of chronic PH. This percutaneous model was created in swine (n=6) by combining distal embolization of dextran beads with selective coiling of the lobar pulmonary arteries (2 procedures per lung over 4 weeks). As controls, findings from this model were compared with those from a standard weekly distal embolization model (n=6) and sham animals (n=4). Survival with the combined embolization model was 100%. At 8 weeks after the index procedure, combined embolization procedure animals had increased mean pulmonary artery pressure (mPA) and pulmonary vascular resistance (PVR) compared to the controls with no effect on left heart or systemic pressures. RV remodeling and RV dysfunction were also present with a decrease in the RV ejection fraction, increase in the myocardial performance index, impaired longitudinal function, as well as cardiomyocyte hypertrophy, and interstitial fibrosis, which were not present in the controls. Pulmonary vascular remodeling occurred in both embolization models, although only the combination embolization model had a decrease in pulmonary capacitance. Taken together, these cardiopulmonary hemodynamic and structural findings identify the novel combination embolization swine model as a valuable tool for future studies of chronic PH.

**Competing Interests:** The authors have declared that no competing interests exist.

## Introduction

Pulmonary hypertension is associated with pathological pulmonary vascular remodeling as well as maladaptive RV remodeling and, ultimately, RV failure that leads to poor clinical outcomes and early death [1]. Vascular remodeling occurs predominantly, but not exclusively, in the pulmonary arterioles and manifests as intimal and medial hypertrophy, inflammation, thrombosis, and fibrosis that disrupts the normal vessel architecture and leads to subtotal luminal obliteration. The RV also undergoes structural and functional remodeling with evidence of hypertrophy and impaired indices of ventricular contraction and relaxation [1]. The finding of pathologically remodeled vessels and RV dysfunction is shared among WHO pulmonary hypertension (PH) Groups, although the pathogenesis of Group 1 PH originates within the vasculature in contradistinction to other forms of PH (Groups 2–5) where pulmonary arteriole remodeling occurs as a consequence of sustained hemodynamic disturbances [2].

Large animal models that are representative of human PH are necessary to bridge the gap between studies in the well-accepted rodent models of experimental PH and clinical testing [3]. Large animal models also offer a unique opportunity to study PH using typical clinical diagnostic methodologies, such as right heart catheterization and advanced imaging techniques, together with a comprehensive characterization of the disease at a cellular and molecular level. This has led to attempts to develop accessible large animal models that recapitulate the pathological and clinical features of human PH. Several models of PH have been created in large animals using advanced surgical procedures such as the subclavian-pulmonary artery shunt overcirculation and pulmonary vein stenosis models [4,5,6]. To overcome the complexity associated with these surgical models, recurrent pulmonary vascular embolization to obstruct the distal pulmonary arterioles has been utilized as a methodology to create a model of PH (Group 4) [7,8,9,10,11,12,13]; however, studies of this model have reported mixed results with some protocols failing to achieve PH cardiopulmonary hemodynamics. There is also no consensus pertaining to the choice of embolic material, timing of administration, and the number of embolization procedures required to create the model. In addition, many of the studies did not evaluate RV function and only examined hemodynamic changes at a time-point $<1$ month after the final embolization procedure thereby calling into the question the long-term durability of those models.

Owing to the lack of information about longer-term pulmonary hemodynamics and RV function in a large animal pulmonary embolization model, the aim of the present study was to determine if this model could develop chronic PH with characteristics of human disease or if the model required modification to achieve chronic PH. We, therefore, hypothesized that only a pulmonary embolization protocol that was sufficient to produce pulmonary vascular (sub) total occlusion would create a model of chronic PH with RV dysfunction. To test this hypothesis, we utilized a novel embolization protocol that combined repeated distal embolization with microspheres, similar to prior studies, with proximal pulmonary coil embolization using silk suture fragments and examined cardiopulmonary hemodynamics and structural changes at 8 weeks.

## Methods

### Experimental design

Sixteen female Yorkshire pigs were included in the study. The pigs were housed in the animal facility until the final follow-up assessment. At the end of the study, animals were euthanized with sodium pentobarbital and the heart and lungs were resected for analysis. The study was performed in accordance with the Guidelines for the Care and Use of Laboratory Animals and

was approved by the Icahn School of Medicine at Mount Sinai Institutional Animal Care and Use Committee.

## Peri-procedural anesthesia

For procedures related to creating the model and at final follow-up, animals were pre-medicated using Telazol (tiletamine/zolazepam) 6.0 mg/kg, intubated, and ventilated with 40% oxygen at 10 ml/kg tidal volume and 15 respirations per minute to maintain an end-tidal $CO_2$ between 35–45 mmHg. General anesthesia was maintained throughout the procedures with propofol 5–8 mg/kg/hr.

## Recurrent embolization model of chronic PH

Two different recurrent pulmonary embolization protocols were utilized to compare the standard distal embolization model (D-Embo) with the combination proximal coiling and distal embolization model (P+D-Embo). The final follow-up assessment was planned for week 8, which was at least 2 weeks after the last embolization procedure. A sham group (n = 4) that did not undergo embolization served as a control and was used as a benchmark of changes over time related to somatic growth. The experimental protocol is shown in Fig 1.

**Distal embolization model (D-Embo)(n = 6).** First, pulmonary angiography was performed using a 5F pigtail catheter to identify branches of the right and left main pulmonary arteries. A 7.5 Fr Swan-Ganz catheter (Edwards Lifesciences) was advanced to the right or left

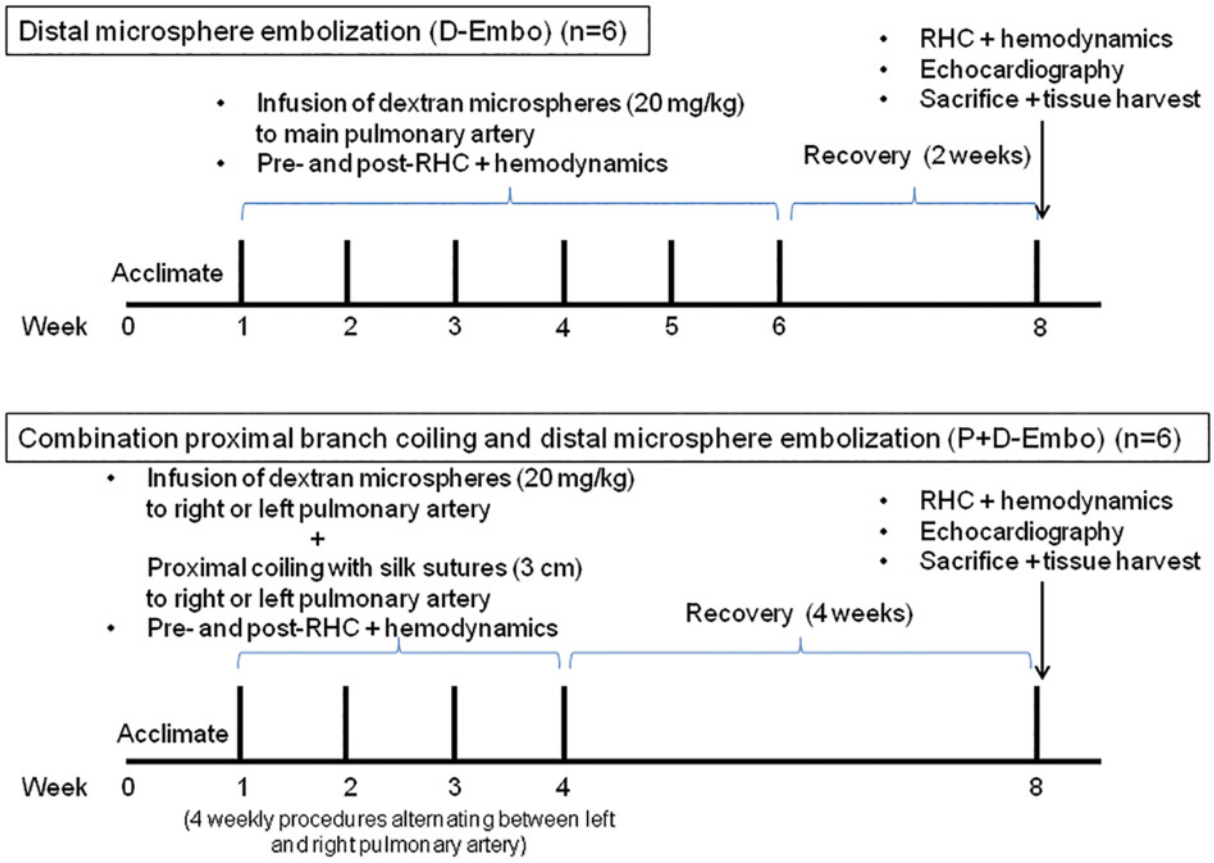


**Fig 1. Study design and experimental protocol.**

doi:10.1371/journal.pone.0124526.g001

pulmonary artery via femoral vein access and dextran microspheres (100–300 μm diameter, coarse Sephadex G-50, Sigma-Aldrich) at a dose of 20 mg/kg were infused through the lumen of the Swan-Ganz catheter on a weekly basis. The dextran microspheres were mixed with 30 ml of sterile 0.9% sodium chloride at least 6 hours prior to the injection. Using this approach, all animals recovered with 100% survival. This dosing regimen was based on the results of a pilot study that demonstrated that infusion of concentrated microspheres (i.e., without dilution in saline) at doses as low as 10 mg/kg led to severe respiratory distress and high early mortality. Once the microspheres were diluted in saline prior to infusion doses as high as 15–20 mg/kg were tolerated without acute morbidity or mortality.

**Proximal + distal embolization model (P+D-Embo) (n = 6).** This model combined distal microsphere embolization with coiling of multiple pulmonary artery branches. To avoid acute severe PH and RV failure as a result of acute bilateral obstruction of the pulmonary arteries, the distal embolization procedure was modified. Using a 7.5 Fr Swan-Ganz (Edwards, Lifesciences) catheter, 20 mg/kg of dextran microspheres were injected through the distal port while the balloon was inflated in the right pulmonary artery. The Swan-Ganz catheter was exchanged for a 5F JR 3.5 coronary guide catheter (Cordis) followed by selective coiling of the main branches of the right pulmonary artery. The coiling procedure was performed by cutting sterile silk sutures into 3 cm long sections and selectively deploying these segments into each branch. The following week, the same procedures were performed on the contralateral lung. Over a period of 4 weeks, the embolization procedures were performed 2 times for each lung per animal.

## Hemodynamic assessment

Cardiopulmonary hemodynamics were recorded using a 7.5 Fr Swan-Ganz catheter (Edwards Lifesciences) that was advanced to the heart via femoral vein access to measure mean right atrial (RA) pressure, mean pulmonary artery pressure (mPA), pulmonary artery occlusion pressure (PAOP), and cardiac output (CO) was measured using the thermodilution method. Pulmonary vascular resistance (PVR) was calculated as (mPAP-PAOP)/CO, and pulmonary artery capacitance as SV/PP, where SV is stroke volume and PP is pulse pressure. CO, SV, PVR and pulmonary artery capacitance were indexed to the body surface area as previously reported [14]. All parameters were recorded during brief periods of end-expiratory breath-hold in anesthetized and ventilated animals.

## Echocardiography

Echocardiographic data were collected at baseline and final follow-up in all animals using a Philips iE33 ultrasound system (Philips Medical Systems, Andover, MA, USA). Cardiac performance was analyzed by measuring the following parameters: 1) anatomical M-mode tricuspid annulus plane systolic excursion (TAPSE); 2) tissue Doppler-derived tricuspid annular systolic velocity; 3) myocardial performance index (MPI); and 4) RV end-systolic and end-diastolic volumes and RV ejection fraction (RVEF) that were obtained from 3D datasets that were analyzed offline with QLAB software (Philips Medical Systems, Andover, MA, USA). All parameters were averaged from three consecutive measurements. For RV volumetric data, interobserver variability was assessed in a subset of 10 animals and estimated using the intraclass correlation coefficient. This parameter was 0.81, 0.96 and 0.93 for end-diastolic volume, end-systolic volume and RVEF, respectively.

## Heart and lung morphology

To assess relative RV hypertrophy, the heart was sectioned into RV and left ventricle (LV), weighed, and RV hypertrophy was assessed using the Fulton index (RV/LV + septum). After

harvests, the heart and lung tissue samples were placed in 10% formaldehyde solution, fixed, processed and tissue blocks were embedded in paraffin. From randomly selected segments harvested from the upper and lower lobes from both lungs, the presence and type of vascular lesions were assessed from 5 μm thick sections stained with Masson's trichrome or hematoxylin and eosin. Distal pulmonary artery remodeling was assessed in 10–12 randomly identified vessels and was quantified by the relative medial thickness (MT) measured as: MT = (WTx2) x100/ED (WT = wall thickness and ED = external diameter) at different vessel diameters. Cardiomyocyte cross-sectional area (CSA) was measured in cardiac sections stained with wheat germ agglutinin (WGA) (conjugated to Oregon Green 488, 10 μg/mL, Invitrogen) and co-stained with phalloidin (conjugated to Alexa fluor 546, 165 nM, Invitrogen). Images of RV cardiomyocyte cell membranes were captured digitally and analyzed using ImageJ software (National Institutes of Health). RV myocardial fibrosis was assessed with Masson's Trichrome staining, quantified, and reported as % area.

### Statistical analysis

All continuous variables are expressed as the mean ± SD. The distribution of continuous variables was assessed graphically using histograms. Normality was determined using Q-Q plots Continuous variables were compared between three groups using one-way analysis of variance or the non-parametric Kruskal-Wallis test, followed by *post hoc* analysis (Tukey HSD method to correct for multiple pairwise comparisons). As the main objective of the study was the development of chronic PVD, hemodynamic changes were computed as the difference between the last follow-up (8 weeks) and the baseline values. For quantitative analyses of histological samples, a mixed model regression was used considering the Group as a fixed factor and the animals within groups as random factors to account for nested measurements within each animal. All statistical analyses were performed using R software version 3.1.0 (http://cran.r-project.org/).

## Results

All animals included in the study completed the embolization procedures per protocol and survived to the 8 week follow-up assessment timepoint. Pulmonary angiograms from before and immediately following the infusion of dextran microspheres (20 mg/kg) revealed that the procedure created acute subtotal luminal obstruction and diminished pulmonary vascular blood flow patterns (S1 and S2 videos). This finding, however, improved over time as the pulmonary angiograms from animals after repeated distal pulmonary embolization procedures demonstrated less luminal obstruction and better recovery of pulmonary blood flow compared to the initial post-embolization study (S3 video). Representative images from angiograms of the pulmonary arterial tree at baseline and immediately after embolization demonstrating acute occlusion of the arterioles are shown in Fig 2.

### Chronic increase in pulmonary artery pressure occurs in proximal + distal embolization model

Although pulmonary artery pressures were elevated acutely ~2-fold after administration of the dextran beads in both models (Fig 3), pulmonary pressures returned to baseline between all of the subsequent embolization procedures in D-Embo animals (shown by the mPA pressure measured pre-embolization at each procedure). By contrast, there was a gradual increase in the mPA over time in P+D-Embo pigs. At the 8-week follow-up examination, indices of pulmonary arterial hypertension were present only in P+D-Embo animals (Table 1). Compared to sham controls and D-Embo pigs, mPA pressures were increased significantly in P+D-Embo pigs (14 ±1 vs. 16 ± 2 vs. 23 ± 4 mmHg, $p<0.05$) with normal PAOP observed in all groups. To

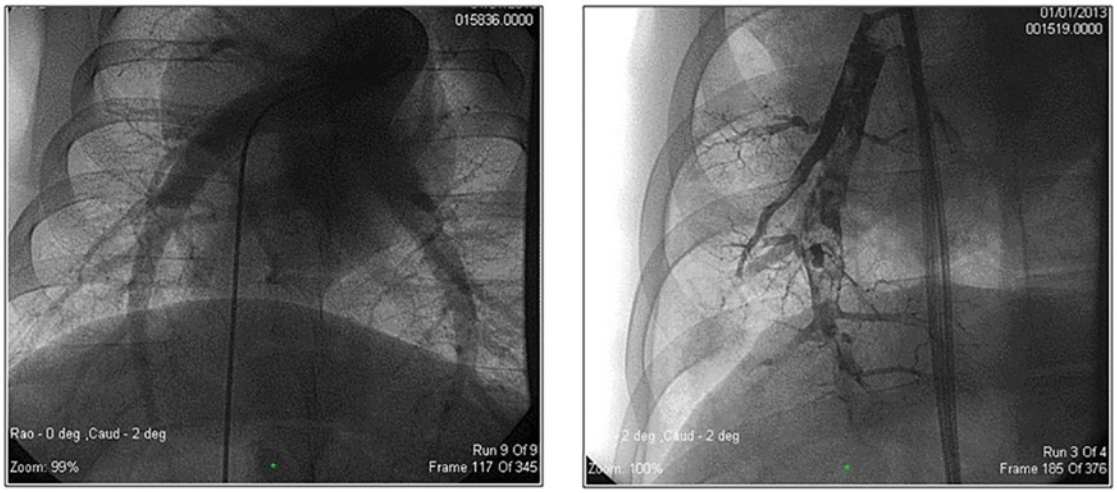


**Fig 2. Infusion of dextran microspheres (100–300 μm) acutely obstructs pulmonary arteries.** Representative still images from pulmonary artery angiographies obtained at (A) baseline or (B) immediately after embolization of microspheres.

doi:10.1371/journal.pone.0124526.g002

examine the effect of the $FiO_2$ on measured mPA pressures, the $FiO_2$ was decreased to 21% for 10 min and mPA pressures were remeasured in sham and P+D-Embo animals. While there was no significant difference in mPA pressures at 21% compared to 40% $FiO_2$ in sham pigs, there was an observed increase in mPA pressure at 21% in P+B-Embo animals (S1 Fig). The PVR index was also increased in P+D-Embo animals (3.9 ±1.6 $WU^*m^2$) compared to shams (2.0 ± 0.4 WU*m2) and D-Embo animals (2.5 ± 0.5 $WU^*m^2$). The pulmonary artery capacitance index, a measure of the pulsatility or compliance of the pulmonary artery, was decreased significantly in P+D-Embo pigs compared to D-Embo pigs (3.9 ±0.5 vs. 2.9 ±0.5, $p<0.05$) and inversely related to the PVR index. Thus, at 8 weeks, the combination embolization pigs all

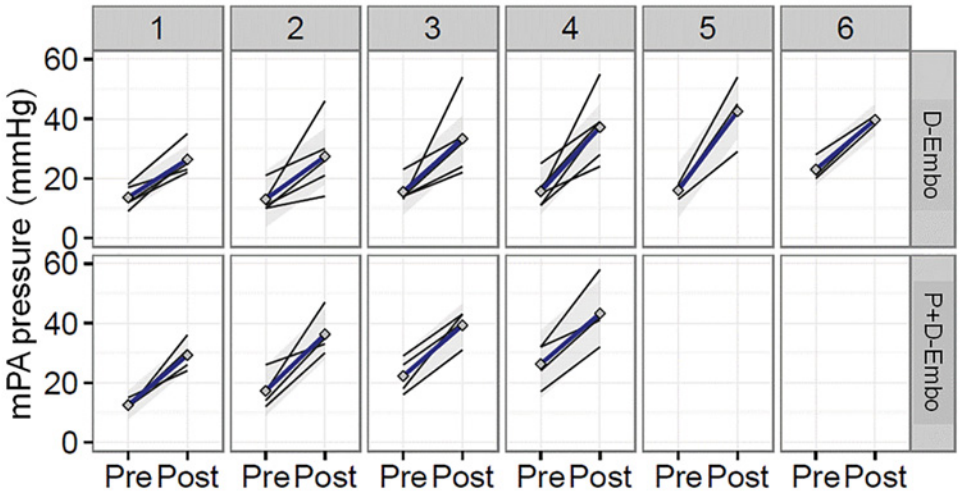


**Fig 3. Acute changes in mPA pressure at the time of consecutive weekly embolization procedures.** Hemodynamic assessments were made by right heart catheterization immediately before and after each weekly infusion of dextran microspheres. Animals in the D-Embo group (n = 6) underwent 6 embolization procedures (top) while pigs in the P+D-Embo group (n = 6) underwent 4 procedures (bottom). Changes for individual animals are plotted with the mean for the group shown as a blue line. mPA, mean pulmonary artery, P+D-Embo, proximal and distal embolization group; D-Embo, distal embolization group.

doi:10.1371/journal.pone.0124526.g003

**Table 1. Cardiopulmonary hemodynamics.**

| | Sham (n = 4) | | D-Embo (n = 6) | | P+D-Embo (n = 6) | | P (ANOVA) |
|---|---|---|---|---|---|---|---|
| | Baseline | 8 weeks | Baseline | 8 weeks | Baseline | 8 weeks | |
| **BW (kg)** [c, d, e] | 16±3 | 30±2 | 15±5 | 22±3 | 19±1 | 26±3 | [a]P<0.05 |
| **HR (bpm)** [d, e] | 69±10 | 65±14 | 85±10 | 72±13 | 62±4 | 71±15 | [b]P<0.05 |
| **Mean AoP (mmHg)** | 88±15 | 96±27 | 75±9 | 74±7 | 78±12 | 82±19 | NS |
| **PAOP (mmHg)** | 5±1 | 5±2 | 5±3 | 6±2 | 3±1 | 9±3 | NS |
| **mPAP (mmHg)** [d, e] | 17±5 | 14±1 | 13±4 | 16±2 | 14±3 | 23±4 | [a]P<0.05 |
| **TPG (mmHg)** | 12±6 | 9±2 | 9±5 | 10±1 | 11±3 | 14±4 | NS |
| **RA pressure (mmHg)** | 3±1 | 2±1 | 3±1 | 4±2 | 2±1 | 2±2 | NS |
| **Cardiac index** | 3.5±1.0 | 4.4±0.4 | 4.1±1.3 | 4.3±0.8 | 3.7±0.4 | 3.7±0.6 | NS |
| **SV index** [e] | 50±8 | 70±9 | 48±15 | 60±9 | 60±6 | 52±6 | [a]P<0.05 |
| **PVR index (WU*m$^2$)** | 3.4±1.1 | 2.0±0.4 | 1.9±0.7 | 2.5±0.5 | 3.0±0.9 | 3.9±1.6 | NS |
| **Capacitance index**[c, d, e] | 4.2±0.9 | 5.3±1.0 | 3.8±12 | 3.9±0.5 | 4.2±0.5 | 2.9±0.5 | [a]P<0.05 |

BW, body weight; HR, heart rate; AoP, aortic pressure; PAOP, pulmonary artery occlusion pressure; mPAP, mean pulmonary artery pressure; TPG, transpulmonary gradient; RA, right atrium; SV, stroke volume; PVR, pulmonary vascular resistance; WU, Wood units.

[a]p<0.05: ANOVA for baseline comparisons.

[b]p<0.05: ANOVA for 8-week follow-up comparisons.

[c]p<0.05 post-hoc comparison: Sham vs. D-Embo.

[d] p<0.05 post-hoc comparison: Sham vs. P+D-Embo.

[e]p<0.05 post-hoc comparison: D-Embo vs. P+D-Embo.

doi:10.1371/journal.pone.0124526.t001

have evidence of chronic PH with increased vascular resistance and decreased compliance, which was not observed in animals that underwent distal embolization alone.

The time course of the rise in mPA pressure and PVR index was also examined in both models (Fig 4). In D-Embo pigs, the peak mPA pressure measured was 21 ± 4 mmHg and was recorded at week 5, one week before the last embolization procedure; however, this increase in

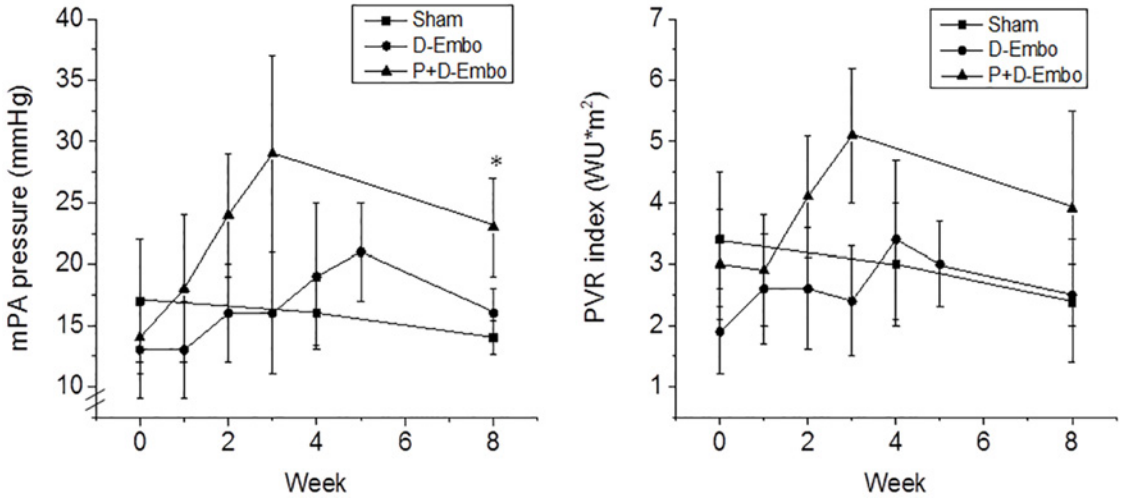


**Fig 4. Temporal changes in mPA pressure and PVR index.** The change over time in mPA pressure (*top*) and PVR index (*bottom*) measured at each embolization procedure and at the 8 week follow-up examination was evaluated in the P+D-Embo group (n = 6), D-Embo group (n = 6) and sham controls (n = 4). mPA, mean pulmonary artery; PVR, pulmonary vascular resistance; P+D-Embo, proximal and distal embolization group; D-Embo, distal embolization group. Data are reported as mean ± SD, *p<0.05 vs. sham, D-Embo by ANOVA.

doi:10.1371/journal.pone.0124526.g004

pressure was normalized at the 8 week follow-up examination and was similar to pressures recorded in sham controls. In contrast, in P+D-Embo pigs, mPA pressures increased by week 2, reached a maximum of 29 ± 8 mmHg (2.1-fold increase over baseline) by week 3, with some evidence of recovery to 23 ± 4 mmHg mmHg by week 8 (1.6-fold increase over baseline). The PVR index followed a similar temporal course with no difference observed between D-Embo animals and sham controls compared to their respective baseline measurements. In P+D-Embo pigs, the PVR index increased to 5.1 ± 1.1 $WU^{*}m^{2}$ at week 3 and by week 8 remained increased 82% over baseline, similar to the temporal trend observed for mPA pressures. These hemodynamic changes occurred without any observed differences between the groups with respect to the cardiac index or mean aortic pressure, both of which were preserved over time.

## Right ventricular dysfunction occurs in the proximal + distal embolization model

Consistent with the finding of PH in P+D-Embo pigs, echocardiographic examination revealed that there was also evidence of RV dysfunction (Table 2). Compared to shams and D-Embo pigs, there was a significant decrease in RVEF in P+D-Embo (70.0 ± 2.7 vs. 68.8 ± 7.0 vs. 58.8 ± 3.7, $p<0.005$) and a significant increase in the myocardial performance index (0.4 ± 0.1 vs. 0.4 ± 0.1 vs. 0.5 ± 0.1, $p<0.006$). Other indices of RV dysfunction were more pronounced in P+D-Embo compared to D-Embo animals, including abnormal longitudinal function as quantified by TAPSE and tissue Doppler imaging-derived peak myocardial velocity.

There was also evidence of RV structural remodeling in P+D-Embo pigs. Compared to shams and D-Embo animals, the RV end-systolic volume index and end-diastolic index was increased significantly in P+D-Embo pigs. There was an increase in RV weight in P+D-Embo pigs (1.14 ± 0.07 vs. 1.18 ± 0.09 vs. 1.42 ± 0.26 gm/kg, $p<0.05$) and RV/LV + septum weight (0.40 ± 0.03 vs. 0.41 ± 0.02 vs. 0.47 ± 0.6 gm/kg, $p<0.05$) indicating that RV hypertrophic remodeling had occurred. To further characterize RV remodeling, myocardial interstitial fibrosis and cardiomyocyte hypertrophy were examined. Compared to sham and D-Embo animals, there was a significant increase in RV interstitial fibrosis in the P+D-Embo pigs (Fig 5). At a cellular level, there was evidence of RV cardiomyocyte remodeling with an increase in cardiomyocyte cross-sectional area observed only in in the P+D-Embo animals (Fig 5).

**Table 2. Echocardiographic RV function and structural remodeling.**

| | Sham (n = 4) | D-Embo (n = 6) | P+D-Embo (n = 6) | P (ANOVA) |
|---|---|---|---|---|
| **EDV index** | 101.7 ± 4.5 | 76.2 ± 14.1 | 104.4 ± 21.0 | 0.048 |
| **ESV index** | 30.5 ± 2.9 | 23.3 ± 4.1 | 43.3 ± 10.7[a,b] | 0.006 |
| **RVEF (%)** | 70.0 ± 2.7 | 68.8 ± 7.0 | 58.8 ± 3.7[a,b] | 0.005 |
| **MPI** | 0.4 ± 0.1 | 0.4 ± 0.1 | 0.5 ± 0.1[a,b] | 0.006 |
| **TDI peak S (cm/s)** | 10.0 ± 0.9 | 8.6 ± 1.1 | 8.0 ± 1.0[a] | 0.034 |
| **TAPSE (mm)** | 24.5 ± 2.4 | 21.6 ± 2.9 | 18.8 ± 2.4[a] | 0.015 |
| **RV weight (g/kg)** | 1.14 ± 0.07 | 1.18 ± 0.09 | 1.42 ± 0.26 | 0.046 |
| **RV/(LV+septum)** | 0.40 ± 0.03 | 0.41 ± 0.02 | 0.47 ± 0.06 | 0.055 |

D-Embo, distal embolization model; P+D-Embo, proximal + distal embolization model; EDV, end-diastolic volume; ESV, end-systolic volume; RVEF, right ventricular ejection fraction; MPI, myocardial performance index; TDI peak S, tissue Doppler imaging peak systolic myocardial velocity; TAPSE, tricuspid annular plane systolic excursion; RV, right ventricle; LV, left ventricle.

[a]$p<0.05$ *post-hoc* comparison: Sham vs. P+D-Embo.

[b]$p<0.05$ *post-hoc* comparison: P+D-Embo vs. D-Embo.

doi:10.1371/journal.pone.0124526.t002

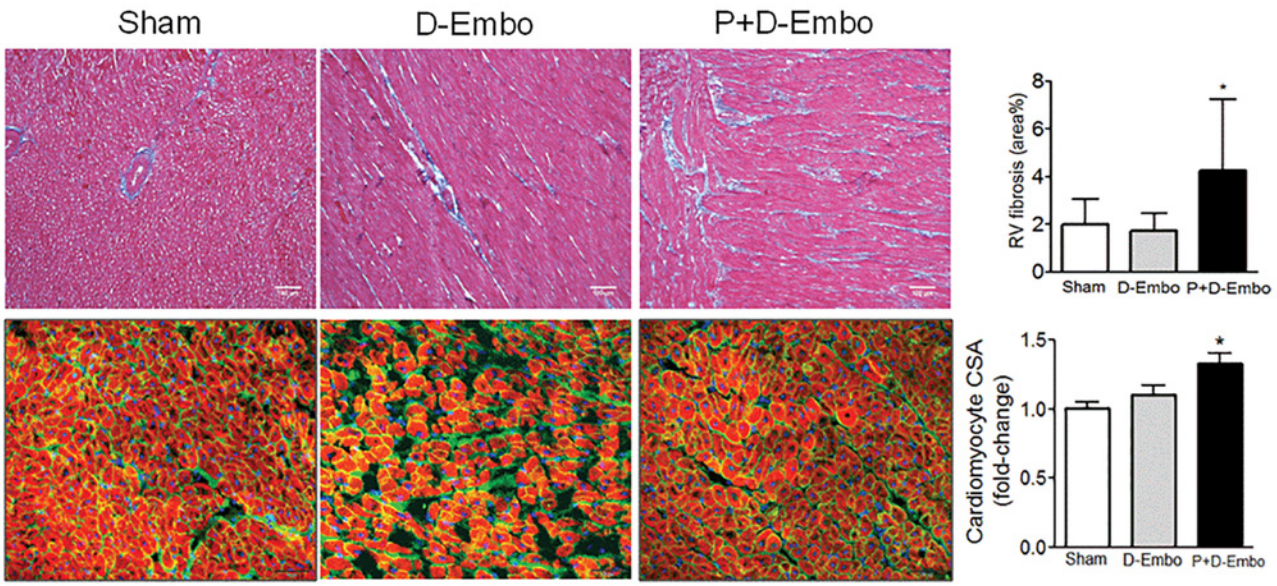


**Fig 5. Right ventricular fibrosis and hypertrophy.** Myocardial fibrosis was examined in RV sections from the P+D-Embo group (n = 6), D-Embo group (n = 6) and sham controls (n = 4) stained with Masson's trichrome and quantified as % area fibrosis (*top*). Cardiomyocyte hypertrophy was evaluated by staining RV sections with wheat germ agglutinin and co-staining with phalloidin to assess cardiomyocyte cross-sectional area (*bottom*). Representative images are shown for each group. P+D-Embo, proximal and distal embolization group; D-Embo, distal embolization group; RV, right ventricular. *p<0.05 vs. sham, D-Embo by ANOVA.

doi:10.1371/journal.pone.0124526.g005

## Pulmonary vascular remodeling is present in the proximal + distal embolization model

Macroscopic examination of the lungs of P+D-Embo pigs showed clusters of silk and fibrin occluding the majority of branches of the pulmonary arteries (Fig 6). In both embolization models,

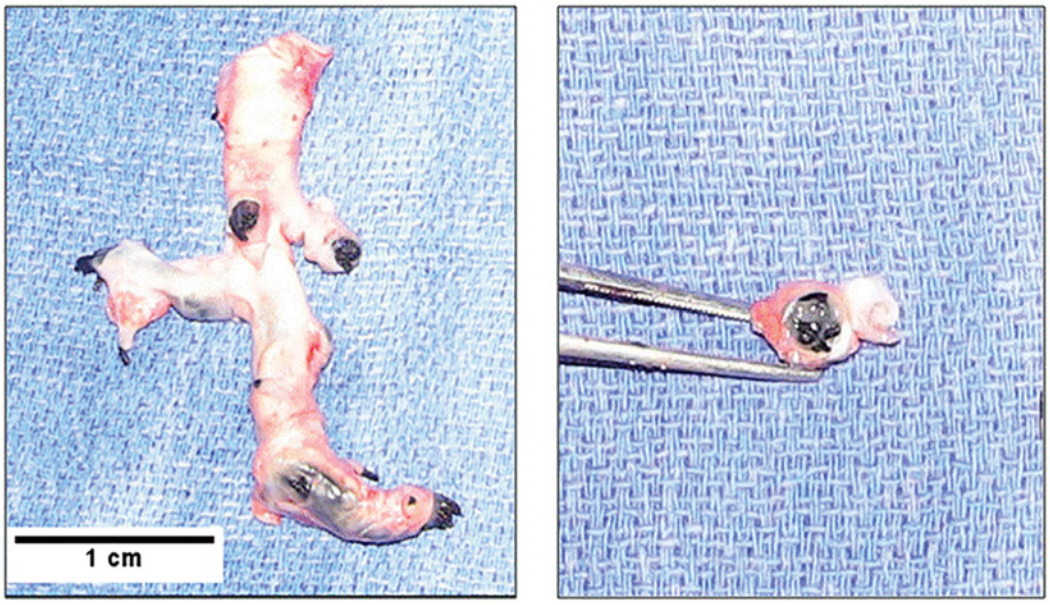


**Fig 6. The combination proximal coiling and distal embolization protocol results in occlusion of pulmonary arteries.** Explanted segments from the right inferior pulmonary artery showing silk coil and fibrin clusters obstructing the vessel lumen with dilation of the vessel. (*left*) Whole vessel segment explant; (*right*) cross-section through vessel showing silk suture and fibrin clusters occluding the lumen.

doi:10.1371/journal.pone.0124526.g006

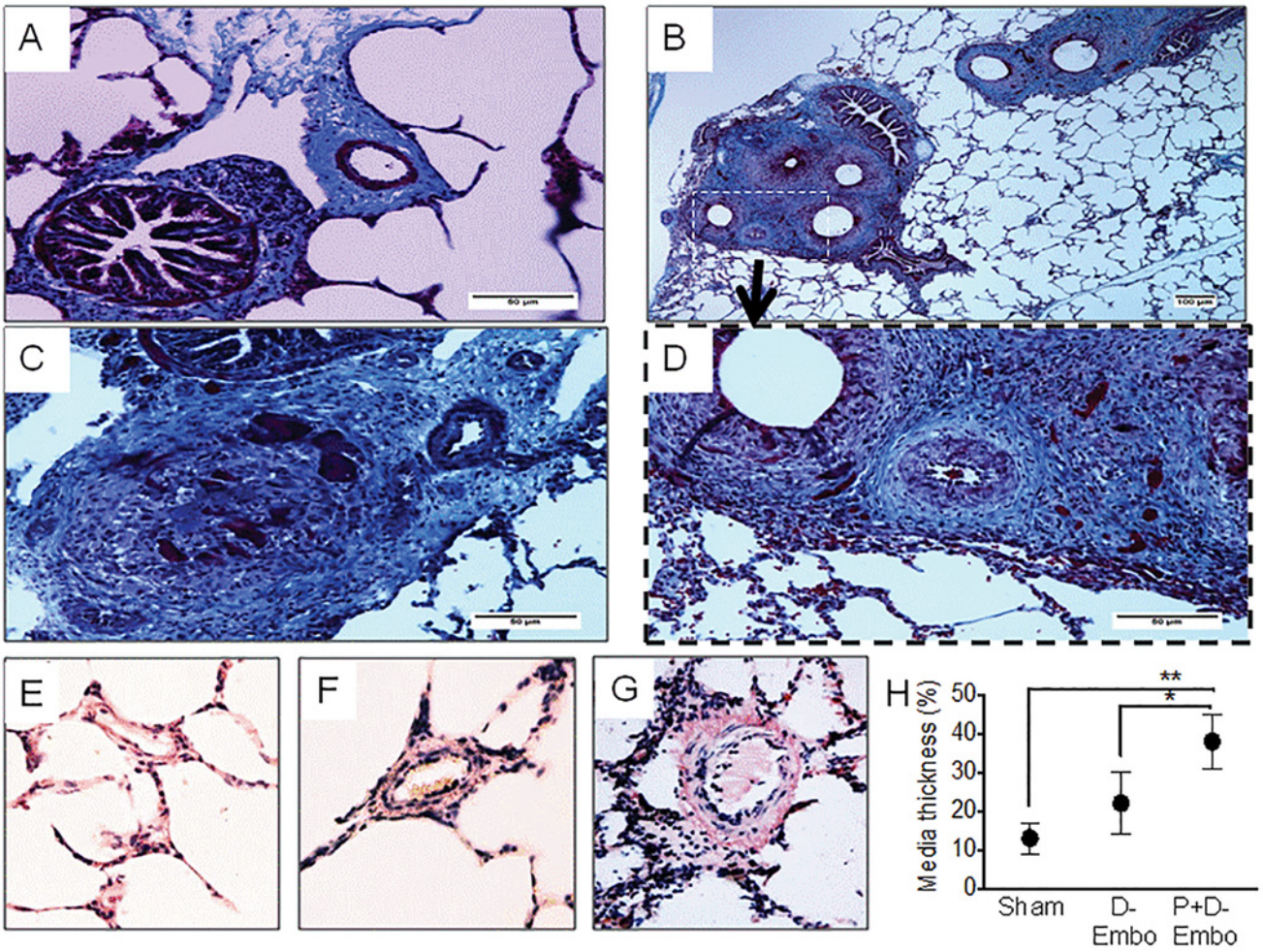


**Fig 7. Pulmonary vascular remodeling.** At 8 weeks, lungs were harvested, processed, and stained with Masson's trichrome to examine pulmonary vascular remodeling. Representative images from A) sham and B-D) embolization models with similar patterns of remodeling, including luminal encroachment and hypertrophic intimal and medial remodeling, were observed for the D-Embo (B, D) and P+D-Embo pigs (C). In selected images (D), microspheres are present in the vessel lumen. There is also extensive perivascular collagen deposition. The distal pulmonary arteries were examined in the periphery of the lung in vessels that were not occluded by beads in sections stained with hematoxylin and eosin. Representative vessels from E) sham, F) D-Embo, and G) P+D-Embo animals are shown. H) Vessel media thickness as an indicator of pulmonary artery remodeling was assessed. P+D-Embo, proximal and distal embolization group; D-Embo, distal embolization group. Scale bars for A, B, C, and D are 60 μm, 100 μm, 60 μm, and 60 μm, respectively. *p<0.05 vs. D-Embo, **p<0.01 vs. sham by ANOVA.

doi:10.1371/journal.pone.0124526.g007

dextran beads were present in the pulmonary artery lumen, which was narrowed significantly as a result of intimal and medial hypertrophic vascular remodeling. There was also evidence of extensive perivascular collagen deposition in the embolization models as compared with the sham controls. To determine the effect of proximal and distal embolization on distal pulmonary artery remodeling, we examined medial thickness in non-occluded distal pulmonary arteries in the lung periphery. This revealed that there was a significant increase in pulmonary arteriole medial thickening in theP+D-Embo animals as compared to the D-Embo and sham pigs (Fig 7).

## Discussion

Translation of scientific and therapeutic findings from PH studies using small animal models into the clinic has been limited, in part, by the lack of accessible large animal models that

recapitulate the essential features of human disease. Investigators have attempted to create large animal models of PH utilizing recurrent intravascular embolization to simulate pulmonary arteriole obstruction with variable results. In many cases, PH did not develop, it occurred acutely but recovered, or studies were not carried out long-term to know if the model was durable over time. In the present study, we describe a novel swine model of chronic pulmonary vascular diseasecreated using a proximal coiling procedure combined with distal embolization (P+D-Embo). The key findings of the present study are: 1) a swine model of chronically elevated pulmonary artery pressures, RV dysfunction, and pulmonary vascular remodeling can be created by the combined embolization procedure; 2) the P+D-Embo protocol adds multiple lobar and segmental artery coiling to the standard D-Embo procedure and requires fewer intrapulmonary artery injections than the distal embolization alone protocol; 3) hemodynamic comparison between P+D-Embo and D-Embo animals reveals that the addition of proximal vessel coiling is an essential element to induce PH; 4) the P+D-Embo model also develops RV structural remodeling and RV dysfunction; and, 5) the procedure is safe with 0% mortality observed over the 8-week follow-up period.

There have been other studies that utilized recurrent embolization techniques to create a PH model in large animals (Table 3) [7,8,9,10,11,12,13,15,16]. These studies have a number of notable differences between them, including the embolic material (e.g., dextran beads, ceramic beads, air), number of procedures required to create the model (e.g., continuous/daily, weekly, biweekly), and the experimental conditions (e.g., mechanical ventilation, $pO_2$, anesthesia) under which the cardiopulmonary hemodynamics were assessed. The importance of these variables is demonstrated by comparing our findings to those from a previous study that performed embolization in pigs using similar doses of microsphere. Our study reported a small, albeit more sustained, increase in mPA pressures and pulmonary hypertension than the other study[16], although pulmonary vascular resistance was similar. Differences between these studies could be explained by a different vascular response to the embolic injury in Yorkshire versus Large-White pigs that were used in each study as well as the different anesthesia protocols and oxygenation conditions at the time of hemodynamic evaluation, as shown in Table 3. The importance of oxygenation conditions is also underscored by our observation that the mPA pressure was lower in anesthetized animals ventilated with 40% $FiO_2$ as compared to 21% $FiO_2$. Another important variable is the time interval between the last embolization procedure and the final assessment (ranging from 1 hour to 6 months). This wide variability in experimental methodology is consistent with the fact that not all embolization protocols developed PH. It has been suggested that the models may have failed owing to pulmonary artery flow redistribution or the progressive recruitment or distension of existing capillaries [17]. It has also been estimated that increases in resting PA pressure don't occur until >50% of the pulmonary circulation is obstructed [17]. Regarding the required amount of beads needed to cause significant levels of PH, Shelub et al [7] estimated that the number of microspheres injected greatly exceeded the number of vessels of similar or smaller diameter than the beads (~300 μm). They further speculated that: 1) flow would still occur despite the impacted beads due to vessel dilatation in response to the acute occlusion, and that 2) maldistribution of beads would spare a significant percentage of vessels that would eventually dilate and contribute to restoring pulmonary blood flow. With respect to the second explanation, we observed an acute increase in pulmonary pressures even at low doses of bead injection, suggesting that acute vasoconstriction may occur and affect the even distribution of beads across the pulmonary vasculature. Accordingly, a much higher dose or modification of the embolization material may be required to create at least moderate elevations in pulmonary pressures. In our study, we solved this issue by increasing the dose of dextran beads delivered (20 mg/kg) and prediluting the beads in saline to increase bead swelling and, thereby, bead diameter to facilitate obstruction. When considering the effect of recurrent pulmonary artery embolization on mPA

**Table 3. Comparison between studies utilizing embolization techniques to create large animal pulmonary hypertension models.**

| 1st Author | Reference in text | Species | Embolic material | Embolizations (n)[a] | N | Oxygenation | Anesthesia during RHC | Recovery period | mPAP | Δ mPAP | Δ mPAP (%) | PVR | Δ PVR | Δ PVR (%) | RV/ LV+S | Δ RV/ LV+S | Δ RV/ LV+S (%) | RV function assessment | Δ RV function (%) |
|---|---|---|---|---|---|---|---|---|---|---|---|---|---|---|---|---|---|---|---|
| D-Embo | Current study | Swine | Sephadex G50 (20 mg/kg) | 6 | 6 | 40% | propofol | 14 days | 16 (2) | 2 | 28 | 2.5 (0.45)[d] | 0.5 | 25 | 0.41 (0.02) | 0.01 | 3 | Echocardiography | None |
| P +D-Embo | Current study | Swine | Sephadex G50 (20 mg/kg) + coil | 4 | 6 | 40% | propofol | 1 month | 23 (4) | 9 | 64 | 3.9 (1.6) [d] | 1.9 | 95 | 0.47 (0.06) | 0.07 | 18 | Echocardiography | -16 (RVEF) |
| Pohlmann *et al*. | 11 | Sheep | Sephadex G50 (0.375 g, ~6 mg/ kg) | 60 | 9 | 21% (SB) | none | 1 day | 35 (9) | 18[b] | 106 | 1.7 (0.66) | 0.82 | 93 | 0.42 (0.03) | 0.07 | 20 | None | - |
| Kim *et al*. | 10 | Canine | ceramic beads (3 mm) | 4 | 5 | 21% | halothane | 6 months | 17 (2) | 5 [b] | 42 | 4.3 (0.83) | 2.1 | 95 | NR | NR | NR | None | - |
| Zhou *et al*. | 15 | Sheep | air (continuous) | 8 weeks | 4 | 21% (SB) | none | 7 days | 34 (5) | 21 [b] | 162 | 4.5 (1.8) | 3.7 | 462 | 0.36 (0.02) | 0.09 | 33 | None | - |
| Weimann *et al*. | 9 | Swine | Sephadex G50 (15 mg/kg) | 3 (days 0, 7 and 49) | 8 | 30% | ketamine | 7 days | 18 (3) | 5 | 38 | 2.3 (0.8) [d] | 0.1 | 5 | NR | NR | NR | None | - |
| Perckett *et al*. | 8 | Sheep | air (continuous) | 12 days | 5 | 21% (SB) | none | 1 hour | 23 (4) | 9 | 64 | 7 (1.54) | 3.36 | 92 | 0.38 (0.13) | 0.06 | 19 | None | - |
| Shelub *et al*. | 7 | Canine | Sephadex G50 | Variable (16–30 weeks) | 5 | 21% (SB) | none | >7 days | 29 (4) | 15 [b] | 107 | 8.3 (2.3) | 6.3 | 315 | 0.54[c] | 0.16 | 42 | None | - |
| Garcia-Alvarez *et al*. | 16 | Swine | Sephadex G50 | 4(3–6) | 9 | 21% (SB) | midazolam | 2 month | 27(3) [e] | 8 | 42 | 3.2 (1.5) [e] | 0.3 | 10 | NR | NR | NR | None | - |
| Mercier *et al*. | 13 | Swine | Histoacryl +Left PA ligation | 5 | 5 | NR | NR | 7 days? | 28.5 (3.8) | 16.9 | 146 | 9.8 (4.5) | 5.1 | 107 | NR | NR | NR | Echocardiography and PV loop | -50 (RVFAC) |

Data expressed as mean (SD) unless stated otherwise. SB: spontaneous breathing.

[a] Per protocol.

[b]Compared with baseline (vs. control group).

[c]Only reported in 2/5 cases.

[d]Indexed (BSA).

[e]Medians (IQR) reported.

NR = not reported. RHC, right heart catheterization; mPAP, mean pulmonary artery pressure; Δ mPAP, change in mean pulmonary artery pressure; PVR, pulmonary vascular resistance; Δ PVR, change in pulmonary vascular resistance; RV/(LV+S), right ventricular weight divided by left ventricular + septum weight (Fulton index); Δ RV/(LV+S), change in right ventricular weight divided by left ventricular + septum weight (Fulton index); RV, right ventricle.

doi:10.1371/journal.pone.0124526.t003

pressure and PVR index, the greatest observed relative change (> 2-fold vs. baseline or controls) in these variables was achieved only in studies where hemodynamic assessments were made following a short (≤ 7 days) recovery period after the last embolization procedure. This finding appears to be independent of animal species, embolization material, or ventilation [8,9,15]. In the current study, we added a proximal embolization procedure together with repeat distal embolization to create the chronic PH model. The use of silk sutures for this purpose is advantageous owing to its ready availability and low cost as compared to commercial coils. The coiling or proximal embolization procedure was performed using silk suture material, which has been used previously to coil cerebral aneurysms[18]. When applied to the pulmonary arterial vasculature, repeated silk suture deployment using angiographic guidance results in progressive occlusion of the pulmonary artery branches. This, in turn, contributed to our finding of increased mPA pressures and PVR one month after the last embolization procedure.

Other non-surgical approaches such as the administration of monocrotaline or hypobaric hypoxia to create PH have been trialed in large animal models. In one study, monocrotaline (12 mg/kg) elevated mPA pressures (34.0 ± 1.7 mmHg) after 6 weeks and echocardiographic evaluation revealed a decreased pulmonary artery acceleration time and pulmonary artery valve ejection time indicating PH and RV dysfunction, respectively. The model was, however, incompletely characterized as PVR, systemic pressures, and other measures of RV function were not reported. These pigs also had an increase in RV weight consistent with RV hypertrophy and pathological examination of the lungs revealed hypertrophic vascular remodeling [19]. Although this model appears promising, it is susceptible to the same criticisms elicited by the monocrotaline rat model. In particular, this model doesn't form obstructive pulmonary vascular lesions and PH has been attributed to sustained vasoconstriction [20,21,22]. Other investigators used chronic hypobaric hypoxia as a mechanism to induce PH; however, this methodology is species specific as it was found to induce PH in calves but not in sheep. Moreover, the inflammatory pulmonary vascular remodeling that occurs is reversible upon exposure to normoxia [3].

In the present study, we conducted a comprehensive analysis of RV structural and functional remodeling using advanced echocardiographic techniques. Using 3D-echocardiography, we found that the P+D-Embo model of PH developed significant RV remodeling with an increased RV end-systolic volume. Global RV performance (increased MPI) and longitudinal function (TAPSE) were also impaired significantly in the P+D Embo model. In prior studies using recurrent embolization models, RV function was not analyzed and reported systematically[23] (Table 3) despite the fact that it is a key contributor to the cardiopulmonary hemodynamics observed in PH and has prognostic implications. Among the studies that reported changes in relative RV mass as an indicator of RV hypertrophy, RV weight increased 18–42%, with greater increases in weight associated with higher mortality and likely indicative of worse RV function [7]. We also examined PA compliance as a measure of RV afterload and found lower PA compliance (increased RV afterload) in the P+D-Embo model [24,25]. This is consistent with the observation that pulmonary artery stiffness is an independent predictor of RV failure and has been shown to add prognostic information to hemodynamic markers of increased afterload such as PVR [24,25]. Moreover, histolopathological analysis of the pulmonary vasculature demonstrated hypertrophic vascular remodeling and increased collagen deposition, which likely contributes to the decrease in PA compliance and has been described previously [16]. Regarding the degree of RV dysfunction in relation to relatively mild hemodynamic chronic severity, our results indicate that decreased capacitance is an important contributor to early impairment of RV function and the development of myocardial hypertrophy and associated interstitial fibrosis,

### Limitations

There are several limitations associated with the findings of our study. Based on our initial goal of examining cardiopulmonary hemodynamics within a sub-acute and longer-term time frame, we examined these parameters 4 weeks after the final embolization procedure in the P+-D-Embo model. It, therefore, remains unknown if the hemodynamic profile changes over a longer follow-up time period. It is also unknown if additional embolization procedures would have resulted in higher mPA pressures after 8 weeks although this is not likely based on the observed trend in pre- and post-embolization mPA pressures. Furthermore, we demonstrated that mPA pressures were actually higher in animals when ventilated with 21% $FiO_2$ than with 40% $FiO_2$ indicating that PH was present in our model although we did not measure mPA pressures in D-Embo animals under these conditions. Another limitation common to all embolization protocols is that the foreign material elicits an inflammatory response and possibly an immune response that may contribute to the observed pulmonary vascular histopathology. We also examined RV structure and function using advanced echocardiographic techniques but did not examine pressure-volume relationships using PV loops, which would have provided additional information about RV function and performance.

## Conclusions

In conclusion, we demonstrate a clinically relevant swine model of pulmonary vascular disease that is created by the combination of a percutaneous proximal coil embolization procedure with distal pulmonary vascular embolization. This requires fewer procedures than previously reported embolization protocols and results in elevated mPA pressure, PVR, pulmonary vascular remodeling, and RV dysfunction at one month after the final procedure. Taken together these findings indicate that the swine P+D-Embo model does recapitulate the cardiopulmonary hemodynamic profile of human PH with RV structural and functional remodeling. Owing to the relative ease with which this model is created as compared to surgical models, it is likely that the combination embolization swine model of PH will serve as a valuable model for future preclinical studies of PH.

## Supporting Information

**S1 Fig. The effect of oxygen on mPA pressures.** To examine the effect of oxygen on mPA pressures, the FiO2 was decreased from 40% to 21% for 10 minutes and mPA pressures were remeasured in sham (n = 4) and P+D-Embo pigs (n = 6). P+D-Embo, proximal and distal embolization group $^{*}p<0.05$ vs. sham, $^{**}p<0.001$ vs. sham.
(TIF)

**S1 Video. Normal pulmonary artery angiogram.**
(MOV)

**S2 Video. Pulmonary artery angiogram immediately after embolization.**
(MOV)

**S3 Video. Pulmonary artery angiogram at the 8 week timepoint.**
(MOV)

## Acknowledgments

We would like to express our great appreciation to Lauren Leonardson for her expertise and valuable technical support.

## Author Contributions

Conceived and designed the experiments: JA KI KMF AGA BI VF RJH JAL. Performed the experiments: JA KI NH LH. Analyzed the data: JA KI KMF NH RJH JAL. Contributed reagents/materials/analysis tools: JA KI NH LH AGA BI. Wrote the paper: JA KI KMF NH AGA BI VF RJH JAL.

## References


1. Champion HC, Michelakis ED, Hassoun PM (2009) Comprehensive invasive and noninvasive approach to the right ventricle-pulmonary circulation unit: state of the art and clinical and research implications. Circulation 120: 992–1007. doi: 10.1161/CIRCULATIONAHA.106.674028 PMID: 19752350
2. Pietra GG, Capron F, Stewart S, Leone O, Humbert M, Robbins IM, et al. (2004) Pathologic assessment of vasculopathies in pulmonary hypertension. J Am Coll Cardiol 43: 25S–32S. PMID: 15194175
3. Stenmark KR, Meyrick B, Galie N, Mooi WJ, McMurtry IF (2009) Animal models of pulmonary arterial hypertension: the hope for etiological discovery and pharmacological cure. Am J Physiol Lung Cell Mol Physiol 297: L1013–1032. doi: 10.1152/ajplung.00217.2009 PMID: 19748998
4. Rondelet B, Kerbaul F, Motte S, van Beneden R, Remmelink M, Brimioulle S, et al. (2003) Bosentan for the prevention of overcirculation-induced experimental pulmonary arterial hypertension. Circulation 107: 1329–1335. PMID: 12628956
5. Silove ED, Tavernor WD, Berry CL (1972) Reactive pulmonary arterial hypertension after pulmonary venous constriction in the calf. Cardiovasc Res 6: 36–44. PMID: 5014277
6. Pereda D, Garcia-Alvarez A, Sanchez-Quintana D, Nuno M, Fernandez-Friera L, Fernandez-Jimenez R, et al. (2014) Swine model of chronic postcapillary pulmonary hypertension with right ventricular remodeling: long-term characterization by cardiac catheterization, magnetic resonance, and pathology. J Cardiovasc Transl Res 7: 494–506. doi: 10.1007/s12265-014-9564-6 PMID: 24771313
7. Shelub I, van Grondelle A, McCullough R, Hofmeister S, Reeves JT (1984) A model of embolic chronic pulmonary hypertension in the dog. J Appl Physiol Respir Environ Exerc Physiol 56: 810–815. PMID: 6706785
8. Perkett EA, Davidson JM, Meyrick B (1991) Sequence of structural changes and elastin peptide release during vascular remodelling in sheep with chronic pulmonary hypertension induced by air embolization. Am J Pathol 139: 1319–1332. PMID: 1836307
9. Weimann J, Zink W, Schnabel PA, Jakob H, Gebhard MM, Martin E, et al. (1999) Selective vasodilation by nitric oxide inhalation during sustained pulmonary hypertension following recurrent microembolism in pigs. J Crit Care 14: 133–140. PMID: 10527251
10. Kim H, Yung GL, Marsh JJ, Konopka RG, Pedersen CA, Chiles PG, et al. (2000) Endothelin mediates pulmonary vascular remodelling in a canine model of chronic embolic pulmonary hypertension. Eur Respir J 15: 640–648. PMID: 10780753
11. Pohlmann JR, Akay B, Camboni D, Koch KL, Mervak BM, Cook KE (2012) A low mortality model of chronic pulmonary hypertension in sheep. J Surg Res 175: 44–48. doi: 10.1016/j.jss.2011.02.049 PMID: 21529838
12. Sato H, Hall CM, Griffith GW, Johnson KF, McGillicuddy JW, Bartlett RH, et al. (2008) Large animal model of chronic pulmonary hypertension. ASAIO J 54: 396–400. doi: 10.1097/MAT.0b013e31817efa85 PMID: 18645357
13. Mercier O, Tivane A, Dorfmuller P, de Perrot M, Raoux F, Decante B, et al. (2013) Piglet model of chronic pulmonary hypertension. Pulm Circ 3: 908–915. doi: 10.1086/674757 PMID: 25006407
14. Kelley KW, Curtis SE, Marzan GT, Karara HM, Anderson CR (1973) Body surface area of female swine. J Anim Sci 36: 927–930. PMID: 4703721
15. Zhou X, Wang D, Castro CY, Hawkins H, Lynch JE, Liu X, et al. (2011) A pulmonary hypertension model induced by continuous pulmonary air embolization. J Surg Res 170: e11–16. doi: 10.1016/j.jss.2011.04.030 PMID: 21696769
16. Garcia-Alvarez A, Fernandez-Friera L, Garcia-Ruiz JM, Nuno-Ayala M, Pereda D, Fernandez-Jimenez R, et al. (2013) Noninvasive monitoring of serial changes in pulmonary vascular resistance and acute vasodilator testing using cardiac magnetic resonance. J Am Coll Cardiol 62: 1621–1631. doi: 10.1016/j.jacc.2013.07.037 PMID: 23954344
17. Burrowes KS, Clark AR, Tawhai MH (2011) Blood flow redistribution and ventilation-perfusion mismatch during embolic pulmonary arterial occlusion. Pulm Circ 1: 365–376. doi: 10.4103/2045-8932.87302 PMID: 22140626

18. Song JK, Eskridge JM, Chung EC, Blake LC, Elliott JP, Finch L, et al. (2000) Preoperative embolization of cerebral arteriovenous malformations with silk sutures: analysis and clinical correlation of complications revealed on computerized tomography scanning. J Neurosurg 92: 955–960. PMID: 10839255

19. Zeng GQ, Liu R, Liao HX, Zhang XF, Qian YX, Liu BH, et al. (2013) Single intraperitoneal injection of monocrotaline as a novel large animal model of chronic pulmonary hypertension in Tibet minipigs. PLoS One 8: e78965. doi: 10.1371/journal.pone.0078965 PMID: 24244396

20. Stenmark KR, McMurtry IF (2005) Vascular remodeling versus vasoconstriction in chronic hypoxic pulmonary hypertension: a time for reappraisal? Circ Res 97: 95–98. PMID: 16037575

21. Bauer NR, Moore TM, McMurtry IF (2007) Rodent models of PAH: are we there yet? Am J Physiol Lung Cell Mol Physiol 293: L580–582. PMID: 17660327

22. Gomez-Arroyo JG, Farkas L, Alhussaini AA, Farkas D, Kraskauskas D, Voelkel NF, et al. (2012) The monocrotaline model of pulmonary hypertension in perspective. Am J Physiol Lung Cell Mol Physiol 302: L363–369. doi: 10.1152/ajplung.00212.2011 PMID: 21964406

23. Guihaire J, Haddad F, Boulate D, Decante B, Denault AY, Wu J, et al. (2013) Non-invasive indices of right ventricular function are markers of ventricular-arterial coupling rather than ventricular contractility: insights from a porcine model of chronic pressure overload. Eur Heart J Cardiovasc Imaging 14: 1140–1149. doi: 10.1093/ehjci/jet092 PMID: 23677917

24. Mahapatra S, Nishimura RA, Sorajja P, Cha S, McGoon MD (2006) Relationship of pulmonary arterial capacitance and mortality in idiopathic pulmonary arterial hypertension. J Am Coll Cardiol 47: 799–803. PMID: 16487848

25. Stevens GR, Garcia-Alvarez A, Sahni S, Garcia MJ, Fuster V, Sanz J (2012) RV dysfunction in pulmonary hypertension is independently related to pulmonary artery stiffness. JACC Cardiovasc Imaging 5: 378–387. doi: 10.1016/j.jcmg.2011.11.020 PMID: 22498327

## Parte 2. Modelos de disfunción ventricular izquierda.

### Introducción a los artículos 3 y 4, y manuscrito 1.

La disfunción ventricular izquierda es un componente esencial en la IC. A menudo, es la primera alteración fisiopatológica que inicia la progresión de la enfermedad. Los dos ejemplos paradigmáticos de disfunción ventricular izquierda en el ámbito clínico son la cardiopatía isquémica y la cardiopatía hipertensiva. En el caso de la cardiopatía isquémica, suele ser un daño miocárdico agudo debido a enfermedad coronaria lo que induce una lesión inicial (infarto agudo de miocardio), tras lo cual se inicia el proceso de remodelado ventricular. En cardiopatía hipertensiva, es la exposición prolongada a una poscarga anormalmente elevada lo que induce un remodelado lentamente progresivo que altera la fisiología cardiaca.

En este apartado, la presente Tesis Doctoral ha contribuido con tres trabajos (dos publicados, y otro en fase de revisión) centrados en la caracterización de aspectos concretos de la cardiopatía isquémica y secundaria a sobrecarga de presión como modelos preclínicos. La aportación personal como doctorando en estos estudios se ha centrado tanto en la creación de estos modelos animales, tanto en los procedimientos percutáneos como quirúrgicos, y esencialmente en la adquisición de imagen y análisis de las mismas. He participado en el diseño de los estudios, así como en el análisis estadístico de los resultados y la discusión de los manuscritos.

Las características de estos modelos, según los resultados de estos trabajos, se resumen en la Figura 3.

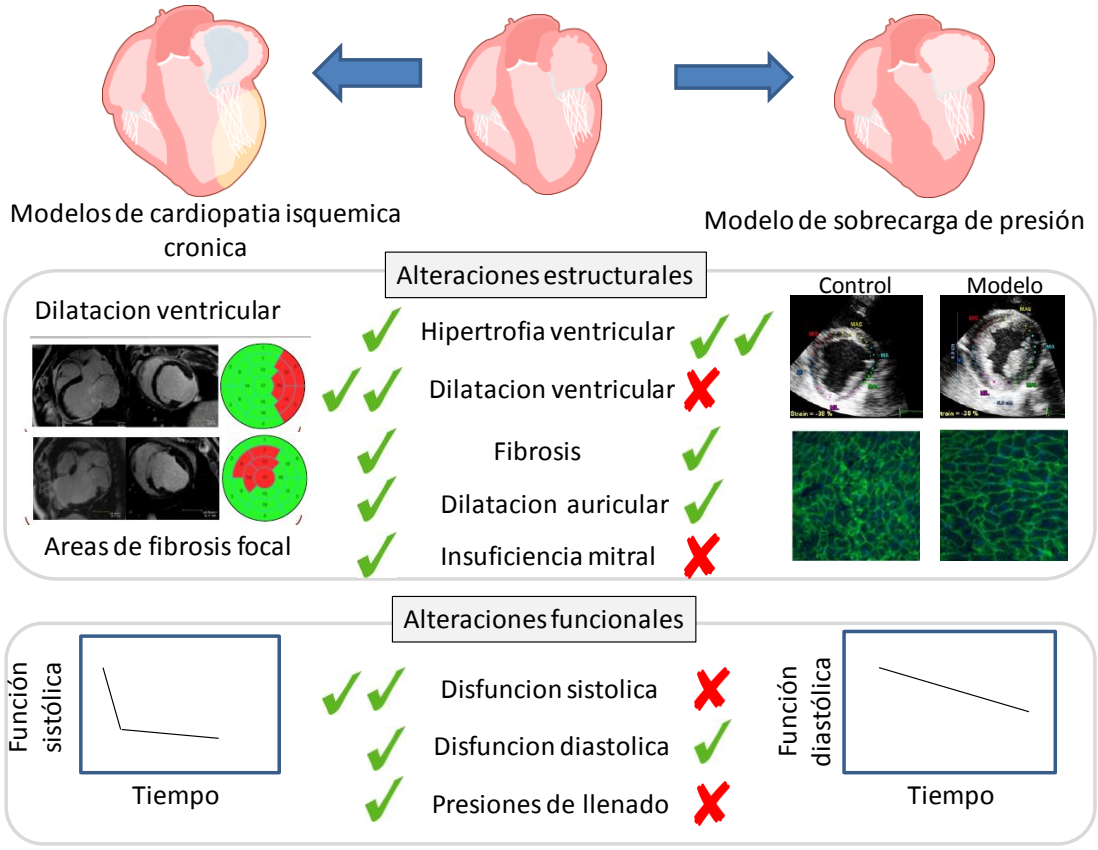


*Figura 3 (Resumen Parte 2, Modelos de disfunción ventricular izquierda). Los modelos de causa isquémica dan lugar a marcadas alteraciones estructurales y funcionales que son bien identificables por técnicas de imagen. En los modelos de sobrecarga de presión, las alteraciones estructurales se producen de forma más progresiva, y los cambios funcionales son más leves.*


Referencias de los artículos.

Artículo 3 [9].

*Ishikawa K, Aguero J, Tilemann L, Ladage D, Hammoudi N, Kawase Y, Santos-Gallego CG, Fish K, Levine RA, Hajjar RJ. Characterizing Preclinical Model of Ischemic Heart Failure: Difference Between LAD and LCx Infarctions. Am J Physiol Heart Circ Physiol. 2014 Nov 15;307(10):H1478-86.*

Artículo 4 [10].

*Ishikawa K, Aguero J, Oh JG, Hammoudi N, A Fish L, Leonardson L, Picatoste B, Santos-Gallego CG, M Fish K, Hajjar RJ. Increased Stiffness is the Major Early Abnormality in a Pig Model of Severe Aortic Stenosis and Predisposes to Congestive Heart Failure in the Absence of Systolic Dysfunction. J Am Heart Assoc. 2015 May 20;4(5).*

Manuscrito 1.

*Aguero J, Galan-Arriola C, Fernandez-Jimenez R, Sanchez-Gonzalez J, Ajmone N, Delgado V, Solis J, Lopez GJ, Molina-Iracheta A, Hajjar RJ, Bax JJ, Fuster V, Ibañez B. Left atrial remodeling after acute myocardial infarction: insight into the role of atrial infarction.*

Artículo 3 [9].

*Ishikawa K, Aguero J, Tilemann L, Ladage D, Hammoudi N, Kawase Y, Santos-Gallego CG, Fish K, Levine RA, Hajjar RJ. Characterizing Preclinical Model of Ischemic Heart Failure: Difference Between LAD and LCx Infarctions. Am J Physiol Heart Circ Physiol. 2014 Nov 15;307(10):H1478-86.*

*Am J Physiol Heart Circ Physiol* 307: H1478–H1486, 2014.
First published September 12, 2014; doi:10.1152/ajpheart.00797.2013.

**TRANSLATIONAL PHYSIOLOGY**

# Characterizing preclinical models of ischemic heart failure: differences between LAD and LCx infarctions

**Kiyotake Ishikawa,[1] Jaume Aguero,[1] Lisa Tilemann,[1] Dennis Ladage,[1] Nadjib Hammoudi,[1] Yoshiaki Kawase,[1] Carlos G. Santos-Gallego,[1] Kenneth Fish,[1] Robert A. Levine,[2] and Roger J. Hajjar[1]**

[1]*Cardiovascular Research Center, Icahn School of Medicine at Mount Sinai, New York, New York; and* [2]*Cardiology, Department of Medicine, Massachusetts General Hospital, Boston, Massachusetts*

Submitted 11 October 2013; accepted in final form 11 September 2014

**Ishikawa K, Aguero J, Tilemann L, Ladage D, Hammoudi N, Kawase Y, Santos-Gallego CG, Fish K, Levine RA, Hajjar RJ.** Characterizing preclinical models of ischemic heart failure: differences between LAD and LCx infarctions. *Am J Physiol Heart Circ Physiol* 307: H1478–H1486, 2014. First published September 12, 2014; doi:10.1152/ajpheart.00797.2013.—Large animal studies are an important step toward clinical translation of novel therapeutic approaches. We aimed to establish an ischemic heart failure (HF) model with a larger myocardial infarction (MI) relative to previous studies, and characterize the functional and structural features of this model. An MI was induced by occluding the proximal left anterior descending artery (LAD; $n = 15$) or the proximal left circumflex artery (LCx; $n = 6$) in Yorkshire pigs. Three pigs with sham procedures were also included. All pigs underwent hemodynamic and echocardiographic assessments before MI, at 1 mo, and 3 mo after MI. Analyses of left ventricular (LV) myocardial mechanics by means of strains and torsion were performed using speckle-tracking echocardiography and compared between the groups. The proximal LAD MI approach induced larger infarct sizes (14.2 ± 3.2% vs. 10.6 ± 1.9%, $P = 0.03$), depressed systolic function (LV ejection fraction; 39.8 ± 7.5% vs. 54.1 ± 4.6%, $P < 0.001$), and more LV remodeling (end-systolic volume index; 82 ± 25 ml/m$^2$ vs. 51 ± 18 ml/m$^2$, $P = 0.02$, LAD vs. LCx, respectively) compared with the LCx MI approach without compromising the survival rate. At the papillary muscle level, echocardiographic strain analysis revealed no differences in radial and circumferential strain between LAD and LCx MIs. However, in contrast with the LCx MI, the LAD MI resulted in significantly decreased longitudinal strain. The proximal LAD MI model induces more LV remodeling and depressed LV function relative to the LCx MI model. Location of MI significantly impacts the severity of HF, thus careful consideration is required when choosing an MI model for preclinical HF studies.

anterior; posterior; remodeling; torsion; sphericity

THE STATISTICAL REPORT FROM the American Heart Association revealed a decline in mortality attributable to cardiovascular diseases by 30.6% in the last decade. However, one out of three patients still die from cardiovascular diseases in the US and the mortality in heart failure (HF) patients remains high (31). Significant progresses in treatment devices as well as modern pharmacotherapy have improved prognoses, while efforts on greater improvements continue. Several novel treatments for HF including gene therapy and cell therapy, and novel pharmaceuticals show promising results in small animal experimental studies. However, structural and physiological differences between human and small animals (27) continue to limit their clinically relevant predictive value for translating to humans. Hence, the need for large animal studies is still required to validate the efficacy and safety of these novel treatments in more clinically relevant models of HF.

There are several large animal models of HF using diverse species. Pigs, dogs, and sheep are frequently used animals in translational experimental studies of cardiovascular diseases (18). Among them, the pig is most common due to similar coronary anatomies to humans, lack of inherent coronary collaterals, and ease of handling (14). HF can be induced by ischemia (23, 34), rapid pacing (1), mitral valve regurgitation (20), etc. Although all the models result in different phenotypes representing different etiology, ischemic HF due to myocardial infarction (MI) is the most widely accepted HF model (13, 18). Not only does this approach recapitulate the most prevalent etiology in human HF, but it also includes left ventricular remodeling and neurohormonal activation, which are important components of HF (6). Several studies have used the porcine ischemic HF model to test various treatments with successful results (8, 24, 29, 35, 37). However, most studies induce MI at the mid-left anterior descending artery (LAD) or at the left circumflex artery (LCx), which are usually not sufficient to cause enough dysfunction that develops severe HF in clinical situation. In patients with severe ischemic HF, who are the candidates for the novel therapies, there usually exist a very large MI or multiple moderate-sized MIs of different coronary territories. Therefore, the ideal preclinical model should have largest MI as possible to represent these populations. Our aims were to establish a HF model with clinically relevant large MI by occluding proximal LAD and to characterize the model by comparing the structural and functional phenotype with that of LCx MI in pigs. In addition to general left ventricular (LV) function parameters, we used echocardiographic speckle-tracking strain analysis to evaluate the functional differences more closely. Speckle-tracking derived strain and torsion have been shown to provide additional mechanistic insights in evaluating LV function (4, 32). Echocardiographic strain in coronary artery disease improves detection of coronary ischemia, assessment of myocardial viability, and prognosis prediction (11). However, the role of strain and torsion in chronic HF after MI is not fully established, and whether the MI location would impact these parameters at chronic stages remains unknown.

Address for reprint requests and other correspondence: K. Ishikawa, Cardiovascular Research Center, Mount Sinai School of Medicine, One Gustave L. Levy Place, Box 1030, New York, NY 10029-6574 (e-mail: kiyotake.ishikawa@mssm.edu).

Accordingly, we investigated how these parameters are linked to physiological and structural presentations in ischemic HF after large anterior MI. Because we took advantage of large animal models that have close physiological profiles to human, our models enable the comparison of strain and torsion while eliminating confounding factors such as comorbidities and time from MI.

## METHODS

*Animal protocols.* All animal protocols complied with the National Institutes of Health *Guide for the Care and Use of Laboratory Animals* and standards of United States regulatory agencies. They were approved by the Institutional Animal Care and Use Committee of the Mount Sinai School of Medicine. Yorkshire pigs (18–22 kg) were premedicated using intramuscular Telazol (8.0 mg/kg; Fort Dodge, IA). After the placement of an intravenous line, animals were intubated and ventilated with 100% oxygen. General anesthesia was maintained with intravenous propofol (6–10 $mg \cdot kg^{-1} \cdot h^{-1}$) throughout the procedure. Electrocardiograms and pulse oximeter measurements were recorded at 5-min intervals. Continuous monitoring with an intravenous saline infusion was maintained for a period of 30 min to stabilize the hemodynamic status. Then, all animals underwent echocardiographic assessment, followed by hemodynamic measurement. Pigs received either proximal LAD MI ($n = 15$, LAD group) or proximal LCx MI ($n = 6$, LCx group), and the cardiac performance was evaluated at 1 and 3 mo after MI. Nine pigs with LAD MI overlap with the pigs previously reported in another study (15). The sham-operated group (Sham group) consisted of three animals that received sham procedure without MI.

*Pressure and volume measurements.* The methods for pressure measurement were previously described in detail (15). Briefly, percutaneous punctures were performed to establish the vascular access to the femoral artery and femoral vein. Heparin (100 IU/kg iv) was then administered to maintain an activated coagulation time of 250–300 s. Swan-Ganz catheter (Edwards Lifesciences, Irvine, CA) was proceeded to the main pulmonary artery, and pressure measurements were collected. Approximately 0.25 × BW(kg) ml of cold saline were injected into the inferior vena cava to obtain cardiac output by the thermodilution method. Next, through the femoral arterial sheath, a Millar catheter (Millar Instruments, Houston, TX) was advanced to the LV to obtain hemodynamic parameters. All measurements were performed after the confirmation of hemodynamic stability for 3 min. An MPVS Ultra System (Millar Instruments) was used to acquire analog signal and convert it to digital data. Data analyses were performed using an iox2 application (EmkaTechnologies, Falls Church, VA).

*MI creation.* After cardiac performance evaluation was completed, a bolus of atropine (0.05 mg/kg) and amiodarone (1–3 mg/kg) were given intravenously or intramuscularly. A 1,000-ml saline solution mixed with atropine (0.1 mg/kg), amiodarone (3 mg/kg), and potassium acetate (20 meq) was continuously infused at the rate of 300 ml/h for the duration of the procedure. A 5-Fr hockey-stick catheter (Cordis, Miami, FL) was advanced to the right coronary artery, and the coronary angiography was performed. The catheter was then exchanged for a 7-Fr hockey-stick catheter (Cordis) and advanced to the left coronary artery. After the coronary angiogram, a 0.014-inch guide wire (Abbott, Park, IL) was advanced into either the LAD or LCx, depending on the animal group. An 8-mm-long, 4.0-mm VOYAGER over-the-wire balloon (Abbott) was advanced to the proximal part of the coronary artery. The balloon was then inflated to 3 to 4 atm for 90–120 min followed by reperfusion (Fig. 1). In two LCx MI pigs, an embolic coil was implanted at the balloon occlusion site after 60 min of coronary occlusion. At the end of the study, these pigs showed similar hemodynamic profiles to the pigs that received 90 min occlusion/reperfusion of the LCx, thus grouped together as the LCx MI group. In case of malignant arrhythmia, direct current shock was applied immediately with continuous chest compression. After confirmation of hemodynamic stability, animals were allowed to recover. Intramuscular injections of nitroglycerine and furosemide were administered. Intravenous saline with amiodarone, atropine, and potassium acetate infusion is decreased to 50 ml/h and was given overnight. The animals were housed in their cages and examined daily for any signs of pain or distress. The visual guidance of the procedure is available in Ishikawa et al (17).

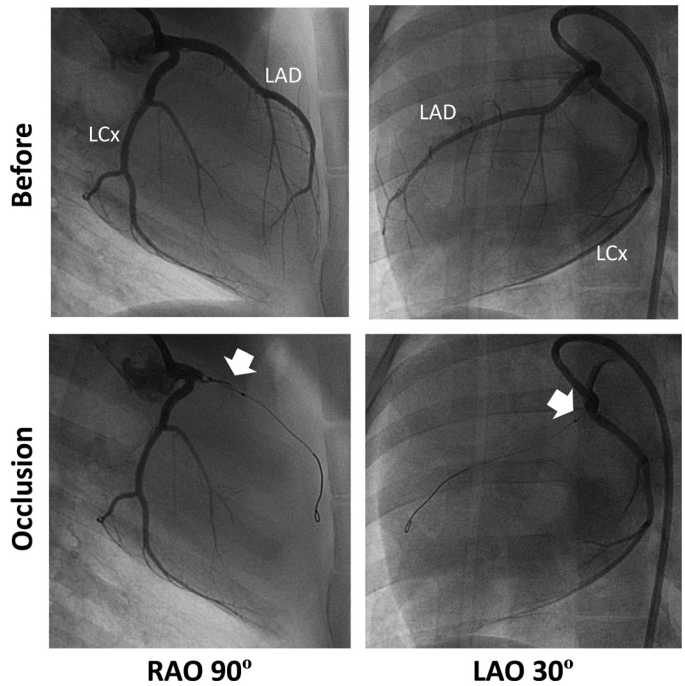


Fig. 1. Representative images of balloon occlusion site. Balloon is inflated at the proximal left anterior descending artery (LAD). Images at *top* show before the occlusion, and images at *bottom* show during the occlusion. Arrows indicate the position of the balloon. LCx, left circumflex artery.

*Echocardiographic analysis.* Comprehensive trans-thoracic echocardiographic studies including Doppler, two-dimensional (2-D), and three-dimensional (3-D) echocardiography were performed at baseline (before MI), 1 mo, and 3 mo. A Philips iE-33 ultrasound system (Philips Medical Systems, Andover, MA) was used to acquire echocardiographic data with a multi-frequency imaging transducer (S5 probe for 2-D images or X3 probe for 3-D images). A subxiphoid approach provided an apical four-chamber view as well as 3-D images of the LV. With the use of the parasternal approach, cross-sectional images of the LV short axis were obtained at the levels of the base, papillary muscle, and apex with a high frame rate (60–100 Hz). The 2-D images were loaded into the Q-lab application (version 7.0; Philips Medical Systems) for strain analysis using a speckle-tracking algorithm. LV volumes and ejection fraction (EF) were obtained from 3-D images. Body surface area (in $m^2$) was calculated as previously described (21), and volume parameters were divided by the body surface area to calculate volume indexes. Longitudinal strain (LS) was obtained from apical four-chamber views. Short axis images from the papillary muscle level were used for the circumferential and radial strain (CS and RS, respectively) analyses. The LV short axis was divided into six segments and categorized into three zones as previously described: ischemic, border, and remote areas. A good inter- and intra-observer agreement has been previously reported with this method (16) and Cronbach's $\alpha$ for inter- and intra-observer variation in the present study were 0.93 and 0.98 for CS, 0.69 and 0.99 for RS, 0.94 and 0.96 for LS, and 0.76 and 0.88 for torsion, respectively. LV short-axis planes of basal and apical levels provided rotation curves

for each level. LV twist was calculated as the instantaneous net difference in rotation between the apical and basal levels, and the peak value was obtained. LV sphericity index was calculated at end diastole using 3-D images as previously reported (22). Left atrium size was measured as a diameter from right superior pulmonary vein to the root of left appendage.

*Survival.* To investigate the survival rate of the pigs that underwent our MI creation protocol, accumulated data of 100 LAD MI and 9 LCx MI pigs in our database were reviewed. Because many of our pigs received some kind of treatment, which may affect the cardiac function after 1 mo, the survival curves were limited to 28 days.

*Postmortem histology.* Hearts were explanted, weighed, and sectioned into six slices. Heart slices were immersed in triphenyl tetrazolium chloride to demarcate the infarct area. Adobe Photoshop CS2 (Adobe Systems, San Jose, CA) was used to quantify the infarction size by digital planimetry.

*Coronary dominance and diagonal branch disparity.* Coronary angiograms of pigs included in survival study were reviewed. Seven pigs were excluded due to ambiguous image of the angiogram. The dominance was defined as previously described (3). In right dominance, both the posterior descending artery and ≥1 posterolateral branches originated from the right coronary artery; in left dominance, posterior descending artery and all posterolateral branches originated from LCx. Balanced, posterior descending artery originated from the right coronary artery, but all posterolateral branches originated from the LCx. To check the diagonal branch disparity, the numbers of large diagonal branch were counted. They were considered large when they had branching or circulated a significant area. When the branch was significantly larger than other branches, it was counted as a major diagonal branch.

*Statistical analysis.* Data are expressed as means ± SD. The Kaplan-Meier method with a log rank test was used to analyze the survival curves. The unpaired *t*-test was used to compare the differences between two groups. For group comparisons, 1-way ANOVA was performed. Levene's test was used to determine whether ANOVA was appropriate. Welch's ANOVA was applied where heterogeneity of variance was indicated. Post hoc analysis was performed using either the Tukey test or the Games-Howell test, depending on the heterogeneity. All $P$ values $<0.05$ were considered statistically significant. Relation between strain and torsion to functional and structural parameters was assessed by Pearson or Spearman correlation as appropriate. Inter- and intra-observer variability was assessed in seven randomly chosen animals from the MI pigs and all three pigs from the sham-operated group.

## RESULTS

A total of 24 pigs were included in the study (LAD, $n = 15$; LCx, $n = 6$; Sham, $n = 3$). One pig from the LCx MI group died at *day 80* without undergoing 3 mo follow up. Postmortem studies indicated no signs of HF, thus malignant arrhythmia was suspected as a cause of death. LVEF decreased significantly 1 mo after MI in both groups, and the dysfunction persisted to the 3-mo time point. There were significant differences in LVEF between LAD and LCx MI at 1 mo and 3 mo (Fig. 2). In contrast, peak LV pressure rate of rise ($dP/dt_{max}$) decreased only in LAD group, whereas LCx and Sham groups had similar values during the study period (Fig. 2). ANOVA revealed that there was a statistical difference only between the Sham and LAD groups at 3 mo; however, direct comparison of LAD versus LCx in MI revealed significantly higher $dP/dt_{max}$ in LCx group both at 1 mo (LCx, 2,204 ± 619 vs. LAD, 1,642 ± 245; $P = 0.007$) and at 3 mo (LCx, 2,142 ± 84 vs. LAD, 1,752 ± 309; $P = 0.02$). Volume indexes showed larger LV sizes in LAD MI pigs with a statistical difference relative to both LCx and Sham group in end-systolic volume index (Fig. 2). Temporal changes of other related parameters are shown in Table 1, indicating decreased systolic function and greater heart remodeling in the LAD group. Interestingly, diastolic function parameters were similarly impaired in the LAD and LCx groups, although statistical significance was only reached when comparing the LAD and Sham groups. Of note, LV end-diastolic pressure was significantly higher in LAD MI

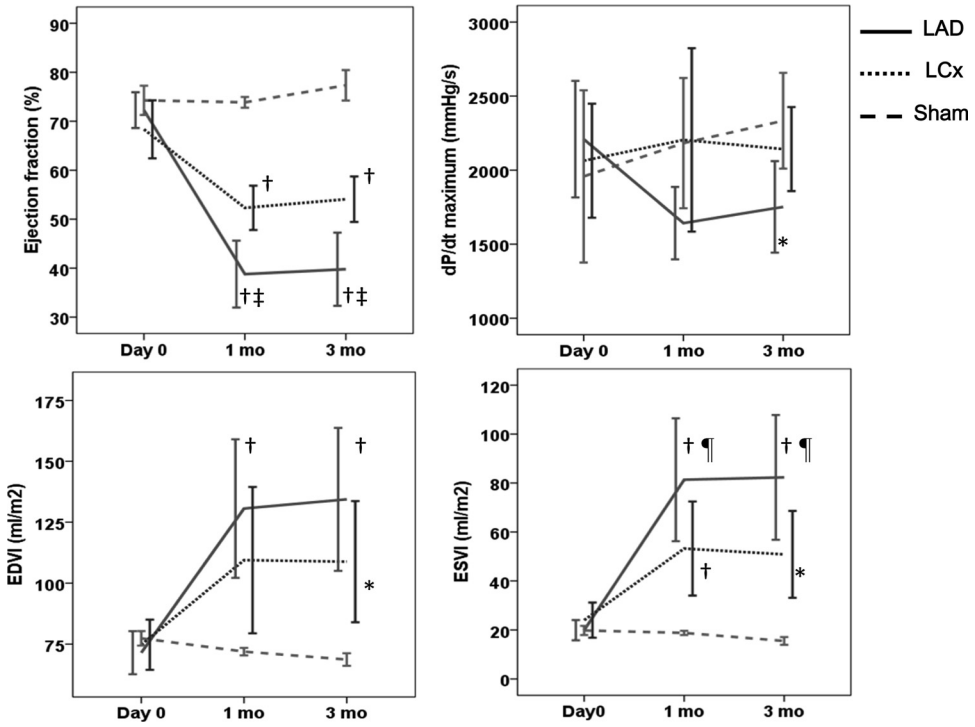


Fig. 2. Temporal changes of systolic parameters and volume indexes. LAD myocardial infarction (MI) had significantly lower ejection fraction and larger end-systolic volume index (ESVI) than both LCx MI and Sham at 1 and 3 mo after the MI. LAD MI showed decreased peak LV pressure rate of rise ($dP/dt_{max}$) after MI; however, LCx MI took similar course to the Sham without significant decrement. Ejection fraction and volume indexes were assessed by 3-dimensional echocardiography. *$P < 0.05$ against Sham; †$P < 0.01$ against Sham; ¶$P < 0.05$ against LCx MI; ‡$P < 0.01$ against LCx MI. EDVI, end-diastolic volume index.

Table 1. *Temporal changes of cardiac parameters after myocardial infarction*

| | Baseline | | | 1 mo | | | 3 mo | | |
|---|---|---|---|---|---|---|---|---|---|
| | LAD | LCx | Sham | LAD | LCx | Sham | LAD | LCx | Sham |
| *n* | 15 | 6 | 3 | 15 | 6 | 3 | 15 | 5 | 3 |
| Body weight, kg | 19.3 ± 1.5 | 19.5 ± 1.5 | 18.7 ± 1.2 | 24.6 ± 1.3 | 24.2 ± 1.8 | 24.3 ± 2.5 | 38.0 ± 3.2 | 40.6 ± 2.8* | 34.3 ± 2.1 |
| Echocardiography | | | | | | | | | |
| Three-dimensional, ml | | | | | | | | | |
| EDV | 36.4 ± 3.5 | 39.0 ± 4.4 | 38.7 ± 1.5 | 78.3 ± 17.1* | 64.9 ± 17.6 | 42.8 ± 3.0 | 107.1 ± 22.9* | 91.0 ± 22.8 | 51.2 ± 1.5 |
| ESV | 10.1 ± 2.0 | 12.5 ± 3.4 | 9.9 ± 1.4 | 48.8 ± 15.1*¶ | 31.6 ± 11.3 | 11.2 ± 0.4 | 65.6 ± 20.0* | 42.6 ± 15.7 | 11.6 ± 1.4 |
| SV | 26.2 ± 2.3 | 26.5 ± 1.4 | 28.8 ± 1.3 | 29.5 ± 4.0 | 33.3 ± 6.5 | 31.6 ± 2.7 | 41.5 ± 6.7¶ | 50.4 ± 8.6* | 39.6 ± 2.6 |
| E/A | 1.27 ± 0.24 | 1.31 ± 0.16 | 1.29 ± 0.24 | 1.16 ± 0.27 | 1.28 ± 0.86 | 1.37 ± 0.17 | 1.03 ± 0.25 | 1.19 ± 0.40 | 1.34 ± 0.35 |
| Left atrium, mm | 33 ± 5 | 35 ± 7 | 35 ± 5 | 38 ± 4 | 39 ± 7 | 36 ± 2 | 44 ± 3* | 44 ± 8 | 38 ± 1 |
| Invasive hemodynamics | | | | | | | | | |
| $LVP_{max}$, mmHg | 109 ± 18 | 102 ± 14 | 100 ± 8 | 115 ± 12 | 110 ± 5 | 111 ± 13 | 122 ± 9 | 122 ± 18 | 129 ± 27 |
| End-diastolic pressure, mmHg | 14.4 ± 4.3 | 11.8 ± 1.5 | 11.1 ± 0.6 | 25.9 ± 9.5*¶ | 15.8 ± 4.5 | 15.9 ± 3.3 | 19.2 ± 6.3¶ | 10.9 ± 3.8 | 16.3 ± 3.5 |
| CI, $l/m^2$ min | 4.0 ± 1.4 | 3.1 ± 0.9 | 2.9 ± 1.0 | 3.7 ± 0.7 | 4.1 ± 0.5 | 4.0 ± 0.8 | 3.7 ± 0.7 | 4.0 ± 1.0 | 3.8 ± 0.9 |
| HR, beats/min | 78 ± 22 | 75 ± 19 | 51 ± 16 | 69 ± 13 | 77 ± 23 | 62 ± 3 | 73 ± 12 | 77 ± 12 | 64 ± 9 |
| $dP/dt_{min}$, mmHg/s | −1,715 ± 614 | −1,491 ± 456 | −1,313 ± 89 | −1,417 ± 367* | −1,508 ± 371 | −2,078 ± 223 | −1,891 ± 393* | −2,018 ± 431 | −2,842 ± 769 |
| τ, ms | 46.4 ± 21.7 | 50.0 ± 24.5 | 47.4 ± 14.1 | 45.6 ± 19.4 | 41.3 ± 12.3 | 29.6 ± 1.2 | 38.8 ± 9.7* | 36.7 ± 3.9 | 25.4 ± 3.5 |

Values are means ± SD. LAD, left anterior descending artery; LCx, left circumflex artery; EDV, end-diastolic volume; ESV, end-systolic volume; SV, stroke volume; E/A, mitral valve early and late ventricular filling velocity ratio; $LVP_{max}$, maximum left ventricular pressure; CI, cardiac index measured by Swan-Ganz; HR, heart rate; $dP/dt_{min}$, minimum peak LV pressure rate of decay. *$P < 0.05$ against sham; ¶$P < 0.05$ against LCx.

group than LCx MI group both at 1 mo and 3 mo time point, indicating severe HF condition.

*Scar size.* Representative images of LV at 3 mo are shown in Fig. 3. Although LAD MI involved apex in all the pigs, LCx MI tended to have larger scar at the base and lesser extent toward the apex. Scar size was larger in LAD pigs compared with LCx (14.2 ± 3.2% vs. 10.6 ± 1.9%, $P = 0.03$); however, LV weight was not different between the groups (Fig. 4).

*Mitral valve regurgitation.* Eight pigs in the LAD MI group (53%) and three pigs in the LCx MI group (60%) developed a Seller's grade of 1 to 2 mitral valve regurgitation, whereas none of the pigs presented with more than a grade 3 mitral valve regurgitation at 3 mo.

*Survival.* Four pigs were excluded from the survival analysis because they reached humane endpoints and were euthanized due to prolonged lameness ($n = 2$) and deaths from intubation problems ($n = 2$). Out of 96 recent pigs, the survival rate of LAD MI at 1 mo was 81% and that of LCx was 88% ($P = 0.62$) (Fig. 5). Whereas most of the nonsurviving pigs died during or within 48 h post-MI creation, there were three deaths in LAD MI group after that period. All three of them had significant amount of pleural effusion, suggesting the involvement of HF for the cause of the deaths.

*LV strain, torsion, and sphericity.* Both RS and CS of ischemic area were significantly lower than those of remote area in MI pigs. RS and CS in the remote area in MI groups were lower compared with the average of all areas of Sham. Similarly, global RS and global CS at the papillary muscle level were reduced in MI pigs. However, there were no significant differences in RS or CS between LAD and LCx (Fig. 6). In contrast, LS was significantly lower in the LAD group compared with the LCx group, while both showed lower values compared with the Sham group (Fig. 6). LV torsion was significantly lower than that of the Sham group, but there was no difference found between LAD and LCx groups. Table 2 shows the relationship of strain and torsion to functional and structural parameters in MI pigs. Whereas RS and CS did not show any significant correlation to these parameters, torsion showed modest correlation to EF, $dP/dt_{max}$, end-systolic volume, and scar size. Moreover, LS showed stronger correlation to these important parameters of physiological and morphological indexes. Pigs with LCx MI had highest LV sphericity index among the groups with significant difference to the Sham group (Fig. 6).

*Coronary dominance and diagonal branch disparity.* Although majority of pigs showed balanced coronary circulation between the left coronary artery and the right coronary artery, there were ~10% each of pigs with either left or right coronary dominance. The dominance was mainly determined by the different balance between the LCx and the right coronary artery. Although the total of the LAD main and side branches circulate similar size of the anterior area, the size and numbers of diagonal branches showed modest variability. Out of 102 pigs with a good quality coronary angiogram, 22% had only one large diagonal branch, whereas 44% had two large branches and 34% had more than three large branches (see METHODS for the definition of large branch). First diagonal branch was the major branch in 27% of the pigs, which can lead to smaller infarct size when the distal of first diagonal branch was occluded during MI induction.

## DISCUSSION

In this study, we have established the successful creation of preclinical HF models with large anterior MIs while maintaining reasonable mortality for at least 3 mo. Additionally, we found that the proximal LAD MI resulted in more severely impaired LV function, larger infarct size, and more remodeled LV compared with LCx MI, but with similar mortality. Furthermore, we compared, for the first time, the myocardial strain and torsion between LAD and LCx MI in chronic stages after MI. Although RS, CS, and torsion did not differ between the different MI groups, LS was significantly lower in LAD MI pigs.

Emerging novel therapies, newly discovered drugs, and evolving technologies are offering promising options for treating patients with severe HF. To validate the efficacy and safety of each treatment, careful evaluation is necessary before it can be translated to the clinic. Large animal preclinical studies in addition to small animal studies are essential because of sim-

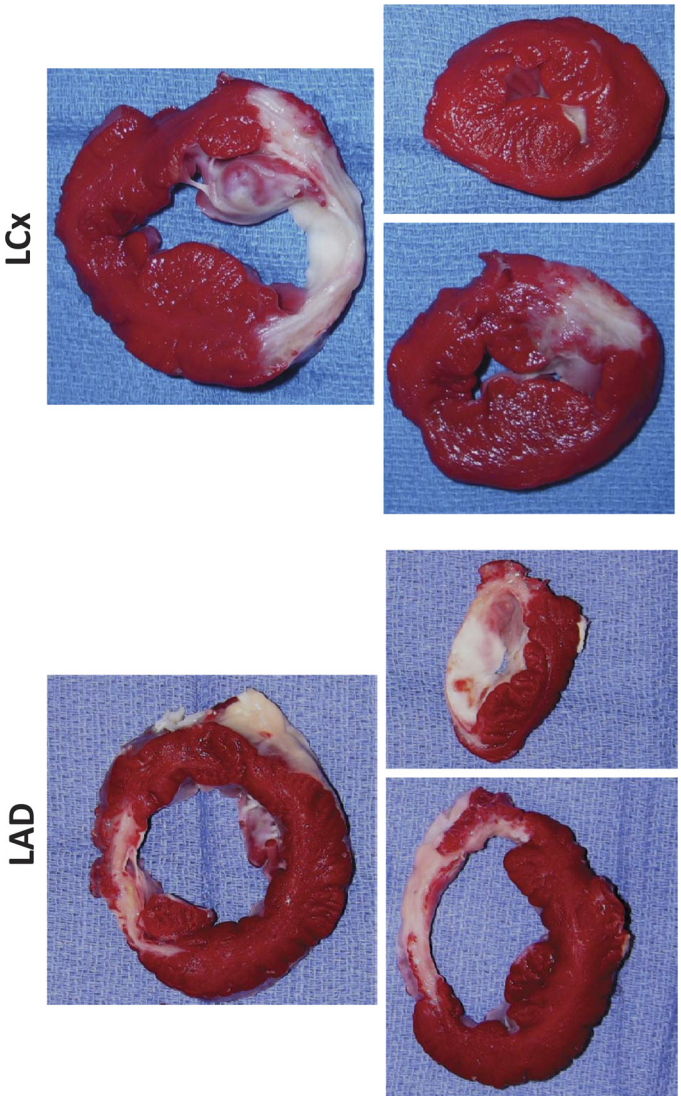


Fig. 3. Representative images of the infarct in LAD and LCx MI. Although the scar in LAD MI involves apex, the scar of LCx MI was shifted toward base with less apical involvement to the left anterior.

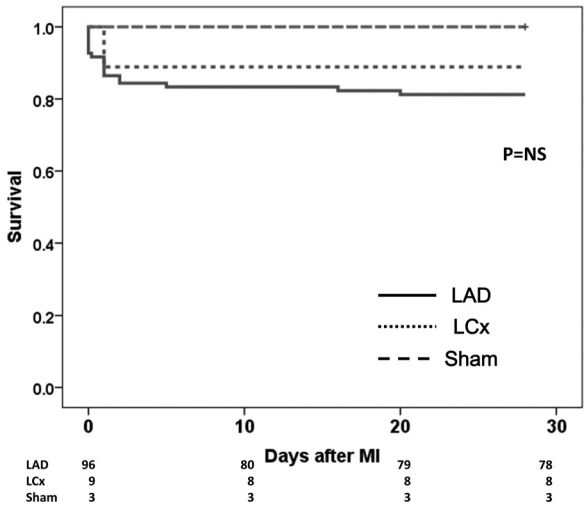


Fig. 5. Survival curves of each group. Similar survival rate up to 1 mo was seen in LAD ($n$ = 96) and LCx MI ($n$ = 9). Note that there are a few deaths after 48 h due to heart failure in LAD group.

ilarities in metabolic rates, anatomy, size, and cardiac functional properties to humans (27). Ideally, the large animal HF models should have significant cardiac dysfunction reflecting the clinical candidates for the novel therapies. However, if the myocardial injury is too severe, the mortality becomes too high. Current ischemic HF models often balance survival rate and cardiac dysfunction; thus the infarct size is somewhat compromised. In most previous studies, the location of coronary occlusion took place at the mid-LAD or LCx. Our proximal LAD MI model results in larger anterior MIs, which mimic the clinical ischemic HF phenotype while maintaining the similar mortality in previous studies (19, 33, 35). It is clear that proximal LAD occlusion induces larger infarct sizes than mid-LAD occlusion, since the first diagonal branch is involved. Although proximal LCx was occluded in our study, most of the parameters indicated a less severe MI relative to the LAD MI model. Moreover, $dP/dt_{max}$ of the LCx MI group was not significantly different than the Sham group. Furthermore, LV volumes were more increased in LAD MI group, indicating more severe post-MI LV remodeling than in the LCx MI group. It has been shown that infarct expansion occurs predominantly in MI associated with the LAD (28). Therefore, the remodeling process is more intensified after LAD MI and thus recapitulates important characteristic of clinical HF development. In accordance with the model of ischemic HF, interstitial fibrosis of the remote myocardium was also observed in our models (data not shown). The model with a larger MI may also have an advantage in evaluating therapeutic efficacy. In fact,

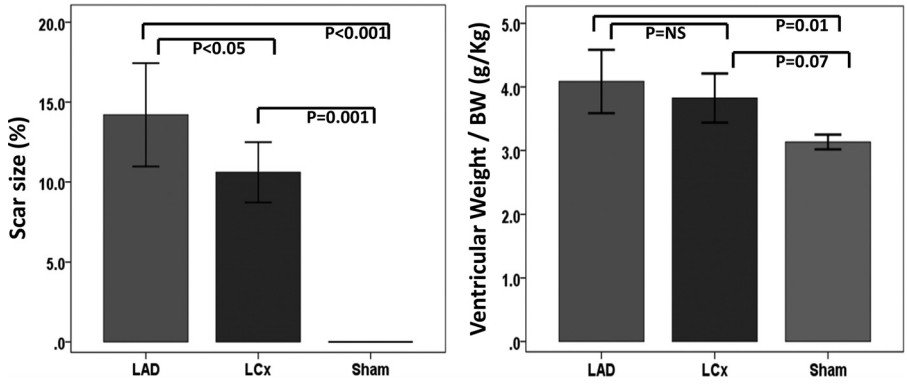


Fig. 4. Scar size and the ventricular weight adjusted by the body weight (BW). Size of the scar was significantly larger in LAD MI than in LCx MI. In LAD MI, despite the initial infarct area of 35–40% assessed by MRI, infarct size becomes to around 15% at 3 mo because of scar thinning and hypertrophy of nonischemic remote area. Ventricular weight increased in MI pigs without statistical difference between the MI groups. NS, not significant.

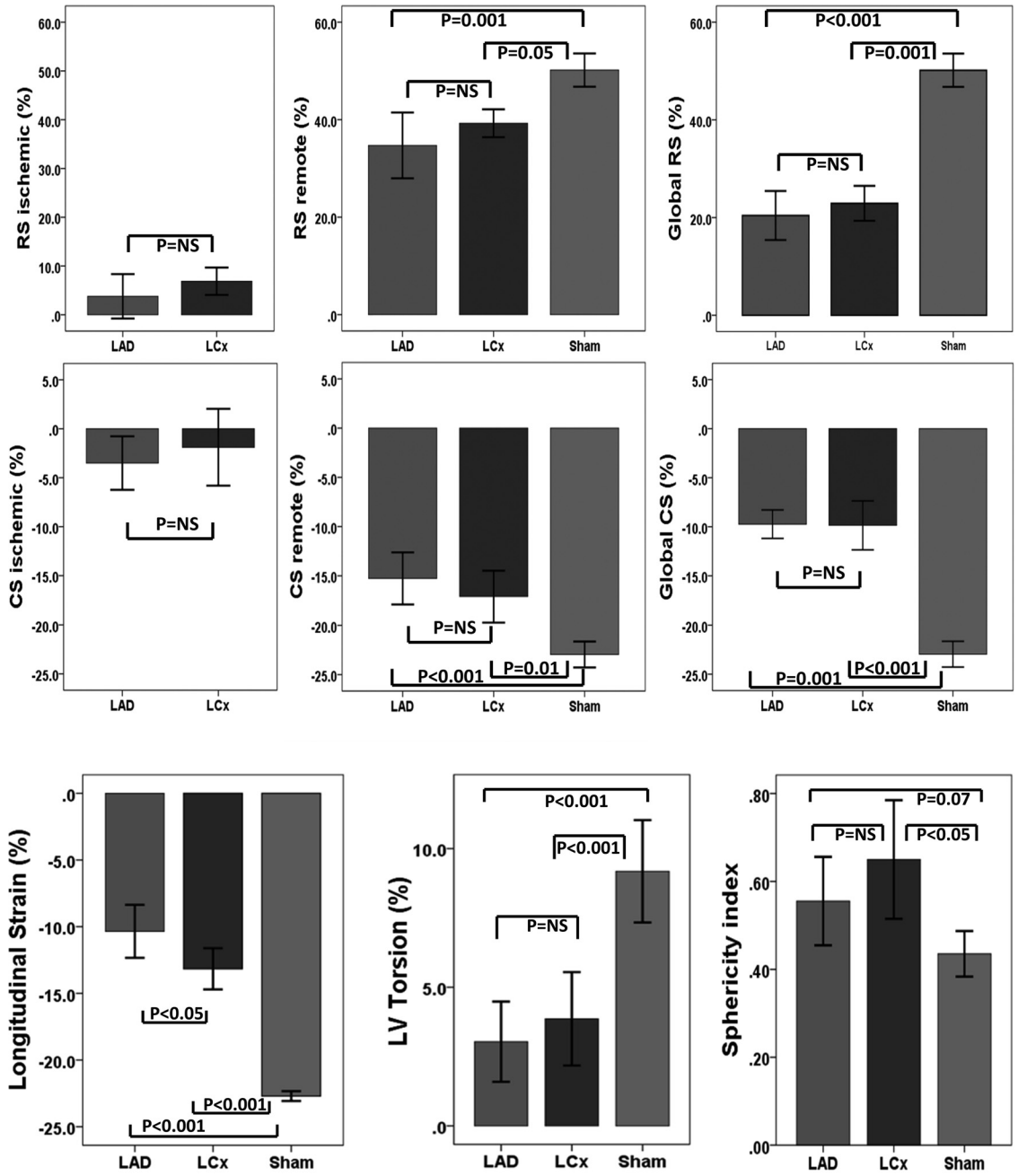


Fig. 6. Left ventricular (LV) strain, torsion, and sphericity by 2-dimensional echocardiography 3 mo after MI. The LV short axis was divided into 6 segments and categorized into 3 zones: ischemic, border, and remote areas. Radial strain (RS) and circumferential strain (CS) were analyzed at the papillary muscle level. Both MI groups presented impaired RS and CS at the remote area, as well as global RS and CS compared with Sham. Sham values are average of all the segments. LAD MI presented significantly lower longitudinal strain (LS) than LCx MI. LV torsion was significantly less in MI groups than in Sham; however, no difference was found between LAD and LCx MI. LV sphericity index was higher in MI pigs than in Sham.

meta-analysis of stem cell therapy in preclinical studies revealed that the LAD-related infarction, when compared with the LCx infarction, benefits more from the treatment (37). This is presumably attributed to the larger infarct size, lower cardiac function, and increased cardiac remodeling (37).

There are several important characteristics of our protocol required to achieve severe dysfunction without raising the mortality. First, we use propofol as anesthetic agent instead of isoflurane. Although isoflurane is an easily administered inhalant anesthetic, it is cardio-protective and a vasodilator (36). Because it acts similar to β-blockers, isoflurane anesthesia may result in smaller infarct sizes. Maintaining blood pressure over 80 mmHg during the coronary occlusion enhances recovery from malignant arrhythmia. Propofol is also beneficial in maintaining higher blood pressures, because the blood lowering effect is much lower than in cases where isoflurane is used (2). When the blood pressure falls below 80 mmHg, fluid load and/or atropine should be administered to maintain the pressure. In cases of malignant arrhythmia, continuous chest compression and immediate cardioversion are critical to pig sur-

Table 2. *Correlation of strain and torsion to functional and structural parameters at 3 mo after myocardial infarction*

| | Ejection Fraction | EDV | ESV | SV | $LVP_{max}$ | $dP/dt_{max}$ | HR | CI | Scar Size |
|---|---|---|---|---|---|---|---|---|---|
| Longitudinal strain | −0.77** | 0.42 | 0.61** | −0.45 | 0.07 | −0.54* | −0.26 | −0.66** | 0.81** |
| Global circumferential strain | −0.07 | 0.17 | 0.17 | 0.25 | 0.21 | −0.31 | 0.24 | −0.34 | 0.17 |
| Global radial strain | 0.30 | −0.27 | −0.34 | −0.04 | −0.2 | 0.13 | −0.03 | 0.41 | −0.42 |
| Torsion | 0.54* | −0.37 | −0.45* | 0.18 | 0.07 | 0.46* | 0.04 | 0.37 | −0.52* |

Values indicate Pearson or Spearman's correlation coefficient, depending on the distribution. Sham-operated animals are not included. $dP/dt_{max}$, peak LV pressure rate of rise. *$P < 0.05$; **$P < 0.01$.

vival during this acute phase. Finally, continuous administration of amiodarone and maintaining the potassium level reduce arrhythmic deaths during the peri-MI period.

Although ischemic MI models are the most frequently used, the differences in LAD MI and LCx MI have not been well documented. The present study investigated the differences in various parameters including systolic and diastolic function and volumetric parameters between different branch MIs. Our results indicate that the LAD MI model induces more LV remodeling and has decreased systolic function relative to the LCx MI model. The infarction area of the LAD MI model was shifted to the apical region, whereas the LCx MI model had basal dominancy. Similar findings were documented in patients with MI when the scar was analyzed with magnetic resonance imaging (5). Although LV rotation is most prominent at the apical LV (26), there was no difference between LAD and LCx MI models in our study. This suggests that mid-ventricular myocardial fibers play important role on generating LV twist mechanics. Notwithstanding, torsion yet showed modest correlation to functional and structural indexes, suggesting the important role in cardiac contraction. Despite the functional differences, myocardial strain analyses revealed no differences in RS and CS at the papillary muscle level between the different MI groups. Meanwhile, LS was significantly lower in the LAD MI group. Hoit et al. investigated the different impact of LAD and LCx ischemia on remote areas in the acute setting and demonstrated that compensatory increases of ejection phase shortening were only present after LCx ischemia (12). However, similar RS and CS in the remote area in our study suggests that this was not the case in chronic phase of MI. Our results indicate diminished longitudinal contraction together with larger infarct size is responsible for the lower cardiac function in LAD MI. Correlation of strain to various functional and structural parameters indicated that LS reflects important features of HF the most, suggesting the usefulness of LS in evaluating chronic ischemic HF. Utility of LS to estimate scar size has been demonstrated in patients with chronic LV dysfunction (30), and our data are consistent with this finding. Despite less remodeling with preserved systolic function in LCx MI compared with LAD MI, sphericity index was higher in LCx MI. Although spherical shape is an important feature of LV remodeling in heart failure (9) and sphericity index is applied as a parameter to assess LV remodeling (7), our data suggest that the location of MI influences this index after MI.

In sheep, Llaneras et al. reported that the ligation of the second and third LCx obtuse marginal branches resulted in a reproducible mitral valve regurgitation over the 8 wk follow up (25). Because mitral valve regurgitation is an important determinant of HF progression in patients after MI, we investigated the prevalence of this phenomenon in our models. However, proximal occlusion of the LCx was unable to induce significant mitral valve regurgitation in our pigs. We therefore conducted a preliminary study to determine whether we can induce ischemic mitral valve regurgitation in pigs. Concurrent occlusion of the LCx and the diagonal branch successfully resulted in reproducible mitral valve regurgitation in 3 pigs (supplementary video). Notwithstanding, all three pigs developed such severe HF that none of the pigs were able to undergo hemodynamic evaluation at 3 mo after the MI induction. This model may be useful for testing surgical or device therapy targeting mitral valve insufficiency at the sub-acute stage of MI; however, more extensive investigation would be required to establish this model.

We observed more variability in the circulatory area of the LCx compared with the LAD in our pigs. The main LAD branch presented similar length, and the variability of the LAD mostly depended on the sizes of the diagonal branches. However, the overall circulatory areas of diagonal branches were relatively similar when taken together. In contrast, the LCx shared the posterior wall with the right coronary artery to the different degree. Although all the LCx MI pigs in our study had balanced coronary arteries, 20% of the pigs have either right coronary artery or LCx dominance. This is a major disadvantage to the LCx MI model, since there is already 10–30% inter-animal variability in various parameters even with similar coronary circulation area. This also applies to the LAD MI model when the distal of first diagonal branch is occluded because the inter-individual size variability is high. By creating an MI using the proximal LAD occlusion approach, we can diminish the impact of differences in diagonal branch disparity. In summary, our results suggest that proximal LAD MI model is more suited to study chronic HF experiments considering that it has larger infarct size, worse LV function, more LV remodeling, and less variability compared with those of the LCx MI model. It is important to note that LCx MI model is still useful for many of the studies that are not targeting advanced HF such as prevention of ischemic-reperfusion injury studies (10).

### *Limitation*

The major limitation in the present study is a small sample size, especially in the LCx MI and sham-operated groups. Although our study might be underpowered to detect small differences between the groups, we found significant differences in LVEF, end-systolic volume, and scar size between LAD and LCx MI pigs. Observing differences in these important parameters clearly indicate that LAD MI has more severe HF compared with LCx MI. Therefore, we believe our primary motivation of establishing a porcine ischemic HF model with clinically relevant large MI was achieved. Although LAD proximal occlusion can minimize the effect of diagonal branch

disparity, there still remains a significant degree of inter-animal variability after MI induction. Uniform dysfunction may be ideal for the preclinical data interpretation; however, the inter-individual variability can be often found in clinical situations as well. Therefore, we believe it reflects the clinical population, and when conducting a translational study, we suggest a comparison of parameters before and after the treatment rather than comparing groups only after treatments. We did not include a distal LAD occlusion model in the present study, and this model may result in similar characteristics to LCx MI. However, because LCx MI was also induced by occlusion of the proximal LCx, we believe comparing proximal LAD MI with proximal LCx MI model is more appropriate.

### *Conclusion*

Occluding the proximal LAD in pigs induces larger infarct size, depressed systolic function, and more extensive cardiac remodeling than the LCx MI model. Location of MI significantly impacts the severity of HF; thus careful consideration is required when choosing an MI model for preclinical HF studies. LAD MI model reflects important features of clinical HF more and thus may be suited for preclinical studies involving HF. Greater impaired LS after LAD MI is one of the key mechanisms for the decreased systolic function over the LCx MI model.

#### ACKNOWLEDGMENTS

We thank Lauren Leonardson for providing excellent technical assistance and expertise.

#### GRANTS

This work is supported by a grant from Leducq Foundation (to R. J. Hajjar) and by National Heart, Lung, and Blood Institute, as a Program of Excellence in Nanotechnology (PEN) Award, Contract No. HHSN268201000045C, and Grants R01-HL-093183, HL-088434, HL-071763, HL-080498, HL-083156, and P20-HL-100396 (to R. J. Hajjar). J. Aguero was supported by Spanish Society of Cardiology (Ischemic Heart Disease section) and Fundacion Alfonso Martin-Escudero. N. Hammoudi was supported by French Federation of Cardiology. D. Ladage was supported by the German Research Foundation.

#### DISCLOSURES

No conflicts of interest, financial or otherwise, are declared by the author(s).

#### AUTHOR CONTRIBUTIONS

Author contributions: K.I., J.A., D.L., Y.K., R.A.L., and R.J.H. conception and design of research; K.I., J.A., L.T., D.L., Y.K., and C.G.S.-G. performed experiments; K.I., J.A., L.T., N.H., and C.G.S.-G. analyzed data; K.I., J.A., L.T., N.H., K.F., R.A.L., and R.J.H. interpreted results of experiments; K.I. and K.F. prepared figures; K.I., K.F., and R.J.H. drafted manuscript; K.I., J.A., L.T., D.L., N.H., Y.K., C.G.S.-G., K.F., R.A.L., and R.J.H. edited and revised manuscript; K.I., J.A., L.T., D.L., N.H., Y.K., C.G.S.-G., K.F., R.A.L., and R.J.H. approved final version of manuscript.

#### REFERENCES

1. **Chow E, Woodard JC, Farrar DJ.** Rapid ventricular pacing in pigs: an experimental model of congestive heart failure. *Am J Physiol Heart Circ Physiol* 258: H1603–H1605, 1990.
2. **Deryck YL, Brimioulle S, Maggiorini M, de Canniere D, Naeije R.** Systemic vascular effects of isoflurane versus propofol anesthesia in dogs. *Anesth Analg* 83: 958–964, 1996.
3. **Goldberg A, Southern DA, Galbraith PD, Traboulsi M, Knudtson ML, Ghali WA.** Coronary dominance and prognosis of patients with acute coronary syndrome. *Am Heart J* 154: 1116–1122, 2007.
4. **Gorcsan J, 3rd, Tanaka H.** Echocardiographic assessment of myocardial strain. *J Am Coll Cardiol* 58: 1401–1413, 2011.
5. **Gotte MJ, van Rossum AC, Marcus JT, Kuijer JP, Axel L, Visser CA.** Recognition of infarct localization by specific changes in intramural myocardial mechanics. *Am Heart J* 138: 1038–1045, 1999.
6. **Haitsma DB, Bac D, Raja N, Boomsma F, Verdouw PD, Duncker DJ.** Minimal impairment of myocardial blood flow responses to exercise in the remodeled left ventricle early after myocardial infarction, despite significant hemodynamic and neurohumoral alterations. *Cardiovasc Res* 52: 417–428, 2001.
7. **Hare JM, Fishman JE, Gerstenblith G, DiFede Velazquez DL, Zambrano JP, Suncion VY, Tracy M, Ghersin E, Johnston PV, Brinker JA, Breton E, Davis-Sproul J, Schulman IH, Byrnes J, Mendizabal AM, Lowery MH, Rouy D, Altman P, Wong Po Foo C, Ruiz P, Amador A, Da Silva J, McNiece IK, Heldman AW, George R, Lardo A.** Comparison of allogeneic vs autologous bone marrow-derived mesenchymal stem cells delivered by transendocardial injection in patients with ischemic cardiomyopathy: the POSEIDON randomized trial. *JAMA* 308: 2369–2379, 2012.
8. **Hatzistergos KE, Quevedo H, Oskouei BN, Hu Q, Feigenbaum GS, Margitich IS, Mazhari R, Boyle AJ, Zambrano JP, Rodriguez JE, Dulce R, Pattany PM, Valdes D, Revilla C, Heldman AW, McNiece I, Hare JM.** Bone marrow mesenchymal stem cells stimulate cardiac stem cell proliferation and differentiation. *Circ Res* 107: 913–922, 2010.
9. **Hees PS, Fleg JL, Lakatta EG, Shapiro EP.** Left ventricular remodeling with age in normal men versus women: novel insights using three-dimensional magnetic resonance imaging. *Am J Cardiol* 90: 1231–1236, 2002.
10. **Hinkel R, Boekstegers P, Kupatt C.** Adjuvant early and late cardioprotective therapy: access to the heart. *Cardiovasc Res* 94: 226–236, 2012.
11. **Hoit BD.** Strain and strain rate echocardiography and coronary artery disease. *Circ Cardiovasc Imaging* 4: 179–190, 2011.
12. **Hoit BD, Lew WY.** Functional consequences of acute anterior vs. posterior wall ischemia in canine left ventricles. *Am J Physiol Heart Circ Physiol* 254: H1065–H1073, 1988.
13. **Houser SR, Margulies KB, Murphy AM, Spinale FG, Francis GS, Prabhu SD, Rockman HA, Kass DA, Molkentin JD, Sussman MA, Koch WJ.** Animal models of heart failure: a scientific statement from the American Heart Association. *Circ Res* 111: 131–150, 2012.
14. **Hughes HC.** Swine in cardiovascular research. *Lab Anim Sci* 36: 348–350, 1986.
15. **Ishikawa K, Chemaly ER, Tilemann L, Fish K, Ladage D, Aguero J, Vahl T, Santos-Gallego C, Kawase Y, Hajjar RJ.** Assessing left ventricular systolic dysfunction after myocardial infarction: are ejection fraction and $dP/dt_{max}$ complementary or redundant? *Am J Physiol Heart Circ Physiol* 302: H1423–H1428, 2012.
16. **Ishikawa K, Kawase Y, Ladage D, Chemaly ER, Tilemann L, Fish K, Sanz J, Garcia MJ, Hajjar RJ.** Temporal changes of strain parameters in the progress of chronic ischemia: with comparison to transmural infarction. *Int J Cardiovasc Imaging* 28: 1671–1681, 2012.
17. **Ishikawa K, Ladage D, Tilemann L, Fish K, Kawase Y, Hajjar RJ.** Gene transfer for ischemic heart failure in a preclinical model. *J Vis Exp* 51: 2778, 2011.
18. **Ishikawa K, Tilemann L, Ladage D, Aguero J, Leonardson L, Fish K, Kawase Y.** Cardiac gene therapy in large animals: bridge from bench to bedside. *Gene Ther* 19: 670–677, 2012.
19. **Iwanaga K, Takano H, Ohtsuka M, Hasegawa H, Zou Y, Qin Y, Odaka K, Hiroshima K, Tadokoro H, Komuro I.** Effects of G-CSF on cardiac remodeling after acute myocardial infarction in swine. *Biochem Biophys Res Commun* 325: 1353–1359, 2004.
20. **Kawase Y, Ly HQ, Prunier F, Lebeche D, Shi Y, Jin H, Hadri L, Yoneyama R, Hoshino K, Takewa Y, Sakata S, Peluso R, Zsebo K, Gwathmey JK, Tardif JC, Tanguay JF, Hajjar RJ.** Reversal of cardiac dysfunction after long-term expression of SERCA2a by gene transfer in a pre-clinical model of heart failure. *J Am Coll Cardiol* 51: 1112–1119, 2008.
21. **Kelley KW, Curtis SE, Marzan GT, Karara HM, Anderson CR.** Body surface area of female swine. *J Anim Sci* 36: 927–930, 1973.
22. **Kono T, Sabbah HN, Stein PD, Brymer JF, Khaja F.** Left ventricular shape as a determinant of functional mitral regurgitation in patients with severe heart failure secondary to either coronary artery disease or idiopathic dilated cardiomyopathy. *Am J Cardiol* 68: 355–359, 1991.
23. **Kupatt C, Hinkel R, von Bruhl ML, Pohl T, Horstkotte J, Raake P, El Aouni C, Thein E, Dimmeler S, Feron O, Boekstegers P.** Endothelial nitric oxide synthase overexpression provides a functionally relevant

angiogenic switch in hibernating pig myocardium. *J Am Coll Cardiol* 49: 1575–1584, 2007.

24. **Leor J, Tuvia S, Guetta V, Manczur F, Castel D, Willenz U, Petnehazy O, Landa N, Feinberg MS, Konen E, Goitein O, Tsur-Gang O, Shaul M, Klapper L, Cohen S.** Intracoronary injection of in situ forming alginate hydrogel reverses left ventricular remodeling after myocardial infarction in Swine. *J Am Coll Cardiol* 54: 1014–1023, 2009.
25. **Llaneras MR, Nance ML, Streicher JT, Lima JA, Savino JS, Bogen DK, Deac RF, Ratcliffe MB, Edmunds LH Jr.** Large animal model of ischemic mitral regurgitation. *Ann Thorac Surg* 57: 432–439, 1994.
26. **Opdahl A, Helle-Valle T, Remme EW, Vartdal T, Pettersen E, Lunde K, Edvardsen T, Smiseth OA.** Apical rotation by speckle tracking echocardiography: a simplified bedside index of left ventricular twist. *J Am Soc Echocardiogr* 21: 1121–1128, 2008.
27. **Piacentino V, 3rd Weber CR, Chen X, Weisser-Thomas J, Margulies KB, Bers DM, Houser SR.** Cellular basis of abnormal calcium transients of failing human ventricular myocytes. *Circ Res* 92: 651–658, 2003.
28. **Pirolo JS, Hutchins GM, Moore GW.** Infarct expansion: pathologic analysis of 204 patients with a single myocardial infarct. *J Am Coll Cardiol* 7: 349–354, 1986.
29. **Pleger ST, Shan C, Ksienzyk J, Bekeredjian R, Boekstegers P, Hinkel R, Schinkel S, Leuchs B, Ludwig J, Qiu G, Weber C, Raake P, Koch WJ, Katus HA, Muller OJ, Most P.** Cardiac AAV9–S100A1 gene therapy rescues post-ischemic heart failure in a preclinical large animal model. *Sci Transl Med* 3: 92ra64, 2011.
30. **Roes SD, Mollema SA, Lamb HJ, van der Wall EE, de Roos A, Bax JJ.** Validation of echocardiographic two-dimensional speckle tracking longitudinal strain imaging for viability assessment in patients with chronic ischemic left ventricular dysfunction and comparison with contrast-enhanced magnetic resonance imaging. *Am J Cardiol* 104: 312–317, 2009.
31. **Roger VL, Go AS, Lloyd-Jones DM, Benjamin EJ, Berry JD, Borden WB, Bravata DM, Dai S, Ford ES, Fox CS, Fullerton HJ, Gillespie C, Hailpern SM, Heit JA, Howard VJ, Kissela BM, Kittner SJ, Lackland DT, Lichtman JH, Lisabeth LD, Makuc DM, Marcus GM, Marelli A, Matchar DB, Moy CS, Mozaffarian D, Mussolino ME, Nichol G, Paynter NP, Soliman EZ, Sorlie PD, Sotoodehnia N, Turan TN, Virani SS, Wong ND, Woo D, Turner MB.** Heart disease and stroke statistics—2012 update: a report from the American Heart Association. *Circulation* 125: e2–e220, 2012.
32. **Sengupta PP, Tajik AJ, Chandrasekaran K, Khandheria BK.** Twist mechanics of the left ventricle: principles and application. *JACC Cardiovasc Imaging* 1: 366–376, 2008.
33. **Suzuki Y, Lyons JK, Yeung AC, Ikeno F.** In vivo porcine model of reperfused myocardial infarction: in situ double staining to measure precise infarct area/area at risk. *Catheter Cardiovasc Interv* 71: 100–107, 2008.
34. **Suzuki Y, Yeung AC, Ikeno F.** The representative porcine model for human cardiovascular disease. *J Biomed Biotechnol* 2011: 195483, 2011.
35. **Toma C, Letts DP, Tanabe M, Gorcsan J 3rd, Counihan PJ.** Positive effect of darbepoetin on peri-infarction remodeling in a porcine model of myocardial ischemia-reperfusion. *J Mol Cell Cardiol* 43: 130–136, 2007.
36. **Urdaneta F, Lobato EB, Kirby DS, Sidi A.** Treating myocardial stunning randomly, with either propofol or isoflurane following transient coronary occlusion and reperfusion in pigs. *Ann Card Anaesth* 12: 113–121, 2009.
37. **van der Spoel TI, Jansen of Lorkeers SJ, Agostoni P, van Belle E, Gyongyosi M, Sluijter JP, Cramer MJ, Doevendans PA, Chamuleau SA.** Human relevance of pre-clinical studies in stem cell therapy: systematic review and meta-analysis of large animal models of ischaemic heart disease. *Cardiovasc Res* 91: 649–658, 2011.

Artículo 4 [10].

*Ishikawa K, Aguero J, Oh JG, Hammoudi N, A Fish L, Leonardson L, Picatoste B, Santos-Gallego CG, M Fish K, Hajjar RJ. Increased Stiffness is the Major Early Abnormality in a Pig Model of Severe Aortic Stenosis and Predisposes to Congestive Heart Failure in the Absence of Systolic Dysfunction. J Am Heart Assoc. 2015 May 20;4(5).*

ORIGINAL RESEARCH

American Heart Association | American Stroke Association

# Increased Stiffness Is the Major Early Abnormality in a Pig Model of Severe Aortic Stenosis and Predisposes to Congestive Heart Failure in the Absence of Systolic Dysfunction

Kiyotake Ishikawa, MD; Jaume Aguero, MD; Jae Gyun Oh, PhD; Nadjib Hammoudi, MD; Lauren A. Fish; Lauren Leonardson, LVT; Belén Picatoste, PhD; Carlos G. Santos-Gallego, MD; Kenneth M. Fish, PhD; Roger J. Hajjar, MD

***Background*—**It remains unclear whether abnormal systolic function and relaxation are essential for developing heart failure in pathophysiology of severe aortic stenosis.

***Methods and Results*—**Yorkshire pigs underwent surgical banding of the ascending aorta. The animals were followed for up to 5 months after surgery, and cardiac function was assessed comprehensively by invasive pressure–volume measurements, 3-dimensional echocardiography, echocardiographic speckle-tracking strain, and postmortem molecular and histological analyses. Pigs with aortic banding (n=6) exhibited significant left ventricular hypertrophy with increased stiffness compared with the control pigs (n=7) (end-diastolic pressure–volume relationship β: 0.053±0.017 versus 0.028±0.009 mm Hg/mL, *P*=0.007); however, all other parameters corresponding to systolic function, including ejection fraction, end-systolic pressure–volume relationship, preload recruitable stroke work, echocardiographic circumferential strain, and longitudinal strain, were not impaired in pigs with aortic banding. Relaxation parameters were also similar between groups. Sarcoplasmic reticulum calcium ($Ca^{2+}$) ATPase protein levels in the left ventricle were similar. There were significant increases in 3-dimensional echocardiographic left atrial volumes, suggesting the usefulness of these indexes to detect increased stiffness. Right atrial pacing with a heart rate of 120 beats per minute induced increased end-diastolic pressure in pigs with aortic banding in contrast to decreased end-diastolic pressure in the control pigs. Histological evaluation revealed that increased stiffness was accompanied by cardiomyocyte hypertrophy and increased perimysial and perivascular fibrosis.

***Conclusion*—**Increased stiffness is the major early pathological process that predisposes to congestive heart failure without abnormalities in systolic function and relaxation in a clinically relevant animal model of aortic stenosis. **(*J Am Heart Assoc.* 2015;4:e001925 doi: 10.1161/JAHA.115.001925)**

**Key Words:** diastolic dysfunction • fibrosis • hypertrophy • stiffness • systolic dysfunction



Transcatheter aortic valve implantation has emerged as an alternative therapeutic approach for patients with aortic stenosis. Implementation of this approach in clinical practice has expanded the population of candidates for aortic valve replacement, including patients with severe aortic stenosis who are considered high risk or ineligible for conventional surgical aortic valve replacement. These patients are often elderly with limited daily physical activity, and patients remain asymptomatic despite vulnerability to developing heart failure (HF); therefore, identifying the patient population with masked HF symptoms has become of increasing importance. To this end, it is essential to understand the underlying pathophysiology of HF development in severe aortic stenosis.

Newer techniques such as echocardiographic strain or magnetic resonance strain imaging allow for more detailed assessments of myocardial function than traditional modalities. Several studies have suggested the association of subnormal systolic function with HF in patients with severe aortic stenosis.[1–5] Meanwhile, others have reported impaired relaxation as a major contributor to HF development in aortic stenosis.[6,7] These changes, however, can be the result of disease progression and not the cause of HF. Consequently, it is not clear whether these abnormalities in systolic function

*From the Cardiovascular Research Center, Icahn School of Medicine at Mount Sinai, New York, NY.*

An accompanying Figure S1 is available at http://jaha.ahajournals.org/content/4/5/e001925/suppl/DC1

**Correspondence to:** Kiyotake Ishikawa, MD, Cardiovascular Research Center, Mount Sinai School of Medicine, One Gustave L. Levy Place, Box 1030, New York, NY 10029-6574. E-mail: kiyotake.ishikawa@mssm.edu

Received February 18, 2015; accepted April 8, 2015.

and relaxation are essential for HF development. We hypothesized that increased left ventricular (LV) stiffness is the major early abnormality in patients with severe aortic stenosis and that it predisposes these patients to congestive HF in the absence of systolic dysfunction or impaired relaxation. A large animal model that mimics human aortic stenosis was developed to test this hypothesis with comprehensive functional and histological assessments.

## Methods

### Animal Protocols

All animal protocols complied with the National Institutes of Health Guide for the Care and Use of Laboratory Animals and standards of US regulatory agencies. Protocols were approved by the institutional animal care and use committee of the Icahn School of Medicine at Mount Sinai. A total of 14 female Yorkshire pigs (Animal Biotech Industries (Danboro, PA)) were included in the study. Seven pigs received aortic banding (AoB) and were compared with control animals composed of 3 sham-operated animals and 4 naïve pigs of similar age at the final time point. Sham-surgery animals were included to provide an overview of changes in various parameters due to animal growth. The long-term animals underwent echocardiographic and hemodynamic assessments at 2 months after surgery, followed by final assessments at 3 to 5 months after surgery (Figure 1).

Yorkshire pigs were premedicated using intramuscular Telazol (8.0 mg/kg; Fort Dodge). After the placement of an intravenous line, animals were intubated and ventilated with 40% oxygen. General anesthesia was maintained with intravenous propofol (8 to 10 mg/kg per hour) throughout the procedure except for surgeries in which isoflurane (2% to 3%) was used. Intravenous saline infusion (body weight × 10 mL) was maintained for a period of 30 minutes under continuous monitoring to correct dehydration from overnight fasting. All animals then underwent echocardiographic assessment, followed by an AoB surgery at day 0 and hemodynamic measurements for other time points.

### Aortic Banding

After an echocardiographic evaluation, pigs (10 to 13 kg) were positioned in the right lateral decubitus position, and left thoracotomy was performed in the third intercostal space. A 3-cm opening was created in the pericardium, and the ascending aorta proximal to the brachiocephalic artery was gently isolated. A 1-cm-thick customized rubber band with a fixed inner radius of 12 mm (approximate inner area of 4.5 $cm^2$) was placed around the aorta and fixed with umbilical tape. The chest was closed, air was evacuated, and animals recovered. Sham animals received pericardial opening without AoB.

### Pressure and Volume Measurements

The methods for pressure measurement were previously described in detail.[8] Briefly, percutaneous punctures were performed to establish vascular access to the femoral artery

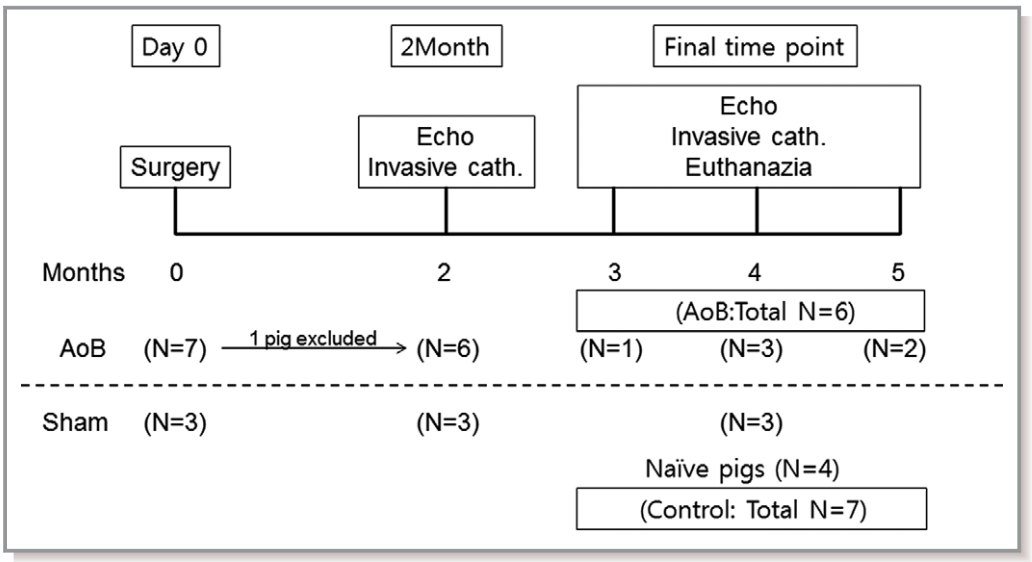


**Figure 1.** Study design and the number of animals. Two groups of animals were included in the study. Control group consists of 3 sham-surgery animals and 4 naïve pigs with similar age and weight to match the numbers of animals in the AoB group. One pig was euthanized at 1 month because of infectious aortic stenosis. AoB indicates aortic banding; cath., catheterization; Echo, echocardiography.

and femoral vein. Heparin (100 IU/kg intravenously) was administered to maintain an activated coagulation time of 150 to 250 seconds. A Swan-Ganz catheter (Edwards Lifesciences LLC) was advanced to the main pulmonary artery, and pressure measurements were collected. Next, through the femoral arterial sheath, a Millar catheter (Millar Instruments) was advanced to the left ventricle to obtain hemodynamic parameters. Approximately 0.25×body weight (in kilograms) milliliter of cold saline was injected into the inferior vena cava to obtain cardiac output by the thermodilution method. All measurements were performed after the confirmation of hemodynamic stability for 3 minutes. Data analyses were performed using an iox2 application (Emka Technologies). At the final time point, an inferior vena cava occlusion was conducted to evaluate the pressure–volume relationship during the preload reduction. The slope of the end-systolic pressure–volume relationship was defined as a measure of contractility. The stiffness constant (β) was determined from a set of relationships between end-diastolic pressure (EDP) and volume, using the following calculation: $EDP=\alpha e^{\beta \cdot EDV}$. EDV indicated end-diastolic volume, and α indicated the curve-fitting constant. After the preload-reduction study, a pacing catheter was advanced through the venous sheath. To evaluate the response of a physiologically relevant increase in heart rate, the right atrium was paced at 120 Hz, and hemodynamic parameters were measured again.

## Echocardiographic Analysis

Comprehensive transthoracic echocardiographic studies including Doppler, 2-dimensional, and 3-dimensional (3D) echocardiograms were performed at baseline (prior to AoB), at 2 months after AoB, and at the final time point. A Philips iE-33 ultrasound system (Philips Medical Systems) was used to acquire echocardiographic data with a multifrequency imaging transducer (S5 probe for 2-dimensional images or X3 probe for 3D images). A subxiphoid approach provided an apical 4-chamber view and 3D images of the left ventricle. Using the parasternal approach, 3D images of the left atrium (Figure S1) and cross-sectional images of the LV short axis were obtained at the levels of the base, papillary muscle, and apex with a high frame rate (60 to 100 Hz). The 2-dimensional images were loaded into the Q-lab application (version 7.0; Philips Medical Systems) for strain analysis using a speckle-tracking algorithm. LV volumes and ejection fraction were obtained from 3D images. Body surface area (in square meters) was calculated as described previously,[9] and volume parameters were divided by body surface area to calculate volume indexes. Longitudinal strain was obtained from apical 4-chamber views. Short-axis images from the papillary muscle level were used for the circumferential strain analysis. Good inter- and intraobserver agreement was reported previously with this method.[10] Tissue Doppler images were analyzed to determine isovolumic relaxation time. Left atrium size was measured as the diameter from the right superior pulmonary vein to the root of the left appendage. The degree of stenosis due to AoB was serially evaluated by maximum velocity and the mean pressure gradient using the continuous-wave Doppler signal at each echocardiographic study by aligning the ultrasound beam with the aortic flow at the level of the banding in the apical view. In the absence of systolic dysfunction, these parameters are used as an established indicator of stenosis severity and allows classification of severe aortic stenosis when the mean gradient is >40 mm Hg, calculated by the simplified Bernoulli equation.[11]

## Postmortem Molecular Analysis and Histology

At the end of the study protocol, the animals were euthanized by intravenous injection of potassium chloride under deep isoflurane anesthesia. Hearts were explanted and weighed, and the left ventricle was sectioned into 5 slices. One middle slice was used for histological and molecular analyses. Samples measuring 1 $cm^3$ were obtained from the anterior wall and preserved both by snap freezing and in formalin. Frozen cardiac tissue was minced and subsequently homogenized in radioimmunoprecipitation assay buffer containing a protease inhibitor cocktail (Sigma-Aldrich). Protein extracts (10 μg) were separated on 10% SDS-PAGE, transferred to a nitrocellulose membrane (Bio-Rad), and probed with antibodies specific for sarcoplasmic reticulum $Ca^{2+}$ ATPase (SERCA2a; Cell Signaling) and phospholamban (Cell Signaling). Peroxidase-conjugated antibodies targeting both primary antibodies (Sigma-Aldrich) and GAPDH (Sigma-Aldrich) were also used. Blots were developed with SuperSignal West Pico (Pierce). Protein band densities were quantified using ImageJ software (National Institutes of Health). Formalin-fixed tissues were embedded in paraffin, sectioned (8 μm), and mounted on positively charged microscope slides. The slides were stained with fluorescein isothiocyanate–labeled wheat-germ agglutinin (Life Technologies) for assessing cell area as an indicator of hypertrophy and with picrosirus red (Abcam) to detect levels of collagen as an indicator of fibrosis.

## Statistical Analysis

Data are expressed as mean±SD unless stated otherwise. The Shapiro–Wilk normality test was conducted to test the normality of the distribution. The unpaired *t* test was used to compare the differences between 2 groups, and the Mann–Whitney *U* test was used as appropriate. A paired *t* test was used to compare changes within the same animal. SPSS version 22.0 (IBM Corp) was used for all statistical analyses. A *P* value <0.05 was considered statistically significant.

## Results

One pig in the AoB group was euthanized at 1 month after the surgery because of worsening general condition. Postmortem evaluation in this pig revealed infectious vegetation at the stenosis site. This pig was excluded from the analysis; therefore, the AoB group consisted of 6 pigs (Figure 1). There was no significant difference in the growth of the pigs, and most functional parameters remained nonsignificant at 2 months after the surgery, although this was most likely due to the small number of pigs in the sham group at this time point (Table 1). In the AoB group compared with the control group, echocardiographic assessments of pressure gradients (mean pressure gradient at

**Table 1.** Temporal Changes of Cardiac Parameters

| | Baseline | | 2 Months | | | Final (3 to 5 Months) | | |
|---|---|---|---|---|---|---|---|---|
| | AoB (n=6) | Sham (n=3) | AoB (n=6) | Sham (n=3) | *P* Value | AoB (n=6) | Control (n=7) | *P* Value |
| BW, kg | 11.5±1.2 | 10.7±0.6 | 24.2±1.9 | 22.7±2.1 | 0.32 | 41.3±7.1 | 37.1±4.4 | 0.22 |
| Days after surgery | 0 | 0 | 57±3 | 55±1 | 0.53 | 121±20 | 107±8† | 0.37 |
| Echocardiography | | | | | | | | |
| Ejection fraction (3DE), % | 70.0±4.8 | 70.4±3.8 | 82.9±13.9 | 85.7±0.61 | 0.75 | 85.2±5.4 | 81.5±6.8 | 0.31 |
| End-diastolic volume index (3DE), mL/m$^2$ | 72.1±16.9 | 78.3±15.7 | 69.4±20.3 | 81.7±7.1 | 0.35 | 81.9±11.7 | 87.1±10.3 | 0.41 |
| End-systolic volume index (3DE), mL/m$^2$ | 21.6±6.1 | 22.9±2.9 | 11.2±7.7 | 11.7±1.3 | 0.92 | 11.8±3.7 | 15.6±4.7 | 0.14 |
| Stroke volume index (3DE), mL/m$^2$ | 50.5±12.2 | 55.5±13.8 | 58.2±21.5 | 70.0±5.8 | 0.39 | 70.1±12.3 | 71.6±13.8 | 0.84 |
| E wave, cm/s | 62.5±11.6 | 72.3±19.1 | 65.8±13.5 | 61.1±3.7 | 0.58 | 61.4±14.1 | 71.1±7.0 | 0.14 |
| E-wave deceleration time, ms | 109±40 | 85±18 | 124±48 | 84±23 | 0.23 | 102±22 | 85±26 | 0.22 |
| A wave, cm/s | 52.6±8.1 | 60.7±12.9 | 66.6±8.4 | 56.5±12.6 | 0.19 | 74.4±13.5 | 70.0±14.5 | 0.58 |
| E/A | 1.20±0.27 | 1.18±0.07 | 1.02±0.36 | 1.12±0.30 | 0.68 | 0.82±0.07 | 1.05±0.22 | 0.03 |
| E', cm/s | 8.4±1.6 | 11.3±1.9 | 7.9±1.6 | 9.9±3.7 | 0.27 | 7.3±1.9 | 10.3±1.5 | 0.01 |
| E/E' | 7.5±1.0 | 6.3±0.6 | 8.5±1.6 | 6.9±2.9 | 0.31 | 8.7±2.3 | 7.0±1.1 | 0.10 |
| IVRT, ms | 71.8±26.3 | 71.1±8.3 | 76.8±14.9 | 70.3±6.0 | 0.39 | 95.1±25.8 | 80.4±8.2 | 0.23 |
| LA diameter, mm | 26.0±3.5 | 27.3±2.5 | 33.8±3.8 | 28.3±3.5 | 0.07 | 42.0±4.2 | 38.6±4.8 | 0.20 |
| Left atrial ejection fraction (3DE), % | 64.3±8.7 | 62.5±4.9 | 61.1±7.4 | 64.4±9.3 | 0.58 | 58.3±6.8 | 63.6±5.4 | 0.14 |
| LA maximum volume index (3DE), mL/m$^2$ | 26.4±2.3 | 26.1±5.1 | 39.2±10.0 | 28.4±2.5 | 0.12 | 51 (34, 66) | 29 (27, 43) | 0.04* |
| LA minimum volume index (3DE), mL/m$^2$ | 9.4±2.7 | 9.7±1.5 | 15.3±5.5 | 10.0±2.3 | 0.16 | 23.1±12.9 | 12.1±2.7 | 0.05 |
| Invasive hemodynamics | | | | | | | | |
| LV maximum pressure, mm Hg | N/A | N/A | 171±34 | 124±17 | 0.07 | 214 (186, 245) | 132 (125, 141) | 0.005* |
| End-diastolic pressure, mm Hg | N/A | N/A | 20.1±4.0 | 13.8±4.4 | 0.07 | 16.7±4.8 | 14.4±3.4 | 0.34 |
| Maximum dP/dt, mm Hg/s | N/A | N/A | 2890±380 | 2055±350 | 0.02 | 2445±387 | 2331±528 | 0.67 |
| dP/dt at pressure 40, mm Hg/s | N/A | N/A | 1609±342 | 1641±226 | 0.89 | 1503±410 | 1644±310 | 0.5 |
| Minimum dP/dt, mm Hg/s | N/A | N/A | −2100±592 | −2277±445 | 0.67 | −2870±1051 | −2612±461 | 0.6 |
| Tau, ms | N/A | N/A | 52.9±11.4 | 59.7±8.4 | 0.39 | 47.2±16.7 | 53.1±8.8 | 0.46 |
| Relaxation time, ms | N/A | N/A | 119±14 | 140±13 | 0.06 | 118±12 | 131±17 | 0.13 |

Mean±SD. 3DE indicates 3-dimensional echocardiography; A, late diastolic transmitral flow velocity; AoB, aortic banding; BW, body weight; dP/dt, peak left ventricular pressure rate; E, early diastolic transmitral flow velocity; E', early diastolic mitral annular velocity; IVRT, isovolumic relaxation time; LA, left atrial; LV, left ventricular; N/A, not available.
*Mann–Whitney *U* test, median (interquartile range).
†Sham pigs.

2 months: 45.4±22.5 versus 1.7±1.2 mm Hg, $P$=0.01; final: 78.1±27.4 versus 3.7±2.1 mm Hg, $P$=0.003) and velocities (maximum velocity ($V_{max}$) at 2 months: 436±77 versus 93±23 cm/s, $P$<0.001; final: 510±130 versus 106±8 cm/s, $P$=0.001) at the banding sites increased significantly after surgery (Figure 2). There were nonsignificant increases in these parameters from 2 months to the final time point ($V_{max}$ $P$=0.16, mean pressure gradient $P$=0.10), suggesting stenosis progression due to animal growth. At the final time point, pigs with AoB presented with significantly higher maximum LV pressure than control pigs. The hearts of the pigs with AoB exhibited significant hypertrophy, demonstrated by a higher ratio of heart weight to body weight (Figure 3).

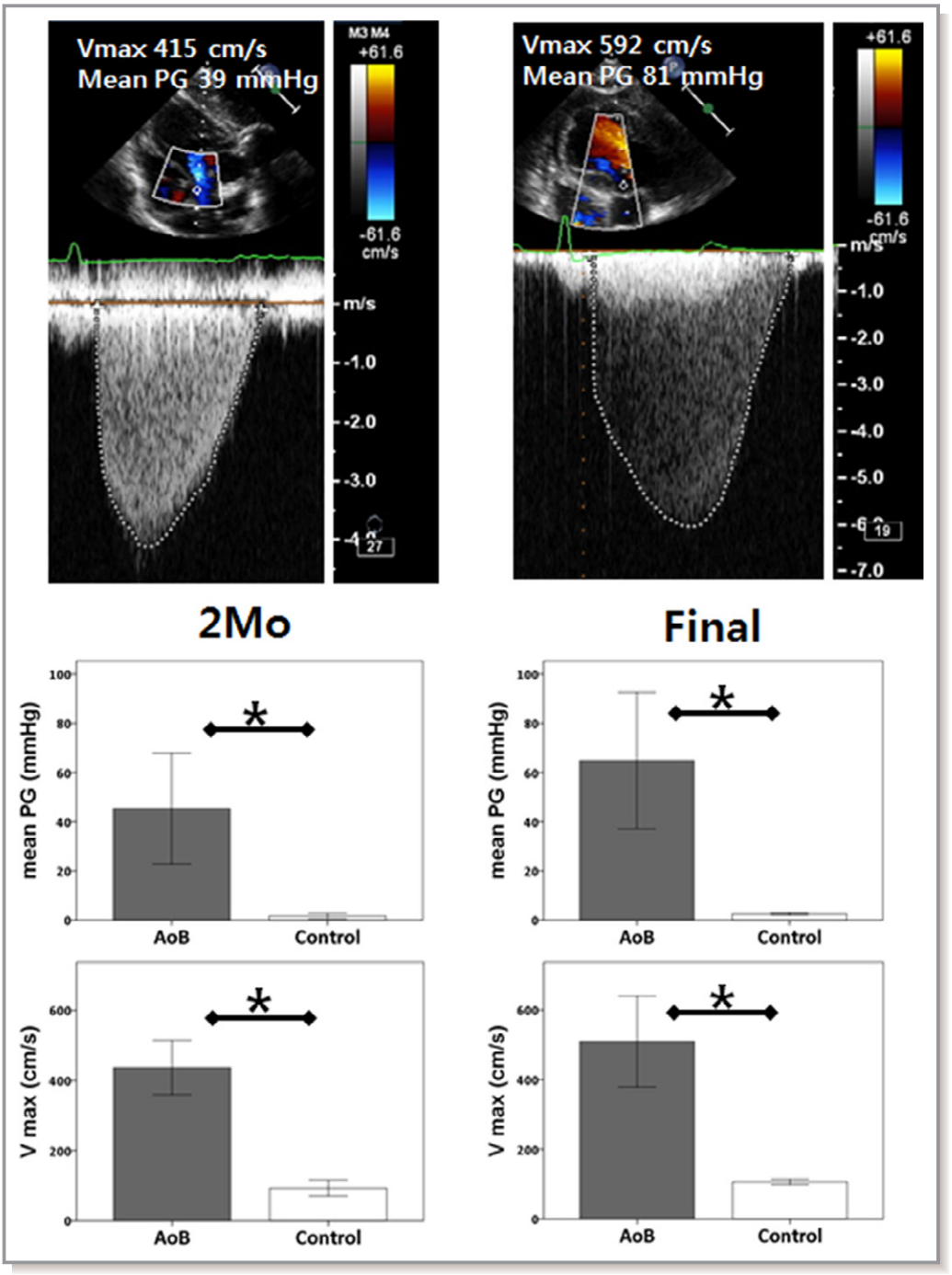


**Figure 2.** Echocardiographic assessment of stenosis at the aortic banding site using continuous Doppler. Both $V_{max}$ and mean PG were significantly increased at 2 months and at final time points in AoB pigs. *$P$<0.05. AoB indicates aortic banding; PG, pressure gradient; $V_{max}$, maximum velocity.

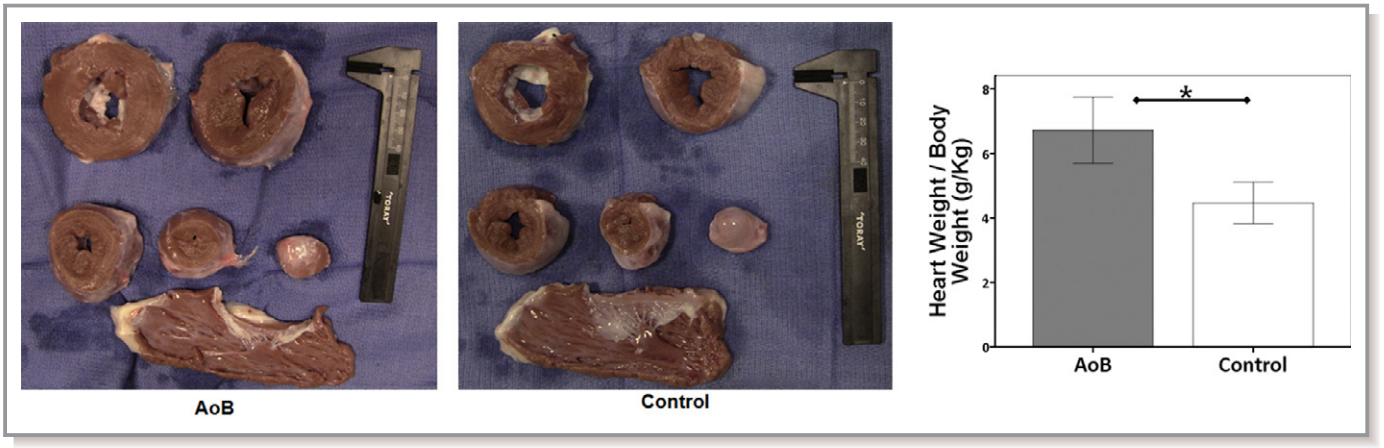


**Figure 3.** Cross-sections of the explanted heart. Macroscopic hypertrophy is apparent in pigs with aortic banding (AoB), with significantly heavier heart weight ($P$=0.001). *$P$<0.05.



Importantly, major systolic and relaxation parameters including LV ejection fraction by 3D echocardiography, peak LV pressure rate of rise, peak LV pressure rate of decline, Tau, and relaxation time were similar between the groups, indicating no depression in contractility and lusitropy in pigs with AoB (Table 1). These observations were supported by the pressure–volume analysis during the preload reduction study, in which higher end-systolic elastance and preload recruitable stroke work were demonstrated without impaired arterial–ventricular coupling (Figure 4, Table 2). Interestingly, LV EDP was not different between the groups, suggesting a compensating condition in pigs with AoB; however, pressure–volume relationship analysis revealed stiffer left ventricles in pigs with AoB, determined by significantly higher β of the end-diastolic pressure-volume relationship (Figure 4, Table 2).

## Echocardiographic Strain and Left Atrial Volumes

Speckle-tracking strain analysis was performed at the final time point. All acquired images were adequate for strain analysis. Although pigs with AoB presented significant hypertrophy, there was no difference in longitudinal or circumferential strain between AoB and sham pigs (Figure 5). Left atrial 3D echocardiographic imaging exhibited significantly higher maximum and minimum left atrial volumes (Table 1).

## Pacing Study

After baseline hemodynamic measurements were acquired, a pacing study was performed to examine the impact of increased heart rate within a physiological range. A pacing rate of 120 beats per minute in the right atrium increased LV EDP in pigs with AoB, whereas LV EDP decreased in the control animals (Figure 6). On average, there was an increase of ≈50% in EDP during pacing in pigs with AoB. These results indicate a propensity for developing congestive HF in these pigs. Changes in LV maximum pressure, LV pressure rate of rise and decline, and Tau were lower in pigs with AoB but did not reach statistical difference.

## Postmortem Histology and SERCA2a Expression

Consistent with the macroscopic presentation, histological evaluation of the left ventricle confirmed cardiomyocyte hypertrophy in pigs with AoB (Figure 7). In addition, myocardium of pigs with AoB had significantly increased collagen volume fractions in both perimysial and perivascular areas (Figure 7). To investigate whether there was molecular evidence of systolic dysfunction, expression of SERCA2a and phospholamban was studied. We found no difference in these protein expression levels between the groups (Figure 8).

## Discussion

In the present study, we demonstrated that increased LV stiffness alone, but not impaired LV systolic function or abnormal relaxation, is the major abnormality at the early stages of severe aortic stenosis in a clinically relevant experimental animal model; however, this increased LV stiffness was associated with a propensity to develop congestive HF in response to the physiological increase in heart rate despite the absence of systolic dysfunction and relaxation abnormalities. Normal systolic function was confirmed by comprehensive cardiac functional analyses including 3D echocardiography, pressure–volume relationship, and speckle-tracking echocardiographic strain. Consistent with our findings that relaxation and systolic function were normal, myocardial SERCA2a protein levels were similar between the groups. In contrast, LV stiffness evaluated by

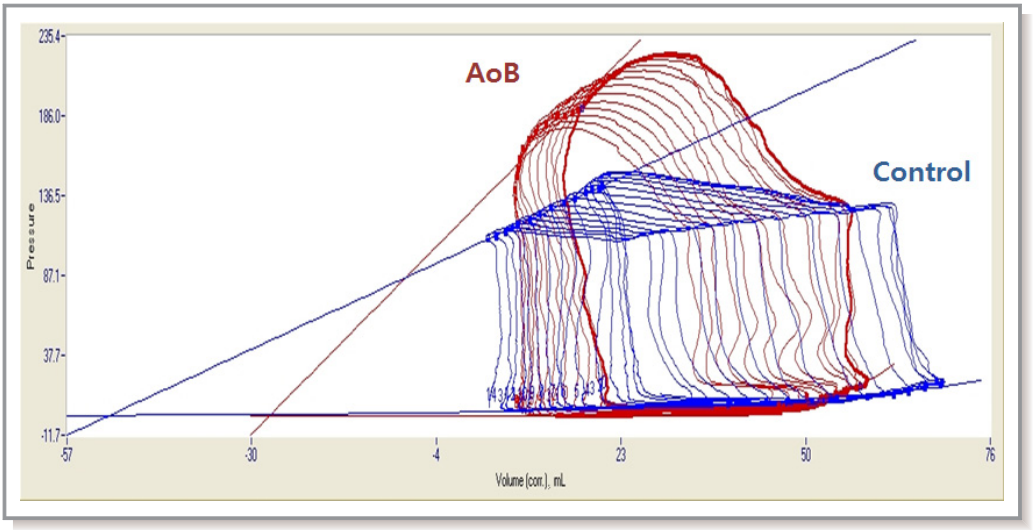


**Figure 4.** Representative pressure–volume loops of AoB and control pigs. Steeper end-systolic pressure–volume relationship was found in pigs with AoB compared with control pigs. Despite similar end-diastolic pressure before occlusion, pigs with AoB presented steeper end-diastolic pressure–volume relationship, indicating stiffer left ventricle. AoB indicates aortic banding; corr., corrected.

pressure–volume loop analysis revealed stiffer left ventricle in pigs after AoB. This finding is consistent with the severe myocardial hypertrophy observed in the pigs with AoB. Moreover, histopathological studies indicated that cardiomyocyte hypertrophy and increased fibrosis are major contributors to increased LV stiffness. To our knowledge, this study is the first to demonstrate isolated increased LV stiffness and its association with HF in the absence of systolic dysfunction and impaired relaxation in severe aortic stenosis, using comprehensive functional analyses.

**Table 2.** Pressure–Volume Loop Relationships

| | AoB (N=6) | Control (n=7) | *P* Value |
|---|---|---|---|
| ESPVR | | | |
| Slope, mm Hg/mL | 4.66 (2.83 to 5.74) | 1.68 (1.13 to 1.90) | 0.005* |
| $V_0$, mL | −29.8±22.0 | −62.9±23.1 | 0.02 |
| Ea/Ees | 0.97±0.61 | 1.68±0.51 | 0.04 |
| PRSW | | | |
| Slope, mm Hg | 176 (103 to 202) | 55 (48 to 81) | 0.008* |
| EDPVR | | | |
| α | 3.03±2.29 | 0.63±0.22 | 0.15 |
| β | 0.053±0.017 | 0.028±0.009 | 0.007 |

AoB indicates aortic banding; α, curve fitting constant; β, stiffness constant; Ea/Ees, arterial elastance/end-systolic elastance; EDPVR, end-diastolic pressure volume relationship; ESPVR, end-systolic pressure volume relationship; PRSW, preload recruitable stroke work; $V_0$, volume axis intercept of end-systolic pressure-volume relationship.
*Mann–Whitney *U* test, median (interquartile range).

Several large animal models of AoB have been developed previously, with use of dogs, pigs, and sheep showing varying results.[6,12–20] Although some studies have reported subnormal systolic function after AoB,[13,15,16] our animals did not develop systolic dysfunction up to 5 months after the surgery, with final LV maximum pressure >200 mm Hg. In contrast, our animals showed supranormal systolic function, as suggested by the increased slope of the end-systolic pressure–volume relationship, the higher preload recruitable stroke work, and the lower arterial–ventricular coupling. The discrepancy may be due to the time point examined after AoB, the age of the animals, and the degree of induced stenosis. The absence of systolic dysfunction with increased stiffness is an attractive feature of our model because it allows for isolation of LV stiffness and systolic dysfunction. This model also may be useful for evaluating various therapeutic approaches targeting HF with preserved ejection fraction; the presentation of this type of HF is similar, with increased myocardial stiffness as a major contributor to development of HF in both diseases.

Relaxation and stiffness are sometimes discussed together as a form of diastolic dysfunction without clear distinction. This is because in many cases, impaired relaxation and increased stiffness coexist in diastolic dysfunction; however, our pigs with AoB presented with increased stiffness without delayed relaxation. Consistent with this finding, it was reported that a mouse model of α-myosin heavy chain missense mutation presented significantly impaired relaxation in the absence of HF or elevated EDP.[21,22] These data suggest that relaxation and stiffness abnormalities do not necessarily parallel and that increased stiffness alone is the key factor for

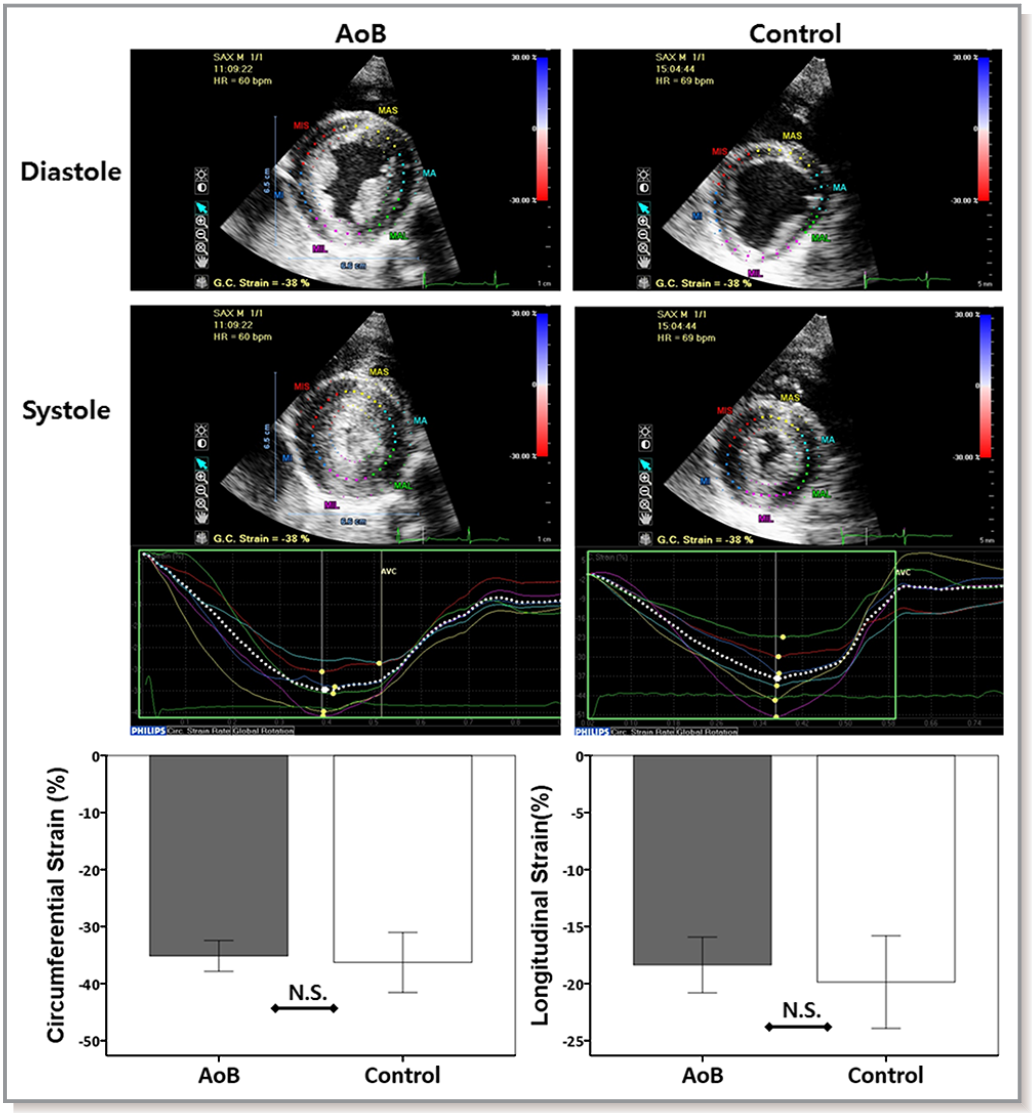


**Figure 5.** Echocardiographic speckle-tracking strain analysis. AoB pigs exhibited thicker wall thickness at both end-diastole and end-systole (top); however, both peak circumferential and longitudinal strains were not different between the groups ($P$=0.63 and $P$=0.45, respectively) (bottom). AoB indicates aortic banding; bpm, beats per minute; GC, global circumferential, HR, heart rate; NS, not significant.

HF induction. They also highlight the importance of distinguishing relaxation and stiffness when evaluating HF with diastolic abnormalities. We found that increased cardiomyocyte hypertrophy and increased fibrosis were potential contributors to increased LV stiffness. A recent study in a rat model of swimming-induced cardiac hypertrophy without significant myocardial fibrosis reported improved LV relaxation without altered stiffness.[23] Although it remains speculative, fibrosis seems to have a significant impact on LV stiffness, although the amount is minor in our model.

Our findings have important clinical implications. If subnormal systolic function or impaired LV relaxation is the key early indicator of HF development in patients with severe aortic stenosis, clinicians can focus on detailed functional imaging studies to identify these abnormalities. Unfortunately, our study demonstrated that this is not the case, and thus patients with severe aortic stenosis are at risk of developing congestive HF without any evidence of systolic dysfunction or impaired relaxation. Instead, increased LV stiffness seems to be the critical early pathological process that predisposes to congestive HF development in this model. Precise measurement of LV stiffness requires pressure–volume loop analysis using invasive catheterization and load-alteration studies. Several formulas for estimating LV stiffness have been proposed,[24,25] but these formulas contain many assumptions, and whether they are always applicable to different disease conditions remains unclear. Consequently, identifying the early manifestation of HF in asymptomatic severe aortic

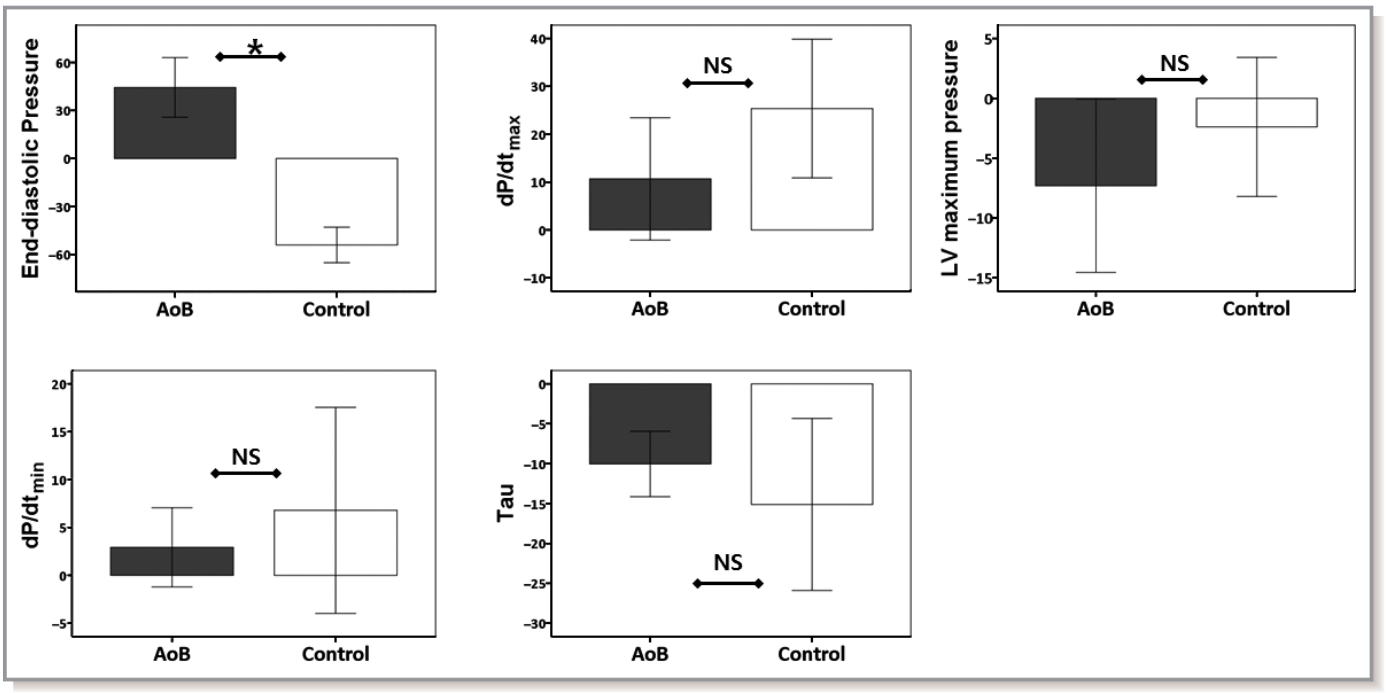


**Figure 6.** Hemodynamic changes induced by pacing study. Pigs received right atrial pacing (120 bpm) with continuous hemodynamic monitoring. End-diastolic pressure decreased in the control group but increased in the AoB group ($P<0.001$), suggesting the propensity of the latter to develop congestive heart failure. Although the parameters did not reach statistical significance, changes in $dP/dt_{max}$, $dP/dt_{min}$, and Tau were smaller in AoB pigs, suggesting limited functional reserve. *$P<0.05$. AoB indicates aortic banding; bpm, beats per minute; $dP/dt_{max}$, peak left ventricular pressure rate of rise; $dP/dt_{min}$, peak left ventricular pressure rate of decline; LV, left ventricular; NS, not significant.

stenosis patients remains challenging. Although most studies of patients with severe aortic stenosis report the presence of diastolic functional abnormalities,[26,27] comprehensive evaluation of specific diastolic parameters is not yet available using standard noninvasive tools; therefore, in current guidelines, diastolic functional parameters are not included in the decision-making process for patients with severe aortic stenosis.[28] Our results demonstrated that 3D echocardiography–derived left atrial volumes were significantly increased in pigs after AoB, and these indexes had superior sensitivity relative to conventional 2-dimensional left atrial diameter to detect the difference between groups. The left atrium is constantly exposed to increased LV filling pressure in a stiff heart, promoting left atrial remodeling. In fact, left atrial remodeling has been proposed as a chronic marker for diastolic dysfunction.[29] Focused evaluation of the left atrium using sophisticated techniques may provide better diagnostic information in patients with severe aortic stenosis. Another approach that may be useful in the detection of early signs of HF in this patient population is fibrosis evaluation, based on our findings. Noninvasive quantification of fibrosis may be performed with serum markers[30] or with cardiac magnetic resonance. In fact, several studies have shown correlation between fibrosis assessed by histology and cardiac magnetic resonance imaging using late gadolinium enhancement[31,32] and T1 mapping[33] in patients with severe aortic stenosis. Because these correlations were evaluated in patients with a relatively large degree of fibrosis, further study is necessary to examine cardiac magnetic resonance sensitivity to small increases in myocardial fibrosis, as found in our study. From a therapeutic point of view, our findings suggest that antihypertrophic and antifibrotic therapies may be beneficial to prevent the development of HF in patients with aortic stenosis.

## Limitations

Due to the nature of animal studies, whether the pigs had HF symptoms remains uncertain, although we did not find any difference in the pig behaviors compared with the sham animals. The propensity for development of congestive HF was determined by increased EDP during the pacing study. Ideally, this should be performed by exercise testing; however, the difficulty of training the pigs for adequate exercise testing and of performing stable placement of the pressure–volume catheter during exercise precluded this option. The pacing method to mimic exercise has been reported previously,[14] and the clear difference in response to pacing in our study suggests the utility of this method to uncover the propensity for HF development in patients with limited exercise ability.

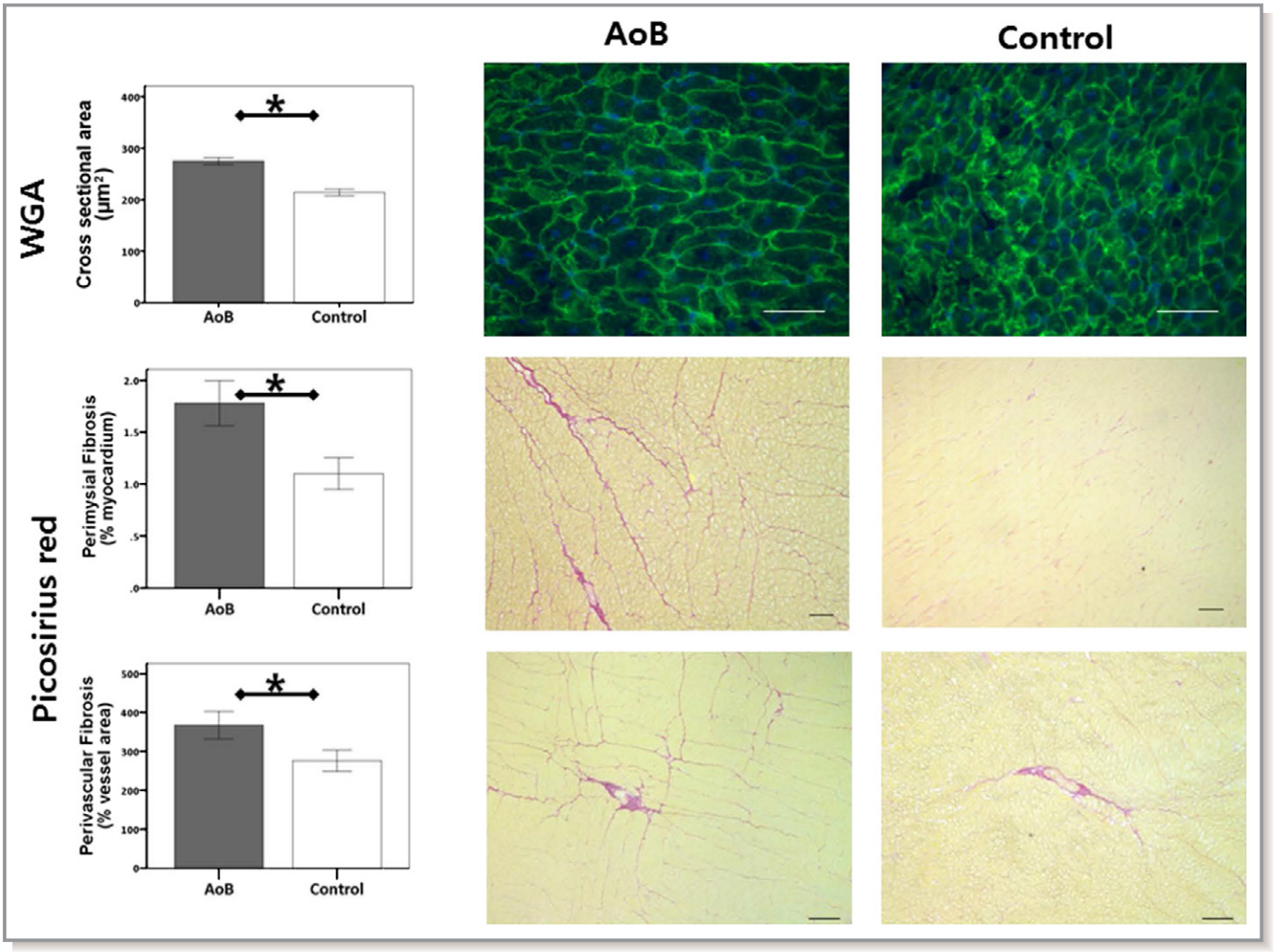


**Figure 7.** Histological characterization of the left ventricular myocardium. AoB pigs presented a significantly larger cardiomyocyte area ($P<0.001$), increased perimysial fibrosis ($P=0.01$), and increased perivascular fibrosis ($P=0.045$). Scale bars indicate 50 μm for WGA figures, 200 μm for perimysial fibrosis figures, and 100 μm for perivascular fibrosis figures. Error bars indicate standard error. *$P<0.05$. AoB indicates aortic banding; WGA, wheat-germ agglutinin.

The supracoronary stenosis in the AoB pig model may differ in the coronary flow pattern from valvular stenosis in humans; however, impaired coronary flow similar to human aortic stenosis has been shown in a dog model of AoB with a banding location similar to ours.[14] Not all animals in the control group underwent sham surgery, and this may have caused unrecognized heterogeneity in this group related to the surgical procedures.

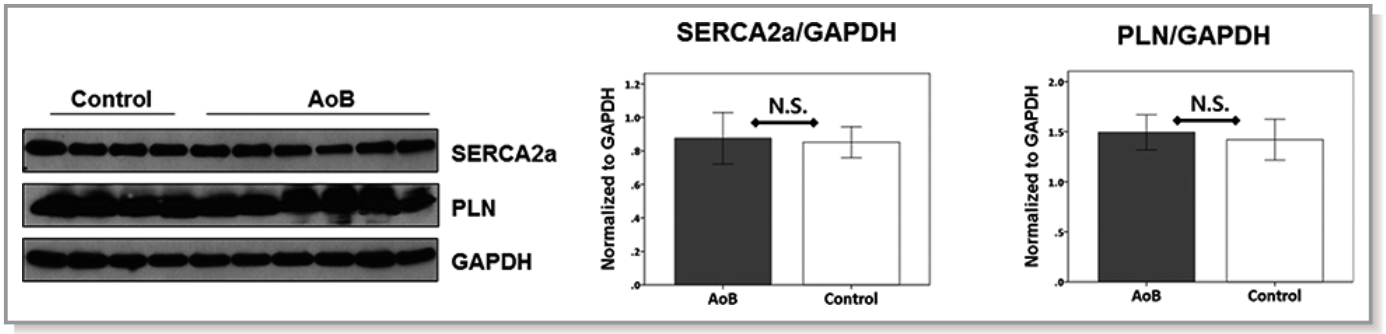


**Figure 8.** SERCA2a and PLN expression in the left ventricle. Both SERCA2a and PLN levels were not different between the AoB and control groups. AoB indicates aortic banding; NS, not significant; PLN, phospholamban; SERCA2a, sarcoplasmic reticulum calcium ($Ca2^{+}$) ATPase.

## Conclusion

Early abnormality in severe aortic stenosis is characterized by increased LV stiffness, whereas systolic dysfunction or impaired relaxation is not necessarily present in this early pathological process. Increased LV stiffness due to cardiomyocyte hypertrophy and increased tissue fibrosis contributes to the propensity to develop congestive HF. Our animal model offers a unique opportunity to study the role of LV stiffness independent of systolic dysfunction and impaired relaxation.

## Sources of Funding

This work is supported by National Institutes of Health R01 HL117505, HL 119046, a National Heart, Lung, and Blood Institute (NHLBI) Program of Gene Therapy Resource Program (GTRP), and Excellence in Nanotechnology (PEN) Award, Contract No. HHSN268201000045C, a P50HL112324, and a Transatlantic Fondation Leducq Grant. Aguero was supported by Spanish Society of Cardiology (Ischemic Heart Disease section) and Fundacion Alfonso Martin-Escudero. NH was supported by a grant from the French Federation of Cardiology.

## Disclosures

None.

## Reference

1. Poulsen SH, Sogaard P, Nielsen-Kudsk JE, Egeblad H. Recovery of left ventricular systolic longitudinal strain after valve replacement in aortic stenosis and relation to natriuretic peptides. *J Am Soc Echocardiogr*. 2007;20:877–884.
2. Dinh W, Nickl W, Smettan J, Kramer F, Krahn T, Scheffold T, Barroso MC, Brinkmann H, Koehler T, Lankisch M, Futh R. Reduced global longitudinal strain in association to increased left ventricular mass in patients with aortic valve stenosis and normal ejection fraction: a hybrid study combining echocardiography and magnetic resonance imaging. *Cardiovasc Ultrasound*. 2010;8:29.
3. Yingchoncharoen T, Gibby C, Rodriguez LL, Grimm RA, Marwick TH. Association of myocardial deformation with outcome in asymptomatic aortic stenosis with normal ejection fraction. *Circ Cardiovasc Imaging*. 2012;5:719–725.
4. Ng AC, Delgado V, Bertini M, Antoni ML, van Bommel RJ, van Rijnsoever EP, van der Kley F, Ewe SH, Witkowski T, Auger D, Nucifora G, Schuijf JD, Poldermans D, Leung DY, Schalij MJ, Bax JJ. Alterations in multidirectional myocardial functions in patients with aortic stenosis and preserved ejection fraction: a two-dimensional speckle tracking analysis. *Eur Heart J*. 2011;32:1542–1550.
5. Lafitte S, Perlant M, Reant P, Serri K, Douard H, DeMaria A, Roudaut R. Impact of impaired myocardial deformations on exercise tolerance and prognosis in patients with asymptomatic aortic stenosis. *Eur J Echocardiogr*. 2009;10:414–419.
6. Marshall KD, Muller BN, Krenz M, Hanft LM, McDonald KS, Dellsperger KC, Emter CA. Heart failure with preserved ejection fraction: chronic low-intensity interval exercise training preserves myocardial $O_2$ balance and diastolic function. *J Appl Physiol*. 2013;114:131–147.
7. Falcao-Pires I, Palladini G, Goncalves N, van der Velden J, Moreira-Goncalves D, Miranda-Silva D, Salinaro F, Paulus WJ, Niessen HW, Perlini S, Leite-Moreira AF. Distinct mechanisms for diastolic dysfunction in diabetes mellitus and chronic pressure-overload. *Basic Res Cardiol*. 2011;106:801–814.
8. Ishikawa K, Chemaly ER, Tilemann L, Fish K, Ladage D, Aguero J, Vahl T, Santos-Gallego C, Kawase Y, Hajjar RJ. Assessing left ventricular systolic dysfunction after myocardial infarction: are ejection fraction and dP/dt(max) complementary or redundant? *Am J Physiol Heart Circ Physiol*. 2012;302:H1423–H1428.
9. Kelley KW, Curtis SE, Marzan GT, Karara HM, Anderson CR. Body surface area of female swine. *J Anim Sci*. 1973;36:927–930.
10. Ishikawa K, Kawase Y, Ladage D, Chemaly ER, Tilemann L, Fish K, Sanz J, Garcia MJ, Hajjar RJ. Temporal changes of strain parameters in the progress of chronic ischemia: with comparison to transmural infarction. *Int J Cardiovasc Imaging*. 2012;28:1671–1681.
11. Baumgartner H, Hung J, Bermejo J, Chambers JB, Evangelista A, Griffin BP, Iung B, Otto CM, Pellikka PA, Quinones M. Echocardiographic assessment of valve stenosis: EAE/ASE recommendations for clinical practice. *J Am Soc Echocardiogr*. 2009;22:1–23.
12. Ghaleb B, Hittinger L, Kim SJ, Kudej RK, Iwase M, Uechi M, Berdeaux A, Bishop SP, Vatner SF. Selective large coronary endothelial dysfunction in conscious dogs with chronic coronary pressure overload. *Am J Physiol*. 1998;274:H539–H551.
13. Tagawa H, Koide M, Sato H, Zile MR, Carabello BA, Cooper G IV. Cytoskeletal role in the transition from compensated to decompensated hypertrophy during adult canine left ventricular pressure overloading. *Circ Res*. 1998;82:751–761.
14. Nakano K, Corin WJ, Spann JF Jr, Biederman RW, Denslow S, Carabello BA. Abnormal subendocardial blood flow in pressure overload hypertrophy is associated with pacing-induced subendocardial dysfunction. *Circ Res*. 1989;65:1555–1564.
15. Moorjani N, Catarino P, Trabzuni D, Saleh S, Moorji A, Dzimiri N, Al-Mohanna F, Westaby S, Ahmad M. Upregulation of Bcl-2 proteins during the transition to pressure overload-induced heart failure. *Int J Cardiol*. 2007;116:27–33.
16. Koide M, Nagatsu M, Zile MR, Hamawaki M, Swindle MM, Keech G, DeFreyte G, Tagawa H, Cooper G IV, Carabello BA. Premorbid determinants of left ventricular dysfunction in a novel model of gradually induced pressure overload in the adult canine. *Circulation*. 1997;95:1601–1610.
17. Nediani C, Formigli L, Perna AM, Ibba-Manneschi L, Zecchi-Orlandini S, Fiorillo C, Ponziani V, Cecchi C, Liguori P, Fratini G, Nassi P. Early changes induced in the left ventricle by pressure overload. An experimental study on swine heart. *J Mol Cell Cardiol*. 2000;32:131–142.
18. Wisenbaugh T, Allen P, Cooper G IV, Holzgrefe H, Beller G, Carabello B. Contractile function, myosin ATPase activity and isozymes in the hypertrophied pig left ventricle after a chronic progressive pressure overload. *Circ Res*. 1983;53:332–341.
19. Yarbrough WM, Mukherjee R, Stroud RE, Rivers WT, Oelsen JM, Dixon JA, Eckhouse SR, Ikonomidis JS, Zile MR, Spinale FG. Progressive induction of left ventricular pressure overload in a large animal model elicits myocardial remodeling and a unique matrix signature. *J Thorac Cardiovasc Surg*. 2012;143:215–223.
20. Ye Y, Gong G, Ochiai K, Liu J, Zhang J. High-energy phosphate metabolism and creatine kinase in failing hearts: a new porcine model. *Circulation*. 2001;103:1570–1576.
21. Georgakopoulos D, Christe ME, Giewat M, Seidman CM, Seidman JG, Kass DA. The pathogenesis of familial hypertrophic cardiomyopathy: early and evolving effects from an alpha-cardiac myosin heavy chain missense mutation. *Nat Med*. 1999;5:327–330.
22. Geisterfer-Lowrance AA, Christe M, Conner DA, Ingwall JS, Schoen FJ, Seidman CE, Seidman JG. A mouse model of familial hypertrophic cardiomyopathy. *Science*. 1996;272:731–734.
23. Radovits T, Olah A, Lux A, Nemeth BT, Hidi L, Birtalan E, Kellermayer D, Matyas C, Szabo G, Merkely B. Rat model of exercise-induced cardiac hypertrophy: hemodynamic characterization using left ventricular pressure-volume analysis. *Am J Physiol Heart Circ Physiol*. 2013;305:H124–H134.
24. Zile MR, Baicu CF, Gaasch WH. Diastolic heart failure–abnormalities in active relaxation and passive stiffness of the left ventricle. *N Engl J Med*. 2004;350:1953–1959.
25. Marino P, Little WC, Rossi A, Barbieri E, Anselmi M, Destro G, Prioli A, Lanzoni L, Zardini P. Can left ventricular diastolic stiffness be measured noninvasively? *J Am Soc Echocardiogr*. 2002;15:935–943.
26. Otto CM, Burwash IG, Legget ME, Munt BI, Fujioka M, Healy NL, Kraft CD, Miyake-Hull CY, Schwaegler RG. Prospective study of asymptomatic valvular aortic stenosis. Clinical, echocardiographic, and exercise predictors of outcome. *Circulation*. 1997;95:2262–2270.
27. Hachicha Z, Dumesnil JG, Pibarot P. Usefulness of the valvuloarterial impedance to predict adverse outcome in asymptomatic aortic stenosis. *J Am Coll Cardiol*. 2009;54:1003–1011.
28. Nishimura RA, Otto CM, Bonow RO, Carabello BA, Erwin JP III, Guyton RA, O'Gara PT, Ruiz CE, Skubas NJ, Sorajja P, Sundt TM III, Thomas JD, Members

AATF. 2014 AHA/ACC guideline for the management of patients with valvular heart disease: executive summary: a report of the American College of Cardiology/American Heart Association Task Force on Practice Guidelines. *Circulation*. 2014;129:2440–2492.

29. Abhayaratna WP, Seward JB, Appleton CP, Douglas PS, Oh JK, Tajik AJ, Tsang TS. Left atrial size: physiologic determinants and clinical applications. *J Am Coll Cardiol*. 2006;47:2357–2363.

30. Jellis C, Martin J, Narula J, Marwick TH. Assessment of nonischemic myocardial fibrosis. *J Am Coll Cardiol*. 2010;56:89–97.

31. Azevedo CF, Nigri M, Higuchi ML, Pomerantzeff PM, Spina GS, Sampaio RO, Tarasoutchi F, Grinberg M, Rochitte CE. Prognostic significance of myocardial fibrosis quantification by histopathology and magnetic resonance imaging in patients with severe aortic valve disease. *J Am Coll Cardiol*. 2010;56:278–287.

32. Weidemann F, Herrmann S, Stork S, Niemann M, Frantz S, Lange V, Beer M, Gattenlohner S, Voelker W, Ertl G, Strotmann JM. Impact of myocardial fibrosis in patients with symptomatic severe aortic stenosis. *Circulation*. 2009;120:577–584.

33. White SK, Sado DM, Fontana M, Banypersad SM, Maestrini V, Flett AS, Piechnik SK, Robson MD, Hausenloy DJ, Sheikh AM, Hawkins PN, Moon JC. T1 mapping for myocardial extracellular volume measurement by CMR: bolus only versus primed infusion technique. *JACC Cardiovasc Imaging*. 2013;6:955–962.

SUPPLEMENTAL MATERIAL

Figure S1. Cited in Methods: echocardiographic analysis

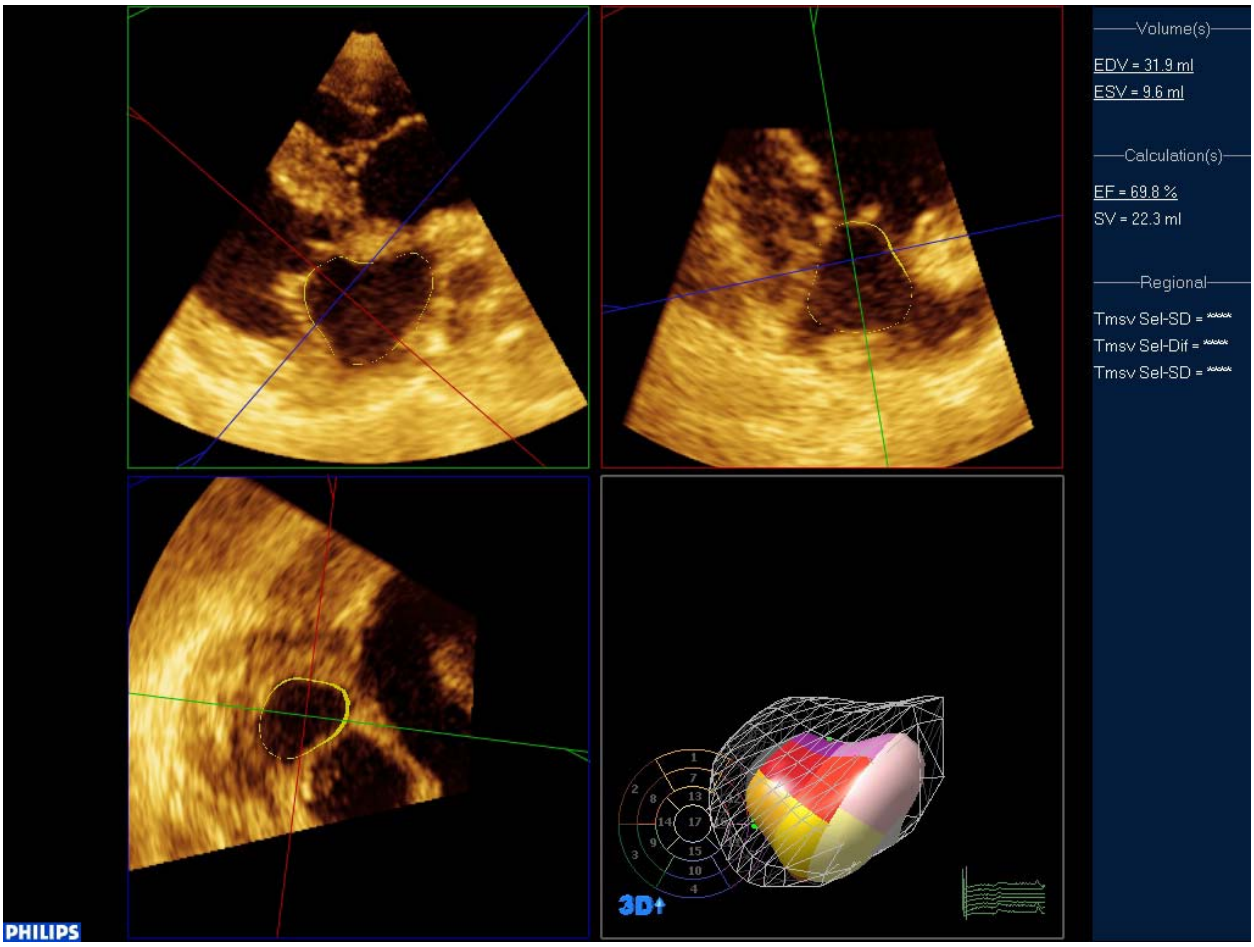


An example of three-dimensional left atrial volume analysis.

Bottom right figure shows the mesh (maximum volume) and color (minimum volume) of the left atrium.

Manuscrito 1.

*Aguero J, Galan-Arriola C, Fernandez-Jimenez R, Sanchez-Gonzalez J, Ajmone N, Delgado V, Solis J, Lopez GJ, Molina-Iracheta A, Hajjar RJ, Bax JJ, Fuster V, Ibañez B. Left atrial remodeling after acute myocardial infarction: insight into the role of atrial infarction.*

**Left atrial remodeling after acute myocardial infarction: insight into the role of atrial infarction**

Jaume Aguero[1], Carlos Galan-Arriola[1], Rodrigo Fernandez-Jimenez[1], Javier Sanchez-Gonzalez[2,1], Nina Ajmone[3], Victoria Delgado[3], Jorge Solis[1,4], Gonzalo J Lopez[1], Antonio de Molina-Iracheta[1], Roger J Hajjar[5], Jeroen J Bax[3], Valentin Fuster[1,5], Borja Ibañez[*1,6].

**Affiliations:**

[1]Centro Nacional de Investigaciones Cardiovasculares Carlos III (CNIC), Madrid, Spain.

[2]Philips Healthcare, Madrid, Spain.

[3]Department of Cardiology, Heart Lung Center, Leiden University Medical Center, Leiden, The Netherlands.

[4]Hospital 12 de Octubre, Madrid, Spain.

[5]The Zena and Michael A. Wiener CVI, Icahn School of Medicine at Mount Sinai, New York, USA.

[6]Cardiology Department, IIS-Fundación Jiménez Díaz Hospital, Madrid, Spain.

***Address for correspondence**:

**Dr. Borja Ibáñez**. MD PhD FESC. Translational Laboratory for Cardiovascular Imaging and Therapy, Centro Nacional de Investigaciones Cardiovasculares Carlos III (CNIC). Melchor Fernández Almagro, 3. 28029, Madrid, Spain. Phone: (+34) 91 453.12.00. Fax: (+34) 91 453 12 45; & Department of Cardiology, Instituto de Investigación Sanitaria, Fundación Jiménez Díaz, Madrid, Spain. E-mail: E-mail: bibanez@cnic.es

**ABSTRACT.**

BACKGROUND. Left atrial (LA) remodeling after acute myocardial infarction (AMI) is poorly characterized and little is known about its determinants and potential impact on ischemic mitral regurgitation and cardiac hemodynamics.

OBJECTIVES. 1) To compare LA remodeling in a pig model of AMI caused either by left anterior descending (LAD) coronary artery occlusion or by left circumflex (LCx) coronary artery occlusion with and without occlusion of the LA branch. 2) To analyze the interplay of LA and LV remodeling and the development of ischemic mitral regurgitation (MR).

METHODS. Three pig models of MI were created: 1) occlusion of the proximal LCx coronary artery with concomitant occlusion of the LA coronary artery (LA infarction, LAI group); 2) occlusion of the proximal LCx coronary artery without involvement of the LA branch (LCx group); and 3) occlusion of the LAD (LAD group). The 3 models were evaluated for structural and functional remodeling of the LA and for LV remodeling and the occurrence of ischemic MR. Animals underwent serial cardiac magnetic resonance (CMR) at 1 and 8 weeks post-AMI to monitor cardiac remodeling parameters. Pulmonary hemodynamics were assessed at 8 weeks post-AMI by right heart catheterization. Animals were sacrificed thereafter, and structural remodeling of the LA was characterized by histological examination.

RESULTS. Compared with the other groups, occlusion of the LCx and LA arteries (LAI) was associated with a greater degree of LA dilation on CMR at 1- and 8-week follow-up. LA coronary occlusion induced severe impairment of LA reservoir function, evident at 1 week post-AMI and persistent at 8-week follow-up; in contrast, in the other groups this dysfunction was less pronounced and not consistent. In the LAI group, atrial infarction was confirmed by extensive fibrotic replacement of the atrial myocardium at 1 and 8 weeks, whereas LCx alone was associated with milder, interstitial fibrosis. All groups showed progressive LV remodeling. Development of ischemic MR was more pronounced in the LAI group than in the LCx group and was evident as early as 1 week post-AMI. The combination of atrial remodeling, LV remodeling, and ischemic MR was associated with pulmonary hypertension measured invasively at 8-week follow-up. In the LAD group, LA remodeling was not observed by CMR or histology, despite a similar degree of LV dysfunction to the other groups.

CONCLUSIONS. We provide the first experimental evidence of the deleterious impact of acute LA infarction during LCx AMI on LA and LV remodeling, with consequent development of ischemic MR. Atrial coronary occlusion induced early and severe LA enlargement, followed by persistent LA functional impairment and extensive fibrosis. The combination of ischemic LA remodeling and MR led to early onset pulmonary hypertension, reflecting post-infarction heart failure.

KEYWORDS. Myocardial infarction, atrial infarction, mitral regurgitation, experimental model, atrial fibrosis.

## Introduction

Chronic heart failure (HF) is a major cause of death and hospital admission. Despite advances in patient care, incident HF in myocardial infarction (MI) survivors remains a major cost burden on health care systems.[1] In the aftermath of an acute MI (AMI), left ventricular ejection fraction (LVEF) is currently the main recommended predictor of future events, including sudden cardiac death and HF.[2] More recently, left atrial (LA) enlargement has been proposed as novel predictor of HF, providing independent prognostic value in addition to LVEF.[3-5]

Excessive dilation of the LA is described in ~15-45% of patients in the early post-MI period.[3-5] However, the main determinants of this finding are not well characterized. The main driver of LA dilation is thought to be increased atrial pressure due to LV dysfunction .[6] However, 2 potentially major contributors to post-MI LA remodeling have scarcely been characterized: ischemic mitral regurgitation (MR) and atrial infarction. Ischemic MR is caused by LV remodeling and distorted valve geometry, resulting in altered leaflet coaptation[8]. Previous studies suggest a close association between ischemic MR and LA remodeling after AMI[9], but the time course of LA remodeling in patients developing ischemic MR has not been described. The incidence and consequences of atrial infarction remain unknown, mainly due to a lack of reliable diagnostic biomarkers[10]. Recently, LA coronary branch occlusion was reported as a complication of percutaneous coronary angioplasty in up to 15% of patients, leading to a higher prevalence of atrial arrhythmias, peri-procedural MI, and mortality.[13] However, the impact of LA infarction on LA structure and physiology has not been explored before, and current knowledge is based mostly on autopsy reports.[14]

The aim of this study was to provide insight into the causes, mechanisms, and consequences of LA remodeling as a complication of AMI. The specific aims were twofold: 1) to evaluate the incidence and progression of post-MI LA remodeling and the interplay among potential contributing factors (ventricular necrosis/remodeling, ischemic MR, and atrial infarction); and 2) to examine the impact of LA remodeling and ischemic MR on the development of post-MI HF. To address these questions, we performed time course studies in porcine AMI models recapitulating LV remodeling, ischemic MR, and LA infarction and evaluated LA remodeling by noninvasive imaging and histology.

**Methods.**

The study was approved by the local institutional animal research committee and conducted in accordance with the National Research Council Guide for the Care and Use of Laboratory Animals. An expanded description of experimental procedures is provided in the Supplementary Methods.

**Study design.** Male large-white pigs (30-35Kg) underwent closed-chest MI by occluding the LAD or LCx coronary arteries. LCx infarctions were conducted with or without associated atrial coronary occlusion (see detailed description below) and were used as a model of ischemic MR. Anterior infarctions were generated by LAD ischemia/reperfusion to provide a post-MI model of LV dysfunction with no or mild ischemic MR. Three experimental groups were created: 1) LCx occlusion (LCx group, n=7), 2) LCx occlusion involving the LA branch and therefore inducing LA infarction(LAI group, n=8), and 3) anterior MI (LAD group, n=18) (Figure 1). An additional 4 healthy pigs served as controls during serial imaging studies. Hearts were examined by cardiac magnetic resonance (CMR) before MI and at 1 and 8 weeks post-MI to evaluate LA and LV remodeling and MR development. Pulmonary hemodynamics were measured invasively by right heart catheterization (RHC) at 8-week follow-up. Animals were sacrificed at 8 weeks post-MI and hearts were excised for histological analysis.

**Model of chronic post-MI ischemic MR and LA infarction.** Pilot experiments (Supplementary Methods and Supplementary Figure 1) enabled us to establish the optimal technique for creating an ischemic MR model in pigs by placing a coronary coil in the proximal segment of moderate-to-large LCx arteries. A 5-French AL-2 guide catheter was used to engage the left coronary artery. The LCx coronary anatomy pattern (including size and distribution of marginal branches) was examined in 2 angiographic projections to select those vessels likely to develop large posterolateral infarcts based on pilot studies. The catheter tip was then was positioned in the proximal LCx artery using a 0.014-inch guide wire. A CMR-compatible steel-alloy embolization coil (MREye, Cook Medical, 3-cm long, 3-mm embolus diameter) was deployed using a 0.035-inch vascular wire. In all animals, total occlusion of the LCx artery was confirmed by angiography within 5 minutes of coil deployment.

To evaluate the effect of acute LA injury during MI, animals undergoing LCx coiling were further classified based on angiographically-determined occlusion of the LA coronary artery (LCx *vs.* LAI groups), which branches off from the proximal LCx segments or less frequently from the mid LCx segment.

**Model of anterior acute MI.** To evaluate the presence and severity of post-MI LA remodeling due to LV necrosis and remodeling in the absence of other potential contributors, anterior infarction was induced with the LAD ischemia/reperfusion protocol previously reported by our group (LAD group).[15] In this model, AMI is achieved by 45-minutes mid-LAD occlusion (distal to the first diagonal branch) followed by reperfusion.[16] This procedure generates consistent transmural infarcts characterized by chamber dilation and systolic dysfunction, consistent with clinical presentation.[16]

**CMR acquisition protocol.** All studies were performed in a Philips 3-T Achieva Tx whole-body scanner (Philips Healthcare, Best, the Netherlands) equipped with a 32-element phased-array cardiac coil. The imaging protocol included a standard segmented cine steady-state free-precession (SSFP) sequence to provide high-quality anatomical references. The imaging parameters for the SSFP sequence were field of view (FOV) 280x280 mm, slice thickness 6 mm with no gap, repetition time (TR) 2.8 ms, echo time (TE) 1.4 ms, flip angle 45, cardiac phases 30, voxel size 1.8x1.8 mm, and number of excitations (NEX) =3.

Delayed enhancement imaging was performed 10 to 15 min after intravenous administration of 0.20 mmol of gadopentetate dimeglumine contrast agent per kg of body weight using an inversion-recovery spoiled turbo field echo (IR-T1TFE) sequence with the following parameters: FOV 280x280 mm, voxel size 1.6x1.6 mm, end-diastolic acquisition, thickness 6 mm with no gap, TR 5.6 ms, TE 2.8 ms, inversion delay time optimized to null normal myocardium.

Forward stroke volume was determined by 2D flow imaging (phase-contrast) performed on cross-sectional views of the ascending aorta, with a velocity-encoded gradient echo sequence using the minimum upper velocity limit without signal aliasing. The following imaging parameters were applied: repetition time/ echo time 5.4/3.4 ms, number of averages 2, slice thickness 8 mm, voxel size 2.5 x 2.5 mm, reconstructed heart phases 40.

**CMR data analysis.** CMR images were analyzed with dedicated software (MR Extended Work Space 2.6, Philips Healthcare, and QMass MR 7.5, Medis, Leiden, the Netherlands) by 2 observers experienced in CMR analysis. Short-axis epicardial and endocardial contours were manually traced to obtain LV volumes at end-diastole (EDV) and end-systole (ESV) and LV mass. Delayed gadolinium-enhanced regions were defined as >50% of maximum myocardial signal intensity (full width at half maximum), and infarct size was defined as a percentage of LV mass.

Given that no volumetric estimation methods have been validated in swine, we quantified LA dimensions based on the mean area in 4- and 2-chamber views. From these views, 3 phasic parameters were derived as follows:

- Reservoir function (%): 100*(Maximal LA area – minimum LA area)/ Maximal LA area
- Conduit function (%): 100*(Maximal LA area – pre-atrial contraction area)/ Maximal LA area
- Booster function (%): 100*(Pre-atrial contraction area – minimum LA area)/ Maximal LA area.

Post-MI MR severity in the ischemic MR groups (LCx and LAI) was quantified using LV forward stroke volume (SV) obtained from a phase-contrast sequence in the ascending aorta. Regurgitant volume (RegVol) and regurgitant fraction (RF) were calculated as follows:

- CineSV = LV end-diastolic volume – LV end-systolic volume
- RegVol= Forward SV – (CineSV)
- RF= RegVol/CineSV

**Histology.** After excision of the heart, tissue samples from the LA anterior wall and mitral leaflets were fixed in 10% neutral buffered formalin, embedded in paraffin wax, and cut into 4 µm sections. Sections stained with Picrosirius red, hematoxylin-eosin, and Masson's trichrome were digitized with a Nanozoomer-RS C110730® scanner (Hamamatsu). The level of collagen organization was evaluated qualitatively by polarized light microscopy of Picrosirius-red-stained sections (Nikon ECLIPSE 90i).

**Invasive measurement of pulmonary pressure.** RHC was performed in the LCx, LAI, and control groups at 8-week follow-up, using a 7.5-Fr Swan-Ganz catheter (Edwards Lifesciences). Hemodynamic measurements were obtained under mechanical ventilation (oxygen inspiratory fraction 30%, tidal volume 7 ml/kg). Cardiac output was measured by the thermodilution method.

**Statistical analysis.** Continuous variables are expressed as medians and interquartile ranges. Between-group comparisons at different time points were performed using one-way ANOVA or the non-parametric Kruskal-Wallis test, followed by post-hoc analyses corrected for multiple comparisons (Holm method). Linear or ordinal associations between different parameters were evaluated using the Pearson or Spearman's correlation coefficient,

as appropriate. Statistical analyses were performed using R version 3.1.1 (http://cran.r-project.org/). Differences were considered significant at p-value < 0.05.

## Results.

Data related to the generation of the 3 porcine MI models are provided in the Supplementary Data. The final analyses were performed in all animals that completed the study protocol (Control group, n=4; LCx group, n=7; LAI group, n=8; and LAD group, n=18). Experimental procedures, study timeline, and experimental groups are summarized in Figure 1.

**Time course of LA dilation after MI.** While LA dilation (at 1 week post-MI) was present in both pig groups undergoing LCx coil occlusion (LCx and LAI groups), it was larger in pigs in the LAI group (Table 1 and Figure 2). In addition, between 1 and 8 weeks post-MI, LA dilation progressed faster in the LAI group. Interestingly, pigs in the LAD group showed no LA enlargement (compared with control pigs) despite the presence of LVEF depression and ventricular chamber remodeling. At 1 week, we found a modest but significant linear association of LA dilation with infarct size (R=0.38, p=0.015) and LVESV (R=0.34, p=0.025).

**LA dysfunction after MI: association with LA dilatation**

Impaired LA reservoir function was observed 1 week after MI in all 3 groups (Table 1 and Figure 3). Early reduction in reservoir function was most prominent in the LAI group (13.8% *vs*. 38.2% in the control group, compared with 24.1% and 27.1% for the LCx and LAD groups, respectively). Between 1 and 8 weeks, markedly impaired LA reservoir function indicated persistent dysfunction in LAI animals (16.5% *vs.* 38.3% in controls), whereas impairment was milder in the LCx (24.1%) and LAD (27.1%) groups, with some animals even showing functional recovery (Figure 3). Atrial contractility, measured from the booster function, followed a similar time course to reservoir function, with the most notable changes occurring in the LAI group (Table 1). Individual animals showed a strong correlation between reservoir and contractile properties (R=0.89, p<0.001). Acute MI impaired atrial conduit function to a similar extent in all groups, but there were no significant differences between 1-week and 8-week follow-up (Table 1).

**LV remodelling post-MI and development of ischemic MR**

Time courses of CMR-derived LV remodeling and ischemic MR parameters across all experimental models are summarized in Table 2. In all experimental groups, post-MI remodeling was characterized by enlarged LV

dimensions and decreased LVEF. Infarct size (quantified by late gadolinium enhancement CMR sequence at 1 week post-MI) was significantly larger in the LCx and LAI occlusion groups than in the LAD group (median infarct size = 37.8%, 37.2%, and 28.1% in the LCx, LAI, and LAD groups, respectively), with LV volume showing a similar pattern (Table 2).

Ischemic MR was estimated from CMR-derived regurgitant volumes and fractions (Table 1). Ischemic MR was mild in the LCx group at 1 week post-MI (RF 4.3%) but markedly increased by 8 weeks (RF 15.6%). In the LAI group, ischemic MR was even more pronounced at 1 week (RF 17.2%) with further progression by 8 weeks (RF 25.1%).

**Impact of LA remodeling and ischemic MR on pulmonary pressure**

Eight weeks after MI, LAI animals had a worse pulmonary hemodynamic profile than controls, with a trend toward high PA pressures and resistances (Table 3). Within the LAI group, 6 of 8 animals had a mean pulmonary artery pressure equal to or greater than 25 mmHg, indicating pulmonary hypertension. In 2 of these pigs, mean pulmonary artery pressure was severe (> 40 mmHg), and these animals had hepatic congestion secondary to heart failure (Supplementary Figure 4). Pulmonary artery pressure was normal in the LCx group (Table 3).

Within the LCx and LAI groups, pulmonary artery pressure correlated better with ischemic MR severity ($R=0.84$, $p<0.001$) and LA enlargement ($R=0.83$, $p<0.001$) than with LV parameters such as LVEF ($R=-0.58$, $p=0.009$) and LVESV ($R=0.47$, $p=0.04$) (Supplementary Figure 5).

**Histology findings: post-infarction left atrial structural remodeling**

The impact of permanent LA coronary occlusion on chamber histology was evaluated in 2 additional animals undergoing the LAI procedure and sacrificed after CMR exam on day-7 post-MI. Compared with healthy tissue, atrial tissue of these animals showed extensive myocardial injury, with cardiomyocyte loss and areas of fibrosis (Figure 4, panels C-H), confirming the effects of atrial infarction in this model. Qualitative assessment by polarized light microscopy revealed immature collagen-fiber organization in these areas, indicating an early post-infarction reparative process in the LA myocardium.

Histological changes at 8 weeks post-MI were evaluated in the atria of animals completing the protocol. Atria were harvested after the final CMR exam. The LAI group showed extensive LA enlargement (Supplementary Figure 2)

associated with pronounced patchy and diffuse interstitial collagen deposition (Figure 4, and Supplementary Figure 3). Conversely, LA tissue from the LCx group was characterized by mild interstitial fibrosis with focal or no fibrotic areas. No pathological changes were observed in atria of LAD animals. The absence of LA remodeling was consistent with the absence of LA disease in the CMR studies in this group.

## Discussion

The present study provides insight into the determinants and consequences of LA remodeling after acute MI in translational large-animal (pig) models evaluated by CMR. Our main findings are as follows: 1) LA infarction as a complication of LCx-dependent infarction results in massive LA remodeling with extensive fibrosis during the first week post-MI. These anatomical LA changes are associated with markedly altered contractile and reservoir function and progression of ischemic MR.; 2) Ischemic MR without concomitant LA infarction is associated with early and progressive LA remodeling, although to a less extent than cases with associated LA infarction; 3) Post-MI LV dysfunction without ischemic MR or LA infarction is associated with mild and transient LA remodeling; 4) The combination of post-MI ischemic MR and LA infarction is associated with early onset pulmonary hypertension and liver congestion, hallmarks of post-MI HF.

### Atrial infarction complicating acute MI induces severe remodeling and persistent LA dysfunction

The most prominent finding of this study is the dramatic impact of LA infarction (secondary to LA coronary artery occlusion) on LA chamber remodeling and the persistent impairment of LA contractile and reservoir physiology. These functional abnormalities reflect extensive fibrotic replacement of the atrial myocardium. The progressive LA chamber dilation and persistent functional impairment seen from the subacute (1 week) to chronic (8 week) phases identifies a specific time course of atrial myopathy. To our knowledge, this is the first experimental evidence of the structural and functional impact of LA infarction, in both the early and late post-MI periods. In this regard, although diagnosis of atrial infarction remains elusive,[13] autopsy reports suggest that its impact is significant.[14] The atrial coronary circulation system is complex[17] and the response of the atrial chamber to ischemia is not well characterized. Prior studies showed that LA coronary ischemia blunted the compensatory booster function during acute occlusion.[18] Left atrial infarction secondary to permanent occlusion of the LA coronary artery (associated with proximal LCx occlusion) resulted in severe atrial fibrosis due to the replacement of extensive areas of cardiomyocyte loss. Collagen staining revealed an immature structure at 7 days post-MI. Conversely, at 8 weeks a well-organized network was observed, with both patchy and interstitial distributions. At this chronic stage, the remodeling of the atrial extracellular matrix was characterized by excessive collagen deposition. The net increase in collagen content likely contributes to this change in LA physiology. In this regard, most previous reports have

focused on fibrotic area or collagen content as markers of extracellular matrix changes in atrial remodeling models, such as chronic atrial pacing, HF,[19] or volume overload.[20]

**Contribution of MR and LV dysfunction to post-MI atrial remodeling**

Our experimental approach did not confirm an independent contribution of isolated LV dysfunction to LA enlargement because LAD occlusion alone, in the absence of ischemic MR or LA infarction, produced no CMR or histological LA abnormalities 8 weeks after MI. However, in the absence of induced LA ischemia, mild degrees of ischemic MR were related to significant atrial enlargement at 7 days. Severe LV dysfunction, and not volume overload (mild at this stage), contributed to the larger infarct size in the LCx group (~38%, vs. 25% in the LAD group). In clinical studies, the severity of LV injury (measured from the degree of enlargement, infarct size, or the presence of diastolic function abnormalities) has been regarded as a key determinant of early post-LA dilation. While the LV is typically larger in patients with LA dilation, restrictive LV filling is found in less than 30% of these patients.[3-5] In addition, moderate or severe MR is described in ~16-45% of patients with early LA dilation,[3-5] suggesting that LA disease after MI is a complex phenomenon, with prior conditions and early acute changes both contributing to the remodeling process. In previous experimental models, LA remodeling was not characterized comprehensively. Chamber dilation was described in very large, proximal LAD infarctions after 3 months of follow up[25] and in the rat model of post-MI HF,[26] whereas most reports on ischemic MR models have focused on valve geometry rather than LA remodeling.[8, 27-29] A limitation of our study in this regard is the absence of MR quantification in the LAD group. However, in our experience, MR after acute anterior MI is infrequent and usually very mild even after induction of proximal LAD occlusions.[22]

**Determinants of LA function after MI and clinical relevance**

In our study, only LCx infarctions with ischemic MR (with or without associated LA infarction) were associated with LA enlargement. Conversely, all 3 groups, including the LAD infarction group, showed a deterioration in LA phasic function after acute MI. However, these changes were severe and permanent only in LCx MI complicated with LA infarction. In the LCx group (with ischemic MR but without LA infarction) and the LAD group, these functional changes were milder and even reversible in some cases. Some clinical studies reported that abnormal LA function post-MI is an independent prognostic marker[7, 21-22]; however, a recent report suggests that LA

reservoir (peak atrial longitudinal strain) is dependent on LA size and LV longitudinal strain.[23] In this regard, our atrial infarction model presents a specific situation, severe fibrosis, in which reservoir function is mostly dependent on the contractile performance of the atria but not the LV.

**Translational impact**

The present study provides evidence of the effects of atrial infarction complicating an acute MI on the LA remodeling process. This direct injury mechanism joins the list of other mechanisms known to contribute to atrial remodeling: volume or pressure overload (mitral valve disease), neurohormonal activation (chronic HF), electrical disturbances (atrial fibrillation-induced remodeling), and inflammation[30]. An important finding of the present study is the impact of mild-to-moderate ischemic MR on the development of pulmonary hypertension. This effect is related to the presence of severe LA remodeling, highlighting the need to evaluate both parameters in the clinical setting.

In addition to impairing LA function and cardiac performance, the infarct-related structural remodeling is likely to deleteriously affect LA electrical activity. In this regard, recent data suggest that atrial coronary occlusion is a relatively frequent complication of percutaneous stenting (~15%), and entails a markedly elevated risk of atrial arrhythmias.[13] This confirms previous experimental observations that link acute LA ischemia to a greater arrhythmia vulnerability than seen with other stimuli occurring during acute MI, such as atrial stretch or neurhormonal activation.[11-12, 31] Patient atrial tissue is infrequently available after acute MI, underscoring the value of experimental studies; however, advances in cardiac imaging provide new bedside tools for evaluating patients after MI. Remodeling of the LA is now considered an important feature and a potential therapeutic target. The present study provides important information for understanding LA remodeling, revealing the consequences of atrial ischemia and ischemic MR on cardiac performance and fibrotic substrate. Early identification and close monitoring of these features may provide new therapeutic opportunities in patients at high risk of developing HF and atrial arrhythmias after MI. In addition, a potential advantage of atrial ischemia modeling is the ability to detect rapid development of extensive fibrotic atrial cardiomyopathy (in the absence of chronic atrial fibrillation), not possible with atrial pacing models,[32] providing a new preclinical tool for understanding LA remodeling.[33]

**Limitations**

Our results are limited to the specific modeling conditions presented, and by the small sample size. As discussed above, ischemic MR and atrial ischemia are clinically relevant scenarios but do not represent the whole clinical spectrum; our findings should thus be interpreted accordingly. The LCx occlusion induced to model atrial ischemia also entailed severe LV remodeling and ischemic MR, limiting our ability to isolate the contribution of each component. The comparison of different animal models provided a more comprehensive description of the LA remodelling process, but at the cost of a loss of statistical power after post-hoc adjustments in some comparisons.

**Conclusions**

The current study provides the first experimental evidence of the impact of LA ischemia after acute MI. In addition to acute chamber enlargement, other hallmarks are severe and persistent atrial function impairment, with a slight recovery after 1 week. Furthermore, this study reveals an interplay between ischemic MR and LA remodeling that should be taken into account during clinical assessment. These models may provide new tools for exploring structural remodeling of the LA.

**References.**


1. Gerber Y, Weston SA, Enriquez-Sarano M, Berardi C, Chamberlain AM, Manemann SM, Jiang R, Dunlay SM and Roger VL. Mortality Associated With Heart Failure After Myocardial Infarction: A Contemporary Community Perspective. *Circulation: Heart Failure*. 2016;9:e002460.

2. O'Gara PT, Kushner FG, Ascheim DD, Casey DE, Chung MK, de Lemos JA, Ettinger SM, Fang JC, Fesmire FM, Franklin BA, Granger CB, Krumholz HM, Linderbaum JA, Morrow DA, Newby LK, Ornato JP, Ou N, Radford MJ, Tamis-Holland JE, Tommaso CL, Tracy CM, Woo YJ and Zhao DX. 2013 ACCF/AHA Guideline for the Management of ST-Elevation Myocardial InfarctionA Report of the American College of Cardiology Foundation/American Heart Association Task Force on Practice Guidelines. *Journal of the American College of Cardiology*. 2013;61:e78-e140.

3. Beinart R, Boyko V, Schwammenthal E, Kuperstein R, Sagie A, Hod H, Matetzky S, Behar S, Eldar M and Feinberg MS. Long-term prognostic significance of left atrial volume in acute myocardial infarction. *J Am Coll Cardiol*. 2004;44:327-34.

4. Meris A, Amigoni M, Uno H, Thune JJ, Verma A, Kober L, Bourgoun M, McMurray JJ, Velazquez EJ, Maggioni AP, Ghali J, Arnold JM, Zelenkofske S, Pfeffer MA and Solomon SD. Left atrial remodeling in patients with myocardial infarction complicated by heart failure, left ventricular dysfunction, or both: the VALIANT Echo study. *Eur Heart J*. 2009;30:56-65.

5. Moller JE, Hillis GS, Oh JK, Seward JB, Reeder GS, Wright RS, Park SW, Bailey KR and Pellikka PA. Left atrial volume: a powerful predictor of survival after acute myocardial infarction. *Circulation*. 2003;107:2207-12.

6. Møller JE, Pellikka PA, Hillis GS and Oh JK. Prognostic Importance of Diastolic Function and Filling Pressure in Patients With Acute Myocardial Infarction. *Circulation*. 2006;114:438-444.

7. Lønborg JT, Engstrøm T, Møller JE, Ahtarovski KA, Kelbæk H, Holmvang L, Jørgensen E, Helqvist S, Saunamäki K, Søholm H, Andersen M, Mathiasen AB, Kühl JT, Clemmensen P, Køber L and Vejlstrup N. Left atrial volume and function in patients following ST elevation myocardial infarction and the association with clinical outcome: a cardiovascular magnetic resonance study. *European Heart Journal - Cardiovascular Imaging*. 2013;14:118-127.

8. Levine RA and Schwammenthal E. Ischemic Mitral Regurgitation on the Threshold of a Solution: From Paradoxes to Unifying Concepts. *Circulation*. 2005;112:745-758.

9. Amigoni M, Meris A, Thune JJ, Mangalat D, Skali H, Bourgoun M, Warnica JW, Barvik S, Arnold JMO, Velazquez EJ, Van de Werf F, Ghali J, McMurray JJV, Køber L, Pfeffer MA and Solomon SD. Mitral regurgitation in myocardial infarction complicated by heart failure, left ventricular dysfunction, or both: prognostic significance and relation to ventricular size and function. *European Heart Journal*. 2007;28:326-333.

10. Lu ML, De Venecia T, Patnaik S and Figueredo VM. Atrial myocardial infarction: A tale of the forgotten chamber. *Int J Cardiol*. 2016;202:904-9.

11. Nishida K, Qi XY, Wakili R, Comtois P, Chartier D, Harada M, Iwasaki YK, Romeo P, Maguy A, Dobrev D, Michael G, Talajic M and Nattel S. Mechanisms of atrial tachyarrhythmias associated with coronary artery occlusion in a chronic canine model. *Circulation*. 2011;123:137-46.

12. Yamazaki M, Avula UM, Bandaru K, Atreya A, Boppana VS, Honjo H, Kodama I, Kamiya K and Kalifa J. Acute regional left atrial ischemia causes acceleration of atrial drivers during atrial fibrillation. *Heart Rhythm*. 2013;10:901-9.

13. Álvarez-García J, Vives-Borrás M, Gomis P, Ordóñez-Llanos J, Ferrero-Gregori A, Serra-Peñaranda A and Cinca J. Electrophysiological Effects of Selective Atrial Coronary Artery Occlusion in Humans. *Circulation*. 2016.

14. Lazar EJ, Goldberger J, Peled H, Sherman M and Frishman WH. Atrial infarction: diagnosis and management. *Am Heart J*. 1988;116:1058-63.

15. Fernandez-Jimenez R, Sanchez-Gonzalez J, Aguero J, Garcia-Prieto J, Lopez-Martin GJ, Garcia-Ruiz JM, Molina-Iracheta A, Rossello X, Fernandez-Friera L, Pizarro G, Garcia-Alvarez A, Dall'Armellina E, Macaya C, Choudhury RP, Fuster V and Ibanez B. Myocardial edema after ischemia/reperfusion is not stable and follows a bimodal pattern: imaging and histological tissue characterization. *J Am Coll Cardiol*. 2015;65:315-23.

16. Fernandez-Jimenez R, Garcia-Prieto J, Sanchez-Gonzalez J, Aguero J, Lopez-Martin GJ, Galan-Arriola C, Molina-Iracheta A, Doohan R, Fuster V and Ibanez B. Pathophysiology Underlying the Bimodal Edema Phenomenon After Myocardial Ischemia/Reperfusion. *J Am Coll Cardiol*. 2015;66:816-28.

17. James TN and Burch GE. The atrial coronary arteries in man. *Circulation*. 1958;17:90-8.

18. Stefanadis C, Dernellis J, Tsiamis E and Toutouzas P. Effects of pacing-induced and balloon coronary occlusion ischemia on left atrial function in patients with coronary artery disease. *Journal of the American College of Cardiology*. 1999;33:687-696.

19. Li D, Fareh S, Leung TK and Nattel S. Promotion of Atrial Fibrillation by Heart Failure in Dogs: Atrial Remodeling of a Different Sort. *Circulation*. 1999;100:87-95.

20. Verheule S, Wilson E, Everett T, Shanbhag S, Golden C and Olgin J. Alterations in Atrial Electrophysiology and Tissue Structure in a Canine Model of Chronic Atrial Dilatation Due to Mitral Regurgitation. *Circulation*. 2003;107:2615-2622.

21. Kühl JT, Møller JE, Kristensen TS, Kelbæk H and Kofoed KF. Left Atrial Function and Mortality in Patients With NSTEMIAn MDCT Study. *JACC: Cardiovascular Imaging*. 2011;4:1080-1087.

22. Antoni ML, ten Brinke EA, Atary JZ, Marsan NA, Holman ER, Schalij MJ, Bax JJ and Delgado V. Left atrial strain is related to adverse events in patients after acute myocardial infarction treated with primary percutaneous coronary intervention. *Heart*. 2011;97:1332-1337.

23. Ersbøll M, Andersen MJ, Valeur N, Mogensen UM, Waziri H, Møller JE, Hassager C, Søgaard P and Køber L. The Prognostic Value of Left Atrial Peak Reservoir Strain in Acute Myocardial Infarction Is Dependent on Left Ventricular Longitudinal Function and Left Atrial Size. *Circulation: Cardiovascular Imaging*. 2013;6:26-33.

24. Kyhl K, Vejlstrup N, Lønborg J, Treiman M, Ahtarovski KA, Helqvist S, Kelbæk H, Holmvang L, Jørgensen E, Saunamäki K, Søholm H, Andersen MJ, Møller JE, Clemmensen P and Engstrøm T. Predictors and prognostic value of left atrial remodeling after acute myocardial infarction. *Open Heart*. 2015;2.

25. Ishikawa K, Aguero J, Tilemann L, Ladage D, Hammoudi N, Kawase Y, Santos-Gallego CG, Fish K, Levine RA and Hajjar RJ. Characterizing preclinical models of ischemic heart failure: differences between LAD and LCx infarctions. *Am J Physiol Heart Circ Physiol*. 2014;307:H1478-86.

26. Boixel C, Fontaine V, Rucker-Martin C, Milliez P, Louedec L, Michel JB, Jacob MP and Hatem SN. Fibrosis of the left atria during progression of heart failure is associated with increased matrix metalloproteinases in the rat. *J Am Coll Cardiol*. 2003;42:336-44.

27. Gorman JH, 3rd, Gorman RC, Plappert T, Jackson BM, Hiramatsu Y, St John-Sutton MG and Edmunds LH, Jr. Infarct size and location determine development of mitral regurgitation in the sheep model. *J Thorac Cardiovasc Surg*. 1998;115:615-22.

28. Jensen H, Jensen MO, Ringgaard S, Smerup MH, Sorensen TS, Kim WY, Sloth E, Wierup P, Hasenkam JM and Nielsen SL. Geometric determinants of chronic functional ischemic mitral regurgitation: insights from three-dimensional cardiac magnetic resonance imaging. *J Heart Valve Dis*. 2008;17:16-22; discussion 23.

29. Llaneras MR, Nance ML, Streicher JT, Lima JA, Savino JS, Bogen DK, Deac RF, Ratcliffe MB and Edmunds LH, Jr. Large animal model of ischemic mitral regurgitation. *Ann Thorac Surg*. 1994;57:432-9.

30. Casaclang-Verzosa G, Gersh BJ and Tsang TSM. Structural and Functional Remodeling of the Left AtriumClinical and Therapeutic Implications for Atrial Fibrillation. *Journal of the American College of Cardiology*. 2008;51:1-11.

31. Alasady M, Shipp NJ, Brooks AG, Lim HS, Lau DH, Barlow D, Kuklik P, Worthley MI, Roberts-Thomson KC, Saint DA, Abhayaratna W and Sanders P. Myocardial infarction and atrial fibrillation: importance of atrial ischemia. *Circ Arrhythm Electrophysiol*. 2013;6:738-45.

32. Martins RP, Kaur K, Hwang E, Ramirez RJ, Willis BC, Filgueiras-Rama D, Ennis SR, Takemoto Y, Ponce-Balbuena D, Zarzoso M, O'Connell RP, Musa H, Guerrero-Serna G, Avula UMR, Swartz MF, Bhushal S, Deo M, Pandit SV, Berenfeld O and Jalife J. Dominant Frequency Increase Rate Predicts Transition from Paroxysmal to Long-Term Persistent Atrial Fibrillation. *Circulation*. 2014;129:1472-1482.

33. Kottkamp H. Fibrotic atrial cardiomyopathy: a specific disease/syndrome supplying substrates for atrial fibrillation, atrial tachycardia, sinus node disease, AV node disease, and thromboembolic complications. *J Cardiovasc Electrophysiol*. 2012;23:797-9.

**Figure Legends.**

**Figure 1.** Study design and experimental procedures. (A) Two porcine models of ischemic MR were created by chronic occlusion of the left circumflex artery: 1, No additional vessel occlusion (LCx); 2, Additional occlusion of the main left atrial branch to induce LA Infarction (LAI). 3, A third model of MI was generated with no ischemic MR by LAD occlusion. (B, C) Typical segmental scar distributions. (D) Timeline of imaging and histology evaluation.

**Figure 2.** Left atrial remodeling after MI. (A) Maximum LA size at 1 and 8 weeks post MI for each group (see Figure 1), indicating progressive LA dilation in the LAI and LCx groups, most pronounced in the former. Controls are non-infarcted pigs. (B-G) Representative end-systolic frames from 3-chamber views; MI group and time point are indicated in each image.

**Figure 3.** Changes in left atrial reservoir function after MI. (A) LA reservoir at 1 and 8 weeks post MI, indicating early (1 week) impairment in all AMI groups, the most severe and persistent (at 8 weeks) corresponding to the LAI group (B) Representative -chamber planimetry images at 8 weeks post MI. Maximum area is delineated by solid contours, and minimum area by red-shading and dashed contours.

**Figure 4.** Histology of LA remodeling. (A) Representative atrial tissue of an LAI pig at 1 week post MI. (B) Endocardium (top) and endocardium in atrial tissue of an LAI pig at 1 week post MI. (C-H) Histological sections of atria from Control and LAI pigs at 1 week post-MI, showing evidence of marked cardiomyocyte loss (E) with extensive fibrosis (F-H). (I-L) Histological sections of atria from the 3 MI at 8 weeks, showing evidence of interstitial fibrosis in the LCx group (J) and severely fibrotic replacement in the LAI group (K), contrasting with the Control and LAD groups (I,L). Scale bars, 1 mm (top row); 200 µm (bottom row). Stainings: Picrosirius Red in brightfield (B, D, F-G) and polarized light microscopy (H); Hematoxylin-eosin (C and E); Masson's trichrome (I-L).

**Table 1. Left atrial remodeling CMR parameters: time course by group**

| | Control (n=4) | | LCx (n=7) | | LAI (n=8) | | LAD (n=18) | |
|---|---|---|---|---|---|---|---|---|
| | Baseline | 8 weeks | 1 week | 8 weeks | 1 week | 8 weeks | 1 week | 8 weeks |
| Maximal area, cm2 | 13.1 (12.7-13.3) | 18.8 (18.2-19.6) | 19.5 (18.6-20.9)* ‡ | 25. (22-27) ‡ | 22.6 (20.3-23.8)* ‡ | 32.6 (27.2-38.9)* † ‡ | 13.2 (12.4-14.5) | 16.2 (14.8-18.2) |
| Maximal indexed area, cm2/m2 | 15.7 (15.2-16.3) | 15.3 (14.8-15.9) | 19.9 (19.0-22.3) * ‡ | 17.0 (16.6-19.1) ‡ | 22.5 (21.4-23.2)* ‡ | 25.1 (19.3-30.0)* † ‡ | 15.4 (13.4-16.4) | 14.3 (12.8-15.0) |
| Minimum area, cm2 | 8.0 (7.7-8.4) | 11.4 (11.1-11.9) | 15.0 (14.3-15.9) * ‡ | 17.0 (16.2-20.4) | 18.9 (17.5-20.7) *† ‡ | 27.3 (22.2-32.8) * † ‡ | 9.7 (8.9-10.7) | 11.6 (9.7-13.4) |
| Minimum indexed area, cm2/m2 | 9.6 (9.1-10.2) | 9.2 (9.0-9.7) | 15.5 (14.5-17.2) * ‡ | 13.4 (10.9-14.4) | 19.2 (17.8-20.6) *† ‡ | 19.8 (15.2-27.7) * † ‡ | 10.9 (10.3-11.5) | 9.6 (8.7-10.8) |
| Reservoir function, % | 38.2 (36.4-39.2) | 38.3 (37.4-38.8) | 24.1 (19.9-28.7)* ‡ | 26.4 (21.7-29.9) | 13.8 (11.2-17.7)* † | 16.5 (9.7-22.5) * ‡ | 27.1 (24.2-30.8)* | 28.6 (25.1-31.6) |
| Conduit function, % | 15.0 (14.9-15.2) | 19.8 (17.7-22.8) | 10.2 (7.1-14.4) | 11.7 (8.1-14.9)* | 7.7 (6.2-9.7) | 8.7 (6.5-10.7)* | 8.1 (5.6-12.3)* | 9.6 (6.9-13.7)* |
| Booster function, % | 27.2 (25.2-28.6) | 22.7 (20.3-24.1) | 15.9 (13.9-18.6)* | 18.5 (15.8-19.6) | 4.4 (2.4-9.9)*†‡ | 8.1 (5.6-15.4)* ‡ | 21.4 (16.3-22.9) | 21.2 (19.7-24.6) |

**Data expressed in median (interquartile range). Pairwise comparisons at each timepoint: *p<0.05 vs Control; †p<0.05 vs LCx; ‡ p<0.05 vs LAD.**

**Table 2. Time course of LV remodeling and MR parameters by study group**

| | Control (n=4) | | LCx (n=7) | | LAI (n=8) | | LAD (n=18) | |
|---|---|---|---|---|---|---|---|---|
| | Baseline | 8 weeks | 1 week | 8 weeks | 1 week | 8 weeks | 1 week | 8 weeks |
| Body weight, kg | 29 (29-29.4) | 55.3 (53.5-57.1) | 37 (35-40)* | 70 (67.3-73.5)* | 39 (34.8-43)* ‡ | 62 (59.8-71) | 34.3 (30.4-37.4) | 54 (45.8-55.8) |
| Left ventricle | | | | | | | | |
| Infarct size, % of LV mass | 0 | 0 | 37.8 (27.2-39.9)* | 18.0 (14.1-18.9)* ‡ | 37.2 (33.2-40.5)* | 23.0 (16.7-27.9)* | 27.0 (23.9-36.4)* | 23.8 (22.1-31.3)* |
| EDV, ml | 92.7 (86.9-98.8) | 118.1 (112.5-125.5) | 132.1 (121.9-142.1)* | 242.5 (180.6-246)* | 135.2 (121.1-141.8)* | 202.9 (190.5-220.4)* | 121.8 (112.0-133.9)* | 173.1 (151.7-201.1)* |
| Indexed EDV, ml/m2 | 111.7 (103.8-120.9) | 96.6 (94-100) | 137.3 (130.1-147.8) | 161.5 (138.3-172.5)* | 139.9 (129.8-143.2) | 149.5 (145.4-154.4)* | 134.6 (130.6-142.1)* | 151.4 (129.6-165.3)* |
| ESV, ml | 47.2 (43.3-50.4) | 40.9 (38.3-43.5) | 84.5 (69.3-91.5)* | 121.4 (101.2-147.5)* | 87.1 (75.4-90.6)* | 128.0 (116.1-144.1)* | 77.1 (66.3-85.4)* | 119.0 (95.9-138.8)* |
| Indexed ESV, ml/m2 | 56.9 (51.7-61.6) | 33.1 (32-34.5) | 90.1 (78.1-95.2)* | 86.2 (76.7-101.7)* | 88.2 (80.2-93.1)* | 92.6 (87.9-101.3)* | 86.1 (78.7-94.2)* | 103.4 (85.9-116.6)* |
| LVEF, % | 50.1 (49.4-50.8) | 66.4 (64.0-68.1) | 35.0 (34.6-38.1)* | 47.3 (36.0-49.0)* ‡ | 36.7 (35.7-37.3)* | 36.6 (33.0-40.1)* | 36.4 (35.1-39.1)* | 30.3 (28.1-33.7)* |
| Mitral | | | | | | | | |

| | | | | | | | | |
|---|---|---|---|---|---|---|---|---|
| regurgitation | | | | | | | | |
| Regurgitant volume, ml | 0.74 ([-1.4]-2.6) | 1.2 ([-0.4]-2.1) | 2.1 (1.9-4.0) | 13.2 (8.7-16.6) | 7.4 (5.8-11.1) | 17.8 (15.5-27.2) | NA | NA |
| Indexed regurgitant volume, ml/m2 | 0.9 ([-1.7]-3.4) | 0.9([-0.3]-1.6) | 2.2 (2-3.9) | 9.6 (6.4-11.3) | 7.5 (5.8-10.7) | 13.8 (12.0-18.9) | NA | NA |
| Regurgitant fraction, % | 1.4 ([-3.3]-5.5) | 1.4([-0.8]-2.4) | 4.3 (3.5-7.9) | 15.6 (11.5-16.8) | 17.2 (11.4-21.1) | 25.1 (23.0-36.3) | NA | NA |

**Abbreviations: LV, left ventricle; EDV, end-diastolic volume; ESV, end-systolic volume; LVEF, LV ejection fraction; NA, not applicable.**

**Data expressed in median (interquartile range). Pairwise comparisons at each timepoint*p<0.05 vs Control; †p<0.05 vs LCx; ‡ p<0.05 vs LAD.**

**Table 3. Hemodynamic data 8 weeks after MI**

| | Control (n=4) | LCx (n=7) | LAI (n=8) |
|---|---|---|---|
| Heart rate, bpm | 51 (46-57) | 58 (48-71) | 75 (57-85) |
| PA wedge pressure, mmHg | 4 (4-5) | 9 (8-10) | 14 (10-17)*† |
| Mean PA pressure, mmHg | 16 (15-16) | 18 (16-20) | 27 (24-34)*† |
| Mean RA pressure, mmHg | 4 (3-4) | 4 (3-4) | 5 (3-6) |
| Cardiac output, l/min | 4.1 (3.6-4.6) | 5.4 (3.9-5.4) | 4 (2.9-4.3) |
| Cardiac index, l/min*m2 | 3.1 (2.7-3.4) | 3.6 (2.8-3.9) | 3.1 (2.2-3.3) |
| Pulmonary vascular resistance, WU | 2.6 (2.3-3.1) | 2.2 (2-2.2) | 3.8 (2.8-5.5)† |
| Pulmonary vascular resistance, WU*m2 | 3.6 (3.2-4.1) | 3.1 (2.9-3.3) | 5.2 (3.6-7.3)† |

**Abbreviations: PA, pulmonary artery; WU, Wood units.**

**Data expressed in median (interquartile range). Pairwise comparisons: *p<0.05 vs Control; †p<0.05 vs LCx**

## Supplementary Methods.

### Experimental procedures

The study was approved by the local institutional animal research committee and conducted in accordance with the National Research Council Guide for the Care and Use of Laboratory Animals. Anesthesia was induced with intramuscular ketamine (20 mg/kg), xylazine (2 mg/kg), and midazolam (0.5 mg/kg) and maintained by continuous intravenous infusion of ketamine (2 mg/kg/h), xylazine (0.2 mg/kg/h), and midazolam (0.2 mg/kg/h). Mechanical ventilation was adjusted to 30% oxygen, 8-10 ml/kg tidal volume at 15 respirations per minute. Arterial and venous femoral access was achieved by the Seldinger technique. During acute MI induction, an unfractioned heparin iv bolus was administered (300 mg/kg) at the beginning of the procedure, and amiodarone was continuously infused (300 mg/h). After the procedure, femoral sheaths were removed and the animals were allowed to recover. At the final time point of each study, animals were sacrificed with pentobarbital sodium and hearts were removed and processed for histological analysis.

### Ischemic MR model

To establish a porcine model of ischemic MR, we evaluated the main factors contributing to the structural LV substrate that underlies changes in mitral-valve geometry. Most animal models have focused on LCx coronary artery infarction induced by surgical or percutaneous approaches, the most common being ligation of 2 oblique marginal branches in the sheep.[29] To select the most effective model of ischemic MR, we first compared angioplasty-balloon-induced ischemia/reperfusion with permanent occlusion induced by deployment of a percutaneous coronary coil. Both approaches produced similar-sized infarcts, but only permanent coronary occlusion produced the typical local remodeling causing ischemic MR during the observation period (Supplementary Figure 1). Second, given the variable LCx artery anatomy in the pig, we evaluated the influence of LCx size on the development of ischemic MR (Supplementary Figure 1). Only moderate-to-large LCx proximal occlusions consistently produced the typical features of ischemic MR and were included in the final analyses. In ~10% of animals, the LCx was too small to create the ischemic MR model with a high probability of success. In all animals included in the study, baseline echocardiograms showed no more than a trace degree of MR before model creation.

The data for the LAD ischemic/reperfusion group were obtained from 18 animals included in a previous, unpublished study in our laboratory. For the descriptive purposes of the present study, we minimized the number of animals needed to evaluate our hypothesis. For this reason, while the main remodeling endpoints were available for all animals in the LAD group (n=18), histological data were available only from a smaller but representative subset (n=5).

The coiling procedure in the proximal LCx was feasible in most animals. Mortality was 28.6% (6/21 animals), and most deaths occurred during the first 2 weeks. In total, 2 animals died due to intraprocedural refractory ventricular fibrillation.

**Supplementary Figures.**

**Supplementary Figure 1.** Comparison of left circumflex artery infarction by proximal LCx ischemia/reperfusion (B) and LCx coil occlusion (C). Images show end-systolic frames of the 3 chamber view. LCx coil occlusion was a superior model of chronic ischemic MR than proximal LCx ischemia/reperfusion, which evidenced minimal or no MR in pilot experiments. In addition, if the LCx was small (C), development of MR was mild in the dominant marginal branch, mid LCx, or even proximal LCx.

**Supplementary Figure 2.** Post-MI LA remodelling at 8 weeks post MI. (A) Control heart. (B) LAI heart (characterized by ischemic MR), showing LA enlargement. (C) LAD heart, showing no LA enlargement. (D,E) Excised LA from a control animal (D) and an LAI animal (E), showing marked dilation and fibrosis after LA infarction and ischemic MR.

**Supplementary Figure 3.** Representative histological sections showing the LA fibrosis pattern in animals developing ischemic MR in the absence of LA infarction (LCx group, left panel) and and in its presence (LAI group, center and right panels). Picrosirius red staining (left and center panels) and Masson's trichrome staining illustrate the extent of fibrosis in different animals from each group, supporting the consistency of the models. Scale bars, 1 mm. Picrosirius red and Masson's trichrome staining are shown for the same samples in F and J and in H and L.

**Supplementary Figure 4.** Representative Masson's-trichrome-stained liver sections from a control animal (A) and from an animal from the LAI group exhibiting pulmonary hypertension 8 weeks after LCx occlusion (B). Scale bars, 1 mm.

**Supplementary Figure 5.** Linear correlations between mean pulmonary artery pressure measured by right heart catheterization and cardiac imaging parameters at 8 weeks post-MI, including only the LCx and LAI groups. (A) Regurgitant fraction. (B) LA maximum area. (C) LA reservoir function. (D) LV ejection fraction. (E) LV end-systolic volume. (F) Table summarizing Pearson correlation coefficients and statistical significance for two-sided test. These results indicate a greater linear association between LA remodelling parameters and ischemic MR severity (by regurgitant fraction) with pulmonary artery pressures.

Figure 1

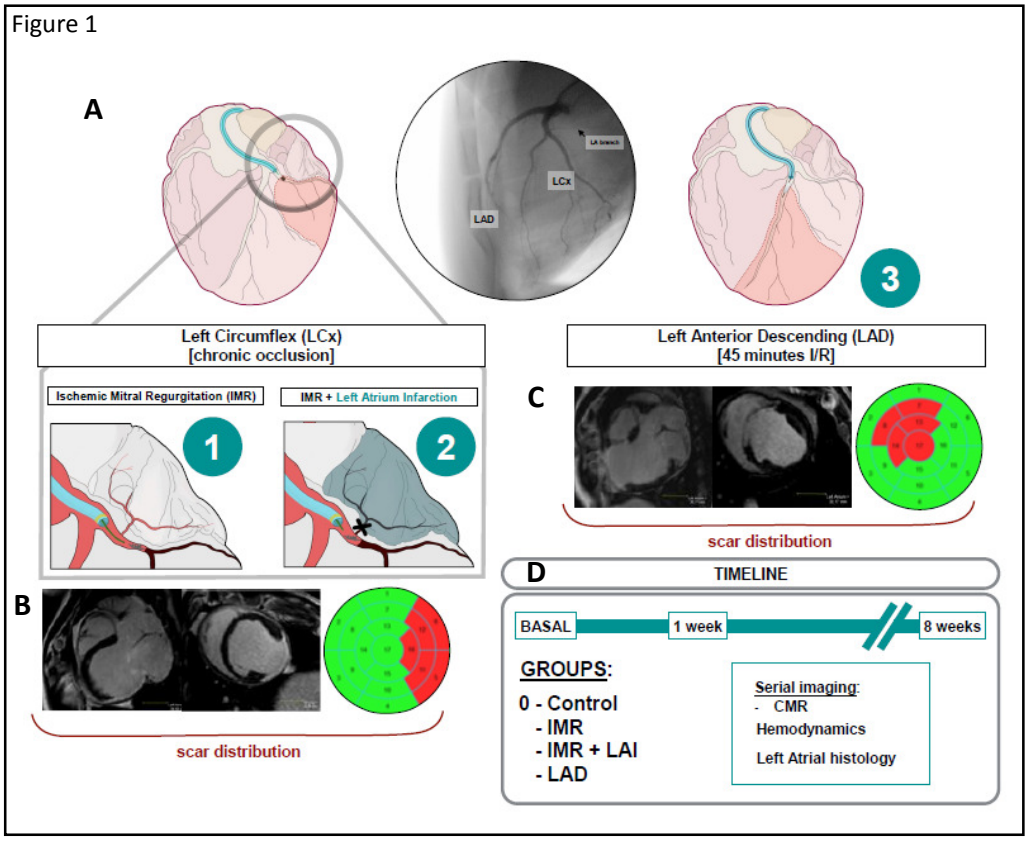


Figure 2

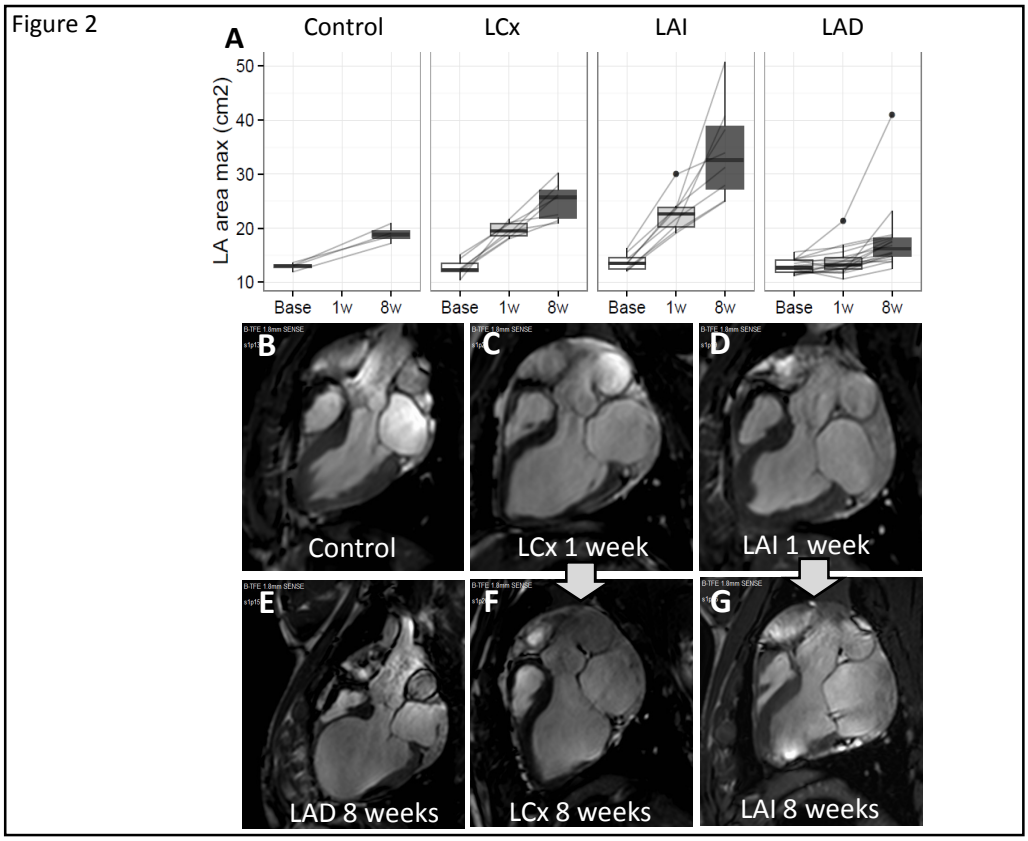

Figure 3

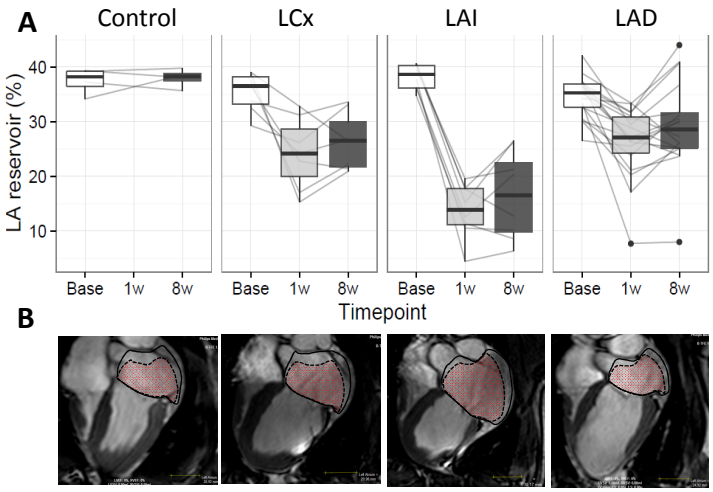


Figure 4

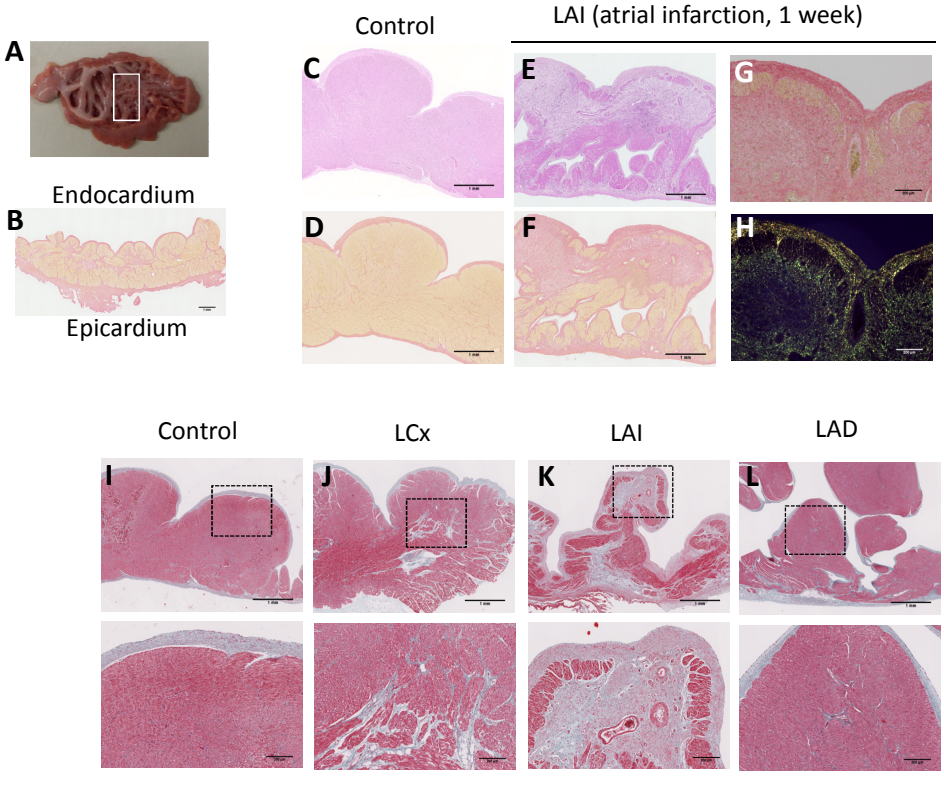

# Supplementary Figures

Supplementary Figure 1.

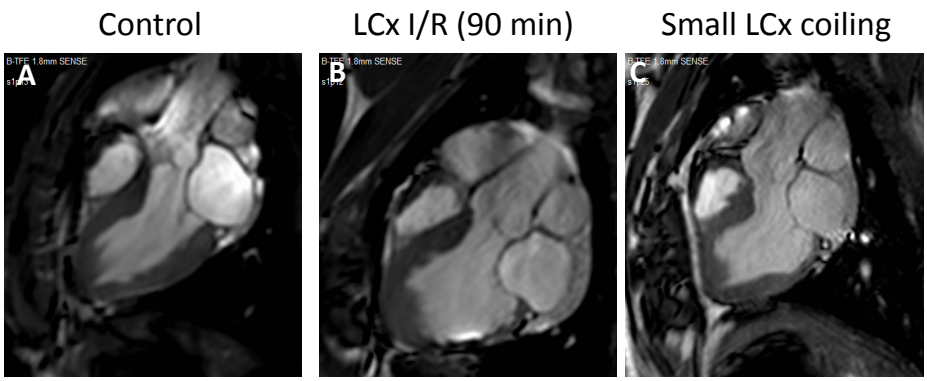

Supplementary Figure 2.

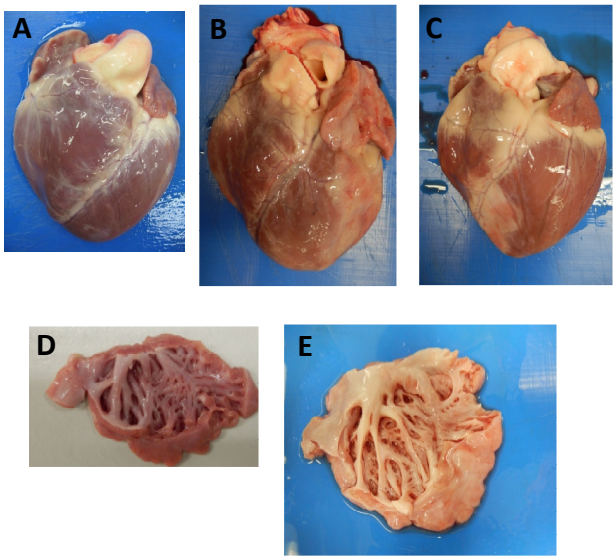


Supplementary Figure 3

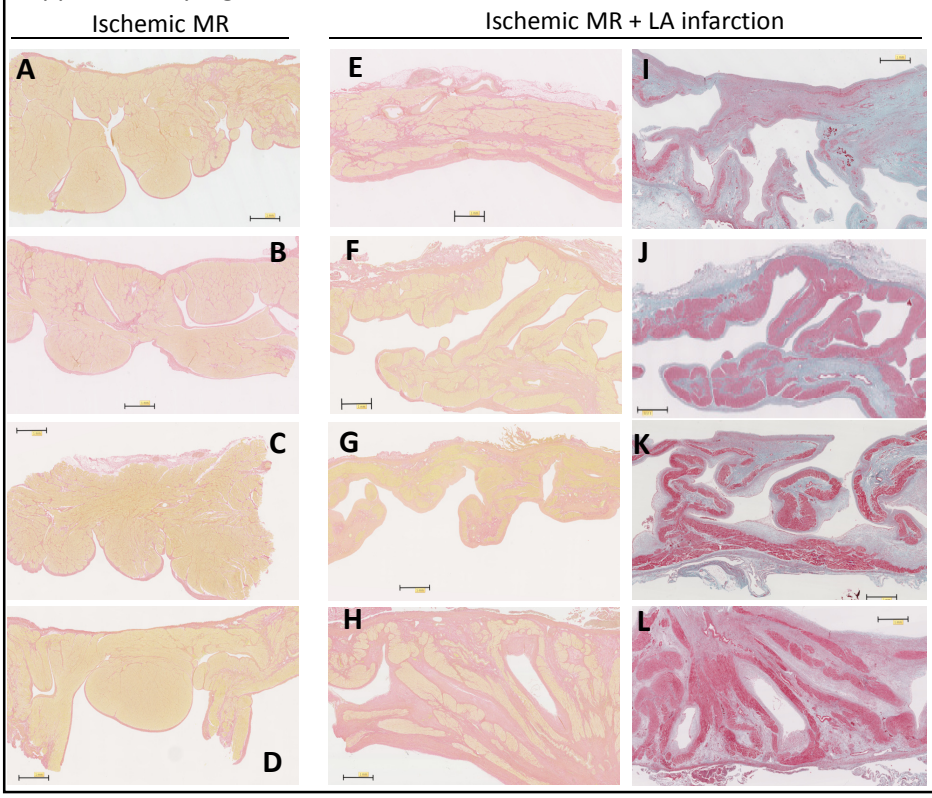

Supplementary Figure 4.

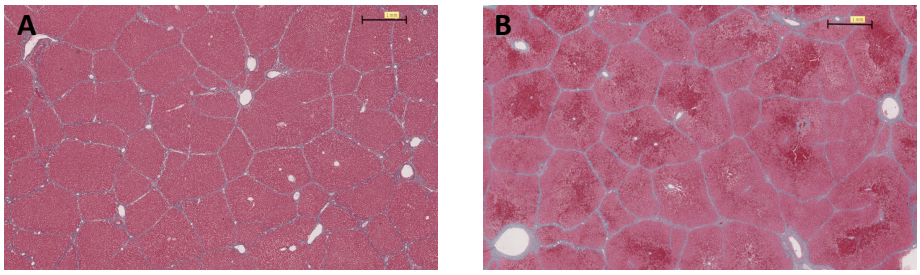


Supplementary Figure 5

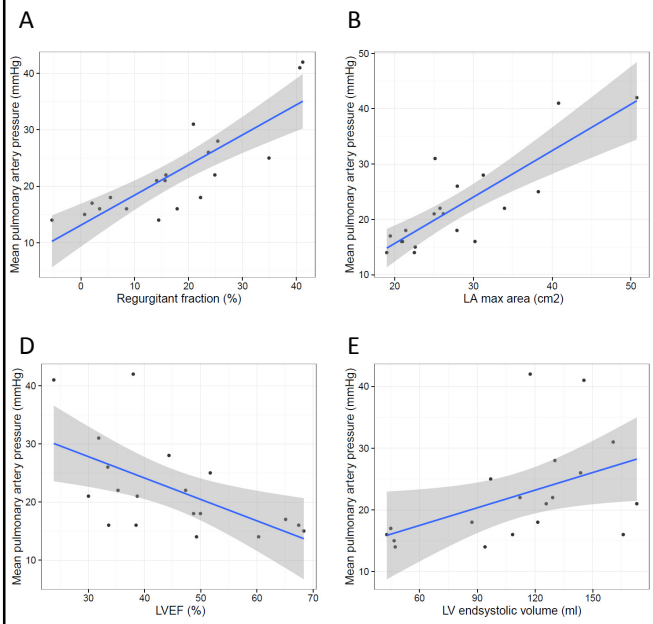


| | R | p |
|---|---|---|
| **RF (%)** | 0.84 | <0.001 |
| **LA max area (cm2)** | 0.83 | <0.001 |
| **LA reservoir (%)** | -0.62 | 0.005 |
| **LV ejection fraction (%)** | -0.58 | 0.009 |
| **LV ESV (ml)** | 0.47 | 0.04 |

**Parte 3. Desarrollo de nuevas terapias experimentales en hipertensión pulmonar.**

**Introducción a los artículos 5 y 6.**

Se trata de un trabajo de investigación aplicada en el ámbito preclínico. Tomando como modelo el descrito y caracterizado en el artículo 1 (Parte 1 de la presente Tesis Doctoral), se puso a prueba una nueva estrategia terapéutica basada en resultados previos del grupo de investigación en un modelo de roedor. La terapia a estudio es un virus adeno-asociado recombinante como vector de expresión de SERCA2a, un enzima implicado en la homeostasis del calcio en el retículo sarcoplasmico.

En este estudio, así como en la revisión metodológica posterior, fui responsable principal del proyecto y mi aportación personal fue necesaria en cada una de las etapas del mismo: diseño, generación de modelos animales, todos los procedimientos experimentales, así como la recogida y análisis de los datos y escritura de manuscritos. En este estudio, también tuve una participación parcial en la generación de vectores virales y realización de protocolos para detección de inmunidad humoral (anticuerpos neutralizantes) antes de la administración de la terapia. Como se indica en el artículo 6, uno de los principales aspectos técnicos previos al desarrollo del estudio de intervención terapéutica fue la puesta a punto del método de administración de vectores virales por vía aérea en el modelo de animal grande, para lo cual nos basamos en la metodología en el modelo de roedor.

La Figura 4 (incluida en el propio artículo 5 como Ilustración central y síntesis del trabajo) resume el diseño y conclusiones de esta parte.

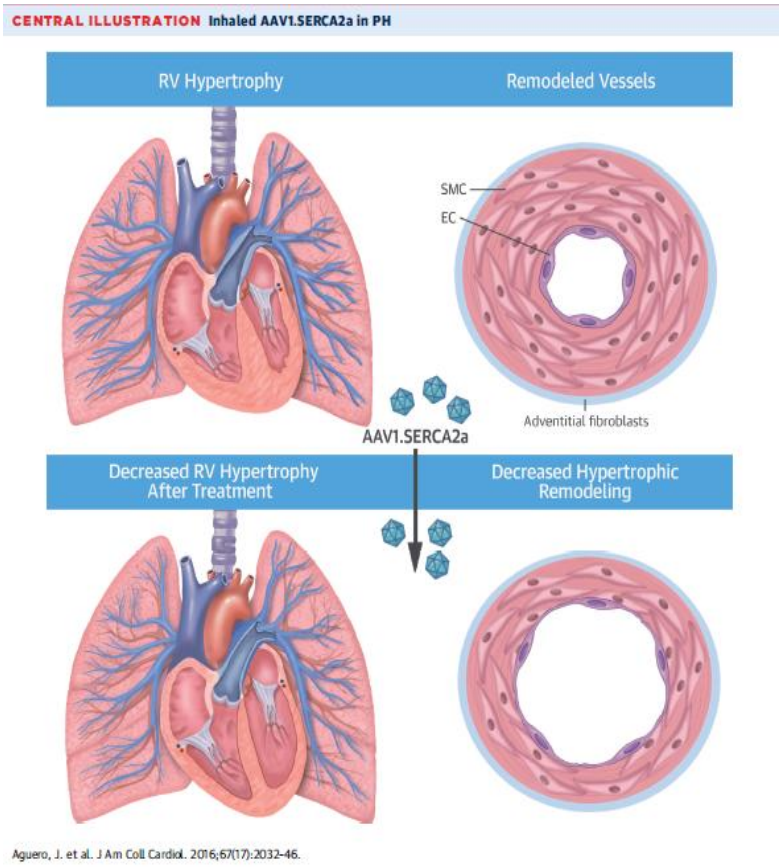


*Figura 4 (Resumen Parte 3, Desarrollo de nuevas terapias experimentales en hipertensión pulmonar). En el modelo de HTP crónica se observan cambios en el remodelado vascular pulmonar. La terapia génica es capaz de enlentecer la progresión de la enfermedad y el desarrollo de disfunción ventricular derecha.*

Referencias de los artículos.

Artículo 5 [11].

*Aguero J, Ishikawa K, Hadri L, Santos-Gallego CG, Fish KM, Kohlbrenner E, Hammoudi N, Kho C, Lee A, Ibanez B, García-Alvarez A, Zsebo K, Maron BA, Plataki M, Fuster V, Leopold JA, Hajjar RJ. Intratracheal Gene Delivery of SERCA2a Ameliorates Chronic Post-Capillary Pulmonary Hypertension in a Large Animal Preclinical Model. J Am Coll Cardiol. 2016 May 3;67(17):2032-46.*

Artículo 6 [14].

*Aguero J, Hadri L, Hammoudi N, Leonardson L, Hajjar RJ, Ishikawa K. Inhaled Gene Transfer for Pulmonary Circulation. Methods Mol Biol. 2017;1521:339-349.*

Artículo 5 [11].

*Aguero J, Ishikawa K, Hadri L, Santos-Gallego CG, Fish KM, Kohlbrenner E, Hammoudi N, Kho C, Lee A, Ibanez B, García-Alvarez A, Zsebo K, Maron BA, Plataki M, Fuster V, Leopold JA, Hajjar RJ. Intratracheal Gene Delivery of SERCA2a Ameliorates Chronic Post-Capillary Pulmonary Hypertension in a Large Animal Preclinical Model. J Am Coll Cardiol. 2016 May 3;67(17):2032-46.*

JOURNAL OF THE AMERICAN COLLEGE OF CARDIOLOGY
© 2016 BY THE AMERICAN COLLEGE OF CARDIOLOGY FOUNDATION
PUBLISHED BY ELSEVIER

VOL. 67, NO. 17, 2016
ISSN 0735-1097/$36.00
http://dx.doi.org/10.1016/j.jacc.2016.02.049

# Intratracheal Gene Delivery of SERCA2a Ameliorates Chronic Post-Capillary Pulmonary Hypertension

## A Large Animal Model

Jaume Aguero, MD,[a,b] Kiyotake Ishikawa, MD,[a] Lahouaria Hadri, PhD,[a] Carlos G. Santos-Gallego, MD,[c] Kenneth M. Fish, PhD,[a] Erik Kohlbrenner, BS,[a] Nadjib Hammoudi, MD, PhD,[a] Changwon Kho, PhD,[a] Ahyoung Lee, PhD,[a] Borja Ibáñez, MD, PhD,[b,d] Ana García-Alvarez, MD, PhD,[b] Krisztina Zsebo, PhD,[e] Bradley A. Maron, MD,[f] Maria Plataki, MD,[a] Valentin Fuster, MD, PhD,[b,g] Jane A. Leopold, MD,[f] Roger J. Hajjar, MD[a]

## ABSTRACT

**BACKGROUND** Pulmonary hypertension (PH) is characterized by pulmonary arterial remodeling that results in increased pulmonary vascular resistance, right ventricular (RV) failure, and premature death. Down-regulation of sarcoplasmic reticulum $Ca^{2+}$-ATPase 2a (SERCA2a) in the pulmonary vasculature leads to perturbations in calcium ion ($Ca^{2+}$) homeostasis and transition of pulmonary artery smooth muscle cells to a proliferative phenotype.

**OBJECTIVES** We assessed the feasibility of sustained pulmonary vascular SERCA2a gene expression using aerosolized delivery of adeno-associated virus type 1 (AAV1) in a large animal model of chronic PH and evaluated the efficacy of gene transfer regarding progression of pulmonary vascular and RV remodeling.

**METHODS** A model of chronic post-capillary PH was created in Yorkshire swine by partial pulmonary vein banding. Development of chronic PH was confirmed hemodynamically, and animals were randomized to intratracheal administration of aerosolized AAV1 carrying the human SERCA2a gene (n = 10, AAV1.SERCA2a group) or saline (n = 10). Therapeutic efficacy was evaluated 2 months after gene delivery.

**RESULTS** Transduction efficacy after intratracheal delivery of AAV1 was confirmed by β-galactosidase detection in the distal pulmonary vasculature. Treatment with aerosolized AAV1.SERCA2a prevented disease progression as evaluated by mean pulmonary artery pressure, vascular resistance, and limited vascular remodeling quantified by histology. Therapeutic efficacy was supported further by the preservation of RV ejection fraction (p = 0.014) and improvement of the RV end-diastolic pressure–volume relationship in PH pigs treated with aerosolized AAV1.SERCA2a.

**CONCLUSIONS** Airway-based delivery of AAV vectors to the pulmonary arteries was feasible, efficient, and safe in a clinically relevant chronic PH model. Vascular SERCA2a overexpression resulted in beneficial effects on pulmonary arterial remodeling, with attendant improvements in pulmonary hemodynamics and RV performance, and might offer therapeutic benefit by modifying fundamental pathophysiology in pulmonary vascular diseases.
(J Am Coll Cardiol 2016;67:2032–46) © 2016 by the American College of Cardiology Foundation.

Listen to this manuscript's audio summary by *JACC* Editor-in-Chief Dr. Valentin Fuster.

From the [a]Cardiovascular Research Center, Icahn School of Medicine at Mount Sinai, New York, New York; [b]Centro Nacional de Investigaciones Cardiovasculares Carlos III (CNIC), Madrid, Spain; [c]Atherothrombosis Research Unit, Cardiovascular Institute, Icahn School of Medicine at Mount Sinai, New York, New York; [d]IIS Fundacion Jimenez-Diaz Hospital, Madrid, Spain; [e]Biovest Consulting, LLC, Santa Barbara, California; [f]Cardiovascular Medicine Division, Brigham and Women's Hospital, Harvard Medical School, Boston, Massachusetts; and the [g]Zena and Michael A. Wiener Cardiovascular Institute, Mount Sinai School of Medicine, New York, New York. This work is supported by National Institutes of Health grants RO1 HL083156, HL093183, HL119046, and P20HL100396 and a National Heart, Lung, and Blood Institute Program of Excellence in Nanotechnology Award; contract HHSN268201000045C (to Dr. Hajjar); and National Institutes of Health R01105301 and U01 125215 (to Dr. Leopold). Part of the work was funded by a Leducq Foundation grant (to Dr. Hajjar). Dr. Aguero was supported by the Fundacion Alfonso Martin-Escudero. Dr. Hammoudi was supported by the French Federation of Cardiology; and has received a research grant from Laboratoires Servier.

Pulmonary hypertension (PH) is a group of pulmonary endovascular diseases with hemodynamic consequences for right ventricular (RV) function that portends a poor clinical prognosis. Although the current classification system for PH segregates patients on the basis of clinical and pathological features, all forms of PH are associated with some degree of aberrant pulmonary vascular remodeling (1). Current pharmacotherapies for PH do not target pulmonary vascular remodeling directly but rather aim to promote pulmonary artery vasodilation and reduce RV afterload as adverse outcomes are driven mainly by the onset of RV failure (2,3).

Epidemiological studies indicate that PH associated with increased pulmonary venous pressure and left heart failure (HF) is the most common cause of chronic PH (4). Furthermore, more than one-half of all patients with HF may develop chronic PH, leading to even more adverse cardiac events (5). Similar to pulmonary arterial hypertension (PAH) (Group 1 PH), left heart disease–related PH (Group 2 PH) has been associated with impaired pulmonary vascular reactivity, endothelial dysfunction, and excessive arteriolar muscularization, indicating that pre-capillary pulmonary vascular remodeling is present concomitant with post-capillary disease (6). Despite this, therapeutics that are effective in PAH are either not effective, have not been tested, or may be contraindicated in patients with left HF and PH (1).

SEE PAGE 2047

Currently available pharmacotherapies were developed to ameliorate disease symptomatology by targeting 1 of 3 main signaling pathways found to be deficient or activated in PH (7). Although several available compounds have shown benefit in Group 1 PH in randomized clinical trials, unresolved issues remain. These include: 1) few studies in patients with Group 2 PH; 2) a lack of evidence of long-term clinical efficacy; 3) uncertainty regarding the effects of drugs on limiting or reversing vascular remodeling in the presence of established disease; 4) the risk of serious adverse effects that limit dose escalation within or between class combination therapy; and 5) the high cost of long-term treatments. Thus, novel approaches are needed.

Gene therapy has evolved over the past several decades due to advances in vector technology and delivery methodologies. In a wide range of chronic disorders, including cardiovascular disease (8,9), efficient gene transfer has been achieved by newly designed recombinant adeno-associated virus (AAV) vectors. Several experimental studies have reported successful modulation of PH signaling pathways in a specific and efficient manner using gene therapy (10). Proof-of-concept studies in rodent PH models have demonstrated the feasibility of gene transfer of molecules related to currently available pharmacotherapies, such as the endothelial isoform of nitric oxide synthase (eNOS) (11) or prostacyclin synthase (12), that hold promise for treating PH in humans.

Abnormal calcium homeostasis in smooth muscle cells (SMCs) contributes to PH pathobiology (13). Chronically increased intracellular calcium levels in pulmonary artery SMCs trigger signaling pathways that are permissive for cellular proliferation, migration, and dedifferentiation, all of which contribute to hypertrophic vascular remodeling (13). Our group has reported previously that sarcoplasmic reticulum $Ca^{2+}$-ATPase pump 2a (SERCA2a) is a key modulator of calcium cycling in both cardiomyocytes and vascular SMCs (14). We recently demonstrated that pulmonary arterial SERCA2a expression is downregulated in the rat monocrotaline model of PH as well as in humans with PAH. Furthermore, we demonstrated in the rat model that selective pulmonary vascular gene transfer of SERCA2a using AAV1 was feasible, ameliorated arterial remodeling, and improved hemodynamic abnormalities and RV function (15).

Despite the evidence that gene therapy targeting SERCA2a has merit, a major hurdle in the translation of novel therapeutics to the clinic is the limited availability of large animal models of PH that recapitulate human disease. Most pre-clinical drug development studies evaluate interventions in rodent models of PH (16), yet there are marked differences between rodent models and human anatomy and physiology (17). Accessible large animal models of chronic PH allow for a more relevant approach to evaluate novel interventions prior to human clinical trials, as they offer similar dosing therapeutic schemes, human-sized delivery tools, and state-of-the-art diagnostic protocols to assess critical

**ABBREVIATIONS AND ACRONYMS**

**AAV** = adeno-associated virus

**AAV1.SERCA2a** = recombinant adeno-associated virus serotype 1 carrying the human SERCA2a transgene

**IQR** = interquartile range

**PAH** = pulmonary arterial hypertension

**PH** = pulmonary hypertension

**RV** = right ventricle

**SERCA2a** = sarcoplasmic reticulum $Ca^{2+}$-ATPase 2a

Dr. Maron is the recipient of an investigator-initiated grant from Gilead Sciences. All other authors have reported that they have no relationships relevant to the contents of this paper to disclose. Drs. Leopold and Hajjar contributed equally to this work. David A. Dicheck, MD, served as Guest Editor for this paper.

Manuscript received January 26, 2016; revised manuscript received February 16, 2016, accepted February 17, 2016.

endpoints such as pulmonary hemodynamics and RV structure and function (18,19). Validating the results of rodent studies in large animal models of chronic PH therefore increases the likelihood of success in drug development at the pre-clinical stage (17).

The objectives of this study were to assess the feasibility of sustained pulmonary vascular SERCA2a gene transfer in a large animal model of chronic post-capillary PH and to evaluate the efficacy of gene transfer on the progression of pulmonary vascular and RV remodeling. On the basis of the encouraging results in a number of studies (12,20,21), including our own proof-of-concept study in a rodent model of PH (15), we tested a novel aerosol inhalation gene delivery strategy to minimize off-target transgene expression and increase safety.

## METHODS

The study was performed in accordance with the Guidelines for the Care and Use of Laboratory Animals, with approval granted by the Icahn School of Medicine at Mount Sinai Institutional Animal Care and Use Committee. Results are reported following the ARRIVE (Animal Research: Reporting of In Vivo Experiments) guidelines. Detailed methodology is available in the Online Appendix.

**STUDY DESIGN.** The study was designed to evaluate the therapeutic effects of SERCA2a gene transfer to the pulmonary vasculature using a novel aerosolized inhalation gene delivery strategy in a large animal model of chronic PH. Specifically, a swine model of chronic post-capillary PH was created surgically by partial banding of the pulmonary venous drainage, as reported previously by our group (18). The model produced a predictable and sustained rise in pulmonary artery (PA) pressures and RV dysfunction. Two months after the banding procedure, animals with established PH were randomized to airway-based AAV1.SERCA2a gene transfer (n = 10) or saline administration (n = 10) and followed for an additional 2 months until the end of the study. A sham-operated group (n = 4) was included as a control for the PH model. The main efficacy endpoints for the study were invasive cardiopulmonary hemodynamic parameters and RV performance indexes (**Figure 1**).

Human recombinant AAV1.SERCA2a and AAV1.LacZ for transduction efficiency studies were produced as described previously (22). The high prevalence of pre-existing or post-exposure neutralizing antibodies is a major hurdle for AAV-based gene therapies in both animal (23) and human studies (24). We therefore quantified neutralizing antibody titers against the AAV1 serotype before and after airway delivery of the

**FIGURE 1 Study Design and Timeline**

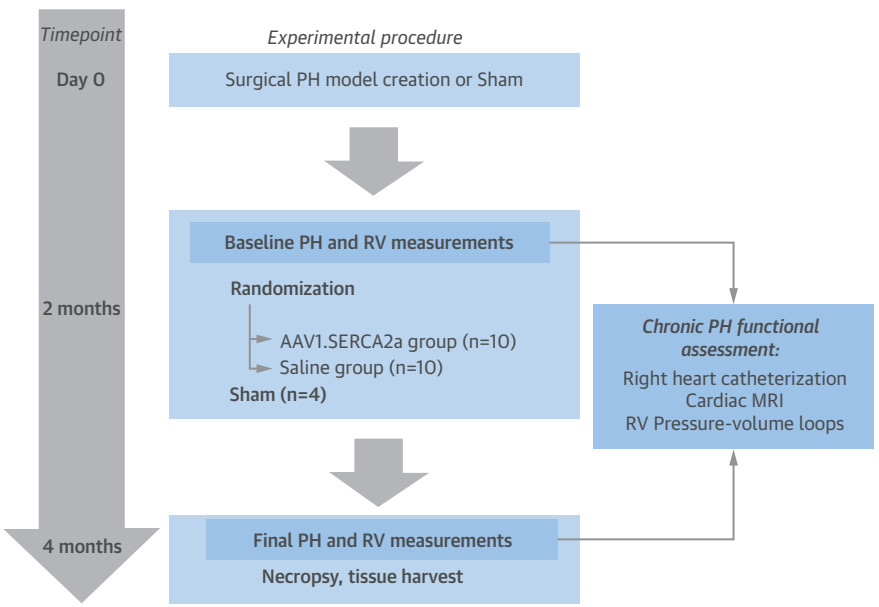


The chronic pulmonary hypertension (PH) model was created surgically by selective banding of pulmonary veins in 10- to 15-kg piglets. Two months later, animals were randomized to aerosolized airway delivery of either recombinant adeno-associated virus serotype 1 carrying the human SERCA2a transgene (AAV1.SERCA2a) or saline. Changes in cardiopulmonary hemodynamics, right ventricular (RV) structure, and RV function were evaluated 2 months after randomization to treatment. Sham-operated animals (n = 4) served as controls. MRI = magnetic resonance imaging.

AAV1 vector using a standardized protocol available in our laboratory (25).

Animals were anesthetized with isoflurane 1% to 2%. AAV1.SERCA2a ($1 \times 10^{13}$ vg) or saline aerosol delivery was performed using the MicroSprayer Aerosolizer (Model IA-1B, Penn-Century, Inc., Wyndmoor, Pennsylvania). This aerosolizer produces particles of ~20 μm; airway delivery of AAVs using this system has been shown to be effective in other large animal models (26). Using fluoroscopic guidance, the aerosol needle was inserted in the airway through the endotracheal tube using a 7-F multipurpose coronary diagnostic catheter with the tip of the catheter positioned near the carina (Online Figures 1A and 1B). The total dose of AAV1.SERCA2a was diluted into 6 ml of sterile saline and aerosolized in 2 ml doses with the animal in the dorsal, right, and left lateral recumbent positions. After virus delivery was completed, the animal was mechanically ventilated for an additional 20 to 30 min with continuous monitoring of the electrocardiogram, hemodynamics, and respiratory parameters. After this time, the animal was recovered fully from the procedure.

Before randomization to the treatment groups, all animals underwent right heart catheterization to measure cardiopulmonary pressures for RV pressure-volume analysis.

At 2 months (baseline) and 4 months (final), cardiac magnetic resonance (CMR) imaging studies were performed with a 3.0-T magnet to examine changes in RV and left ventricular (LV) structure and function.

**HISTOLOGY.** After the animals were euthanized, the RV and LV were sectioned and weighed, and RV hypertrophy was assessed by the following ratio: RV/(LV + septum). Heart and lung tissue samples were placed in 10% neutral buffered formalin solution and were subsequently fixed, processed, embedded in paraffin, and sectioned into 5-μm-thick sections for histology and morphometry analyses.

Protein quantification of SERCA2a was performed in lung and RV tissue homogenates and standardized using β-actin as described previously (15). Immunostaining was performed on acetone-fixed lung sections as reported previously (15), using primary antibodies as described in the Online Appendix.

**STATISTICAL ANALYSIS.** Continuous variables are expressed as median with interquartile range (IQR) unless otherwise specified. The invasive cardiopulmonary hemodynamic parameters and invasive RV performance indexes are reported as the mean change estimate with 95% confidence intervals (CIs) for each group. The study groups were compared at the time of randomization (baseline) using 1-way analysis of variance (with post hoc comparisons between groups performed using the Holm-Bonferroni method or Dunnett's multiple comparisons method), and change over time was evaluated by the group × time interaction of the repeated measures analysis of variance model. A p value $<0.05$ was considered statistically significant for all comparisons.

## RESULTS

Two months after the model was created, PH was confirmed hemodynamically by invasive right heart catheterization prior to the delivery of aerosolized AAV1.SERCA2a or saline; this time point was considered the baseline for future studies that evaluated the effectiveness of gene transfer. After an additional 2 months following aerosol inhalation delivery of the randomized treatment, a final assessment of cardiopulmonary hemodynamics, vascular remodeling, and RV structure and function was performed (**Figure 1**).

In a pre-dosing study that established the time course of hemodynamic compromise in the swine chronic PH model, we found that the onset of RV failure was associated with rapid disease progression and early death. Thus, to ensure that we would have sufficient power to examine the effects of AAV1.SERCA2a gene transfer on pulmonary vascular and RV endpoints, we excluded from randomization those animals found to have a mean PA pressure >45 mm Hg or a low cardiac index ($<2.5$ l/m$^2$) at right heart catheterization, as these measures were associated with RV failure and early death (Online Table 1). At baseline (once the PH was confirmed), compared with sham control subjects (n = 4), we documented a significant increase in mean PA pressure in PH pigs randomized to saline (n = 10) and AAV1.SERCA2a (n = 10) (median 17 mm Hg [IQR: 15 to 18 mm Hg] vs. 26 mm Hg [IQR: 23 to 30 mm Hg] vs. 23 mm Hg [19 to 28 mm Hg], respectively; p = 0.004). There were no significant between-group differences with respect to body weight, pulmonary artery wedge pressure (PAWP), mean aortic pressure, or heart rate. Cardiac index was increased in PH pigs compared with sham control subjects (p = 0.004), which is a recognized feature of this model that has been described previously (18,27) (**Table 1**).

After randomization, 3 animals died during the 2-month treatment follow-up period (2 in the saline group and 1 in the AAV1.SERCA2a group). In all 3 deaths, there were no complications that occurred during or after the airway inhalation gene therapy delivery procedure. The deaths occurred more than 1 month after randomization and were not attributable to the intervention. At necropsy, there was no evidence of lung infiltrates or infection; however, all

**TABLE 1 Cardiopulmonary Hemodynamics***

| | Sham | | Saline | | AAV1.SERCA2a | | p Value (ANOVA) | |
|---|---|---|---|---|---|---|---|---|
| | Baseline (n = 4) | Final (n = 4) | Baseline (n = 10) | Final (n = 8) | Baseline (n = 10) | Final (n = 8) | Baseline (Between Groups) | Group/Time Interaction |
| Body weight, kg | 21.5 (21-22.8) | 34 (31.5-36.3) | 20.5 (19-23) | 30.5 (28.5-32.5) | 22.5 (20.5-24.8) | 36 (34-37.3) | 0.547 | 0.237 |
| Heart rate, beats/min | 61 (55-66) | 75 (74-76) | 73 (71-84) | 73 (64-99) | 68 (57-82) | 78 (71-86) | 0.071 | 0.684 |
| Mean aortic pressure, mm Hg | 92 (89-99) | 121 (116-125) | 85 (80-93) | 103 (90-127) | 84 (81-90) | 112 (104-127) | 0.242 | 0.695 |
| Systolic PA pressure, mm Hg | 22 (21-22) | 23 (22-24) | 34 (30-44) | 70 (59-87) | 34 (28-38) | 40 (33-44) | <0.001† | 0.003†§ |
| Diastolic PA pressure, mm Hg | 10 (9-10) | 10 (9-10) | 15 (12-20) | 35 (29-46) | 14 (11-17) | 18 (15-20) | 0.014 | 0.004†§ |
| Mean PA pressure, mm Hg | 17 (15-18) | 16 (15-17) | 26 (23-30) | 54 (43-63) | 23 (19-28) | 29 (26-31) | 0.004†‡ | 0.003†§ |
| PA wedge pressure, mm Hg | 10 (8-10) | 9 (7-9) | 12 (10-14) | 15 (11-18) | 9 (5-11) | 12 (10-14) | 0.244 | 0.482 |
| Diastolic pulmonary gradient, mm Hg | 0 (0-2) | 0 (0-2) | 5 ([-1]-8) | 22 (10-26) | 4 (2-6) | 6 (1-9) | 0.281 | 0.01†§ |
| RA pressure, mm Hg | 4 (3-5) | 2 (1-2) | 2 (2-3) | 4 (3-5) | 4 (3-5) | 2 (1-3) | 0.044§ | 0.001†§ |
| Cardiac index, l/min/m$^2$ | 3.38 (3.29-3.51) | 4.52 (4.3-4.86) | 4.33 (4.13-5.13) | 3.70 (3.14-4.68) | 4.06 (3.53-5.04) | 5.43 (4.71-5.76) | 0.004† | 0.052 |
| Stroke volume index, ml/m$^2$ | 58 (54-61) | 60 (57-65) | 57 (51-70) | 51 (43-74) | 59 (50-71) | 65 (59-78) | 0.870 | 0.269 |
| PVR index, WU/m$^2$ | 1.93 (1.29-3.03) | 1.56 (1.49-1.85) | 2.83 (2.55-4.38) | 10.3 (5.14-12.21) | 3.17 (2.3-4.8) | 3.17 (1.8-4) | 0.459 | 0.002†§ |
| SVR index, WU/m$^2$ | 26 (24.6-28.7) | 27 (25.3-27.1) | 17.5 (17-22.4) | 27.4 (21.2-31.7) | 19.4 (18-22) | 21.9 (20.5-24.5) | 0.052 | 0.055 |

Values are median (interquartile range [IQR]). *Baseline was at 2 months after model creation and final was at 4 months after model creation (and 2 months after gene transfer). †Pairwise post hoc $p < 0.05$ sham versus saline. ‡Pairwise post hoc $p < 0.05$ for sham versus AAV1.SERCA2a. §Pairwise post hoc $p < 0.05$ for saline versus AAV1.SERCA2a.

AAV1.SERCA2a = recombinant adeno-associated virus serotype 1 carrying the human SERCA2a transgene; ANOVA = analysis of variance; PA = pulmonary artery; PVR = pulmonary vascular resistance; RA = right atrium; SVR = systemic vascular resistance; WU = Wood units.

3 animals had evidence of severe right HF, including hepatomegaly and ascites, implicating this as the primary cause of death. From these nonsurvivors, the only available outcome measurement was RV weight obtained at the time of heart explantation and is reported in Online Table 1. One animal (AAV1.SERCA2a group) that survived to the final time point had clear evidence of pneumonia with respiratory insufficiency and failure to thrive; this animal was excluded from the analyses (Online Table 1). Of the remaining animals that completed the study, no signs of pulmonary infection or congestion were identified at necropsy. In all cases, aerosol inhalation delivery of either AAV1.SERCA2a or saline was well tolerated and did not result in respiratory or hemodynamic instability.

**SERCA2a GENE TRANSFER AND CARDIOPULMONARY HEMODYNAMICS.** First, transduction efficiency of the AAV1 vector was examined using airway delivery of AAV1.LacZ. Examination of lung tissue sections stained for β-galactosidase demonstrated abundant transduction of the distal pulmonary airways and vessels (Online Figure 2). Further evaluation of the main PAs and vessels in the RV and LV revealed that these vessels were not transduced, indicating that aerosolized inhalation of AAV1.SERCA2a delivered the transgene to the target vasculature effectively and that there was no unanticipated gene transfer to cardiac vessels or other nontarget organs (Online Figures 3 and 4). Thus, the observed cardiopulmonary hemodynamic effects of treatment with aerosolized AAV1.SERCA2a are due to transduction of the distal pulmonary vessels and effects on pulmonary vascular remodeling as opposed to targeting the RV.

At the end of the study, 8 animals from the AAV1.SERCA2a-treated group and 8 animals from the saline-treated group were available for analysis. Although mean PA pressures in the sham control subjects did not change during the study, the increase in mean PA pressure was significantly larger in PH pigs randomized to saline compared with AAV1.SERCA2a (median 54 mm Hg [IQR: 43 to 63 mm Hg] vs. 29 mm Hg [IQR: 26 to 31 mm Hg]; $p < 0.05$) (**Figures 2A and 2B**). Compared with baseline, mean PA pressure continued to increase in PH pigs randomized to saline (median 26 mm Hg [IQR: 23 to 30 mm Hg] vs. 54 mm Hg [IQR: 43 to 63 mm Hg]; paired Student *t* test $p = 0.005$); however, compared with baseline, disease progression was limited in the AAV1.SERCA2a PH pigs (median 23 mm Hg [IQR: 19 to 28 mm Hg] vs. 29 mm Hg [IQR: 26 to 31 mm Hg]; paired Student *t* test $p = 0.064$) (**Table 1**, **Figures 2A and 2B**). Corresponding to the observed changes in PA pressure, indexed pulmonary vascular resistance (PVR) was increased significantly in the saline-treated group but not in animals receiving AAV1.SERCA2a (median 10.3 Wood U/m$^2$ [IQR: 5.1 to 12.2 Wood U/m$^2$] vs. 3.17 Wood U/m$^2$ [IQR: 1.8 to 4.0 Wood U/m$^2$]; $p < 0.05$) (**Figures 2C and 2D**), suggesting that treatment with AAV1.SERCA2a had a beneficial effect on pulmonary vascular remodeling. There was a parallel increase in the diastolic pulmonary gradient in the saline group (median 5 mm Hg [IQR: −1 to 8 mm Hg] to 22 mm Hg [IQR: 10 to 26 mm Hg]; $p < 0.05$) that was not present in AAV1.SERCA2a-treated animals

**FIGURE 2** Pulmonary Hemodynamics

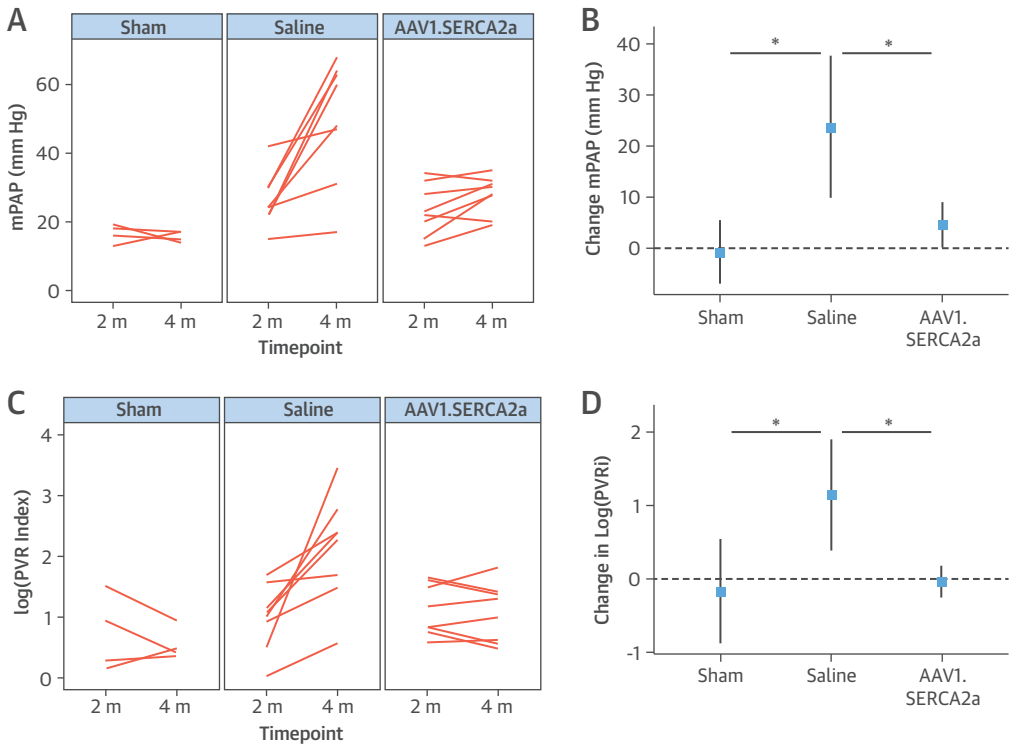


Individual changes from baseline (2 months [m]) to study's end (4 months) are reported for each animal following right heart catheterization to evaluate the effect of adeno-associated virus serotype 1 carrying the human SERCA2a transgene (AAV1.SERCA2a) therapy on cardiopulmonary hemodynamics. **(A)** The mean pulmonary artery pressure (mPAP) and **(C)** pulmonary vascular resistance index (PVRi) reported as well as the corresponding mean changes for each study parameter **(B and D)** demonstrate improvement with AAV1.SERCA2a. Sham (n = 4), saline (n = 8), AAV1.SERCA2a (n = 8). *p < 0.05. PVR = pulmonary vascular resistance.

(median 4 mm Hg [2 to 6 mm Hg] vs. 6 mm Hg [1 to 9 mm Hg]; p = NS). We also found that the cardiac index, which was increased at baseline in PH pigs, was decreased in the saline group by the end of the study, but improved in animals treated with AAV1.SERCA2a, although there was no significant difference between these groups (p = 0.112) (**Table 1**).

To confirm that the observed effects of AAV1.SERCA2a on cardiopulmonary hemodynamics were attributable to gene transfer to the pulmonary vasculature and not an effect of the degree of partial venous banding, we also examined the degree of constriction imposed by the banding procedure over time using Doppler echocardiography (Online Figure 5). Compared with sham control subjects, Doppler velocities in the pulmonary veins in animals with PH at the time of randomization to treatment with AAV1.SERCA2a or saline were increased 3- to 4-fold with no between-group differences. Two months after administration of AAV1.SERCA2a or saline, Doppler velocities remained elevated, with no difference observed between the groups or compared with baseline. Thus, the effect of AAV1.SERCA2a on cardiopulmonary hemodynamics resulted from transduction of the pulmonary vessels (Online Table 2).

**SERCA2a GENE TRANSFER AND HYPERTROPHIC PA REMODELING.** Increased medial thickness and hypertrophic PA remodeling are the main indexes of vascular remodeling observed in this porcine model of chronic PH (18,27). In the present study, compared with sham control subjects, PH pigs randomized to saline had significantly increased medial thickness of vessels <100 μm (p < 0.01) and vessels >100 μm (p < 0.01). Although there was some evidence of pulmonary arteriole remodeling in PH pigs treated with AAV1.SERCA2a, there was significantly less medial thickness of vessels <100 μm (p < 0.05) and >100 μm (p < 0.05) compared with that observed in

**FIGURE 3 Pulmonary Vascular Remodeling**

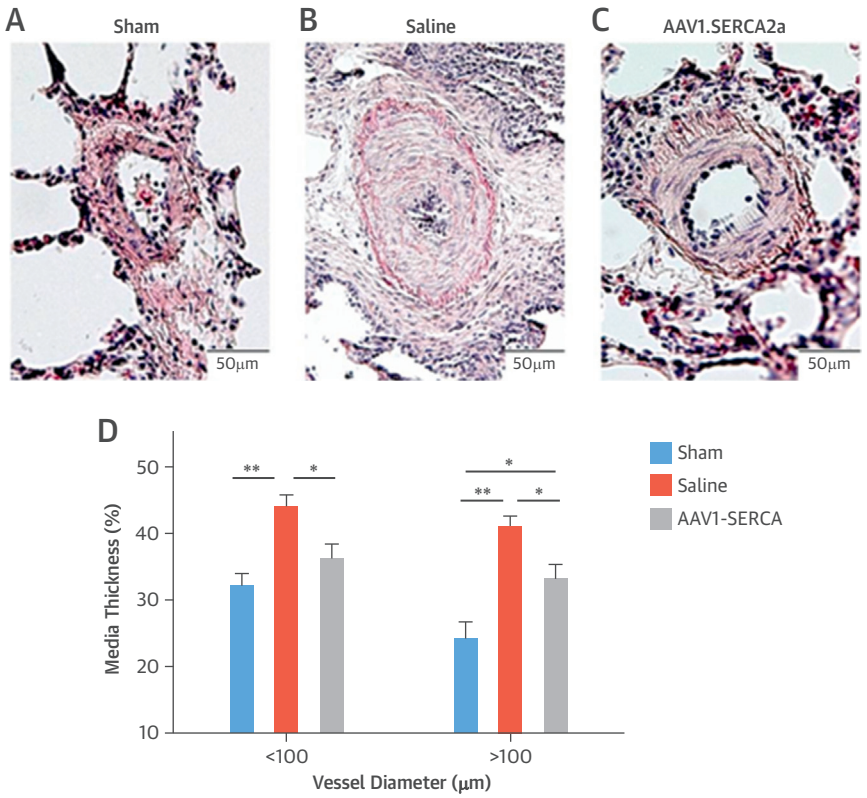


Distal vascular remodeling is ameliorated in adeno-associated virus serotype 1 carrying the human SERCA2a transgene (AAV1.SERCA2a)–treated animals compared with the saline group. Representative hematoxylin-eosin staining is shown for **(A)** sham (n = 4), **(B)** saline-treated (n = 8), and **(C)** AAV1.SERCA2a-treated (n = 8) animals. **(D)** Medial thickness was quantified for pulmonary arteries of <100 and >100 μm diameter. Data are mean ± SEM. *$p < 0.05$; **$p < 0.01$.

saline-treated PH pigs (Figure 3). These findings agreed with the hemodynamic data described earlier.

Next, to determine if the observed findings in the pulmonary vessels could be attributed to SERCA2a gene transfer, we analyzed the association of vascular remodeling with SERCA2a protein expression. Consistent with our observations in patients with PAH (15), SERCA2a protein was decreased in lung homogenates in the saline group compared with sham subjects; however, significantly higher SERCA2a levels were detected in the AAV1.SERCA2a-treated animals (Figure 4A). Immunofluorescence imaging of pulmonary vessels with dual labeling of SERCA2a and α-smooth muscle actin or SERCA2a and eNOS revealed that SERCA2a was detected primarily in the medial layers of the distal pulmonary arteries with some expression in the endothelium as well as the distal airway epithelium (Figure 4B, Online Figure 6). The abundance of SERCA2a detected in vessels of animals treated with AAV1.SERCA2a was greater than that observed in the saline-treated group (Figure 4B).

In a prior study performed in a rodent model of PH, we found that SERCA2a expression was inversely related to STAT3, which has been shown to regulate PA remodeling. To determine if this mechanism was operative in our porcine model, we first examined STAT3 phosphorylation in lung tissue homogenates. Compared with saline-treated PH pigs, animals treated with AAV1.SERCA2a had a lower level of STAT3 phosphorylation ($p < 0.01$) (Online Figure 7). As STAT3 has been identified as a mechanism that regulates bone morphogenetic protein receptor, type II (BMPR2) expression, we next examined this relationship in PA SMCs infected with an adenovirus encoding SERCA2a. Compared with cells infected with an adenovirus encoding β-galactosidase as a control, SERCA2a-infected cells had decreased STAT3 phosphorylation ($p < 0.005$) and a trend toward increased expression of

**FIGURE 4 Lung and Pulmonary Artery SERCA2a Protein Expression**

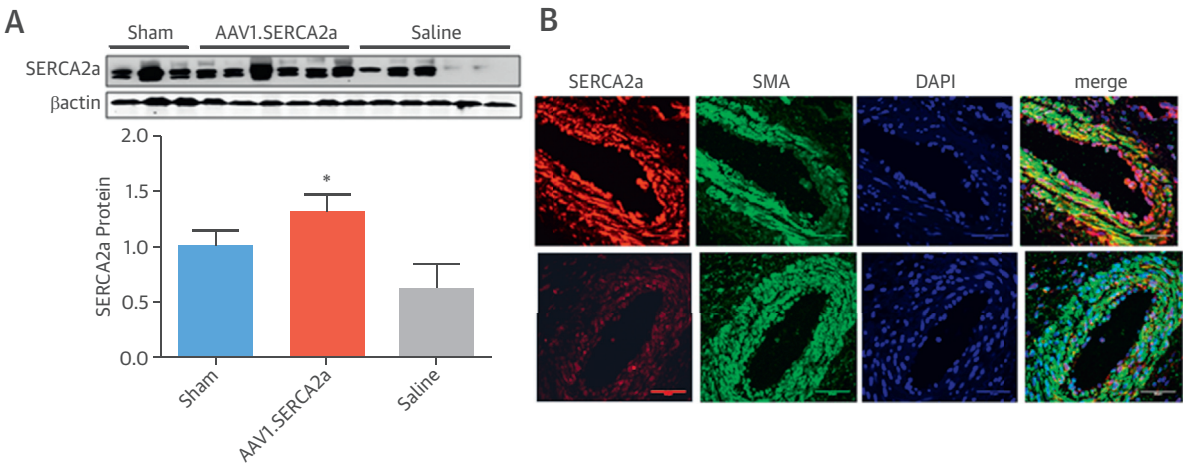


**(A)** Sarcoplasmic reticulum $Ca^{2+}$-ATPase 2a (SERCA2a) protein expression was quantified in lung homogenates by Western blotting. Representative blots are shown with densitometry data provided below comparing sham (n = 3), adeno-associated virus serotype 1 carrying the human SERCA2a transgene (AAV1.SERCA2a)-treated (n = 6), and saline-treated (n = 6) animals. *p < 0.05 vs. saline. **(B)** Representative immunofluorescence images from confocal microscopy showing specific localization of SERCA2a protein **(red)** in pulmonary vessels and distal airway epithelium in AAV1.SERCA-treated **(top)** and saline-treated **(bottom)** animals. **Green** and **blue** staining localize to α-smooth muscle actin (SMA) and 4′,6-diamidino-2-phenylindole (DAPI), respectively. **Bar** = 50 μm.

BMPR2 (p = 0.07), suggesting that this may be a mechanism by which SERCA2a gene transfer improves pulmonary vascular remodeling (Online Figure 8).

**EFFECT ON RV STRUCTURE AND PERFORMANCE.** To evaluate the effect of pulmonary vascular gene transfer of SERCA2a on changes in RV remodeling and global function, serial CMRs were performed before randomization and at the final time point. Animals subsequently randomized to saline or AAV1.SERCA2a were found to have similar RV volume, RV ejection fraction (EF), and indexed RV mass at baseline. Similarly, there were no between-group differences with respect to LV volume or LVEF (Table 2).

In the saline group, RV function worsened by the study's end, with a decrease in RVEF that was associated with an increase in RV end-diastolic and end-systolic volume indexes as well as an increase in RV mass (paired Student *t* test p = 0.130) (Table 2, Figures 5A and 5B). In PH pigs randomized to AAV1.SERCA2a, however, RVEF remained relatively stable over the 2-month follow-up period post-gene transfer.

**TABLE 2 CMR Analysis of Ventricular Structure and Function***

| | Saline | | AAV1.SERCA2a | | p Value† | |
|---|---|---|---|---|---|---|
| | Baseline (n = 9) | Final (n = 5) | Baseline (n = 10) | Final (n = 8) | Baseline | Group/Time Interaction |
| RV EDV, ml/m$^2$ | 108 (99–129) | 161 (110–165) | 111 (104–138) | 132 (124–156) | 0.710 | 0.878 |
| RV ESV, ml/m$^2$ | 45 (40–57) | 82 (54–91) | 48 (41–55) | 51 (45–66) | 0.971 | 0.101 |
| RVEF, % | 58 (56–64) | 50 (44–51) | 59 (58–63) | 61 (56–63) | 0.754 | 0.008 |
| RV mass, g/m$^2$ | 56 (49–69) | 62 (57–63) | 64 (55–71) | 59 (55–62) | 0.489 | 0.014 |
| Stroke volume, ml/m$^2$ | 58 (55–64) | 55 (37–64) | 69 (52–71) | 71 (57–81) | 0.200 | 0.084 |
| LV EDV, ml/m$^2$ | 87 (78–93) | 89 (66–108) | 97 (92–105) | 109 (105–112) | 0.090 | 0.022 |
| LV ESV, ml/m$^2$ | 31 (29–33) | 33 (28–42) | 38 (35–40) | 38 (33–43) | 0.157 | 0.571 |
| LVEF, % | 64 (63–67) | 61 (61–62) | 62 (58–63) | 65 (63–66) | 0.620 | 0.085 |

Values are median (IQR). *Baseline was at 2 months after model creation and final was at 4 months after model creation (and 2 months after gene transfer). †Independent samples Student *t* test.

CMR = cardiac magnetic resonance imaging; RV = right ventricular; EDV = end-diastolic volume; EF = ejection fraction; ESV = end-systolic volume; LV = left ventricular; other abbreviations as in Table 1.

**FIGURE 5 RV Remodeling**

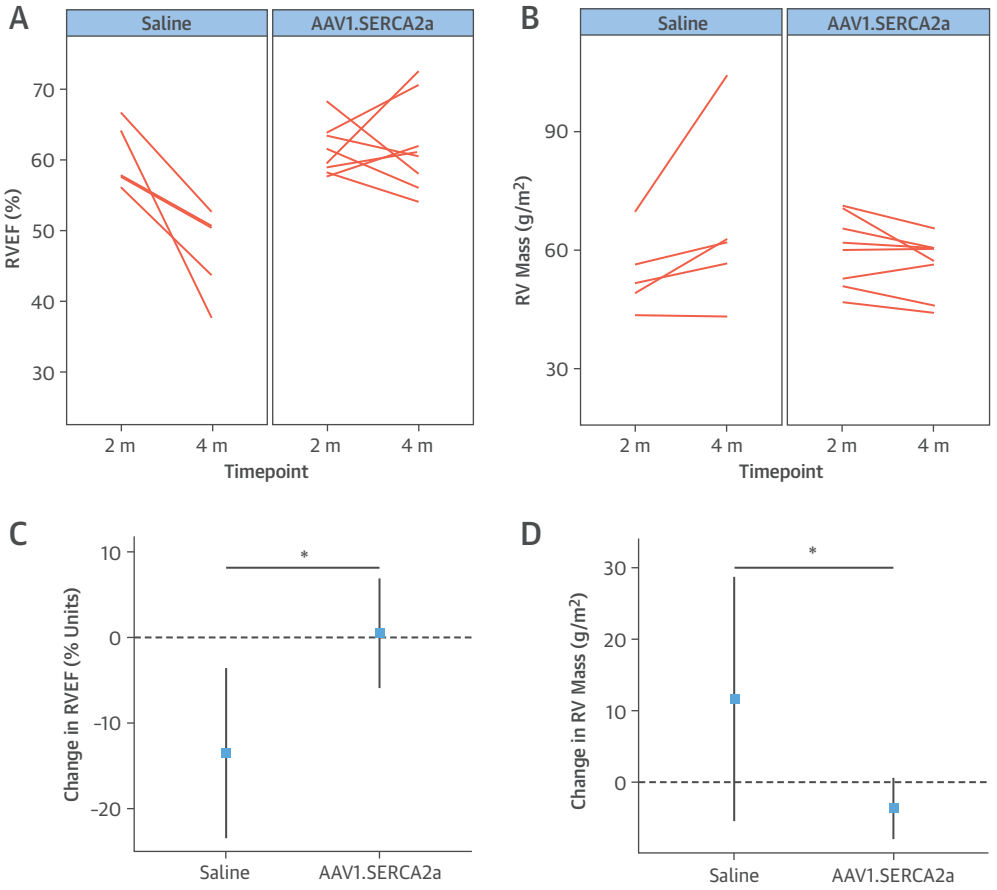


Serial cardiac magnetic resonance imaging (CMR) was performed to examine the effect of aerosolized adeno-associated virus carrying SERCA2a (AAV1.SERCA2a) on RV structural remodeling. At the end of the 2-month treatment period, CMR-derived measures of **(A)** right ventricular ejection fraction (RVEF) and **(B)** indexed RV mass were preserved in the AAV1.SERCA2a-treated pigs (n = 8) but decreased in saline-treated pigs (n = 5). Mean change estimates with 95% confidence intervals are shown for **(C)** RVEF and **(D)** RV mass. *p < 0.05. Abbreviations as in Figure 1.

Indeed, compared with saline-treated animals, the change in RVEF in AAV1.SERCA2a-treated PH pigs was significantly less (p = 0.008), and there was a decrease in RV mass (p = 0.014) (Figures 5C and 5D). At the end of the study, explanted hearts were weighed as a more solid measure of RV mass. There was a significant increase in RV/LV + septum in the saline group compared with sham control subjects (p = 0.006), with a nonsignificant decrease in relative RV weight in AAV1.SERCA2a animals.

To assess RV function further at the end of the treatment period, RV pressure-volume relationships were examined (Figure 6). At baseline, all measures were similar between animals randomized to saline and AAV1.SERCA2a (Table 3). At the end of the study, RV end-systolic pressure-volume relationship or elastance, a measure of RV contractility, was improved in AAV1.SERCA2a-treated animals compared with the saline group (p = 0.043). The change in arterial elastance (Ea), or RV afterload, was significantly higher in saline-treated animals compared with AAV1.SERCA2a-treated pigs (p = 0.005). Moreover, the increase in pulmonary Ea was not compensated by an increase in end-systolic pressure-volume relationship in the saline group, whereas an improved Ea was observed in the AAV1.SERCA2a-treated animals, suggesting better RV-PA coupling. Among diastolic parameters, a marked improvement in end-diastolic pressure-volume relationship (i.e., RV compliance) was observed in the AAV1.SERCA2a group compared with the saline group (p = 0.006) (Table 3, Figure 6). In both PH groups, a significant degree of pathological fibrosis was found in the RV myocardium compared with the sham control subjects, with no quantitative

**FIGURE 6** Indexes of RV Performance

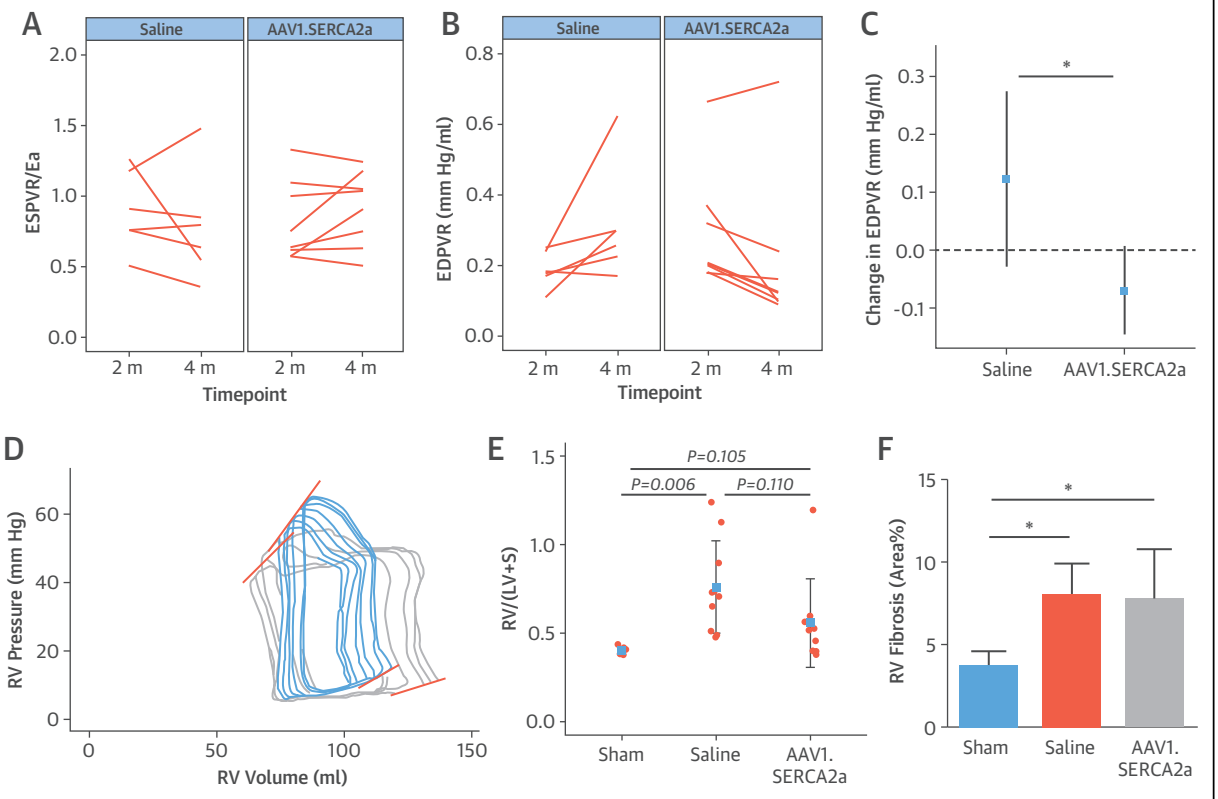


At randomization and after the 2-month treatment period, RV pressure–volume relationships were assessed invasively and reported for animals randomized to saline (n = 6) or AAV1.SERCA2a (n = 8). End-systolic pressure–volume relationship (ESPVR) **(A)** and end-diastolic pressure–volume relationship (EDPVR) **(B)** slopes are shown, together with mean change estimate for EDPVR **(C)**. **(D)** Representative pressure-volume loop volume reduction series from saline-treated **(blue)** and AAV1.SERCA2a-treated **(gray)** animals show steeper slopes for the saline group. **(E)** Relative RV weight from explanted hearts expressed as RV/left ventricle + septum (LV+S). **(F)** Myocardial interstitial fibrosis was assessed as collagen fractional area, which was quantified in RV free wall tissue by picrosirius red staining. *p < 0.05. Ea = arterial elastance; other abbreviations as Figure 1.

**TABLE 3** RV Invasive Pressure-Volume Loop Measurements*

| | Saline | | AAV1.SERCA2a | | p Value† | |
|---|---|---|---|---|---|---|
| | Baseline (n = 10) | Final (n = 6) | Baseline (n = 10) | Final (n = 8) | Baseline | Group/Time Interaction |
| PA Ea, mm Hg/ml | 1.25 (0.96 to 1.54) | 1.88 (1.09 to 2.09) | 1.02 (0.81 to 1.32) | 0.81 (0.61 to 0.96) | 0.653 | 0.005 |
| ESPVR slope, mm Hg/ml | 1.13 (0.64 to 1.40) | 0.92 (0.74 to 1.40) | 0.77 (0.63 to 1.15) | 0.63 (0.53 to 0.76) | 0.216 | 0.043 |
| Vo, ml | −4.9 (−18.3 to 2.1) | −14 (−30.3 to −5.2) | −10.5 (−18.2 to 2.3) | −24.8 (−37.1 to 3.8) | 0.856 | 0.6 |
| ESPVR/Ea | 0.84 (0.69 to 1.18) | 0.72 (0.57 to 0.84) | 0.74 (0.62 to 0.97) | 0.97 (0.72 to 1.08) | 0.434 | 0.167 |
| dP/dt max, mm Hg/s | 624 (591 to 800) | 764 (690 to 875) | 662 (493 to 731) | 690 (671 to 861) | 0.551 | 0.84 |
| EDPVR slope, mm Hg/ml | 0.21 (0.17 to 0.32) | 0.28 (0.23 to 0.30) | 0.27 (0.20 to 0.37) | 0.12 (0.10 to 0.18) | 0.391 | 0.006 |
| dP/dt min, mm Hg/s | −623 (−732 to −468) | −907 (−1,039 to −629) | −486 (−628 to −406) | −560 (−626 to −474) | 0.372 | 0.097 |
| Tau, ms | 33 (26 to 41) | 37 (34 to 40) | 33 (31 to 37) | 34 (32 to 36) | 0.301 | 0.423 |

Values are median (IQR). *Baseline was at 2 months after model creation and final was at 4 months after model creation (and 2 months after gene transfer). †Independent samples Student *t* test.

dP/dt = peak RV pressure rate of rise (max) or decline (min); Ea = arterial elastance; EDPVR = end-diastolic pressure–volume relationship; ESPVR = end-systolic pressure–volume relationship; PA = pulmonary artery; Tau = time constant of isovolumic relaxation; Vo = volume intercept of the ESPVR slope; other abbreviations as in Tables 1 and 2.

differences detected between the treatment groups. Compared with control subjects, SERCA2a expression in the RV was decreased in saline-treated and AAV1.SERCA2a-treated (both $p < 0.05$) PH animals with no between-group difference in SERCA2a expression (Online Figure 9). This suggests that any observed improvements in RV function in AAV1.SERCA2a-treated animals are more likely to be attributed to reduced afterload than a higher RV SERCA2a expression.

**ALDOSTERONE LEVELS AND NEUTRALIZING ANTIBODIES.** Aldosterone levels were measured at study's end as an additional indication of right HF status. Aldosterone levels were elevated in saline-treated pigs compared with control subjects, with lower levels detected in AAV1.SERCA2a-treated animals (mean ± SD: 30.6 ± 5.2 vs. 76.6 ± 7.3 vs. 51.4 ± 7.1 mg/dl; $p < 0.02$). In almost all animals receiving airway delivery of aerosolized AAV1.SERCA2a or AAV1.LacZ vectors, neutralizing antibody titers increased by the end of the study, whereas no change in titers was found in animals from the saline group that were not exposed to any AAV1 viral vectors (Online Figure 10).

## DISCUSSION

In this study, we report for the first time a successful AAV-based gene therapy intervention that modulated progression of chronic PH in a large animal model. We provide data that support feasibility, efficiency, and safety of airway distribution and transduction of small pulmonary vessels using an aerosolized AAV1 vector as a novel delivery method for gene therapy in PH. We also describe the beneficial effects of selective vascular SERCA2a gene transfer using this approach. In this study, PA transduction with aerosolized AAV1.SERCA2a improved cardiopulmonary hemodynamics and RV functional parameters in a chronic PH model that recapitulates the clinical features of the disease seen in patients with chronic post-capillary PH (**Central Illustration**). These data indicate that AAV1.SERCA2a therapy slowed the progression of PH in a clinically relevant large animal model and confirm the potential therapeutic role of SERCA2a as a novel target in PH patients. Our data also extends the "proof-of-concept" strategy of aerosolized gene transfer of SERCA2a (15) by demonstrating efficacy in a truly pre-clinical animal model of PH. As there are no established therapies that target prevention of pulmonary vascular remodeling, a fundamental pathophysiology of PH, our findings offer an innovative option to treat patients with PH.

The time course of PH and pulmonary arteriolar remodeling in the swine model of chronic PH has been established. In this model, increases in PA pressure occur prior to a rise in pulmonary vascular resistance. This, in turn, precedes RV remodeling, dysfunction, and, ultimately, failure (19). In the current study, we found that the progression of disease through these stages was ameliorated by intratracheal administration of aerosolized AAV1.SERCA2a. This was demonstrated by stabilization of the mean PA pressure and PVR at the end of the 2-month follow-up period. These observations also agreed with pulmonary vascular remodeling assessed by medial thickness scores of small (<100 μm) and medium (>100 μm) vessels. We further confirmed that SERCA2a was down-regulated in the PAs in the swine model of chronic PH compared with sham control subjects, similar to what was observed in human PAH pulmonary arterioles and in the rat monocrotaline-induced PH model (15). Of note, pulmonary vascular SERCA2a abundance was markedly higher in AAV1.SERCA2a-treated animals compared with the saline group, indicating that there was efficient vessel transduction and that restoring PA SERCA2a levels prevented disease progression.

These observations support previous reports from our group regarding the association of SERCA2a down-regulation with adverse vascular remodeling in both the pulmonary (15) and coronary circulations (28). In the hypertensive pulmonary vasculature, gene transfer of SERCA2a exerted antiproliferative effects by blocking the STAT3-NFAT pathway in SMCs (15). Additionally, in vitro studies revealed that SERCA2a overexpression restored eNOS to basal levels (15). These mechanistic studies provide the molecular basis for the observed beneficial effects of SERCA2a in pulmonary vascular remodeling in the present model.

RV failure is the main determinant of clinical outcome in patients with PH (29). In our chronic PH model treated with AAV1.SERCA2a, hemodynamic improvements were paralleled by the preservation of RV performance as evaluated by systolic, diastolic, and remodeling parameters quantified by serial CMR and pressure-volume relationships. In a previous report, we comprehensively analyzed the onset of RV failure in this model of chronic PH and found that the progression of vascular disease was responsible for nonadaptive RV remodeling and uncoupling from the pulmonary circulation leading to RV failure (18). In the present study, the most relevant differences between treatment groups were found in diastolic function as assessed by end-diastolic pressure-volume relationship. The fact that beneficial effects observed in RV

**CENTRAL ILLUSTRATION** **Inhaled AAV1.SERCA2a in PH**

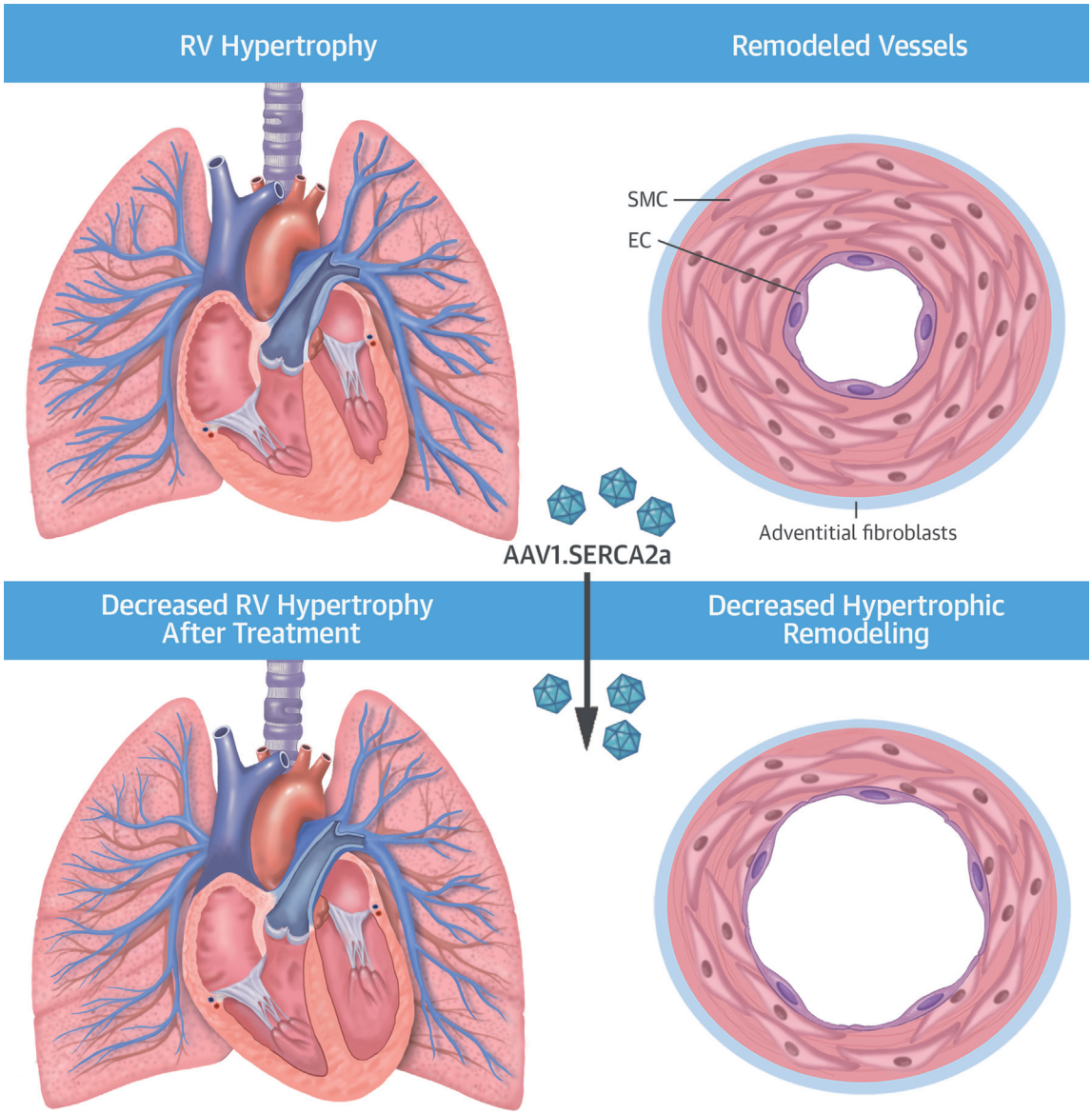


Aguero, J. et al. J Am Coll Cardiol. 2016;67(17):2032–46.

Chronic pulmonary hypertension (PH) is associated with increased right ventricular (RV) afterload and vascular remodeling, leading to right ventricular hypertrophy (RVH) that results from distal pulmonary artery hypertrophic remodeling. Airway gene delivery of recombinant adeno-associated virus serotype 1 carrying the human SERCA2a transgene (AAV1.SERCA2a) limits RV hypertrophy and failure by attenuating the progression of pulmonary artery hypertrophic remodeling in a swine model. EC = endothelial cell; SMC = smooth muscle cell.

performance were not paralleled by differences in interstitial fibrosis between treatment groups suggests that RV performance improvement likely reflected hemodynamic changes and could not be attributed to the prevention or reversal of RV fibrosis. Interestingly, reports using CMR have shown that RV failure may occur even in the presence of a favorable hemodynamic response to vasodilator drugs in PAH patients (3). This also underscores the need for a better understanding of the intrinsic mechanisms of RV structural and functional remodeling to affect the clinical outcome of this patient population (3).

In the past 2 decades, several groups have explored gene therapy as a strategy to improve or correct PH in rodent models (10), under the premise that specific vascular targeting of therapeutics would increase efficacy and decrease systemic side effects. Successful experiences have been reported in the selective modulation of eNOS (30) and prostacyclin synthase (12,31,32), aiming to enhance sustained availability of short-lived endothelial factors, such as NO or prostacyclin, which are known to be deficient in PH. Other targets of interest that have been studied in small animal models of PAH include vascular growth factors (33), BMPR2 (34,35), apoptosis (mutant survivin) (20), calcitonin-gene related peptide (36), and voltage-gated potassium channels (21). However, only a hybrid strategy based on the administration of bone marrow–derived endothelial-like progenitor cells overexpressing eNOS is currently in the clinical study (37). This reflects the complexity of advancing pre-clinical research in the area of gene or cell therapy in PH as well as the need for testing new interventions in relevant animal models of disease (17).

A major aspect in the pre-clinical development of gene therapy as a treatment modality is an optimal delivery method. Due to potential off-target expression of the transgene, organ specificity is a major goal to prevent adverse effects, and to this extent, large animal models have provided an invaluable framework in the field of cardiovascular gene therapy (38). We chose airway delivery of viral vectors on the basis of a number of previous rodent studies that demonstrated feasibility and selectivity to target the distal pulmonary vasculature (12,15,20,21,30,32–34,36,39). The present study is the first to report feasibility of AAV1 gene delivery to the distal pulmonary vessels in a large animal model using an intratracheal sprayer device. A previous report showed the advantages of such a device to deliver AAV vectors to the distal airway compared to oral nebulization or direct catheter instillation. This study also reported that the particle dimensions generated by the microsprayer (~20 μm) did not affect the viability of AAV particles due to their small size (~20 nm) (40). Thus, optimization and future advances in delivery device technology should further improve the ability to transduce the distal pulmonary vessels and minimize the invasiveness of the procedure.

Safety represents a significant concern in the evaluation of nonconventional treatments such as gene or cell therapy. In recent years, gene therapy studies focusing on chronic disorders have shifted to using recombinant AAV as vectors due to their ability to achieve sustained transgene expression, the fact that no human disease is currently attributed to AAV infection, and the very low integration rate of AAV into the host genome (8). Conversely, frequent AAV exposure in humans has led to a high prevalence of neutralizing antibodies that limit the proportion of patients who are candidates for this therapy and make repeated administrations of the AAV vector inefficient (25,41). In the present study, as seen in clinical trials in patients with cystic fibrosis (42), airway administration of AAV led to a high rate of seroconversion. The inability to perform repeated administrations was considered a major hurdle in the development of gene therapies in cystic fibrosis programs and must be addressed to increase the broad applicability of gene therapies using AAV vectors for PH.

Overall, AAV vectors have shown a good safety profile in several clinical trials (43), leading to the regulatory approval of the first AAV1-based gene therapy to treat a human disease (44). Furthermore, compared with other viral vectors (i.e., adenovirus) used in gene therapy studies, AAVs elicit almost no inflammatory response and are nonpathogenic in humans, although they have a smaller packaging capacity, limiting the size of the transgene. With respect to AAV1.SERCA2a, the first clinical trial of this vector and transgene in patients with advanced HF has been reported (45), including long-term follow-up (~3 years) (46), indicating that this therapy was safe when delivered by intracoronary administration.

**STUDY LIMITATIONS.** In our model of chronic post-capillary PH, the partial venous banding procedure may lead to remodeling of the banded pulmonary veins with potential implications for cardiopulmonary pressures. Although we investigated pulmonary venous inflow and the PA diastolic pressure at several time points to ensure that there were no differences between animals, we did not assess inferior lung lobe vein remodeling histologically (47). Thus, we cannot exclude an effect of AAV1.SERCA2a on pulmonary vein remodeling. We also believe that PAWP accurately reflects left atrial pressure in our model; however, it is possible that PAWP was elevated artificially due to damping or other measure-related issues. The study was also performed with a small sample size that may have limited power and limited follow-up (8 weeks after gene delivery). Therefore, future studies focusing on long-term efficacy and safety endpoints are warranted prior to advancing airway gene delivery to the clinic.

## CONCLUSIONS

Our findings indicate that AAV1-based gene therapy was efficacious in PH and position pulmonary

vascular SERCA2a gene transfer via aerosol inhalation delivery as a therapeutic modality in PH and other related pulmonary vascular diseases.

**ACKNOWLEDGMENT** The authors thank L. Leonardson for her expertise and valuable technical support.

**REPRINT REQUESTS AND CORRESPONDENCE:** Dr. Roger J. Hajjar, Cardiovascular Research Center, Icahn School of Medicine at Mount Sinai, One Gustave Levy Place, #1030, New York, New York 10029. E-mail: roger.hajjar@mssm.edu.

## PERSPECTIVES

**COMPETENCY IN MEDICAL KNOWLEDGE:** Down-regulation of SERCA2a is associated with progressive distal PA hypertrophic remodeling and RV dysfunction in patients with chronic post-capillary PH. Aerosolized delivery of AAV1.SERCA2a in a large animal model of this disease favorably influences PA remodeling and improves RV function.

**TRANSLATIONAL OUTLOOK:** Further studies are needed to translate this therapy to patients with this disease.

## REFERENCES

**1.** Galie N, Hoeper MM, Humbert M, et al. Guidelines for the diagnosis and treatment of pulmonary hypertension: the Task Force for the Diagnosis and Treatment of Pulmonary Hypertension of the European Society of Cardiology (ESC) and the European Respiratory Society (ERS). Eur Heart J 2009;30:2493–537.

**2.** Benza RL, Miller DP, Gomberg-Maitland M, et al. Predicting survival in pulmonary arterial hypertension: insights from the Registry to Evaluate Early and Long-Term Pulmonary Arterial Hypertension Disease Management (REVEAL). Circulation 2010;122:164–72.

**3.** van de Veerdonk MC, Kind T, Marcus JT, et al. Progressive right ventricular dysfunction in patients with pulmonary arterial hypertension responding to therapy. J Am Coll Cardiol 2011;58:2511–9.

**4.** Strange G, Playford D, Stewart S, et al. Pulmonary hypertension: prevalence and mortality in the Armadale echocardiography cohort. Heart 2012;98:1805–11.

**5.** Vachiery JL, Adir Y, Barbera JA, et al. Pulmonary hypertension due to left heart diseases. J Am Coll Cardiol 2013;62:D100–8.

**6.** Delgado JF, Conde E, Sanchez V, et al. Pulmonary vascular remodeling in pulmonary hypertension due to chronic heart failure. Eur J Heart Fail 2005;7:1011–6.

**7.** Taichman DB, Ornelas J, Chung L, et al. Pharmacologic therapy for pulmonary arterial hypertension in adults: chest guideline and expert panel report. Chest 2014;146:449–75.

**8.** Hajjar RJ. Potential of gene therapy as a treatment for heart failure. J Clin Invest 2013;123:53–61.

**9.** Ginn SL, Alexander IE, Edelstein ML, et al. Gene therapy clinical trials worldwide to 2012—an update. J Gene Med 2013;15:65–77.

**10.** Reynolds PN. Gene therapy for pulmonary hypertension: prospects and challenges. Expert Opin Biol Ther 2011;11:133–43.

**11.** Champion HC, Bivalacqua TJ, Greenberg SS, et al. Adenoviral gene transfer of endothelial nitric-oxide synthase (eNOS) partially restores normal pulmonary arterial pressure in eNOS-deficient mice. Proc Natl Acad Sci U S A 2002;99:13248–53.

**12.** Gubrij IB, Martin SR, Pangle AK, et al. Attenuation of monocrotaline-induced pulmonary hypertension by luminal adeno-associated virus serotype 9 gene transfer of prostacyclin synthase. Hum Gene Ther 2014;25:498–505.

**13.** Kuhr FK, Smith KA, Song MY, et al. New mechanisms of pulmonary arterial hypertension: role of Ca(2)(+) signaling. Am J Physiol Heart Circ Physiol 2012;302:H1546–62.

**14.** Kawase Y, Hajjar RJ. The cardiac sarcoplasmic/endoplasmic reticulum calcium ATPase: a potent target for cardiovascular diseases. Nat Clin Pract Cardiovasc Med 2008;5:554–65.

**15.** Hadri L, Kratlian RG, Benard L, et al. Therapeutic efficacy of AAV1.SERCA2a in monocrotaline-induced pulmonary arterial hypertension. Circulation 2013;128:512–23.

**16.** Stenmark KR, Meyrick B, Galie N, et al. Animal models of pulmonary arterial hypertension: the hope for etiological discovery and pharmacological cure 2009;297:L1013–32.

**17.** Sutendra G, Michelakis ED. Pulmonary arterial hypertension: challenges in translational research and a vision for change. Sci Transl Med 2013;5:208sr5.

**18.** Aguero J, Ishikawa K, Hadri L, et al. Characterization of right ventricular remodeling and failure in a chronic pulmonary hypertension model. Am J Physiol Heart Circ Physiol 2014;307:H1204–15.

**19.** Aguero J, Ishikawa K, Fish KM, et al. Combination proximal pulmonary artery coiling and distal embolization induces chronic elevations in pulmonary artery pressure in swine. PLoS One 2015;10:e0124526.

**20.** McMurtry MS, Archer SL, Altieri DC, et al. Gene therapy targeting survivin selectively induces pulmonary vascular apoptosis and reverses pulmonary arterial hypertension. J Clin Invest 2005;115:1479–91.

**21.** Pozeg ZI, Michelakis ED, McMurtry MS, et al. In vivo gene transfer of the O2-sensitive potassium channel Kv1.5 reduces pulmonary hypertension and restores hypoxic pulmonary vasoconstriction in chronically hypoxic rats. Circulation 2003;107:2037–44.

**22.** Karakikes I, Hadri L, Rapti K, et al. Concomitant intravenous nitroglycerin with intracoronary delivery of AAV1.SERCA2a enhances gene transfer in porcine hearts. Mol Ther 2012;20:565–71.

**23.** Ishikawa K, Fish KM, Tilemann L, et al. Cardiac I-1c overexpression with reengineered AAV improves cardiac function in swine ischemic heart failure. Mol Ther 2014;22:2038–45.

**24.** Jaski BE, Jessup ML, Mancini DM, et al. Calcium upregulation by percutaneous administration of gene therapy in cardiac disease (CUPID Trial), a first-in-human phase 1/2 clinical trial. J Card Fail 2009;15:171–81.

**25.** Rapti K, Louis-Jeune V, Kohlbrenner E, et al. Neutralizing antibodies against AAV serotypes 1, 2, 6, and 9 in sera of commonly used animal models. Mol Ther 2012;20:73–83.

**26.** Beck SE, Laube BL, Barberena CI, et al. Deposition and expression of aerosolized rAAV vectors in the lungs of Rhesus macaques. Mol Ther 2002;6:546–54.

**27.** Pereda D, Garcia-Alvarez A, Sanchez-Quintana D, et al. Swine model of chronic post-capillary pulmonary hypertension with right ventricular remodeling: long-term characterization by cardiac catheterization, magnetic resonance, and pathology. J Cardiovasc Transl Res 2014;7:494–506.

**28.** Hadri L, Bobe R, Kawase Y, et al. SERCA2a gene transfer enhances eNOS expression and activity in endothelial cells. Mol Ther 2010;18:1284–92.

**29.** Vonk-Noordegraaf A, Haddad F, Chin KM, et al. Right heart adaptation to pulmonary arterial hypertension: physiology and pathobiology. J Am Coll Cardiol 2013;62:D22–33.

**30.** Champion HC, Bivalacqua TJ, D'Souza FM, et al. Gene transfer of endothelial nitric oxide synthase to the lung of the mouse in vivo: effect on agonist-induced and flow-mediated vascular responses. Circ Res 1999;84:1422–32.

**31.** Ito T, Okada T, Mimuro J, et al. Adenoassociated virus-mediated prostacyclin synthase

expression prevents pulmonary arterial hypertension in rats. Hypertension 2007;50:531–6.

**32.** Nagaya N, Yokoyama C, Kyotani S, et al. Gene transfer of human prostacyclin synthase ameliorates monocrotaline-induced pulmonary hypertension in rats. Circulation 2000;102:2005–10.

**33.** Partovian C, Adnot S, Raffestin B, et al. Adenovirus-mediated lung vascular endothelial growth factor overexpression protects against hypoxic pulmonary hypertension in rats. Am J Respir Cell Mol Biol 2000;23:762–71.

**34.** McMurtry MS, Moudgil R, Hashimoto K, et al. Overexpression of human bone morphogenetic protein receptor 2 does not ameliorate monocrotaline pulmonary arterial hypertension. Am J Physiol Lung Cell Mol Physiol 2007;292:L872–8.

**35.** Reynolds AM, Holmes MD, Danilov SM, et al. Targeted gene delivery of BMPR2 attenuates pulmonary hypertension. Eur Respir J 2012;39:329–43.

**36.** Champion HC, Bivalacqua TJ, Toyoda K, et al. In vivo gene transfer of prepro-calcitonin gene-related peptide to the lung attenuates chronic hypoxia-induced pulmonary hypertension in the mouse. Circulation 2000;101:923–30.

**37.** Granton J, Langelben D, Kutryk MB, et al. Endothelial NO synthase gene-enhanced progenitor cell therapy for pulmonary arterial hypertension: The PHACeT Trial. Circ Res 2015;117:645–54.

**38.** Ishikawa K, Aguero J, Naim C, et al. Percutaneous approaches for efficient cardiac gene delivery. J Cardiovasc Trans Res 2013;6:649–59.

**39.** Budts W, Pokreisz P, Nong Z, et al. Aerosol gene transfer with inducible nitric oxide synthase reduces hypoxic pulmonary hypertension and pulmonary vascular remodeling in rats. Circulation 2000;102:2880–5.

**40.** Beck SE, Laube BL, Barberena CI, et al. Deposition and expression of aerosolized rAAV vectors in the lungs of rhesus macaques. Mol Ther 2002;6:546–54.

**41.** Louis Jeune V, Joergensen JA, Hajjar RJ, et al. Pre-existing anti-adeno-associated virus antibodies as a challenge in AAV gene therapy. Hum Gene Ther Methods 2013;24:59–67.

**42.** Moss RB, Rodman D, Spencer LT, et al. Repeated adeno-associated virus serotype 2 aerosol-mediated cystic fibrosis transmembrane regulator gene transfer to the lungs of patients with cystic fibrosis: a multicenter, double-blind, placebo-controlled trial. Chest 2004;125:509–21.

**43.** Kaufmann KB, Büning H, Galy A, et al. Gene therapy on the move. EMBO Mol Med 2013;5:1642–61.

**44.** Gaudet D, Methot J, Dery S, et al. Efficacy and long-term safety of alipogene tiparvovec (AAV1-LPLS447X) gene therapy for lipoprotein lipase deficiency: an open-label trial. Gene Ther 2013;20:361–9.

**45.** Jessup M, Greenberg B, Mancini D, et al. Calcium Upregulation by percutaneous administration of gene therapy in cardiac disease (CUPID): A phase 2 trial of intracoronary gene therapy of sarcoplasmic reticulum Ca2+-ATPase in patients with advanced heart failure. Circulation 2011;124:304–13.

**46.** Zsebo K, Yaroshinsky A, Rudy JJ, et al. Long-term effects of AAV1/SERCA2a gene transfer in patients with severe heart failure: analysis of recurrent cardiovascular events and mortality. Circ Res 2014;114:101–8.

**47.** Gerges C, Gerges M, Lang MB, et al. Diastolic pulmonary vascular pressure gradient: a predictor of prognosis in "out-of-proportion" pulmonary hypertension. Chest 2013;143:758–66.

**KEY WORDS** aerosol delivery, gene therapy, pig models, pulmonary vascular remodeling, right ventricular function

**APPENDIX** For a supplemental Methods section as well as supplemental figures and tables, please see the online version of this article.

Artículo 6 [14].

*Aguero J, Hadri L, Hammoudi N, Leonardson L, Hajjar RJ, Ishikawa K. Inhaled Gene Transfer for Pulmonary Circulation. Methods Mol Biol. 2017;1521:339-349.*

# Chapter 24

# Inhaled Gene Transfer for Pulmonary Circulation

**Jaume Aguero, Lahouaria Hadri, Nadjib Hammoudi, Lauren Leonardson, Roger J. Hajjar, and Kiyotake Ishikawa**

## Abstract

Chronic pulmonary hypertension (PH) is associated with right ventricular failure and high mortality regardless of the underlying disease. Currently, therapies can improve clinical outcomes in specific subsets of patients, but have little impact on the progression of pulmonary vascular remodeling. Upon new advances in vector development and delivery techniques, gene therapy is a novel strategy in this field with the potential of overcoming the main limitations of approved drug therapies: modulation of novel anti-remodeling targets and selective pulmonary vasculature targeting with minimal systemic effects. In the recent years, several reports have shown that gene transfer to the pulmonary vascular system is feasible in rodent models of PH. Our group has focused on the translation of airway delivery of viral vectors in small and large animals. Here, we describe a procedure to achieve vector transduction at the distal vasculature in animal models of PH and the methods to evaluate the outcomes of this intervention as a promising new approach in pulmonary vascular diseases.

**Key words** Airway delivery, Gene therapy, Pulmonary hypertension, Large animal model, Adeno-associated virus, Right ventricular failure, Vascular remodeling, Pulmonary vascular disease

## 1 Introduction

Pulmonary vascular disease (PVD) is defined by the development of vessel wall remodeling changes in the distal pulmonary vasculature, and is a consequence of a heterogeneous group of clinical conditions [1]. In the clinical setting, PVD is characterized by progressive dyspnea and exercise intolerance, and diagnosis relies on the detection of pulmonary hypertension (PH) upon right heart catheterization. PH is defined by a mean pulmonary artery (PA) pressure above 25 mmHg [1], and based on available clinical studies, underlying PVD is suspected by additional hemodynamic abnormalities in the pulmonary circulation, such as increased pulmonary vascular resistance (PVR), transpulmonary gradient or diastolic to PA wedge pressure differences [1–3]. The main determinant of prognosis in patients suffering PH is the impact of sustained high afterload on right ventricular function, leading to premature heart failure and death [4].

Kiyotake Ishikawa (ed.), *Cardiac Gene Therapy: Methods and Protocols*, Methods in Molecular Biology, vol. 1521
DOI 10.1007/978-1-4939-6588-5_24, © Springer Science+Business Media New York 2017

Current therapeutic options for chronic PH are largely dependent on the clinical classification for each patient undergoing the diagnostic process [1]. Advances in the cellular and molecular mechanisms involved in Group 1 PH (also designated as pulmonary arterial hypertension, PAH) have led to novel drug developments targeting the main pathways including endothelin receptor antagonists, prostacyclin analogs and activators of the soluble guanylate cyclase (sGC)/cGMP axis (phosphodiesterase five inhibitors, and more recently, sGC activators) [1]. Clinical trials for these drugs have focused on Group 1 PH, while some benefit may be present in other groups with novel agents [5, 6], in particular groups 2 (PH due to left heart disease) and 4 (chronic thromboembolic PH).

Limitations for the widespread use of current vasodilator drugs include the frequency of systemic, undesired side effects, lack of long-term sustained clinical benefits, as well as a high economic cost of these treatments [1]. In addition, during the past few years, the unraveling of novel molecular mechanisms involved in PH have set growing interest in developing more specific, target-driven therapeutic strategies. In this regard, gene therapy may overcome some of the limitations of current treatments, by selectively modulating novel pathways that are not targeted by any drug at present [7]. Recently, several studies by independent groups have shown the potential therapeutic benefit of modulating a variety of molecular targets using gene therapy [7, 8]. For instance, endothelial NOS, prostacyclin synthase or BMPR2 have been successfully modulated in the pulmonary vasculature leading to improved hemodynamics in animal models of PH [9–11].

In order to develop gene therapy strategies for PH, vectors that efficiently target the pulmonary vasculature and provide sustained expression of the gene of interest are needed. In this regard, advances in viral vector technology have made available the recombinant adeno-associated viruses (AAV)s that allow different tissue tropisms based on the capsid proteins composition, while eliciting minimal immune response. In addition, delivery methods that preferentially transduce the lung vasculature with minimal exposure of the vector to off-target tissues are essential to guarantee the feasibility, safety, and translatability of this strategy for PH patients [12].

The purpose of this protocol is to describe a novel airway delivery method of vectors in large animal models of PH that efficiently transduces the distal pulmonary circulation and elicits improvements in vascular remodeling and hemodynamics.

## 2 Materials

### 2.1 Animal Preparation and PH Model Creation

*For Anesthesia Induction and Maintenance*

1. Telazol (tiletamine/zolazepam).
2. Isoflurane.

3. Propofol.
4. Fentanyl patch.
5. Prophylactic antibiotics.
6. Respirator suitable for swine with adjustable inspiratory oxygen concentration.
7. ECG and pulse oxymetry monitor.

*For Surgical PH Model Creation in Swine*

8. Surgical suite and sterile drapes.
9. Standard surgical tools: Scissors, forceps, scalpel. Bioabsorbable and Nylon sutures, Silicone Thoracic Drain 20Fr., Gauzes.
10. Cotton Umbilical Tape 1/8″ × 18″.
11. A 3.5-mm diameter plastic cylinder.
12. Furosemide.

***2.2 Functional Evaluation of PH in Large Animals: Hemodynamic and Echocardiography Assessments***

1. Procedure room equipped with a fluoroscopy system (C-arm).
2. Standard cath pack for sterile percutaneous angiographies (syringes, towels, bowls, gauze).
3. Sheath introducer 8 French.
4. Swan-Ganz Catheter 7 French.
5. Capnograph.
6. Blood gas analyzer.
7. Pressure transducers.

***2.3 Airway Gene Delivery***

1. Procedure room equipped with a fluoroscopy system (C-arm).
2. MicroSprayer® Aerosolizer and accompanying syringes (Model IA-1B, Penn-Century, Inc.) customized for large animal experiments (in 20–40 kg Yorkshire swine, a 50 cm-length tip is optimal, but needs to be designed according to the animal species and the proximal airway to carina distance).
3. Multipurpose coronary diagnostic catheter shortened to fit the Sprayer (7 Fr).
4. Viral vector encoding reporter gene (lacZ or GFP) or the therapeutic gene of interest.
5. Ambu bag.
6. Airway filter with high filtration efficiency.
7. Personal protective equipment (PPE) including gloves, masks, gown, and eye protection.

***2.4 Evaluation of the Transduction Efficiency Using β-Galactosidase Expression***

1. O.C.T. Compound.
2. Glass slides.
3. Cryotome.
4. X-Gal staining kit.

5. Neutral buffered 10% formalin solution.
6. Primary antibodies against reporter gene or gene of interest.
7. Brightfield and confocal microscope.

## 3 Methods

### 3.1 Animal Preparation and PH Model Creation

1. Fast the animals overnight. Administer prophylactic antibiotics prior to surgery.
2. Anesthesia is induced with intramuscular administration of 6.0 mg/kg Telazol (tiletamine/zolazepam). Orotracheal intubation is performed first by trained personnel, and peripheral oxygen saturation and heart rate are continuously monitored (*see* **Note 1**). A peripheral ear vein access is subsequently obtained.
3. For surgical procedures (surgical PH model creation), inhaled isoflurane (1–3%) is adjusted according to animal sedation status. Analgesia after the procedure is provided using postoperative 25–50 μg/h fentanyl patch. During the procedure, oxygen saturation, heart rate, and systemic blood pressure are continuously monitored. Animals are given prophylactic antibiotics twice daily for 5 days after the thoracotomy.
4. Surgical creation of the PH model in swine. A left lateral thoracotomy at the fifth intercostal space is performed under sterile conditions (*see* **Note 2**). Remove the lung from surgical site by applying a wet gauze and squeeze (*see* **Note 3**). Obtain a good view of the left atrial posterior wall where pulmonary veins enter. Widen the incision if necessary.
5. The superior left pulmonary vein and the common inferior pulmonary vein are carefully dissected in the extrapericardial space close to the left atrium. Consistent degree of venous stenoses are achieved by placing a cotton umbilical tape around a 3.5-mm diameter plastic cylinder that is subsequently removed once the tape is tightly secured (*see* **Note 4**).
6. Close the chest in layers, making sure that all air is evacuated using a drainage chest tube. Furosemide 4 mg/kg is given after the procedure to prevent acute pulmonary edema [13, 14].

### 3.2 Functional Evaluation of PH in Large Animals: Hemodynamic and Echocardiography Assessments

1. Follow the same anesthesia induction as in Subheading 2.2. Use intravenous propofol 8–10 mg/kg/h for hemodynamic evaluation (*see* **Note 5**).
2. Transthoracic echocardiography can be used for right ventricle (RV) noninvasive imaging and is convenient to perform within the animal facility. Apical views of the RV can be obtained with the animal on right lateral recumbency by placing the probe in the sub-xiphoid position. Modified apical views of the RV and

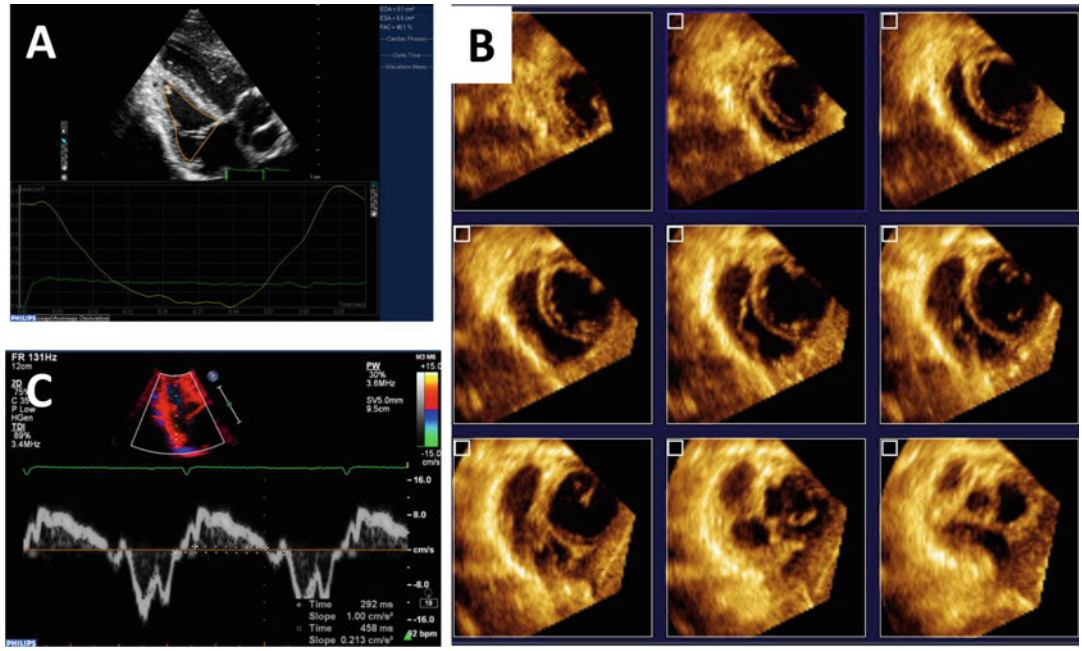


**Fig. 1** Right ventricular noninvasive characterization using echocardiography allows evaluation of the PH model and the changes induced by therapeutic gene transfer. Two- (**a**) and three (**b**) dimensional datasets can be obtained from modified apical views in swine models, as well as the Doppler spectral signal (**c**) for time intervals and Tei index

3D datasets can be acquired with ECG gating (Fig. 1). Offline analyses provides quantitative information of RV dimensions and performance [13].

3. Under sterile conditions, a femoral vascular access is obtained using the Seldinger technique. For right heart catheterization with a 7 French Swan-Ganz catheter, an 8-Fr sheath is placed in the femoral vein (*see* **Note 6**). As an alternative, the jugular veins can also be accessed in swine but care must be taken to avoid undesired carotid artery punctures.
4. Positioning of the Swan-Ganz catheter to obtain right side hemodynamics is achieved using fluoroscopic guidance (C-arm). Calibrate pressure sensor carefully. This is particularly important when measuring right side pressures as they are often much lower than left side pressures. Before measurements are obtained, hemodynamic stability must be obtained and the catheter locations should be confirmed for every measurement (*see* **Note 7**).

### *3.3 Airway Gene Delivery*

1. Therapies should be preceded by hemodynamic measurements to obtain baseline values. Gene delivery can be performed subsequently. Connect an airway filter to the tracheal tube.
2. Research personell in the operating room should take appropriate precautions for vectors (*see* **Notes 8** and **9**).

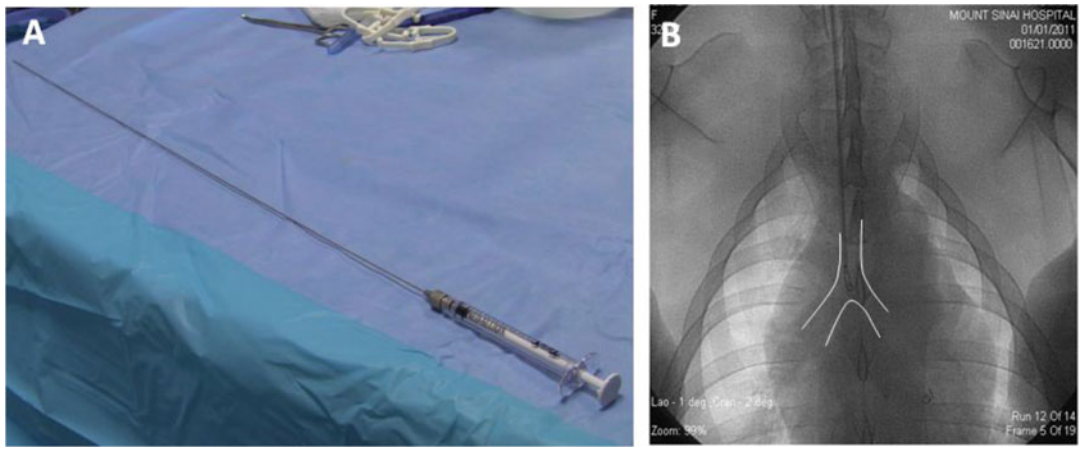


**Fig. 2** Intratracheal gene delivery requires a MicroSprayer device (**a**) that is placed near the carina guided by fluoroscopy (**b**)

3. The vector is prepared in the injection syringes (*see* **Note 10**).
4. The aerosolizer device is inserted carefully through the endotracheal tube and the position of the tip determined using fluoroscopic guidance (*see* **Note 11**). By inserting the aerosolizer tip in a 7 Fr multipurpose coronary diagnostic catheter, cut to fit the Sprayer inside, the device can be advanced in the trachea while avoiding undesired damage in the tracheal mucosa. Once the tip of the aerosolizer is 2–3 cm proximal to the tracheal bifurcation, the multipurpose coronary diagnostic catheter is gently pulled back a few cm (Fig. 2).
5. The total vector dose is split into three equal aliquots that will be injected in the dorsal, right, and left lateral recumbent positions, allowing at least 5 min between each injection (*see* **Note 12**).
6. Injection of the vector solution should be coordinated to the inspiration phase. Also, pre-injection alveolar recruitment maneuvers using the Ambu will facilitate a more even and distal distribution of the vector.
7. After vector delivery is completed, mechanically ventilate for an additional 20–30 min with continuous monitoring of the EKG, hemodynamics, and respiratory parameters.
8. Once the observation period is finished without complications, the animal is recovered. The vector leak from the airway is minimal; however, keep the precaution materials on throughout the procedure.

### *3.4 Evaluation of the Transduction Efficiency*

1. Humanly euthanize the animals after an appropriate time post-gene delivery to allow transgene expression. Through a median sternotomy, lung tissue from both side of the lungs at different lobes are collected. Remove blood from the tissue specimens by perfusing the vessels with PBS (*see* **Note 13**).

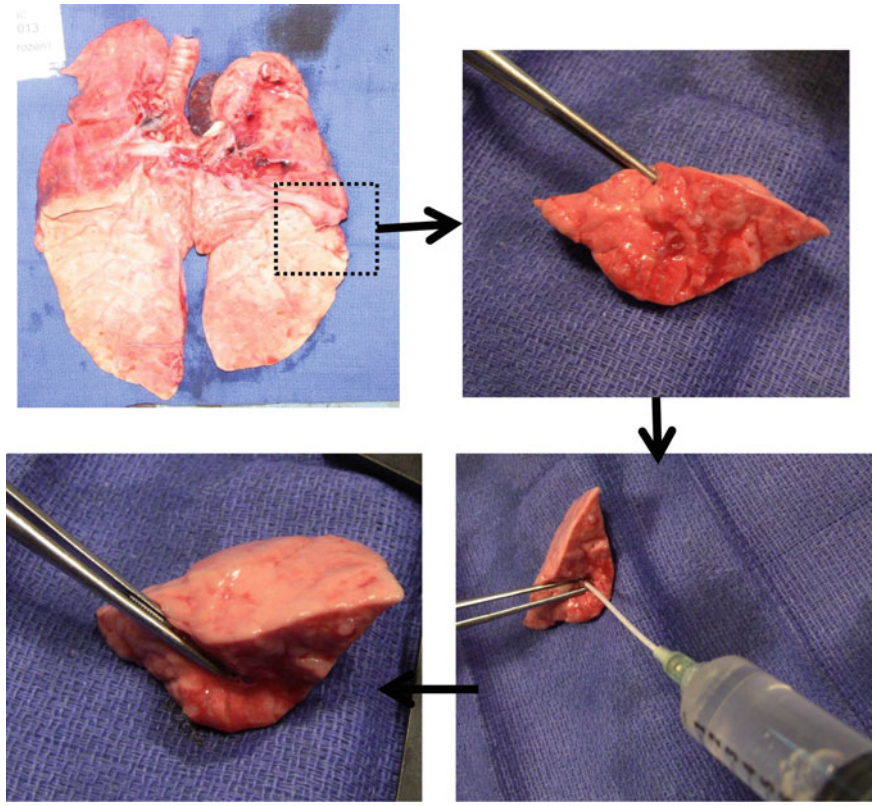

**Fig. 3** Lung tissue is inflated with OCT for easier handling and ulterior staining techniques

2. For lung tissue fixation, gently insufflate the airway with 50% OCT in PBS, embed in labeled OCT molds and freeze the blocks. Using a cryotome, sections (8–10 μm) are prepared on glass slides for subsequent staining (*see* **Note 14**) (Fig. 3).
3. The staining technique to detect transgene expression depends on the reporter or protein of interest. For vectors with the lacZ reporter, the product of β-galactosidase activity can be detected in brightfield microscopy using the X-Gal staining kit. However, detection of β-galactosidase using specific primary antibodies is more sensitive and can be more precisely localized using confocal microscopy. For specific proteins of interest, primary antibodies that are well validated in swine tissue are needed. Colocalization with specific cell type markers such as alpha-smooth muscle actin (for smooth muscle cells) or endothelial NOS (endothelial cells) allows a more clear identification of preferential cell type of gene expression (*see* **Note 15**) (Fig. 4).

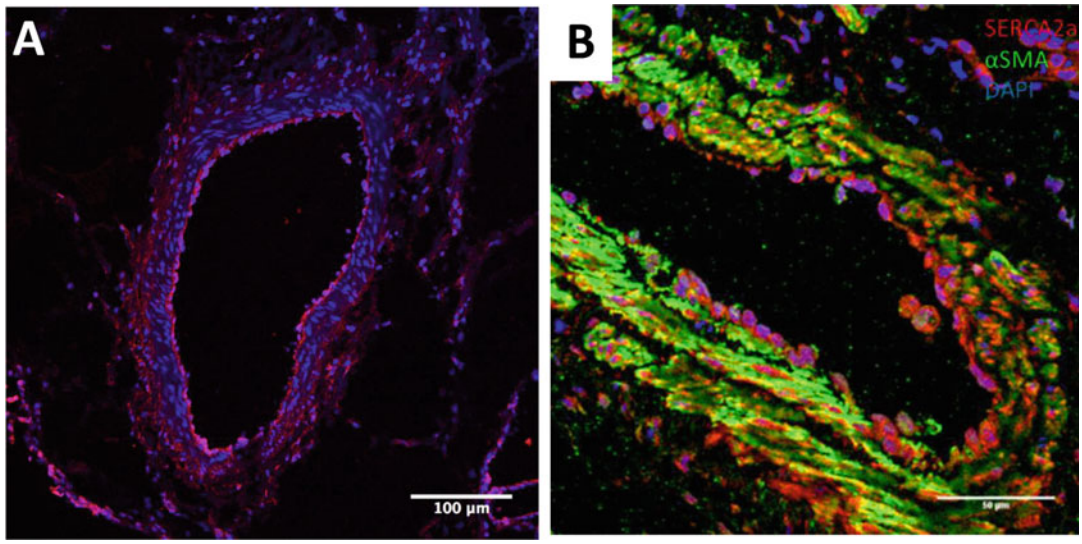


**Fig. 4** Assessment of transgene expression can be performed using immunofluorescent staining. Four weeks after the delivery procedure, β-galactosidase protein is found in the pulmonary vasculature (*pink*, **a**). Upon delivery of the AAV1.CMV.SERCA2a vector, overexpression of SERCA2a protein (*red*, **b**) colocalizes with smooth muscle cells (*green*, **b**)

## 4 Notes

1. In animals with moderate to severe PH, hypoxia can significantly worsen the hemodynamics and animals can easily die from brief hypoxia. Oxygen should be supplied continuously during the preparation, and rapid intubation and immediate ventilation is necessary to prevent prolonged hypoxemia that may influence the stability of the hemodynamic evaluation.
2. When entering the pleural cavity, use caution not to injure the lung. Cutting the pleural membrane during the expiration will reduce the risk of accidental injury.
3. Lungs can be inflated using an Ambu bag after banding the pulmonary veins.
4. The optimal degree of vein stenosis depends of the animal growth rate. Applying too tight of a stenosis can cause subacute lung edema that develops 2–3 h after surgery. The data provided applies to female Yorkshire swine with BW 10–13 kg.
5. Some anesthesia drugs such as isoflurane have a strong vasodilatory effect and can mask mild PH.
6. Guidance of the percutaneous puncture using vascular echography minimizes the number of attempts and vascular injury, and is advisable if repeated right heart catheterization procedures to monitor hemodynamics overtime are planned.

7. Appropriate ventilation parameters are set depending on the investigators needs. The following parameters provide stable and reproducible conditions under general anesthesia in our experience: oxygen inspiratory fraction 40%, 10 ml/kg tidal volume at 15 respirations per minute to maintain an end-tidal $CO_2$ between 35 and 45 mmHg as determined by capnography. A portable blood gas analyzer provides a detailed blood gas profile that can be particularly informative in diseased animals. Cardiac output is determined by thermodilution.
8. When testing vectors that can affect research personnel, personal protective equipment including gloves, gowns, shoe covers, respirators, face shields and safety glasses must be worn during the viral vector delivery procedures and animal necropsies. The risk of infection by exposure to an infectious aerosol must be minimized by primary containment and multiple secondary barriers such as specialized ventilation systems, air treatment systems to decontaminate or remove agents from exhaust air, and controlled access zones.
9. We have previously used AAV vectors using this delivery method [12]. According to the NIH Guidelines, recombinant AAVs in which the transgene does not encode either a potentially oncogenic gene product or toxins, and are produced in the absence of a helper virus can in most cases be handled at Biosafety Level 1. Decontamination of working areas is recommended. Experiments must be performed in accordance with the Guidelines for the Care and Use of Laboratory Animals and approved by the Institutional Animal Care and Use Committee for the use of AAV in these animals.
10. If the vector should be kept cold to maintain its activity, vector preparation should be done by a second operator after placing the Sprayer in the appropriate position.
11. An L-shape connector with a hole for inserting the sprayer will facilitate the procedure and reduce vector leak from the animal.
12. Raising the head by 20 cm will facilitate a more distal deposition of the injected solution.
13. Lung adhesions at the site of surgical manipulation is frequent in these animal models. This may limit the integrity of certain regions of the lung parenchyma.
14. Cryosectioning of the lung OCT block may be challenging especially when incomplete airway insufflation is present. As an alternative, prior fixation in 10% formalin can be used. In formalin-fixed paraffin blocks, deparaffination and the antigen retrieval step with sodium citrate pH 6.0 may yield good immunostaining results for many of the antibodies.
15. Due to cellular turnover, the gene expression signal detected using different techniques may fade overtime.

## Acknowledgments

This work is supported by NIH P50 HL112324, R01 HL119046, R01 HL117505, R01 HL128099, R01 HL129814, R01HL131404, & T32 HL007824 (R. J. H.), and a Transatlantic Leducq Foundation grant. We would like to acknowledge the Gene Therapy Resource Program (GTRP) of the National Heart, Lung, and Blood Institute, National Institutes of Health for providing some of the gene vectors used in these studies. J.A. was supported by the Fundacion Alfonso Martin-Escudero. N.H. was supported by the French Federation of Cardiology.

### References

1. Galie N, Hoeper MM, Humbert M, Torbicki A, Vachiery JL, Barbera JA, Beghetti M, Corris P, Gaine S, Gibbs JS, Gomez-Sanchez MA, Jondeau G, Klepetko W, Opitz C, Peacock A, Rubin L, Zellweger M, Simonneau G (2009) Guidelines for the diagnosis and treatment of pulmonary hypertension: the Task Force for the Diagnosis and Treatment of Pulmonary Hypertension of the European Society of Cardiology (ESC) and the European Respiratory Society (ERS), endorsed by the International Society of Heart and Lung Transplantation (ISHLT). Eur Heart J 30(20):2493–2537. doi:10.1093/eurheartj/ehp297, ehp297 [pii]
2. Lau EMT, Manes A, Celermajer DS, Galiè N (2011) Early detection of pulmonary vascular disease in pulmonary arterial hypertension: time to move forward. Eur Heart J 32:2489. doi:10.1093/eurheartj/ehr160
3. Vachiery JL, Adir Y, Barbera JA, Champion H, Coghlan JG, Cottin V, De Marco T, Galie N, Ghio S, Gibbs JS, Martinez F, Semigran M, Simonneau G, Wells A, Seeger W (2013) Pulmonary hypertension due to left heart diseases. J Am Coll Cardiol 62(25 Suppl): D100–D108.doi:10.1016/j.jacc.2013.10.033, S0735-1097(13)05876-2 [pii]
4. Sutendra G, Michelakis ED (2013) Pulmonary arterial hypertension: challenges in translational research and a vision for change. Sci Transl Med 5(208):208sr205. doi:10.1126/scitranslmed.3005428, 5/208/208sr5 [pii]
5. Ghofrani H-A, D'Armini AM, Grimminger F, Hoeper MM, Jansa P, Kim NH, Mayer E, Simonneau G, Wilkins MR, Fritsch A, Neuser D, Weimann G, Wang C (2013) Riociguat for the treatment of chronic thromboembolic pulmonary hypertension. N Engl J Med 369(4):319–329. doi:10.1056/NEJMoa1209657
6. Gheorghiade M, Greene SJ, Butler J et al (2015) Effect of vericiguat, a soluble guanylate cyclase stimulator, on natriuretic peptide levels in patients with worsening chronic heart failure and reduced ejection fraction: the socrates-reduced randomized trial. JAMA 314(21):2251–2262
7. Reynolds PN (2011) Gene therapy for pulmonary hypertension: prospects and challenges. Expert Opin Biol Ther 11(2):133–143. doi:10.1517/14712598.2011.542139
8. Reynolds AM, Holmes MD, Danilov SM, Reynolds PN (2012) Targeted gene delivery of BMPR2 attenuates pulmonary hypertension. Eur Respir J 39(2):329–343. doi:10.1183/09031936.00187310
9. Meng L-K, Liu C-G (2010) Gene therapies for pulmonary hypertension—from experimental trials to bedside aspects. Eur J Cardiothorac Surg 37(2):407–419. doi:10.1016/j.ejcts.2009.06.045
10. Hadri L, Kratlian RG, Benard L, Maron BA, Dorfmuller P, Ladage D, Guignabert C, Ishikawa K, Aguero J, Ibanez B, Turnbull IC, Kohlbrenner E, Liang L, Zsebo K, Humbert M, Hulot JS, Kawase Y, Hajjar RJ, Leopold JA (2013) Therapeutic efficacy of AAV1.SERCA2a in monocrotaline-induced pulmonary arterial hypertension. Circulation 128(5):512–523. doi:10.1161/CIRCULATIONAHA.113.001585,CIRCULATIONAHA.113.001585 [pii]
11. Granton J, Langleben D, Kutryk MJ, Camack N, Galipeau J, Courtman D, Stewart DJ (2015) Endothelial NO-synthase gene-enhanced progenitor cell therapy for pulmonary arterial hypertension: the PHACeT trial. Circ Res 117:645. doi:10.1161/circresaha.114.305951
12. Aguero J, Ishikawa K, Hadri L, Santos-Gallego CG, Fish KM, Kohlbrenner E, Hammoudi N, Kho C, Lee A, Ibáñez B, García-Alvarez A, Zsebo K, Maron BA, Plataki M, Fuster V,

Leopold JA, Hajjar RJ (2016) Intratracheal Gene Delivery of SERCA2a Ameliorates Chronic Post-Capillary Pulmonary Hypertension: A Large Animal Model. J Am Coll Cardiol. 2016;67(17):2032–46. doi:10.1016/j.jacc.2016.02.049

13. Aguero J, Ishikawa K, Hadri L, Santos-Gallego C, Fish K, Hammoudi N, Chaanine A, Torquato S, Naim C, Ibanez B, Pereda D, Garcia-Alvarez A, Fuster V, Sengupta PP, Leopold JA, Hajjar RJ (2014) Characterization of right ventricular remodeling and failure in a chronic pulmonary hypertension model. Am J Physiol Heart Circ Physiol 307(8):H1204–H1215. doi:10.1152/ajpheart.00246.2014, ajpheart.00246.2014 [pii]
14. Pereda D, Garcia-Alvarez A, Sanchez-Quintana D, Nuno M, Fernandez-Friera L, Fernandez-Jimenez R, Garcia-Ruiz JM, Sandoval E, Aguero J, Castella M, Hajjar RJ, Fuster V, Ibanez B (2014) Swine model of chronic postcapillary pulmonary hypertension with right ventricular remodeling: long-term characterization by cardiac catheterization, magnetic resonance, and pathology. J Cardiovasc Transl Res 7(5):494–506. doi:10.1007/s12265-014-9564-6

# 6. Discusión.

La caracterización de modelos animales preclínicos en el ámbito de las enfermedades cardiovasculares tiene dos objetivos generales:

1) Descriptivo-analítico: consiste en generar modelos e identificar si las principales características propias de la enfermedad de interés están presentes. Para ello las técnicas de imagen cardiovascular desempeñan un papel clave. En modelos de animal grande o preclínicos, es posible emplear los mismos biomarcadores de imagen que en los estudios en humanos, favoreciendo la traslación de nuevos hallazgos al ámbito clínico. En esta fase es importante definir si la gravedad de las alteraciones es similar a la patología en humanos, y describir el curso temporal de dichas alteraciones (cambios predominantemente agudos frente a crónicos, progresión temporal de las alteraciones, y posibilidad de mejoría espontánea que pueda confundir el efecto de una intervención). El objetivo final es determinar la relevancia o validez del modelo clínico respecto a la enfermedad de interés.

2) Modelo de intervención para probar nuevas terapias. Una vez definida la relevancia clínica del modelo, e identificados los biomarcadores en los que se basará la efectividad de un nuevo tratamiento, se pasa a ensayar la nueva estrategia frente a un grupo control.

En la presente Tesis Doctoral se han desarrollado y caracterizado modelos animales preclínicos enfocados en aspectos muy concretos de la enfermedad cardíaca crónica: 1) la hipertensión pulmonar crónica y disfunción ventricular derecha, y 2) la disfunción ventricular izquierda, así como el uso aplicado de uno de estos modelos con fines terapéuticos. Aunque los artículos presentados como parte de esta Tesis incluyen una Discusión pormenorizada de sus contenidos, es importante proporcionar una perspectiva más amplia e integral del ámbito de aplicación de este tipo de investigación en cada uno de los apartados previamente desarrollados.

**Modelos de HTP y desarrollo de nuevas terapias.** En la literatura hay escasas referencias sobre la creación de modelos animales preclínicos en hipertensión pulmonar crónica. Esto se debe en gran medida a la heterogeneidad de esta patología por lo que respecta a las causas, mecanismos y fenotipos clínicos. De los dos modelos que hemos caracterizado[7-8], uno de ellos presentaba un fenotipo cercano a la patología que se deseaba modelizar y se consideró clínicamente relevante, lo que permitió continuar la línea de investigación sobre terapias experimentales en el ámbito de la transferencia génica. Este estudio[11] ha sido la primera experiencia sobre terapia génica en hipertensión pulmonar

crónica en un modelo preclínico, y supuso la continuación de una línea de investigación iniciada unos años antes por nuestro propio grupo en modelos in vitro y en roedores[12]. La terapia que se puso a prueba fue, a su vez, la primera terapia génica empleada en pacientes con insuficiencia cardíaca crónica en el ensayo CUPID[13]. Pese a todo, los modelos animales de hipertensión pulmonar siguen siendo un campo en desarrollo con aspectos no resueltos y deben interpretarse con cautela los resultados de las nuevas intervenciones[15]. Respecto a la aplicación de los modelos descritos, nuestro grupo ha publicado nuevos estudios sobre nuevos conceptos en el diagnóstico y tratamiento de esta enfermedad que necesitan ser validados en humanos[16-17].

Si bien existen descripciones previas de modelos de hipertensión pulmonar, el enfoque en el remodelado del VD es novedoso en ambas publicaciones, gracias a la definición del patrón oro mediante curvas de presión-volumen, y su combinación con técnicas de imagen multimodalidad. Recientemente, diversos documentos y revisiones de expertos han destacado la relevancia de caracterizar los cambios en el VD en modelos preclínicos para entender mejor el efecto de las nuevas terapias[18].

**Modelos de disfunción del VI.** La disfunción del VI ha sido la característica central de la IC en estudios preclínicos y en ensayos clínicos. Si bien hoy sabemos que la IC es un síndrome más complejo y que requiere una visión más amplia para diagnosticar y tratar adecuadamente a los pacientes, la mayoría de terapias se han orientado a mejorar la función del VI. En este sentido, los modelos de infarto han sido descritos ampliamente en la literatura, fundamentalmente para estudios sobre regeneración miocárdica. En uno de los trabajos de la presente Tesis Doctoral evaluamos las ventajas e inconvenientes de estos modelos de cardiopatía isquémica. Un aspecto controvertido en la literatura es la idoneidad de estos modelos post-infarto para probar terapias “no regenerativas” de tipo farmacológico o terapia génica. Esto supone describir no sólo cambios globales en el remodelado ventricular, si no también cambios regionales en miocardio remoto (no infartado) que sean susceptibles de tratamientos dirigidos. En relación a estos resultados descritos en la presente Tesis Doctoral, recientes estudios en pacientes han sugerido que los cambios en el miocardio remoto detectables por técnicas de imagen son importantes en el remodelado global a largo plazo[19], y podrían indicar que tratamientos específicos podrían ser efectivos. Respecto a la caracterización de modelos de cardiopatía isquémica, nuestro grupo ha estudiado recientemente los cambios regionales dinámicos en el territorio infartado mediante técnicas de imagen avanzada, que han contribuido a una mejor comprensión del daño por isquemia y reperfusión del miocárdio[20-22] y potencial desarrollo de nuevas terapias.

La caracterización del modelo de cardiopatía isquémica ha facilitado el desarrollo de estudios sobre nuevas terapias en este contexto. Nuestros grupos de investigación han publicado gracias a estas descripciones y a la experiencia adquirida en estos modelos, diversos trabajos basados en nuevas dianas terapéuticas en terapia génica mediante vectores virales[23-25], nuevas aplicaciones de tratamientos farmacológicos y nuevas modalidades de reperfusión miocárdica para prevenir el remodelado ventricular[26-27].

En modelos de cardiopatía isquémica hemos caracterizado la insuficiencia mitral funcional debida a remodelado del VI. Así mismo, hemos descrito por primera vez en un modelo experimental las consecuencias de la isquemia auricular prolongada en el sustrato fibrótico, y el deterioro funcional auricular asociado a este daño. Con el reciente desarrollo de terapias percutáneas para el tratamiento de valvulopatías en el ámbito del intervencionismo estructural, consideramos que este modelo ofrece características únicas para probar nuevos dispositivos en fenotipos específicos de insuficiencia mitral isquémica.

La caracterización del modelo de sobrecarga de presión no permitió, sin embargo, su desarrollo hacia estudios terapéuticos. Tras comprobar que el fenotipo observado pese a un largo seguimiento no era óptimo para ser objeto de intervención terapéutica, fue descartado para este propósito. A diferencia de lo que hemos podido observar en el modelo porcino, en modelos de roedor se ha descrito que la sobrecarga de presión da lugar a un remodelado inicialmente adaptativo, que posteriormente progresa a disfunción del VI, lo que ha favorecido de este modelo in vivo de IC. La ausencia de esta transición en el modelo preclínico de animal grande supone una limitación importante de su relevancia para evaluar nuevas terapias. A este respecto cabe destacar que, si bien un modelo similar se había empleado para la evaluación preclínica de un tratamiento en IC[28], los resultados positivos no fueron posteriormente confirmados en la fase clínica[29], lo cual podría deberse entre otras cosas a los problemas de relevancia clínica de este modelo. Sin embargo, un modelo similar ha permitido a nuestro grupo desentrañar aspectos mecanísticos novedosos en el remodelado eléctrico y propensión a arritmias cardíacas en el contexto de la hipertrofia ventricular (en revisión).

**Papel de los modelos preclínicos en investigación traslacional.** Los modelos de animal grande son un eslabón importante en la investigación traslacional de nuevos descubrimientos desde el laboratorio a la clínica. Su papel principal es el de confirmar los beneficios de terapias seleccionadas en modelos más sencillos (in vitro, roedor, simulaciones in silico) en un modelo más complejo, y a su vez más cercano a la enfermedad en humanos, así como evaluar aspectos relacionados con la bioseguridad. La presente

Tesis Doctoral se enmarca en este contexto englobando investigación traslacional en terapia génica cardiovascular, y modulación del sistema adrenérgico. Así pues, los modelos de cardiopatía isquémica se emplearon en la validación preclínica de nuevas dianas terapéuticas mediante transferencia génica[12, 23-25, 30-32] y modulación farmacológica de la señalización adrenérgica[33]. En algunos casos, se ha podido avanzar hasta fases clínicas que han confirmado los resultados observados en el modelo animal[34].

Los modelos preclínicos presentan pese a todo lo expuesto anteriormente, limitaciones importantes que deben ser tenidas en cuenta. La principal es la dificultad para capturar aspectos complejos de la enfermedad cardiovascular, en particular la gran heterogeneidad de los fenotipos, y que a menudo está relacionada con el envejecimiento de los pacientes y las comorbilidades. Esta complejidad puede explicar que un tratamiento exitoso en fases preclínicas no produzca ningún beneficio en ensayos clínicos. Estas diferencias entre la enfermedad en el modelo animal y los pacientes pueden ser más profundas respecto al potencial efecto de terapias avanzadas como la regeneración celular y la transferencia génica. En estos casos, intervienen además las diferencias interespecies en la respuesta inmune al producto administrado, lo cual influye de manera decisiva en la efectividad del mismo. Esta es una de las explicaciones que se ha postulado en diversas líneas de investigación traslacional en regeneración celular miocárdica, y más reciente en terapia génica, que mostraron ausencia de beneficio clínico en pacientes pese a haber demostrado eficacia en modelos preclínicos[13, 35].

### Limitaciones.

Los comentarios anteriores sobre estos modelos animales ponen de manifiesto potenciales aplicaciones, pero a su vez importantes limitaciones:

- Necesidades de infraestructura, coste económico y personal experto. La investigación preclínica en modelos de animal grande requiere una gran inversión en infraestructura que permita asumir los cuidados necesarios de estas especies animales, así como equipamientos costosos para crear y evaluar mediante técnicas de imagen. Así mismo hace falta personal experimentado en técnicas de investigación preclínica, y en imagen clínica.

- La puesta a punto de un modelo requiere una gran inversión de recursos y tiempo, que a menudo obliga a descartar esta opción. Con frecuencia, hallazgos publicados en la literatura respecto a determinados modelos pueden no ser reproducibles de forma fiable, lo

que obliga a cambios de protocolo o en el modelo seleccionado. Una vez caracterizado el modelo, puede que este no reúna los aspectos deseados por lo que obliga a descartarlo.

- Con todo ello, la investigación preclínica puede resultar poco rentable y es necesario definir claramente a qué se va a aplicar el modelo y justificar el tiempo y elevado coste que requerirá su puesta a punto.

# 7. Conclusiones.

1. Los modelos preclínicos son un paso necesario para demostrar la eficacia de nuevas dianas terapéuticas antes de iniciar los primeros ensayos en humanos. Permiten a su vez llevar a cabo estudios de bioseguridad.

2. Las técnicas de imagen cardiovascular son una herramienta clave en la caracterización de modelos preclínicos, y permiten definir los criterios de beneficio clínico en estudios de validación de nuevas terapias.

3. Los modelos preclínicos en el ámbito de la HTP crónica presentan características clínicamente relevantes respecto a las alteraciones de la circulación pulmonar y el remodelado ventricular derecho. La selección del modelo animal, métodos de evaluación y duración del seguimiento son críticos para evaluar nuevas terapias experimentales en estudios preclínicos.

4. Los modelos de IC secundaria cardiopatía isquémica presentan características clínicamente relevantes y pueden ser evaluados de forma precisa mediante técnicas de imagen avanzada.

5. Los modelos de sobrecarga de presión presentan cambios típicos de fases precoces de la enfermedad, y eso limita su aplicación en estudios de IC establecida.

6. Los modelos de HTP crónica han permitido evaluar el potencial de nuevas estrategias de terapia génica dirigida de forma selectiva a dianas terapéuticas específicas, y abren un nuevo campo en este grupo de enfermedades.

# 8. Bibliografía.


1. Roger VL. Epidemiology of Heart Failure. *Circulation Research*. 2013;113:646.
2. Dixon JA and Spinale FG. Large Animal Models of Heart Failure. *Circulation: Heart Failure*. 2009;2:262.
3. Pleger ST, Brinks H, Ritterhoff J, Raake P, Koch WJ, Katus HA and Most P. Heart Failure Gene Therapy. *Circulation Research*. 2013;113:792.
4. Tilemann L, Ishikawa K, Weber T and Hajjar RJ. Gene Therapy for Heart Failure. *Circulation Research*. 2012;110:777.
5. Samson R, Jaiswal A, Ennezat PV, Cassidy M and Le Jemtel TH. Clinical Phenotypes in Heart Failure With Preserved Ejection Fraction. *Journal of the American Heart Association*. 2016;5.
6. Houser SR, Margulies KB, Murphy AM, Spinale FG, Francis GS, Prabhu SD, Rockman HA, Kass DA, Molkentin JD, Sussman MA and Koch WJ. Animal Models of Heart Failure. *Circulation Research*. 2012;111:131.
7. Aguero J, Ishikawa K, Hadri L, Santos-Gallego C, Fish K, Hammoudi N, Chaanine A, Torquato S, Naim C, Ibanez B, Pereda D, Garcia-Alvarez A, Fuster V, Sengupta PP, Leopold JA and Hajjar RJ. Characterization of right ventricular remodeling and failure in a chronic pulmonary hypertension model. *Am J Physiol Heart Circ Physiol*. 2014;307:H1204-15.
8. Aguero J, Ishikawa K, Fish KM, Hammoudi N, Hadri L, Garcia-Alvarez A, Ibanez B, Fuster V, Hajjar RJ and Leopold JA. Combination proximal pulmonary artery coiling and distal embolization induces chronic elevations in pulmonary artery pressure in Swine. *PLoS One*. 2015;10:e0124526.
9. Ishikawa K, Aguero J, Tilemann L, Ladage D, Hammoudi N, Kawase Y, Santos-Gallego CG, Fish K, Levine RA and Hajjar RJ. Characterizing preclinical models of ischemic heart failure: differences between LAD and LCx infarctions. *Am J Physiol Heart Circ Physiol*. 2014;307:H1478-86.
10. Ishikawa K, Aguero J, Oh JG, Hammoudi N, Fish LA, Leonardson L, Picatoste B, Santos-Gallego CG, Fish KM and Hajjar RJ. Increased stiffness is the major early abnormality in a pig model of severe aortic stenosis and predisposes to congestive heart failure in the absence of systolic dysfunction. *J Am Heart Assoc*. 2015;4.
11. Aguero J, Ishikawa K, Hadri L, Santos-Gallego CG, Fish KM, Kohlbrenner E, Hammoudi N, Kho C, Lee A, Ibanez B, Garcia-Alvarez A, Zsebo K, Maron BA, Plataki M, Fuster V, Leopold JA and Hajjar RJ. Intratracheal Gene Delivery of SERCA2a Ameliorates Chronic Post-Capillary Pulmonary Hypertension: A Large Animal Model. *J Am Coll Cardiol*. 2016;67:2032-46.
12. Hadri L, Kratlian RG, Benard L, Maron BA, Dorfmuller P, Ladage D, Guignabert C, Ishikawa K, Aguero J, Ibanez B, Turnbull IC, Kohlbrenner E, Liang L, Zsebo K, Humbert M, Hulot JS, Kawase Y, Hajjar RJ and Leopold JA. Therapeutic efficacy of AAV1.SERCA2a in monocrotaline-induced pulmonary arterial hypertension. *Circulation*. 2013;128:512-23.
13. Greenberg B, Butler J, Felker GM, Ponikowski P, Voors AA, Desai AS, Barnard D, Bouchard A, Jaski B, Lyon AR, Pogoda JM, Rudy JJ and Zsebo KM. Calcium upregulation by percutaneous administration of gene therapy in patients with cardiac disease (CUPID 2): a randomised, multinational, double-blind, placebo-controlled, phase 2b trial. *Lancet*. 2016;387:1178-86.
14. Aguero J, Hadri L, Hammoudi N, Leonardson L, Hajjar RJ and Ishikawa K. Inhaled Gene Transfer for Pulmonary Circulation. *Methods Mol Biol*. 2017;1521:339-349.
15. Rubin LJ. Are Animal Models in Pulmonary Hypertension Relevant to the Clinical Disease? *Journal of the American College of Cardiology*. 2016;67:2047.
16. Garcia-Alvarez A, Garcia-Lunar I, Pereda D, Fernandez-Jimenez R, Sanchez-Gonzalez J, Mirelis JG, Nuno-Ayala M, Sanchez-Quintana D, Fernandez-Friera L, Garcia-Ruiz JM, Pizarro G, Aguero J, Campelos P, Castella M, Sabate M, Fuster V, Sanz J and Ibanez B. Association of myocardial T1-mapping CMR with hemodynamics and RV performance in pulmonary hypertension. *JACC Cardiovasc Imaging*. 2015;8:76-82.
17. Garcia-Alvarez A, Pereda D, Garcia-Lunar I, Sanz-Rosa D, Fernandez-Jimenez R, Garcia-Prieto J, Nuno-Ayala M, Sierra F, Santiago E, Sandoval E, Campelos P, Aguero J, Pizarro G, Peinado VI,

Fernandez-Friera L, Garcia-Ruiz JM, Barbera JA, Castella M, Sabate M, Fuster V and Ibanez B. Beta-3 adrenergic agonists reduce pulmonary vascular resistance and improve right ventricular performance in a porcine model of chronic pulmonary hypertension. *Basic Res Cardiol*. 2016;111:49.
18. Sutendra G and Michelakis ED. Pulmonary arterial hypertension: challenges in translational research and a vision for change. *Sci Transl Med*. 2013;5:208sr5.
19. Carrick D, Haig C, Rauhalammi S, Ahmed N, Mordi I, McEntegart M, Petrie MC, Eteiba H, Lindsay M, Watkins S, Hood S, Davie A, Mahrous A, Sattar N, Welsh P, Tzemos N, Radjenovic A, Ford I, Oldroyd KG and Berry C. Pathophysiology of LV Remodeling in Survivors of STEMI: Inflammation, Remote Myocardium, and Prognosis. *JACC: Cardiovascular Imaging*. 2015;8:779-789.
20. Fernandez-Jimenez R, Garcia-Prieto J, Sanchez-Gonzalez J, Aguero J, Lopez-Martin GJ, Galan-Arriola C, Molina-Iracheta A, Doohan R, Fuster V and Ibanez B. Pathophysiology Underlying the Bimodal Edema Phenomenon After Myocardial Ischemia/Reperfusion. *J Am Coll Cardiol*. 2015;66:816-28.
21. Fernandez-Jimenez R, Sanchez-Gonzalez J, Aguero J, Del Trigo M, Galan-Arriola C, Fuster V and Ibanez B. Fast T2 gradient-spin-echo (T2-GraSE) mapping for myocardial edema quantification: first in vivo validation in a porcine model of ischemia/reperfusion. *J Cardiovasc Magn Reson*. 2015;17:92.
22. Fernandez-Jimenez R, Sanchez-Gonzalez J, Aguero J, Garcia-Prieto J, Lopez-Martin GJ, Garcia-Ruiz JM, Molina-Iracheta A, Rossello X, Fernandez-Friera L, Pizarro G, Garcia-Alvarez A, Dall'Armellina E, Macaya C, Choudhury RP, Fuster V and Ibanez B. Myocardial edema after ischemia/reperfusion is not stable and follows a bimodal pattern: imaging and histological tissue characterization. *J Am Coll Cardiol*. 2015;65:315-23.
23. Ishikawa K, Fish K, Aguero J, Yaniz-Galende E, Jeong D, Kho C, Tilemann L, Fish L, Liang L, Eltoukhy AA, Anderson DG, Zsebo K, Costa KD and Hajjar RJ. Stem cell factor gene transfer improves cardiac function after myocardial infarction in swine. *Circ Heart Fail*. 2015;8:167-74.
24. Ishikawa K, Fish KM, Tilemann L, Rapti K, Aguero J, Santos-Gallego CG, Lee A, Karakikes I, Xie C, Akar FG, Shimada YJ, Gwathmey JK, Asokan A, McPhee S, Samulski J, Samulski RJ, Sigg DC, Weber T, Kranias EG and Hajjar RJ. Cardiac I-1c overexpression with reengineered AAV improves cardiac function in swine ischemic heart failure. *Mol Ther*. 2014;22:2038-45.
25. Tilemann L, Lee A, Ishikawa K, Aguero J, Rapti K, Santos-Gallego C, Kohlbrenner E, Fish KM, Kho C and Hajjar RJ. SUMO-1 gene transfer improves cardiac function in a large-animal model of heart failure. *Sci Transl Med*. 2013;5:211ra159.
26. Garcia-Ruiz JM, Fernandez-Jimenez R, Garcia-Alvarez A, Pizarro G, Galan-Arriola C, Fernandez-Friera L, Mateos A, Nuno-Ayala M, Aguero J, Sanchez-Gonzalez J, Garcia-Prieto J, Lopez-Melgar B, Martinez-Tenorio P, Lopez-Martin GJ, Macias A, Perez-Asenjo B, Cabrera JA, Fernandez-Ortiz A, Fuster V and Ibanez B. Impact of the Timing of Metoprolol Administration During STEMI on Infarct Size and Ventricular Function. *J Am Coll Cardiol*. 2016;67:2093-104.
27. Garcia-Ruiz JM, Galan-Arriola C, Fernandez-Jimenez R, Aguero J, Sanchez-Gonzalez J, Garcia-Alvarez A, Nuno-Ayala M, Dube GP, Zafirelis Z, Lopez-Martin GJ, Bernal JA, Lara-Pezzi E, Fuster V and Ibanez B. Bloodless reperfusion with the oxygen carrier HBOC-201 in acute myocardial infarction: a novel platform for cardioprotective probes delivery. *Basic Res Cardiol*. 2017;112:17.
28. Bishu K, Hamdani N, Mohammed SF, Kruger M, Ohtani T, Ogut O, Brozovich FV, Burnett JC, Linke WA and Redfield MM. <span hwp:id="article-title-1" class="article-title">Sildenafil and B-Type Natriuretic Peptide Acutely Phosphorylate Titin and Improve Diastolic Distensibility In Vivo</span><span hwp:id="article-title-49" class="sub-article-title">Clinical Perspective</span&gt. *Circulation*. 2011;124:2882.
29. Redfield MM, Chen HH, Borlaug BA and et al. Effect of phosphodiesterase-5 inhibition on exercise capacity and clinical status in heart failure with preserved ejection fraction: A randomized clinical trial. *JAMA*. 2013;309:1268-1277.
30. Kho C, Lee A, Jeong D, Oh JG, Chaanine AH, Kizana E, Park WJ and Hajjar RJ. SUMO1-dependent modulation of SERCA2a in heart failure. *Nature*. 2011;477:601-5.

31. Yaniz-Galende E, Chen J, Chemaly E, Liang L, Hulot JS, McCollum L, Arias T, Fuster V, Zsebo KM and Hajjar RJ. Stem cell factor gene transfer promotes cardiac repair after myocardial infarction via in situ recruitment and expansion of c-kit+ cells. *Circ Res*. 2012;111:1434-45.
32. Aguero JL, M. Ishikawa, K. Route TESI: Main Street for MSC? *Circ Res*. 2017.
33. Ibanez B, Prat-Gonzalez S, Speidl WS, Vilahur G, Pinero A, Cimmino G, Garcia MJ, Fuster V, Sanz J and Badimon JJ. Early metoprolol administration before coronary reperfusion results in increased myocardial salvage: analysis of ischemic myocardium at risk using cardiac magnetic resonance. *Circulation*. 2007;115:2909-16.
34. Ibanez B, Macaya C, Sanchez-Brunete V, Pizarro G, Fernandez-Friera L, Mateos A, Fernandez-Ortiz A, Garcia-Ruiz JM, Garcia-Alvarez A, Iniguez A, Jimenez-Borreguero J, Lopez-Romero P, Fernandez-Jimenez R, Goicolea J, Ruiz-Mateos B, Bastante T, Arias M, Iglesias-Vazquez JA, Rodriguez MD, Escalera N, Acebal C, Cabrera JA, Valenciano J, Perez de Prado A, Fernandez-Campos MJ, Casado I, Garcia-Rubira JC, Garcia-Prieto J, Sanz-Rosa D, Cuellas C, Hernandez-Antolin R, Albarran A, Fernandez-Vazquez F, de la Torre-Hernandez JM, Pocock S, Sanz G and Fuster V. Effect of early metoprolol on infarct size in ST-segment-elevation myocardial infarction patients undergoing primary percutaneous coronary intervention: the Effect of Metoprolol in Cardioprotection During an Acute Myocardial Infarction (METOCARD-CNIC) trial. *Circulation*. 2013;128:1495-503.
35. Fisher SA, Doree C, Mathur A and Martin-Rendon E. Meta-Analysis of Cell Therapy Trials for Patients with Heart Failure - An Update. *Circulation Research*. 2015.